Final Report

North Carolina Department of Transportation

Research project No. HWY-2005-22

Analysis and Testing of a Bridge Deck Reinforced With GFRP Rebars

By

Janos Gergely, Ph.D., P.E.
Principal Investigator

David M. Boyajian, Ph.D.
Principal Investigator

David T. Young, Ph.D., P.E.
Principal Investigator

Christopher R. Frank, B.S.C.E., E.I.
Graduate Research Assistant

Iosif F. Szabo, Ph.D., E.I.
Post-Doctoral Fellow

Department of Civil Engineering
University of North Carolina at Charlotte
9201 University City Boulevard
Charlotte, NC 28223

April 3, 2007

Technical Report Documentation Page

1. Report No. FHWA/NC/2006-35	2. Government Accession No.	3. Recipient's Catalog No.
4. Title and Subtitle Analysis and Testing of a Bridge Deck Reinforced with GFRP Rebars		5. Report Date April 3, 2007
		6. Performing Organization Code
7. Author(s) Janos Gergely, David M. Boyajian, David T. Young, Christopher R. Frank, and Iosif F. Szabo		8. Performing Organization Report No.
9. Performing Organization Name and Address University of North Carolina at Charlotte, Civil Engineering Department 9201 University City Blvd, Charlotte, NC 28223		10. Work Unit No. (TRAIS)
		11. Contract or Grant No.
12. Sponsoring Agency Name and Address North Carolina Department of Transportation Research and Analysis Group 1 South Wilmington Street Raleigh, North Carolina 27601		13. Type of Report and Period Covered Final Report 7/1/04-12/31/06
		14. Sponsoring Agency Code HWY-2005-22
Supplementary Notes:		

16. Abstract

The present project had two main objectives, to experimentally and analytically investigate a bridge deck reinforced with glass fiber reinforced polymer rebars, and to perform durability tests on four rebar types.

An analytical investigation was performed using the finite element software ANSYS for both the actual bridge deck, and for the reduced size laboratory experiment. In addition, laboratory experiments were also performed on an 11 ft long bridge deck model built inside the structures lab. Except for the length of the girder-deck model, the true scale was used for every other dimension. Three different tests were performed on the model, and the test data verified the analytical results. Once completed, this bridge located in Macon County was instrumented and tested using two loaded tandem trucks.

For the durability testing, four different types of Glass Fiber Reinforced Polymer (GFRP) reinforcement provided by different rebar vendors were evaluated under exposure to an alkaline environment at different temperatures. For the moisture tests, a total of 96 specimens were monitored for changes in length, diameter, and weight. A total 128 unscathed samples and 64 "nicked" samples – simulating defects to the rebars that might occur on the field site – were tested in tension to determine the rate of degradation in tensile properties. Concrete cylinders were poured, and 168 pullout specimens were tested (84 at $5Ø_b$ and 84 at $8Ø_b$).

17. Key Words GFRP rebars, bridge deck, composite durability	18. Distribution Statement		
19. Security Classif. (of this report) Unclassified	20. Security Classif. (of this page) Unclassified	21. No. of Pages 211	22. Price

Form DOT F 1700.7 (8-72) **Reproduction of completed page authorized**

DISCLAIMER

The contents of this report reflect the views of the authors and not necessarily the views of the University. The authors are responsible for the facts and the accuracy of the data presented herein. The contents do not necessarily reflect the official views or policies of either the North Carolina Department of Transportation or the Federal Highway Administration at the time of publication. This report does not constitute a standard, specification, or regulation.

ACKNOWLEDGEMENTS

The research documented in this report was sponsored by the North Carolina Department of Transportation (NCDOT). A Technical Advisory Committee (TAC) provided valuable guidance and technical support for this research project. The project TAC committee included Allen Raynor (Chair), Greg Perfetti, Ron Hancock, Tom Koch, Gichuru Muchane, David Green, Christopher Peoples, and Richard Lakata.

The authors also wish to thank for the following persons and companies:

- Mr. Frankie Smith, Plant Manager, Carolina Prestress, Charlotte, NC - for donating the 4 AASHTO Type III prestressed girders.
- Topical Inc., Atlanta, GA - for donating 6 Stay-in Place metal forms and 4 support angles.
- General Materials, LLC, Charlotte, NC - for donating 70 plastic rebar chairs.
- Unitex, Kansas City, MO - for donating 1 gallon of PRO-POXY 204 medium viscosity multipurpose bonding adhesive.
- Trent Anderson and Larry Wiggins, NCDOT Resident Engineer's Office, Andrews, NC - for providing constant construction progress reports.
- Steve Lamb, Project Superintendent, Taylor and Murphy Construction CO, INC, Asheville, NC - for continuous update from the bridge construction site.
- Mr. Doug Gremmel, Hughes Brothers, Seward, NE - for donating 20 13′ #3 GFRP rebars
- Sam Steere, Concrete Protection Products Inc. (Pultrall), Dallas, TX - for donating 13 20′ #3 GFRP Rebars
- Mr. Leroy Heston, Kodiak, Kodiak Fiberglass Rebar - for donating 20 13′ #3 GFRP rebars.
- Mr. Kem Tilley, Tillco, Marshall, Arkansas - for donating 20 13′ #3 GFRP rebars.

Executive Summary

The present project had two main objectives, to experimentally and analytically investigate a bridge deck reinforced with glass fiber reinforced polymer rebars, and to perform durability tests on four rebar types. An analytical investigation was performed using the finite element software ANSYS for both the actual bridge deck, and for the reduced size laboratory experiment. These analyses confirmed the predicted deck behavior, resulting in punching shear failure modes at load levels significantly higher than the HS-20 wheel loads.

In addition, laboratory experiments were also performed on an 11 ft long bridge deck model built inside the structures lab. Except for the length of the girder-deck model, the true scale was used for every other dimension. Three different tests were performed on the model, and the test data verified the analytical results. As anticipated, the concrete deck failed in punching shear, a brittle failure mode, at load levels an order of magnitude higher than the design values, proving the large safety margin built into the actual bridge currently being constructed. This behavior and failure mode was similar to a traditional steel-reinforced concrete bridge deck's behavior; and considering the fact that the GFRP strain levels at deck failure were only about 15% of ultimate values, the FRP reinforcement ratio used in this project could be reduced in future designs. Once completed, this bridge located in Macon County was instrumented and tested using two loaded tandem trucks, with satisfactory results confirming all major design assumptions.

For the durability testing, four different types of Glass Fiber Reinforced Polymer (GFRP) reinforcement provided by four separate rebar vendors were evaluated under exposure to an alkaline environment to simulate the naturally-occurring high pH solution of the concrete porewater at different temperatures. For the moisture tests, a total of 96 specimens were monitored for changes in length, diameter, and weight. A total of 128 unscathed samples (US), and 64 nicked (NK) samples simulating defects to the rebars that might occur on the field site, were tested in tension to determine the rate of degradation in terms of strength. Finally, 168 cylindrical-concrete pullout specimens at two different development lengths relative to the #3 rebar diameter (d_b) — 84 at $5d_b$ and 84 at $8d_b$ — were cast to gain an understanding of the magnitudes of stresses required to induce slippage. As anticipated, the tensile specimens experienced a decrease in strength and stiffness with increased duration and temperature; a similar observation was seen for the bond strengths of the pullout specimens. Of special noteworthiness was the large potential for moisture ingression that was observed within the reinforcement which, in turn, was found to result in sizable longitudinal and, even more pronounced, hoop strains. It must be stated, however, that this was the case for the bare rebars, and in order to fully qualify this assertion for embedded rebars within concrete structures having adequate cover, additional tests would have to be performed to ascertain differential strain readings. Overall, it was determined that GFRP rebars offer a good alternative to steel or Epoxy Coated Rebars (ECR) — both of which are prone to corrosion — as a means of internal reinforcement particularly for concrete structures in or near marine environments, or for bridge decks in cold regions for which de-icing agents are used.

Table of Contents

LIST OF TABLES

LIST OF FIGURES

1. Introduction

The North Carolina Department of Transportation (NCDOT) is currently investigating the structural stability and alkali durability of Glass Fiber Reinforced Polymer (GFRP) rebars. The present project has two main objectives, to experimentally and analytically investigate a bridge deck reinforced with glass fiber reinforced polymer rebars, and to perform durability tests on four rebar types.

A bridge in Macon County is currently being replaced by a bridge that will utilize GFRP rebars in the deck, instead of the more traditional epoxy coated steel rebars. The new bridge has two 50' exterior spans, and one 60' interior span. In this project the interior span of this bridge was investigated in more details (see Figure 1.1). The cross section of the bridge is composed by four AASHTO Type III prestressed girders and an 8" cast in place deck reinforced with GFRP rebars manufactured by Hughes Brothers (see Figure 1.2).

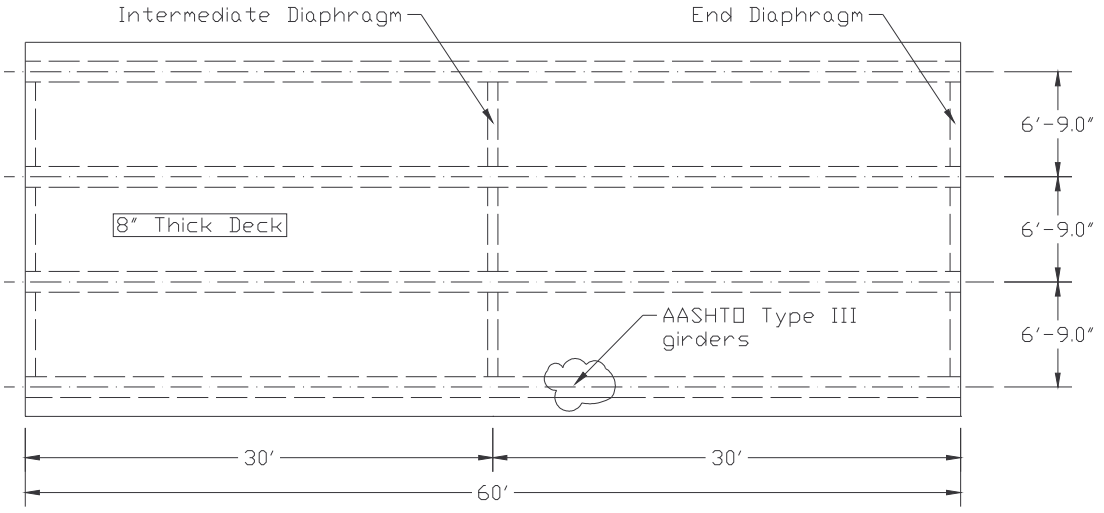

Figure 1.1 Plan View of Interior Span

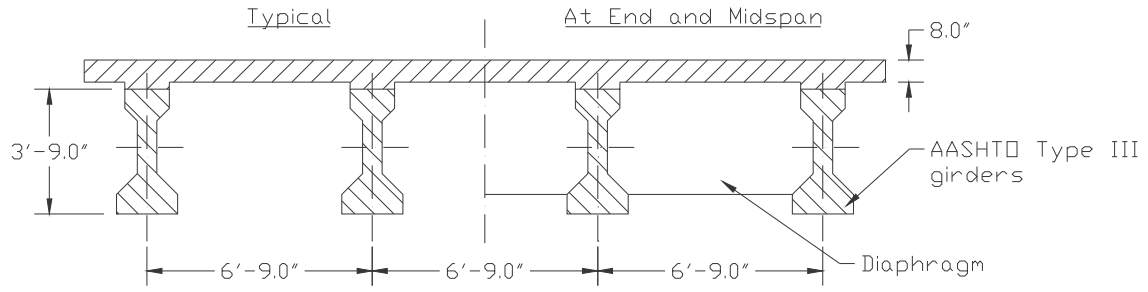

Figure 1.2 Cross Section of Bridge Deck

The experimental phase of this project includes large-scale laboratory tests, and in-situ static and dynamic tests of the actual bridge. In order to compare the results of Hassan and Rizkalla (2003) to the proposed experimental setup, a numerical comparison was done using the ANSYS (2002) advanced finite element computer program.

The purpose of the durability phase of this project is to determine the rate of absorption and any changes that may acquire while in the controlled alkali environment, the percentage decrease of the tensile strength of the rebar over a defined time period, and to determine the effects of the alkali environment has on the bond strength of the rebar to the concrete.

In the first few months of the projects, arrangements were made to receive the 100 gallon chambers that would be used to perform the durability testing on the absorption, tensile, and bond-slip specimens. At the same time, preparations were made with local GFRP manufactures to request the needed GFRP rebar. Starting in 2005, preparations were made for storage of the durability chambers, having them wired and working properly, filled with water, and has each chamber heated to their designated temperature.

At the same time, the chemical ratio was being figured through a recommended ratio from Dr. Indrajit Ray of the University of West Virginia (2005). Once the ratio was determine, it was then approved by Ray. After initial investigation, it was determine that the concrete mix design was inadequate, therefore was reduced in compressive strength. Small batches were conducted to determine an adequate mix design for the bond-slip

specimens. During the first part of March, the bond-slip specimens were prepared and poured over a period of four days. Once the specimens had been poured, the molds were properly removed and the specimens were placed in a curing chamber.

2. Literature Review

A review of the literature was conducted on bridge decks, GFRP rebars relative to optimal shapes, absorption on small specimens immersed in an alkali environment, tensile testing, and the gaging of bond-slip on various concrete strengths and rebar sizes.

2.1 Previous Research on Bridge Decks

Hassan and Rizkalla (2003) and (2004) found that the failure mode for continuous bridge deck slabs, having a span-to-depth ratio of 10 or less, is due to punching shear. Consequently, traditional design procedures using flexural theory will provide unnecessarily high levels of reinforcement. Also, the presence of transverse reinforcement in bridge deck slabs has a negligible effect on the punching shear capacity.

2.2 Finite Element GFRP Rebar Analysis

With the development of GFRP rebars as a substitute for steel, different manufacturers have engineered a variety of shapes and surfaces through the pultrusion process all of which are aimed at improving the bond surface. Methods include the double wrapping of a helical fiber around the rebar glass fiber core and sand-coating. Kadioglu and Pidaparti (2004) used finite element analysis to consider four different types of rebar configurations: standard circular cross-section, circular cross-section with helical wrapping/deformation on the surface, square cross-section, and circular rebar with square sections at mid-sides. The aforementioned rebars were investigated under axial, bending, and torsional loading. It was determined that a circular rebar with 6 square ribs with a 1° offset offered the best configuration under axial and torsional loads. The authors stated that more cases had to be considered to determine the optimal rebar. Due to availability of the rebar, the authors suggestion was not used during this investigation.

From Benmokrane et al. (1996), during the preliminary investigation on the effects of

deforming the rebars by sand coating on the bond strength, the authors determined that adding deformations such as surface coating of sand particles (similar to that of Sam Steere's CPPI – Pultrall) further enhanced the bond performance. The authors do note that reducing the deformation pitch yielded no further enhancement to the bond strength; however, the investigation did not address sand particle rebar, only uncoated GFRP rebar with ribs.

2.3 Previous Research on Absorption of GFRP Rebars

An experimental program was conducted by Tannous and Saadatmanesh (1999) on a series of shorter bar segments that were 4″ long. These segments were exposed to the following environments:

(1) water (H2O) at 77°F
(2) saturated Ca(OH)2 solution with pH of 12.0 at 77°F
(3) saturated Ca(OH)2 solution with pH of 12.0 at 140°F
(4) HCl solution with pH of 3.0 at 77°F
(5) NaCl 3.5% by weight solution at 77°F
(6) NaCl + CaCl2 (2:1) 7% by weight solution at 77°F (Scotwood Industries, 1992)
(7) NaCl + MgCl2 (2:1) 7% by weight solution at 77°F (Wendover 1992)
(8) ultraviolet radiation at the rate of 31.7 × 10-6 J/s/cm2 (2.04 × 10-4 J/s/in2)

Four different types of AR (alkali resistant) glass bars were tested: 10 mm (#3 Bar) AR glass/polyester (a.k.a. 10ARP), 10 mm AR glass/vinyl ester (a.k.a. 10ARV), 19.5 mm (#6 Bar) AR glass polyester (a.k.a. 20APR), and 19.5 mm AR glass/vinyl ester (a.k.a. 20ARV), where the number represents the bar diameter and the letter stands for the material properties. Under acidic and ultraviolet conditions, there were no significant or noticeable changes. For the bars immersed in pure water, the moisture content, Mm and diffusion coefficient, D, were higher for polyester rebars than for vinyl ester. For the alkaline environment at room temperature, Mm and D were lower for the vinyl ester bars, indicating that the vinyl ester bars were better coated than the polyester bars. At the

elevated temperature, Mm and D were both higher as expected. It was observed that the higher temperature alkaline specimens performed similarly to those in the room temperature alkaline environments.

The determination of the amount of absorption in the GFRP bars was also conducted during Vijay's Ph.D. dissertation (1999). The bar size was half the size (2″) of that used in the previous experiment. The bars were immersed in tap water, marine (salty) water, and alkaline environments at room temperature, freeze-thaw temperatures (12°F and 120°F), and an extra elevated temperature of 150°F (65.6°C). Changes in weights and dimensions were continuously monitored for 540 days, where readings were recorded every day during the first two weeks, and later once every two weeks. At 200 days, it was noticed that the alkaline immersion produced at least twice the moisture absorption by weight compared to the other conditions. It was determined that moisture absorption increased with temperature, with bars in the alkaline environment experiencing the maximum increase. On average, the alkaline conditioning produced two to three times the moisture content when compared to tap water and salt-water conditioning. Vijay also stated that the higher absorption of alkaline solution in relation to other solutions is an indication of the relative degradation in tensile strength of the GFRP bars, as anticipated in the accelerated aging tests.

2.4 Previous Research on Tensile Testing of GFRP Rebars

Benmokrane et al. (2001) researched the durability of various types of GFRP reinforcement, and considered the following: an effective loading system and evaluated the performance of the rebars due to different resins, fibers, surface coatings, and manufacturing techniques. From these properties, the researchers would identify the best combination to optimize the GFRP rebar in an alkaline environment. Three different rebars, two being sand-coated and the third having lubs or protrusions on its surface, were tested in three different environments: sodium hydroxide solution, simulated pore water, and humid concrete. The researchers concluded that a sodium solution was the most aggressive of the three and, consequently, the most efficient way to conduct durability

testing to examine the specimens embedded in concrete (2001). The researchers recommended that a GFRP rebar should consist of vinyl ester resin with surface coatings to improve the imperfections that result from the pultrusion process and to protect the rebar surface at the same time (2001). Overall, such GFRP rebars were found to be adequately durable in alkaline environments with stress levels corresponding to 24-30% of the ultimate strength.

Vijay (1999) conducted uniaxial tension tests using a loading apparatus similar to the one for this research work. Vijay also used schedule 80 steel pipes for the gripping mechanisms, where the GFRP tensile specimens were 48" (1220 mm), with a gage length of 36" (915 mm). Instrumentation that was used was strain gauges mounted at midspan. Two bars for each duration and environment condition were tested, where Vijay observed that the alkaline conditioning was more detrimental to the tensile strength of the GFRP bars versus the salt water solution. During testing, it was noted that the bars tested in the alkaline environments had "necking" failures, followed by the failure of the inner core of the bar. Vijay tested a sand coated rebar and a C-bar with no protective coating. The reduction in strength was 32.2% at room temperature over 15 months for the sand coated bars and 30% at room temperature over 30 months for the C-bar.

Cusson and Xi (2002) conducted an investigation of fiber-reinforced polymer reinforcement in low temperature environments for the Colorado Department of Transportation (CDOT). It should be noted that the tensile testing system used by the researchers is the same that was suggested via Hughes Bros. and was used during the current investigation for the NCDOT. Three manufactures and two different size bars were analyzed for this project. The bars were exposed to freeze-thaw cycling for 12-hour period, ranging in temperature from -20 ^{o}F to 68 ^{o}F (three hour freeze-thaw cycle). The researchers concluded that the degree of deterioration of the FRP bars depends on the temperature ranges and the number of freezing-thawing cycles applied (2002), where ~10% of the bars tensile strength was lost under the temperature conditions.

2.5 Previous Research on Bond of GFRP Rebars to Concrete

Malvar (1995) also tested four different types of GFRP bars in 3″ (76 mm) diameter, 4″ long concrete cylinders with silicone rubber spacers used to eliminate the bearing stresses of the concrete specimen during testing. The concrete mix proportions were 1:3.02:1.35:0.55 for cement, sand, ⅜″ (9.5 mm) gravel, and water, yielding a compressive strength of 4220 psi (29 MPa). Malvar found that small surface deformations – about 5.4% of the nominal rebar diameter – yielded a maximum bond stress of up to five times the concrete tensile strength, similar to that as observed with the steel reinforcing bars; however, it was suggested that the rebar deformations should not be glued to the surface, but be developed during the pultrusion process since the deformations could fail during loading. The bond strength of the GFRP bars was 1.2 to 1.5 times smaller than those of the steel bars, along with larger variations found in the indentation depths which caused larger variations in the bond strength. It was also noted that the bond strength could be increased by increasing the confining pressure around the specimen.

Muruts and Nad (1998) conducted pullout tests on rectangular GFRP bars at four different embedment lengths of 5.75″, 7.625″, 9.75″, and 11.625″ (145 mm, 195 mm, 245 mm, and 295 mm) using 6″ (150 mm) ×12″ (304.8 mm) concrete cylinders. During testing, it was concluded that the controlling factor in terms of the bond strength appeared to be the resin type rather than the fiber type. Also, it appeared that the tests with the smaller development lengths showed adequate bond strengths whereas the longer embedment length specimens attained ultimate tensile strength levels, as expected.

Vijay (1999) conducted two types of pullout tests (similar to what was conducted in this research): the general ACI pullout tests and pullout tests of bundled bars. The cylinders that were used for the pullout tests were 6" × 12" (152.4 mm × 304.8 mm) with a development length of 3.5" (88.9 mm). Vijay only considered tap water, salt water (3% NaCl), and freeze-thaw conditions – no alkaline environment was investigated. For the sand coated bars, the bond stress was found to be 2026 psi (14 MPa) with an increase in bond strength of 14% for bars under tap water at freeze-thaw conditions and a loss of

5.3% for bars exposed to salt water at room temperature, both for a duration of 15 months. During the analysis of bond-stress versus slippage of the bar, Vijay compared the relationship of GFRP bars and concrete to have a comparable or better slip modulus to those of steel and concrete, and found that the GFRP bars exhibited superior bond properties over steel (C-bar and sand coated bar being 33.5% and 55.5% higher, respectively, over that of steel). For the bundled bar investigation, a two bar-bundle, a three bar-bundle, and a four bar-bundle were fastened to the extended bar with a bond length of 2.5" (63.5 mm) embedded within the concrete. Vijay concluded that a perimeter of a single bar with an equivalent area could be used for calculating the bond strength, which was found to be proportional to the perimeter of the bundled bars (1999).

3. ANSYS Finite Element Model Calibration

The ANACAP software (an extension of the ABAQUS advanced finite element computer program) was used in a previous study by Hassan and Rizkalla (2003) to model a GFRP reinforced bridge deck, utilizing the software's advanced nonlinear capabilities to model complex behavior of reinforced concrete. In their analysis, only one quarter of the 60' bridge span was considered due to symmetry planes in both principal directions (see Figure 3.1).

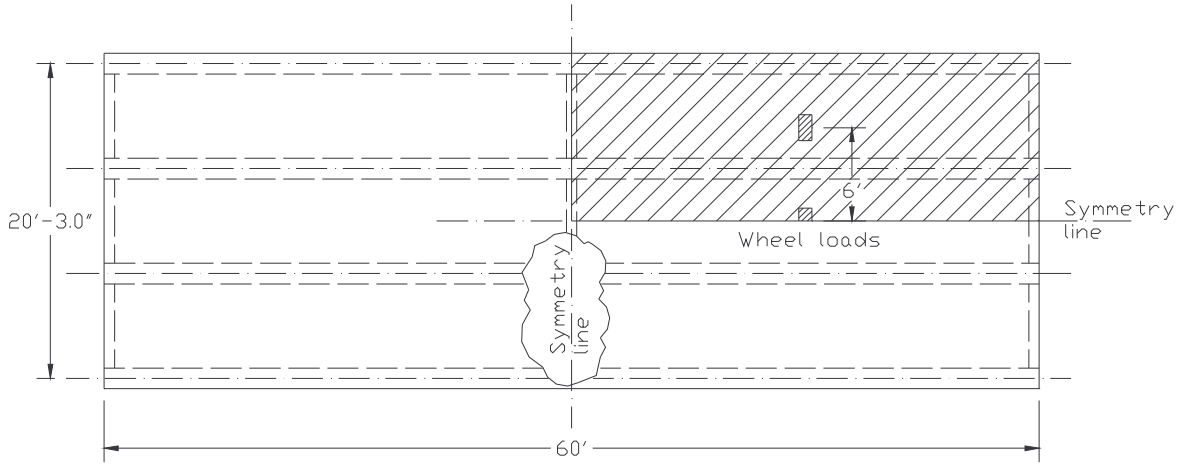

Figure 3.1 Quarter of Bridge Span Modeled

3.1 ANSYS Finite Element Model – Actual Bridge Span

At UNC Charlotte a similar numerical model was developed using the ANSYS finite element software. In order to validate this numerical model, similar assumptions were made to the Hassan and Rizkalla (2003) model. They were as follows:

- One quarter of the bridge span was modeled due to the existing 2 symmetry planes.
- Adjust the size of the finite elements to provide a fine mesh in the most affected areas, and to reduce the analysis execution time.
- An equivalent cross-section was used for the girders, resulting in simpler sections with similar moment of inertia and area as the actual AASHTO Type III girders.

- Use two wheel loads representing an axle of a design truck applied 15' from the girder supports.
- The transverse spacing between the wheel loads was 6', as specified in the AASHTO Standard Specifications for Highway Bridges (1998).
- Each wheel load was applied as point loads applied in the nodes of a 10" × 20" contact surface area.

The finite element model analyzed with the ANSYS software is presented in the Figure 3.2, and the batch input file is enclosed in the Appendix A.

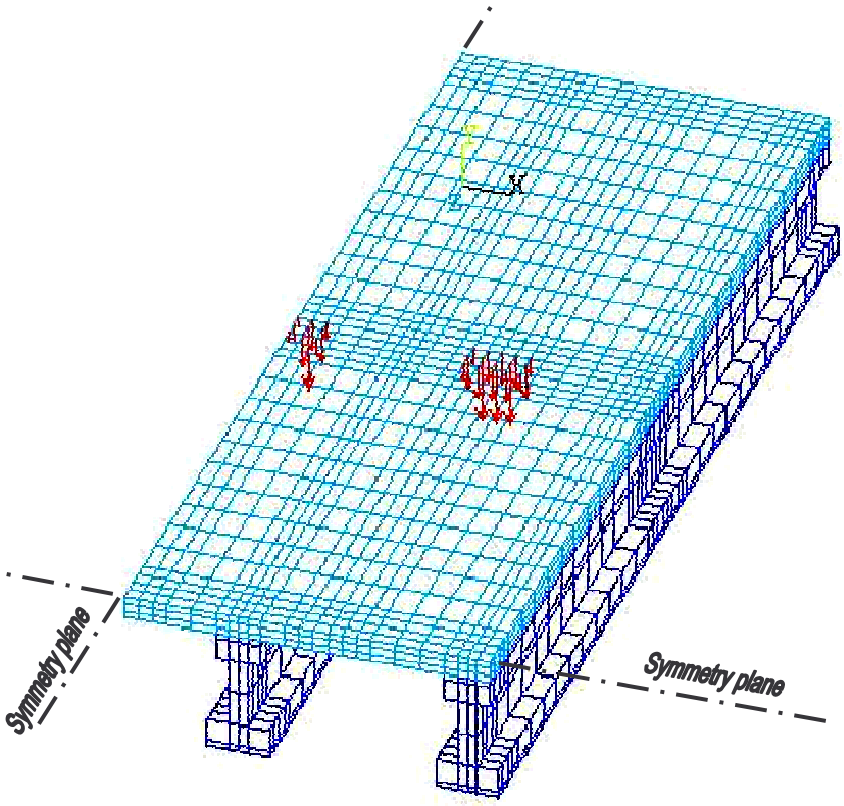

Figure 3.2 ANSYS Finite Element Model

Two element types were used in the numerical model, the SOLID65 for the concrete elements, and the LINK8 for the prestressing strands. The SOLID65 element includes the GFRP rebars in the form of smeared reinforcement. SOLID65 is used for the 3-D modeling of solids with or without reinforcing bars (rebar). This solid is capable of cracking in tension and crushing in compression. In concrete applications, for example,

the solid capability of the element may be used to model the concrete while the rebar capability is available for modeling reinforcement behavior. The element is defined by eight nodes having three degrees of freedom at each node: translations in the nodal x, y, and z directions. Up to three different rebar specifications could be defined.

The most important aspect of this element is the treatment of nonlinear material properties. The concrete is capable of cracking (in three orthogonal directions), crushing, plastic deformation, and creep. The rebars on the other hand, are subjected to tension and compression, but not shear. As it was mentioned, the girders were modeled using a simplified cross-section. The 8" concrete deck-slab was divided into three layers. The smeared GFRP rebars were considered in the top and bottom layers of the deck slab with a 1.25" cover (see Figure 3.2).

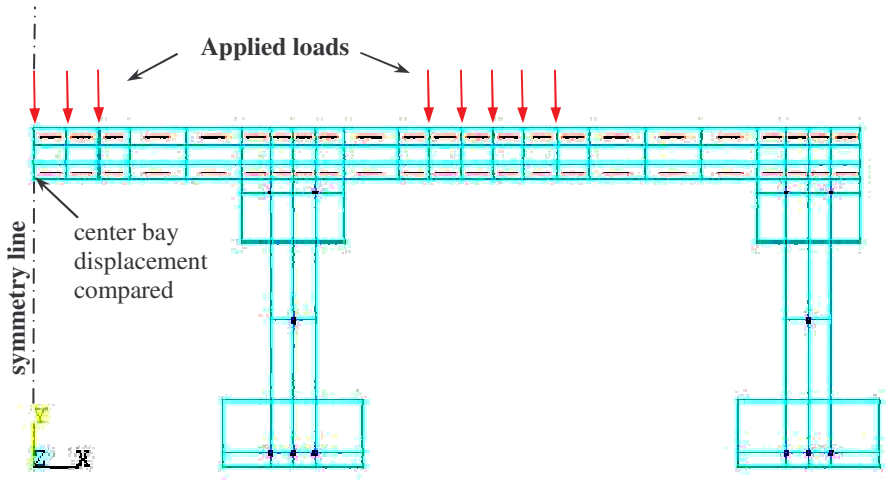

Figure 3.3 Smeared GFRP Reinforcement and Equivalent Prestressing Tendons

The prestressing strands were included using the LINK8 element, applied at the intersection nodes of the SOLID65 elements. LINK8 is a spar which may be used in a variety of engineering applications. This element can be used to model trusses, sagging cables, links, springs, etc. The 3-D spar element is a uniaxial tension-compression element with three degrees of freedom at each node: translations in the nodal x, y, and z directions. As in any pin-connected structural element, no bending was considered. Plasticity, creep, stress stiffening, and large deflection capabilities were included.

The prestressing effect was applied through an initial strain, an option offered by this element. As a result of an initial parametric investigation, it was found that the maximum initial strain numerically possible was 0.0045 in/in, instead of the 0.0052 in/in considered by Hassan and Rizkalla (2004).

For the behavior of the concrete elements, the material characteristics predefined in the "Concrete Non-Metal Plasticity" model were used to generate a multilinear isotropic model (MISO). The MISO curve was generated as is presented in Kachlakev et al. (2001). The modulus of elasticity E and the tensile strength f_r were derived from the nominal value of the ultimate compressive strength f'_c. During the analysis, same convergence problem was faced due to low shear transfer coefficient β_t. After a few preliminary analyses, a 0.25 value was considered to be used in further investigations. This value is similar to other researchers' findings. See Table 3.1 for a comparison of the material characteristics for the two concrete structural members used in the analyses. For the reinforcements (GFRP and prestressing tendons), a perfectly elasto-plastic bilinear isotropic (BISO) model was considered, as presented in Table 3.2.

Table 3.1 Concrete Properties

Material property	Deck	Girder
Modulus of elasticity E [ksi]	3,370	4,030
Compressive strength f'_c [psi]	3,500	5,000
Tensile (rupture) strength f_r [psi]	444	530
Shear transfer coefficient β_t	0.25	0.25
Poisson's ratio ν	0.2	0.2

Table 3.2. Reinforcing Material Properties

Material Property	Smeared GFRP rods	Steel Prestressing tendons
Modulus of elasticity E [ksi]	5900	29000
Ultimate tensile strength F_u [ksi]	72	270
Poisson's ratio ν	0.3	0.3

3.2 ANACAP and ANSYS Results Comparison

For a direct comparison of the two numerical investigations performed at NCSU and UNCC, the net slab deformation of the middle bay under the wheel load was considered (see Figure 3.4). As it can be seen, the two models yielded close to identical results, giving confidence in future analyses using the ANSYS model.

Hassan and Rizkalla (2004) terminated the numerical analysis when the punching shear failure criterion developed by Kinnunen and Nylander (1960) was satisfied. Based on this, the punching load is determined when the circumferential compressive strain of the concrete reaches a critical value of 0.0019 in/in at a distance of B/2+y from the loaded area (see Figures 3.5 and 3.6); where B is the diameter of the idealized load area, and y is the location of centre of rotation of concrete wedges causing punching failure, which can be approximated by 0.1d, where d is the thickness of slab.

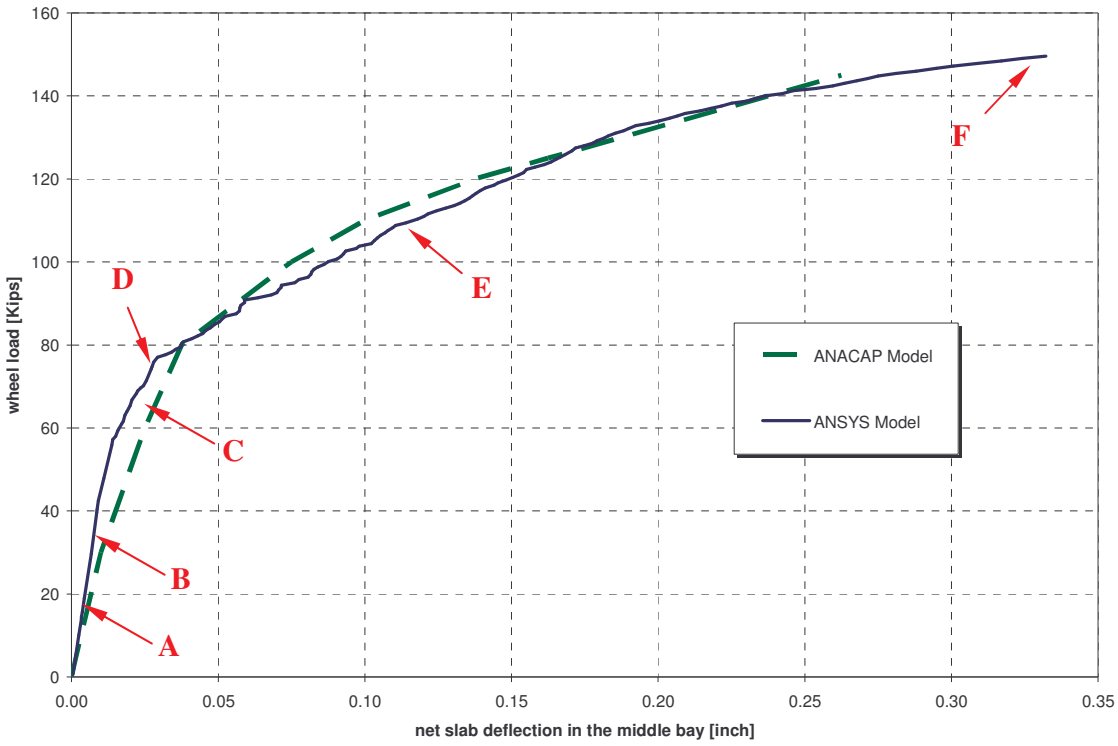

Figure 3.4 Comparison of ANACAP and ANSYS Numerical Results

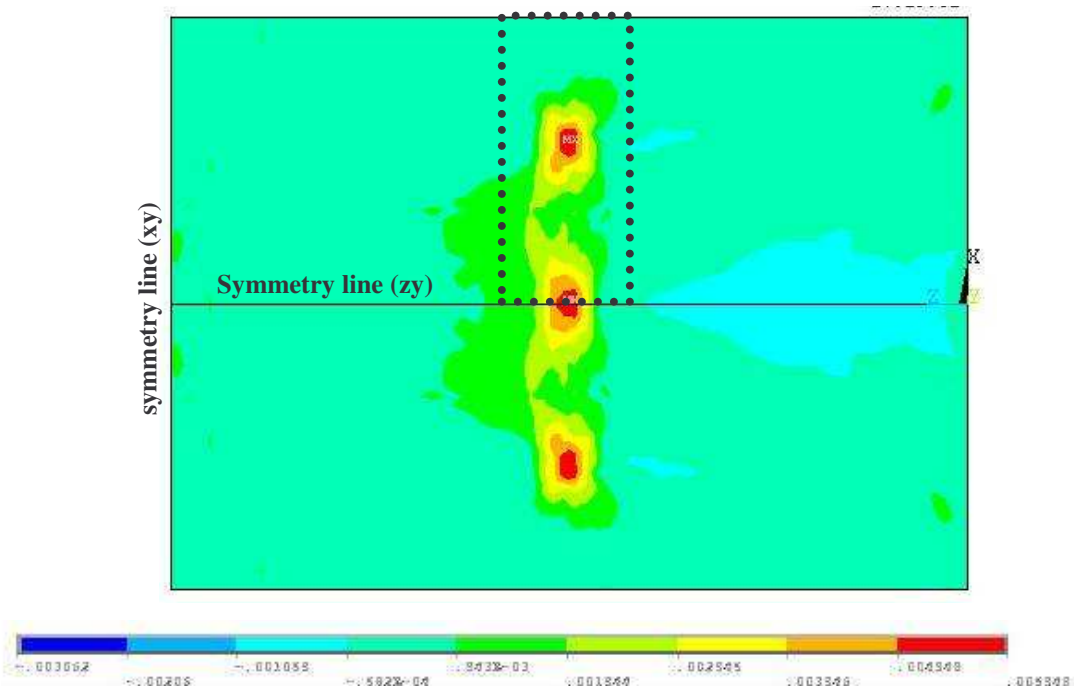

Figure 3.5 Bridge Deck FE Contour Plot

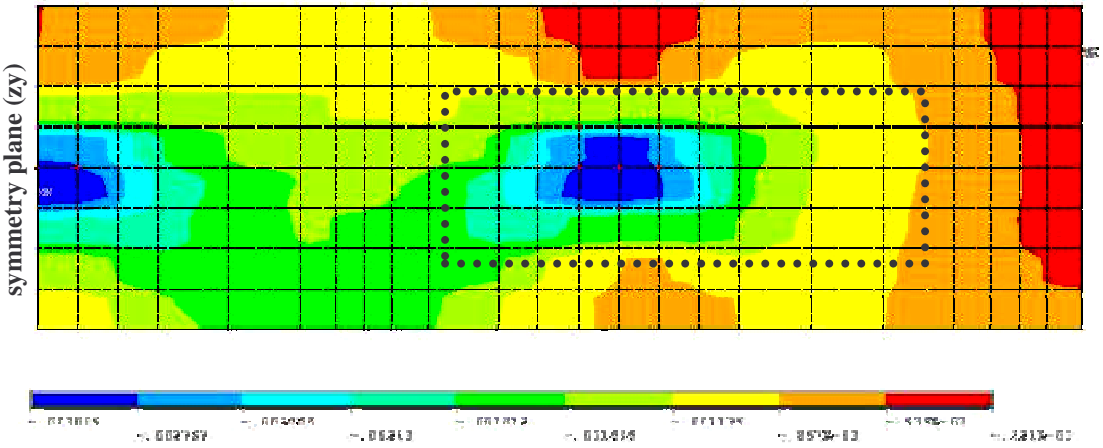

Figure 3.6 Isolated Area in Figure 3.5, Enlarged and Rotated 90° CW

From Figure 3.7 it can be seen that the compressive strain values at the theoretical punching circumference are close to the value of 0.0019 in/in as recommended by Kinnunen and Nylander (1960).

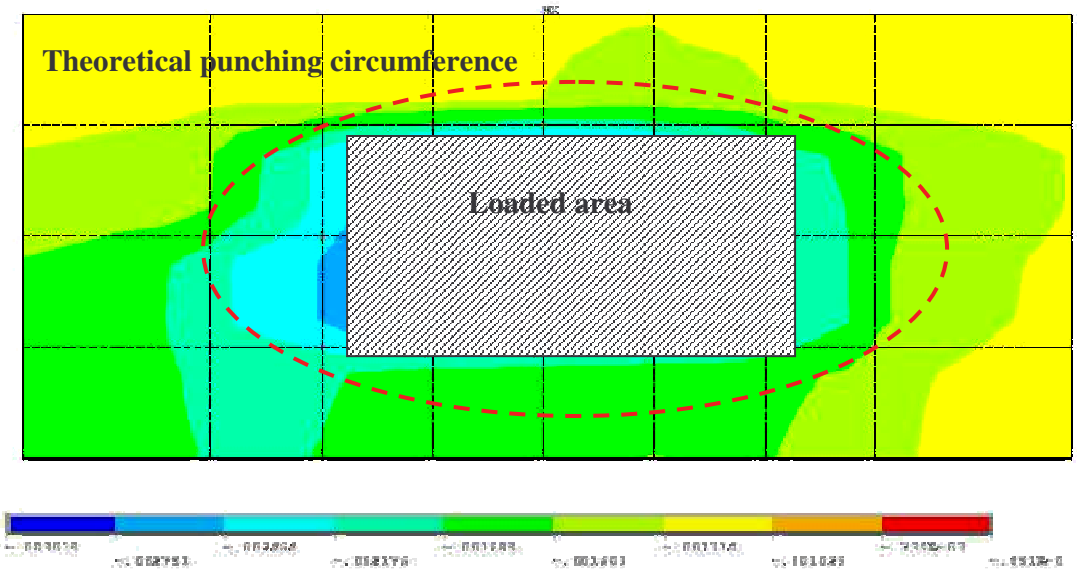

Figure 3.7 Compression Strain Around Loaded Area

The results of the two numerical investigations are slightly different, however, considering the magnitude of this difference, it can be concluded that the ANSYS model gave very similar results as the ANACAP model. Later, this numerical model was compared to the laboratory tests with satisfactory results.

3.3. Numerical Results Discussion

The following few figures are presented in order to illustrate the deformed shape of the structure and the cracking sequence under wheel loading. In Figures 3.8 and 3.9 the undeformed shape is represented by the dashed lines. In Figures 3.10 through 3.15 the cracking sequence is illustrated for the points A through F located on the load-displacement curve given in Figure 3.4.

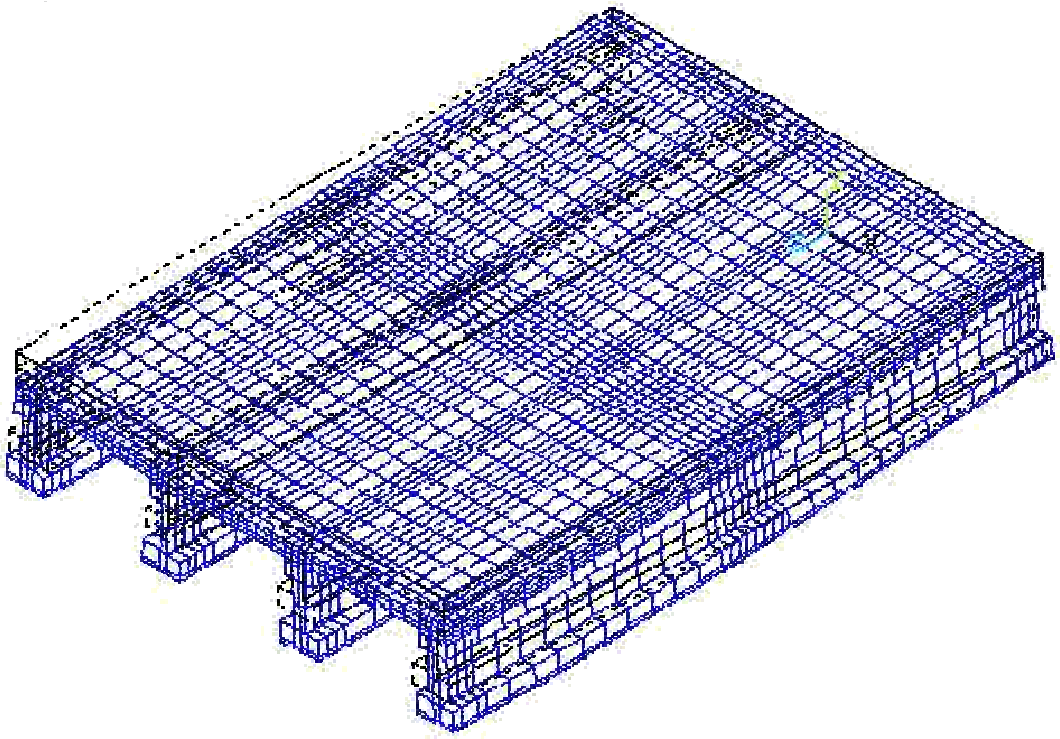

Figure 3.8 General View of the Deformed Shape (Half of the Bridge)

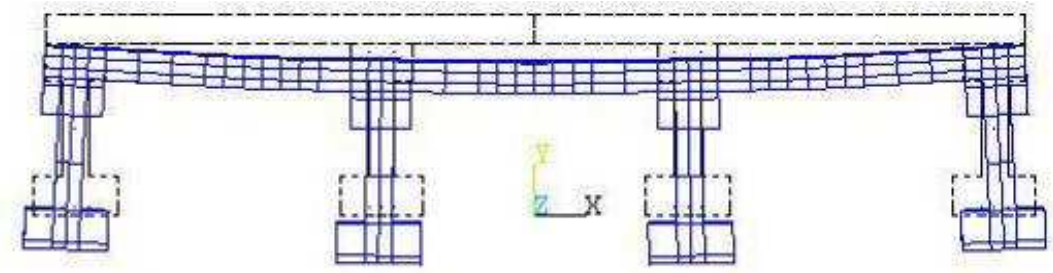

Figure 3.9 Transverse View of the Deformed Shape

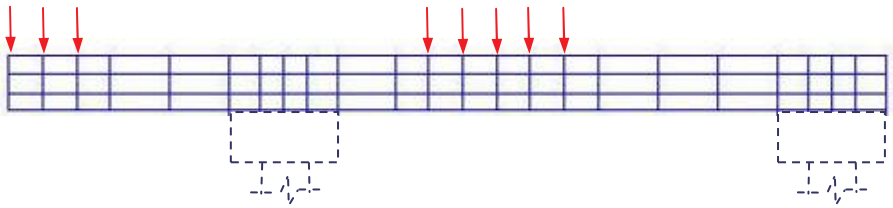

Figure 3.10 Crack Propagation at Point A (at 25 Kips Vertical Load)

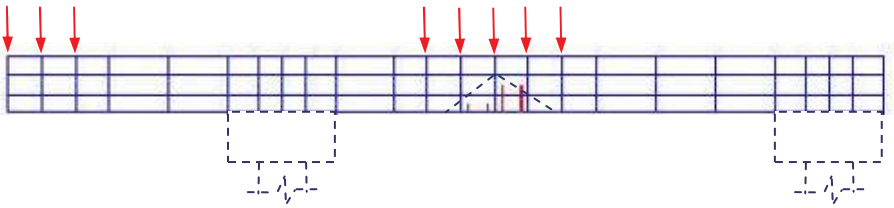

Figure 3.11 Crack Propagation at Point B (at 40 Kips Vertical Load)

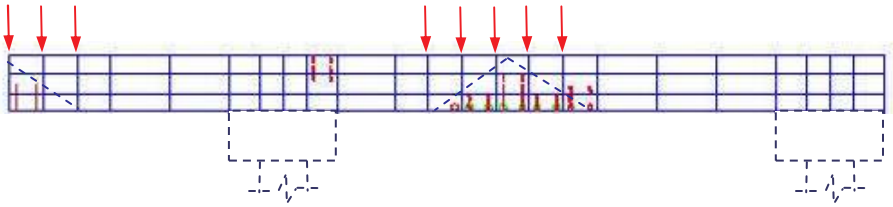

Figure 3.12 Crack Propagation at Point C (at 76 Kips Vertical Load)

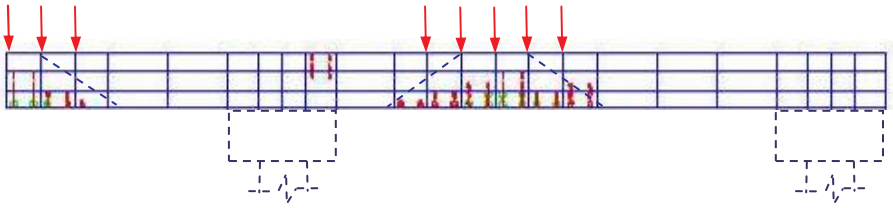

Figure 3.13 Crack Propagation at Point D (at 79 Kips Vertical Load)

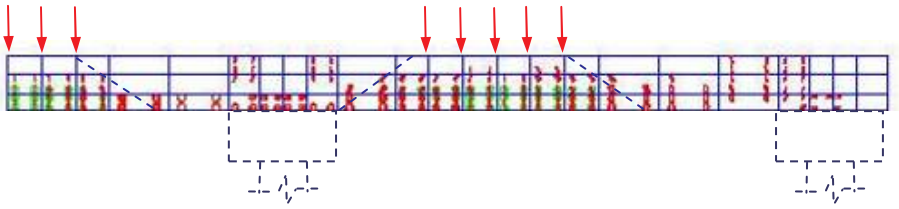

Figure 3.14 Crack Propagation at Point E (at 109 Kips Vertical Load)

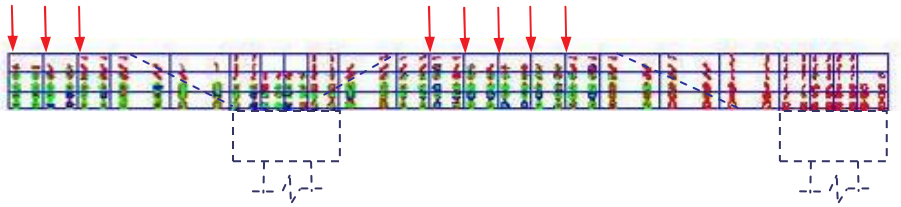

Figure 3.15 Crack Propagation at Point F (at ultimate load)

These figures clearly show the progressive crack development throughout the bridge cross section up to failure. Also, the diagonal cracks in the deck illustrate the punching shear plane developed under the simulated wheel load.

3.4 Prestressed Girder Model Calibration

In order to verify the ANSYS finite element model for the girder, and the actual behavior of the 11 ft prestressed girder used in the lab experiment, a three point loading test was done on one of the prestressed girders. Strain transducers and displacement transducers were attached to the girder to record the strain level at the top and bottom flange, and the overall deformation of the girder. See Figure 3.16 for loading setup.

Figure 3.16 Prestressed Girder Testing

A comparison of the average mid-span deformation from the test and ANSYS model is presented in Figure 3.17. As it can be seen, the two curves show a comparable flexural stiffness, except for the 40-80 Kips load range. For some reason, the analytical model indicates stiffening in this load range. Outside this range however, the two results are almost identical.

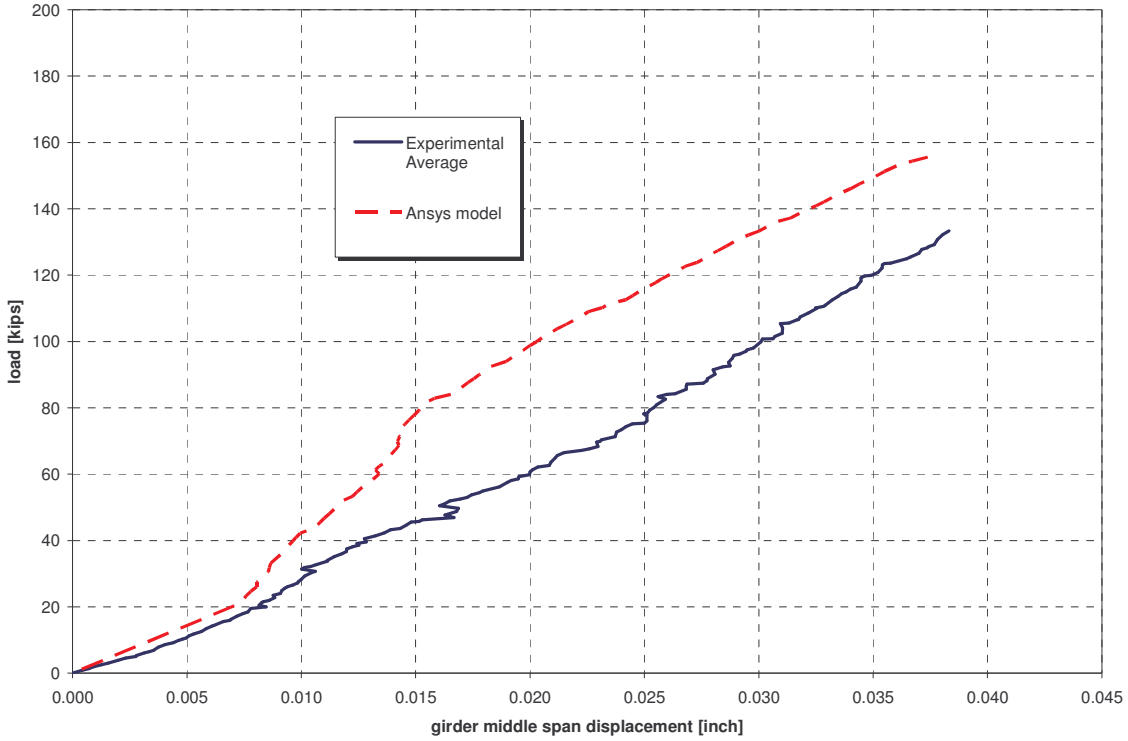

Figure 3.17 Prestressed Girder Behavior: FE Model vs. Experiment

3.5 ANSYS Finite Element Model

Based on the FE model validated through the ANACAP results, and the girder experimental data, an analytical study was done for the experimental model prior to the laboratory tests. The construction details of the lab model are presented later in this report. The actual concrete properties for deck and girder used are presented in Table 3.3. For the reinforcement mechanical properties see Table 3.2.

Table 3.3 Actual Concrete Properties

Material Property	Deck	Girder
Modulus of elasticity E [ksi]	4,680	4,700
Compressive strength f'_c [psi]	6,760	7,600*
Tensile (rupture) strength f_r [psi]	450	634

* Information supplied by the prestressed girder manufacturer

3.6 Laboratory Model - Numerical Results

Figures 3.18 through 3.22 show some of the analytical results of the lab model. These analyses were performed in order to predict the behavior of the lab model, and to estimate the failure load for the load testing setup TEST 1 (more details on the loading setups are presented later).

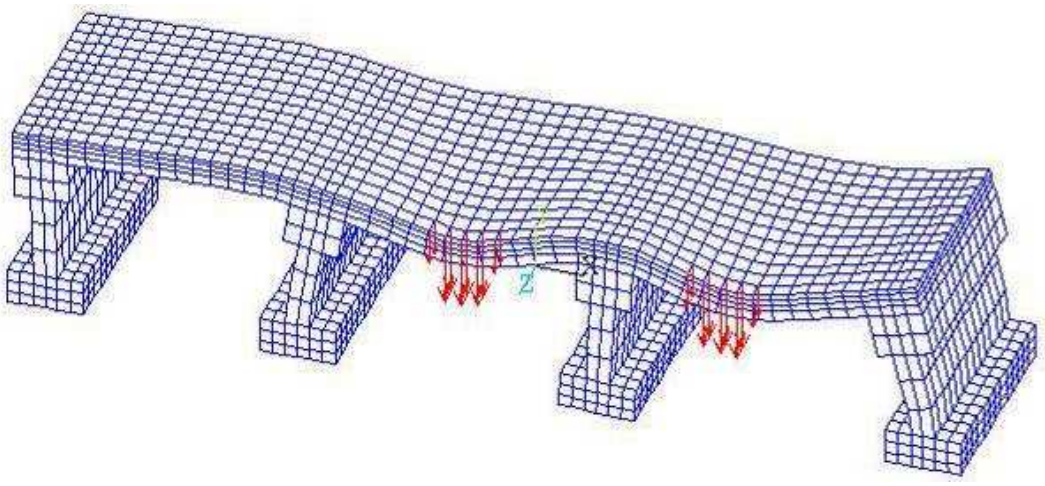

Figure 3.18 General View of the Deformed Shape (Half of the Lab Model)

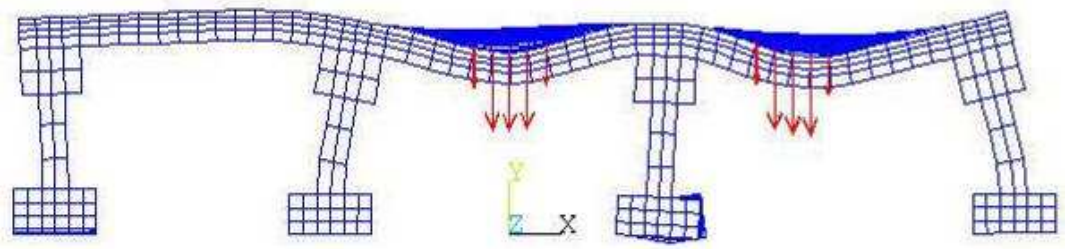

Figure 3.19 Transverse View of the Deformed Lab Model

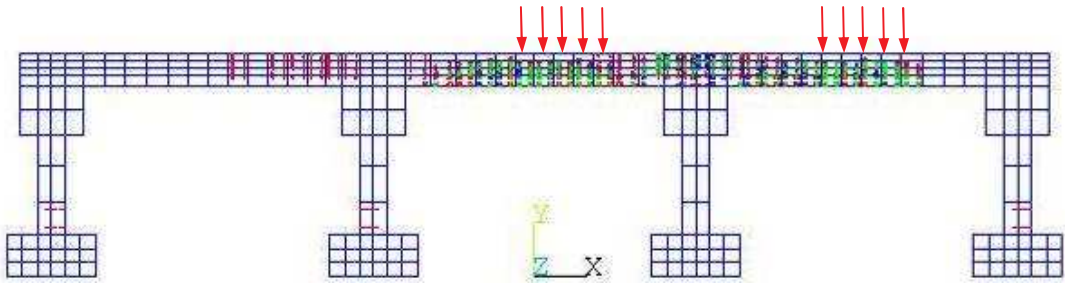

Figure 3.20 Cracking Pattern at Ultimate Load

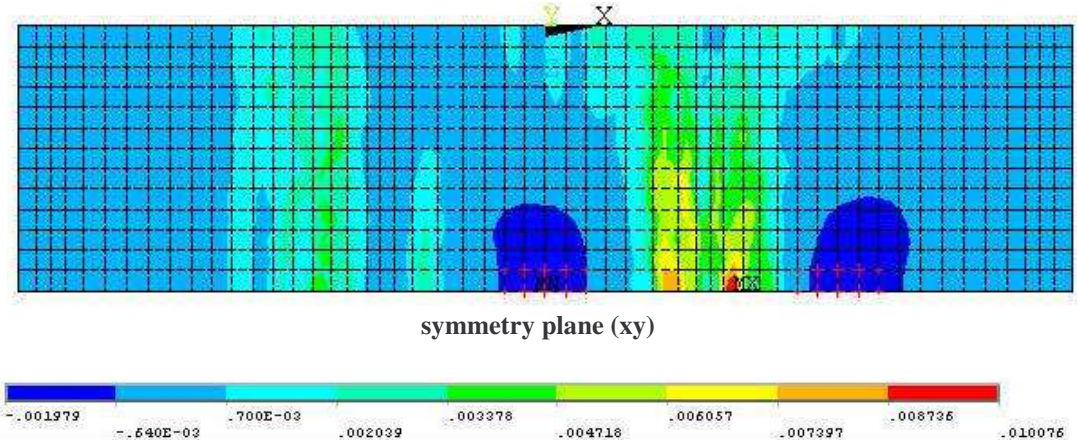

Figure 3.21 Strain Distribution – Deck Top Surface

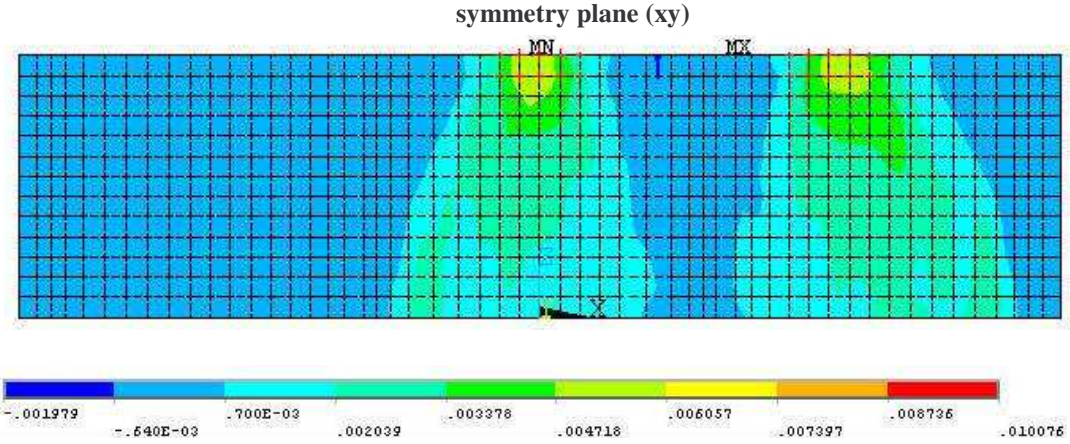

Figure 3.22 Strain Distribution – Deck Bottom Surface

The predicted ultimate load was 183 Kips at each wheel location. This force was used to design/check the load frame and the individual load setup components. In Figure 3.23 the load-displacement curves, resulted from the numerical analysis, are presented for Bays 1 and 2.

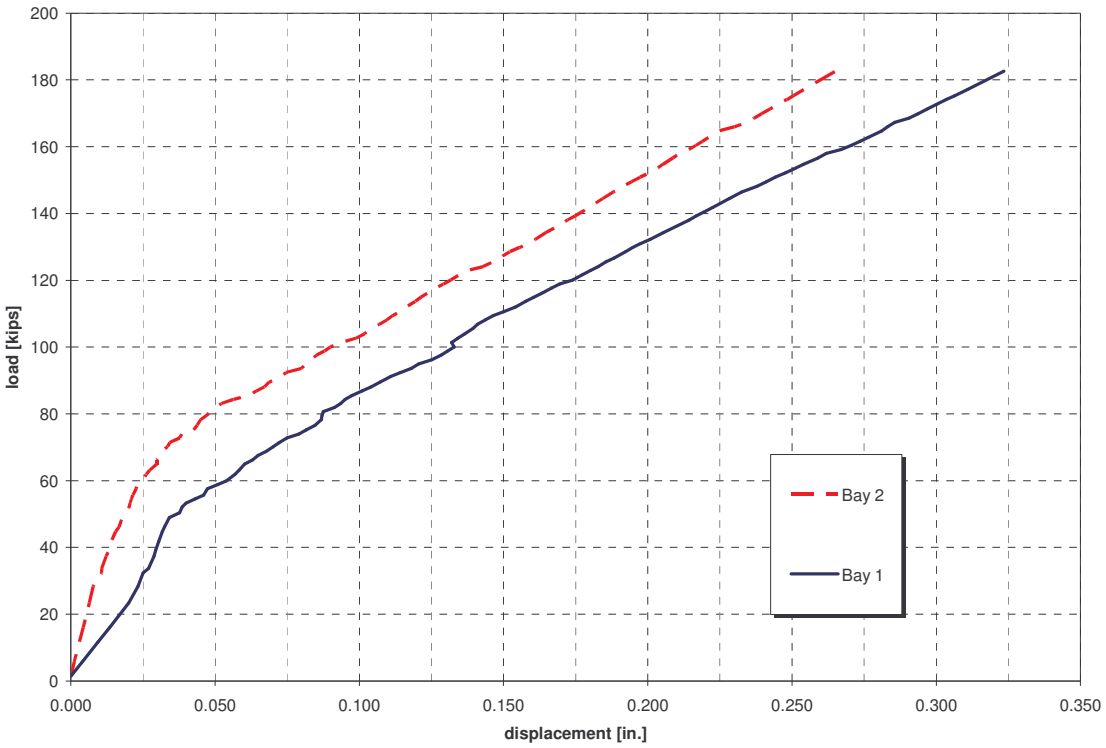

Figure 3.23 Lab Model Load-displacement Curves

3.7 Numerical Results versus Design Specifications

In the AASHTO Standard Specifications for Highway Bridges (1998) the ultimate capacity of a slab loaded with a concentrated load is assumed to be governed by punching shear at 0.5d from the load's footprint. The shear strength V_n can not be taken larger then V_c, defined in Eq. 8-58 as:

$$V_c = \left(2 + \frac{4}{\beta_c}\right)\sqrt{f_c'}\,b_o d \;\le 4\sqrt{f_c'}\,b_0 d$$

where: β_c = is the ratio of long side to short side of concentrated load or reaction area

f'_c = is the specified compressive strength of concrete (psi)

b_o = is the perimeter of the critical section (in)

d = is the distance from extreme compression fiber to centroid of tension reinforcement (in)

For the project dimensions and material properties, the shear capacity is:

$$V_c = \left(2 + \frac{4}{2}\right)\sqrt{6760}(86.25)6.56 = 186149.5\,\text{lbs} = 186.2\ \text{Kips}$$

The AASHTO LRFD Bridge Design Specifications (2004) uses a slightly different approach, and the nominal shear resistance V_n is defined in Eq. 5.13.3.6.3-1 as:

$$V_n = \left(0.063 + \frac{0.126}{\beta_c}\right)\sqrt{f_c'}\,b_o d_v \;\le\; 0.126\sqrt{f_c'}\,b_o d_v$$

where: β_c = is the ratio of long side to short side rectangle through which the concentrated load or reaction force is transformed

f'_c = is the specified compressive strength of concrete (ksi)

b_o = is the perimeter of the critical section (in)

d_v = is the effective shear depth taken as the distance measured perpendicular to the neutral axis, between the resultants of the tensile and compressive forces due to flexure; it need not be taken to be less the greater of 0.9d or 0.72h (in)

$$d_v = d - \frac{a}{2} \;=\; 6.56 - \frac{1.25}{2} = 5.94\ in \begin{cases} > 0.9(6.56) \;=\; 5.91\ in \\ > 0.72(8.0) \;=\; 5.76\ in \end{cases}$$

For this project, the shear capacity is calculated as:

$$V_n = \left(0.063 + \frac{0.126}{2}\right)\sqrt{6.76}(83.74)5.94 = 162.9 \ \ Kips$$

As it can be seen, there is a 14% difference between the two design provisions. The numerical result was closer to the calculations using the AASHTO Standard Specifications for Highway Bridges (1998).

4. Laboratory and Field Tests

4.1 Laboratory Test Setup and Instrumentation

In order to verify the predicted behavior of the bridge, an experimental model was built and tested in the Structures Lab of the University of North Carolina at Charlotte. The lab specimen was built based on the actual bridge's design. The cross sectional dimensions are presented in the Figure 4.1. The length of the specimen was 10'-10". The prestressed girders were AASHTO Type III.

In order to fully utilize the lab specimen, Bay 3 was built with Stay in Place (SIP) metal form for the concrete deck. The actual bridge will have these SIP forms, but in order to have the same conditions as in the numerical investigation, Bays 1 and 2 had no SIP forms.

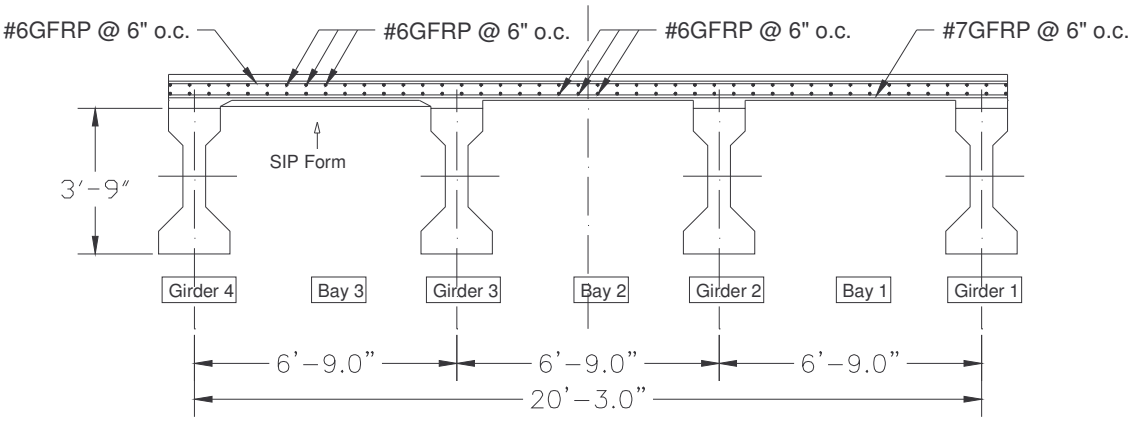

Figure 4.1 Experimental Model Details

The concrete for the deck was Class AA, as it was assigned in the project specifications in Concrete Mix Design Proportions No. 842VF7604E. The compressive strength and the splitting tensile strength were determined according to ASTM C39/C 39M and ASTM C 496. The resulted 28 days compressive strength was f'_c = 6760 psi, and the splitting tensile strength was f_r = 450 psi.

The ASLAN 100 #6 and #7 GFRP rebars were purchased from Hughes Brothers Inc. Details of the deck reinforcement, concrete cover and built-up over the prestressed concrete girder are presented in Figure 4.2.

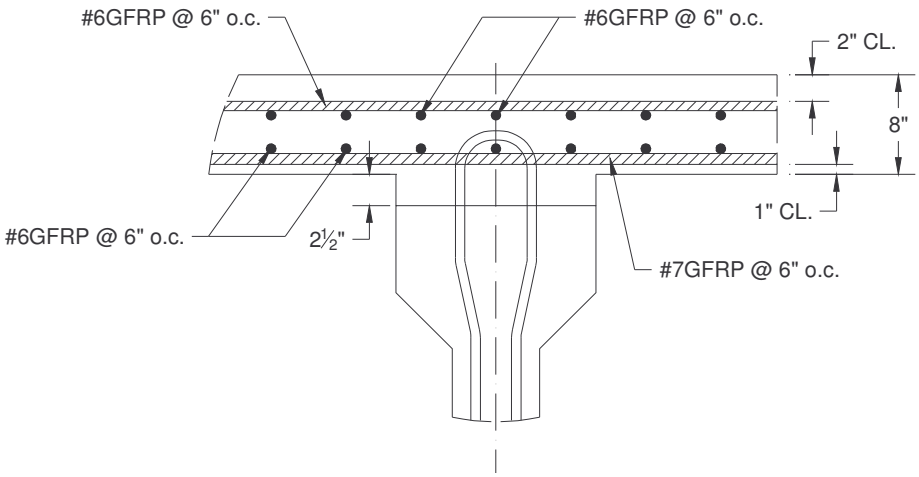

Figure 4.2 Reinforcement Details for the Concrete Deck

The removable formwork was constructed of plywood and dimension lumber. The plywood forms were supported on the floor by 4"x6' timber posts (Figures 4.3 and 4.4). In the bottom reinforcing layer the transverse reinforcement was laid on plastic spacer chairs and tied using nylon zip ties (See Figure 4.5). The longitudinal rebars were laid on the transversal rebars and tied together. For the top layer, the longitudinal bars were placed first and the transverse rebars second. After positioning the transverse rebars on high plastic chairs as presented in Figure 4.6, the longitudinal and transverse rebars were tied together. The plastic rebar chairs and plastic ties were used according to the GFRP rebar manufacturer's requirements. Also, the two reinforcement layers were adequately secured to the formwork, in order to avoid their floating to the top surface of the fresh concrete.

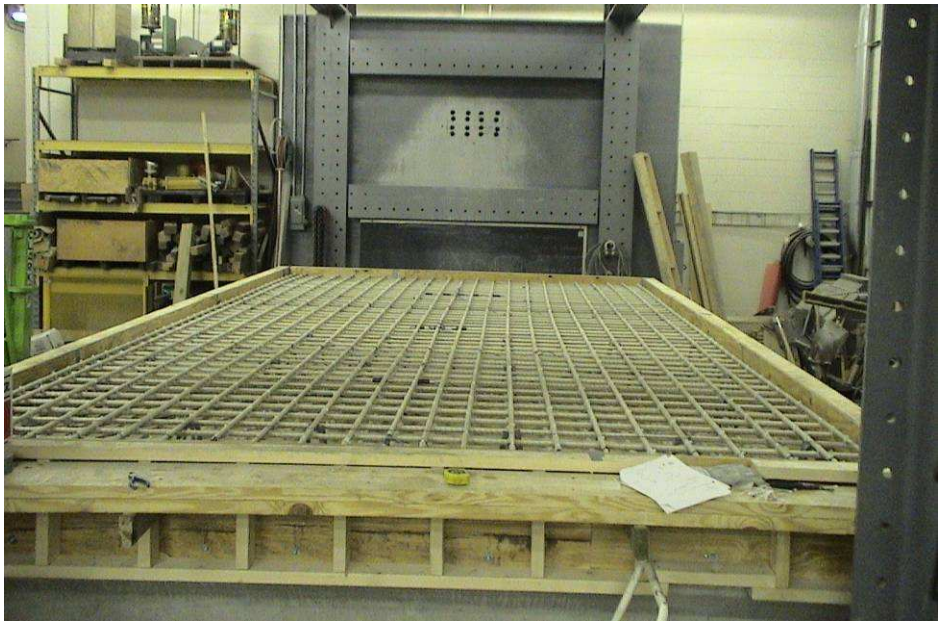

Figure 4.3 Reinforcement Details of Laboratory Model

Figure 4.4 Formwork Details of Laboratory Model

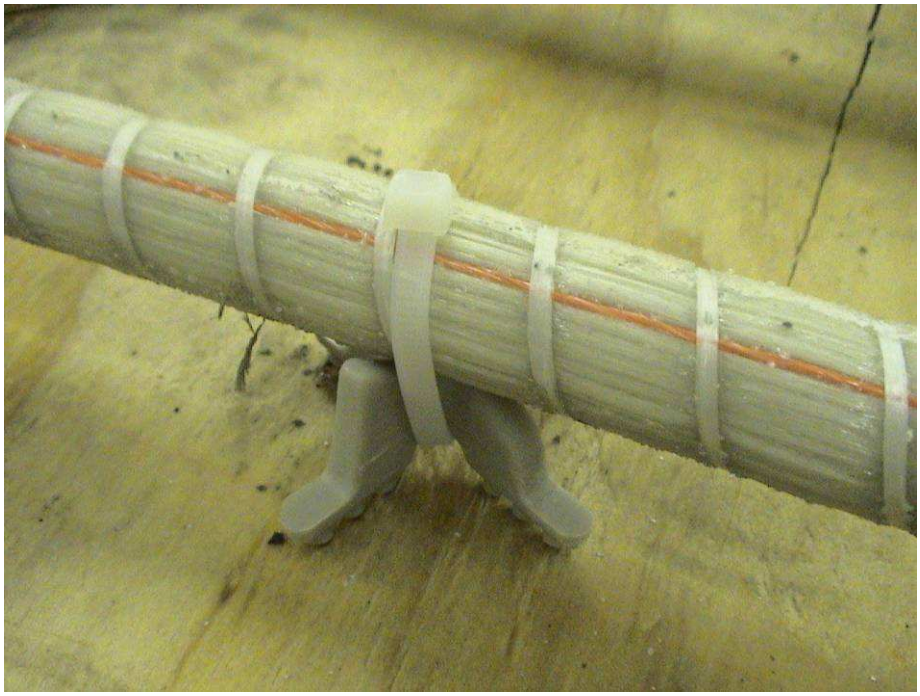

Figure 4.5 Bottom Reinforcement Layer on Plastic Chair

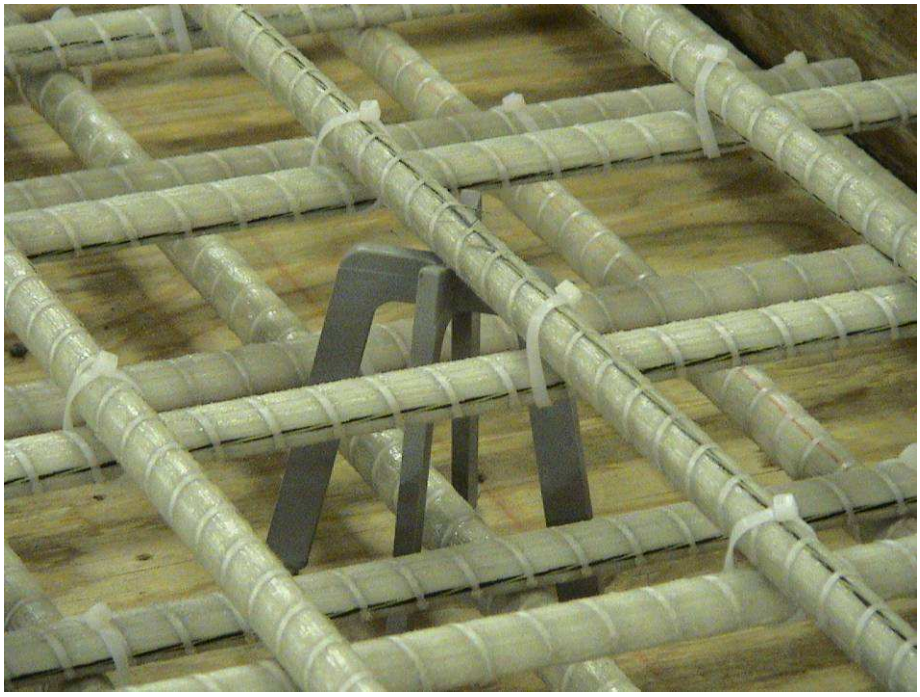

Figure 4.6 Top Reinforcement Layer on Plastic Chair

The concrete was placed using a ¾ cubic yard concrete bucket that was moved with the loading fame's overhead crane. During placement, the concrete was properly vibrated.

The approximate amount of concrete used was 6½ cubic yards. From this concrete batch, 4"x 8" cylinders were collected to later determine the compressive and tensile strengths. After finishing the surface, the deck was covered with plastic sheeting, and regularly sprayed with water. The lateral formwork was removed after 2 days, then the bottom forms at 8 days.

Figure 4.7 Concrete Placement for the Laboratory Deck Model

The Type III prestressed girders didn't satisfy the minimal shear reinforcement requirements for the girder ends. This, in addition by the short girder length (10'-10"), resulted in small cracks forming on the bottom part of the web (See Figure 4.8) after prestress release. A calculation based on AASHTO Standard Specifications for Highway Bridges (1998) proved the presence and extent of the cracks. In order to compensate for the required shear reinforcement, and to avoid a possible horizontal shear surface development, the girder ends were strengthened using carbon fiber reinforced polymer (CFRP) laminates (see Figure 4.9). Also, Figure 4.10 shows details of the strengthened girder-ends.

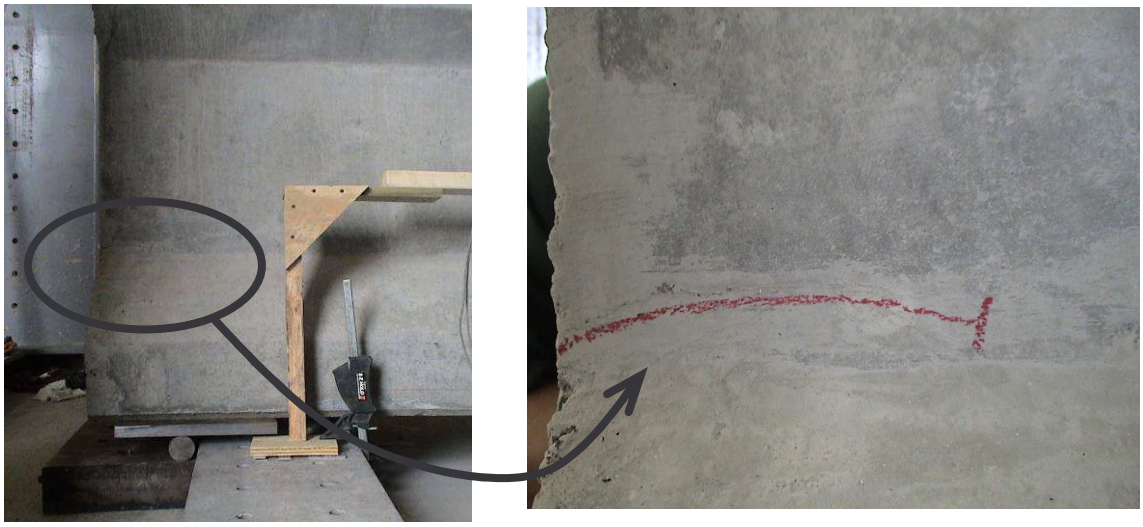

Figure 4.8 Initial Cracking in the Web of the Girder Ends

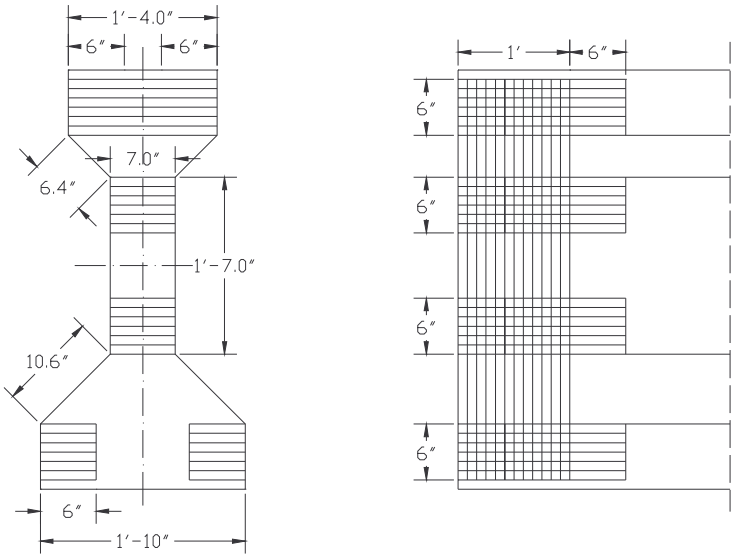

Figure 4.9 Carbon Fiber Reinforced Polymer (CFRP) Laminate Design

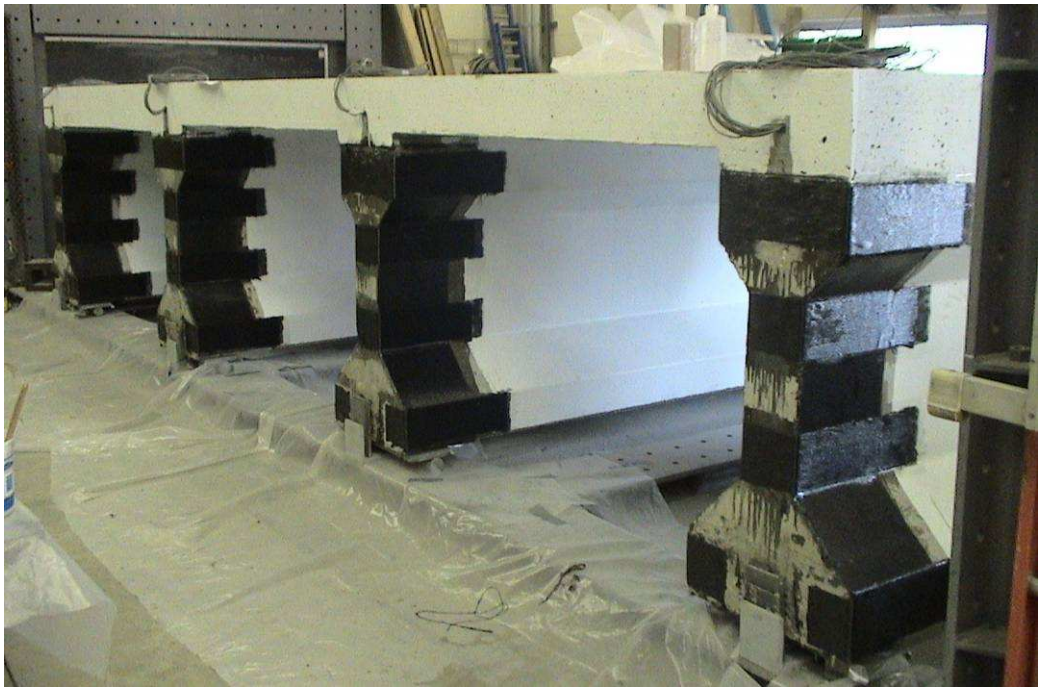

Figure 4.10 Strengthened Girder Ends

The Lab model had strain (internal and external), displacement, and load monitoring instruments. A total of 72 strain gages were used, that were positioned on the GFRP rebar in the concrete deck. 31 strain gages were positioned on the bottom reinforcing layer, mainly under the loaded area, and 41 strain gages were positioned on the top reinforcing layer, under the loading area and over the girders. The strain gages were type EA-05-250BG-120 manufactured by Vishay Micro Measurements. See Figure 4.11 for strain gage placing and protection detail. Further details are provided in Figures A.1 and A.2 in Appendix A.

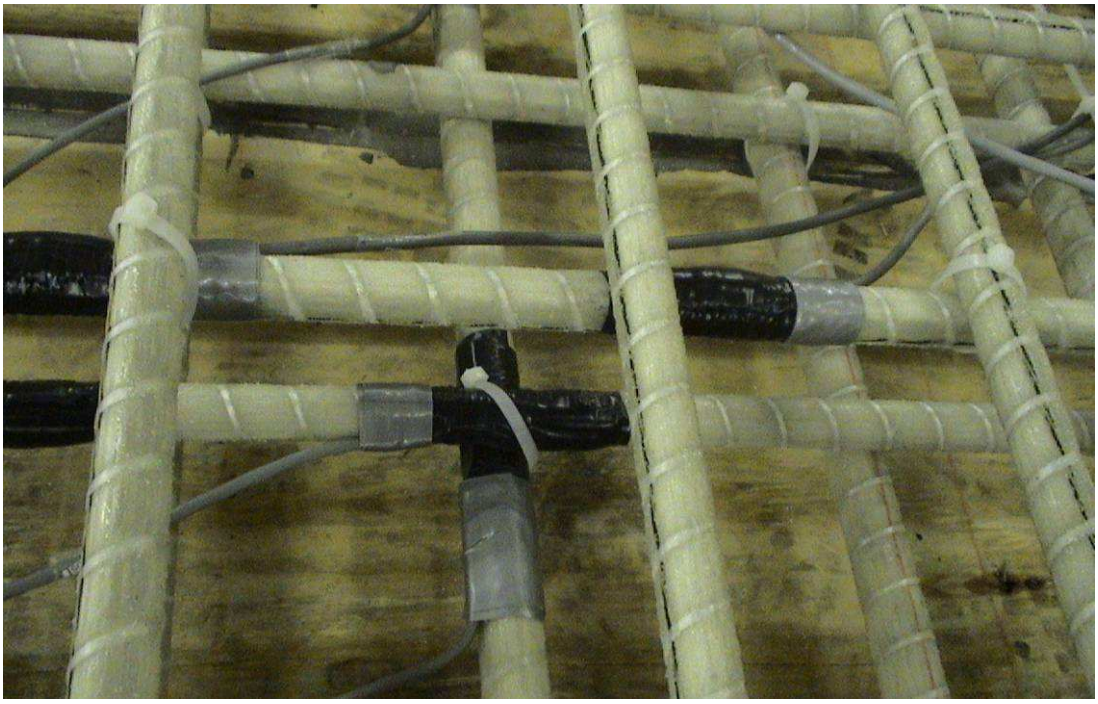

Figure 4.11 Strain Gages on the GFRP Rebar

The 16 strain transducers were positioned in the center of the girder's span, at the bottom and top flange of the girder. They monitored the strain level in the prestressed girders under the loading. 16 displacement transducers were used, and they monitored the displacement of the girder and the deck under the loading area. The strain transducers were type Intelliducer manufactured by Bridge Diagnostics Inc., and the displacement transducers were type PT510 Cable Extension Transducers with 20 inches range manufactured by Celesco Transducer Inc. See Figure 4.12 for strain and displacement transducer details example, and Figures A.3 trough A.7 (Appendix A) for positioning.

To load the lab model, a Power Team RSS2503 hydraulic cylinder was used with a 250 tons capacity. To monitor eventual uneven distribution of the load in the case of TEST 1, two load cells (PSCN-300 K Canister Load Cell) were inserted between the distribution beam and the loading pads. In order to have a realistic load distribution under the nominal 10" × 20" loading area, dimensions specified by AASHTO Standard Specifications for Highway Bridges (1998), rubber pads were used with similar mechanical characteristics to vehicle tires.

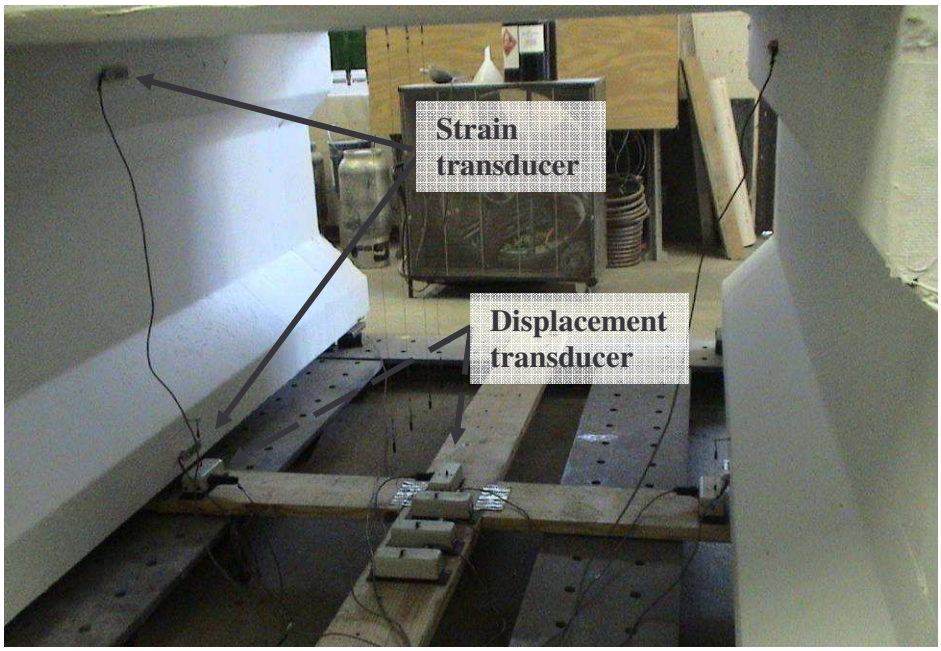

Figure 4.12 Strain Transducers and Displacement Transducers

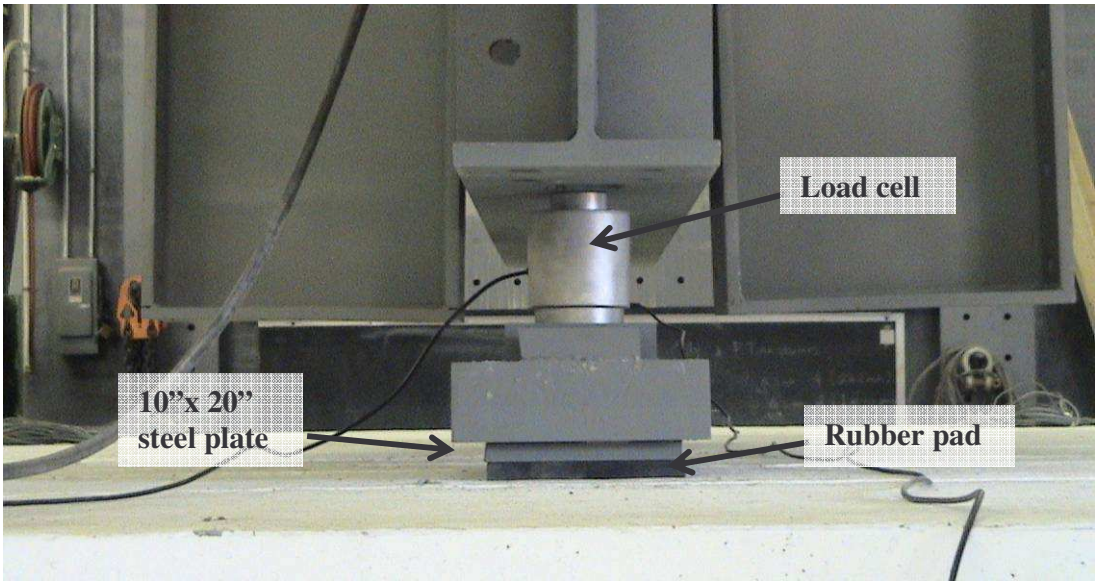

Figure 4.13 Load Cell and Distribution Plates

4.2 Laboratory Test Results

After a discussion with the NCDOT TAC committee it was decided to have a two-point loading test, not a three-point test as the original numerical model suggested. First of all, it was not realistic to have a three-point loading situation on the actual bridge; this would mean that two HS25 trucks are positioned side by side with a common tire footprint. Also, a simplified analysis showed that the difference in the load redistribution is less than 12% between the two load cases. In the following, this test is referenced as TEST 1. Two extra tests were also performed, TEST 2 and TEST 3. The loading setup and discussion of results are presented in the following.

4.2.1 Experimental Results – TEST 1

The layout for the two point loading setup is shown in Figure 4.14. As it was described earlier, two load cells were used to monitor the eventual difference between the two loading points.

16 strain transducers and 16 displacement transducers were used in the test to monitor the prestressed girder's strain level and deformation, and the deformation of the deck. See Figure A.5 for displacement transducer locations for this test. Only 38 strain gages were read at this test, and they were in critical locations, such as the region under the loading area and over the concrete girders (to capture negative moment strain values). See Figures A.1 and A.2 for strain gage positions and numbering. A general view of the actual Lab model during the test is shown in Figure 4.15.

The load was applied in 50 Kips load steps until failure, and released to 0 Kips after each load step. The ultimate load reached was 155 Kips in the first bay, where the slab failed first. The load registered in the second bay was 170 Kips. See Figures 4.16 and 4.17 for the failure mode of the concrete deck.

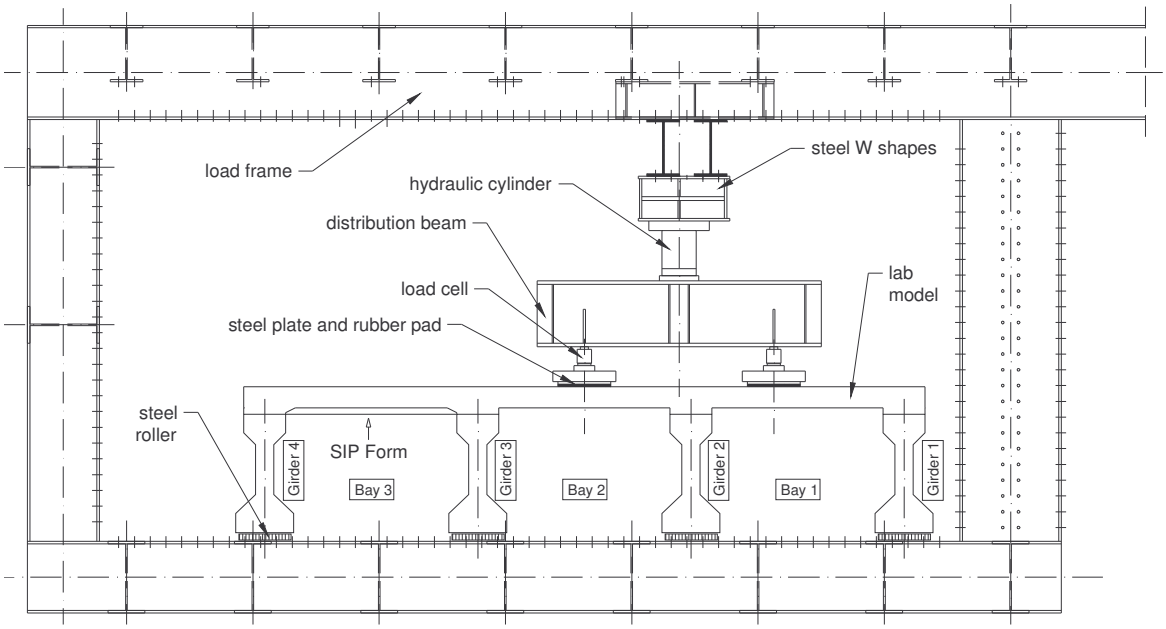

Figure 4.14 Experimental Setup for TEST 1

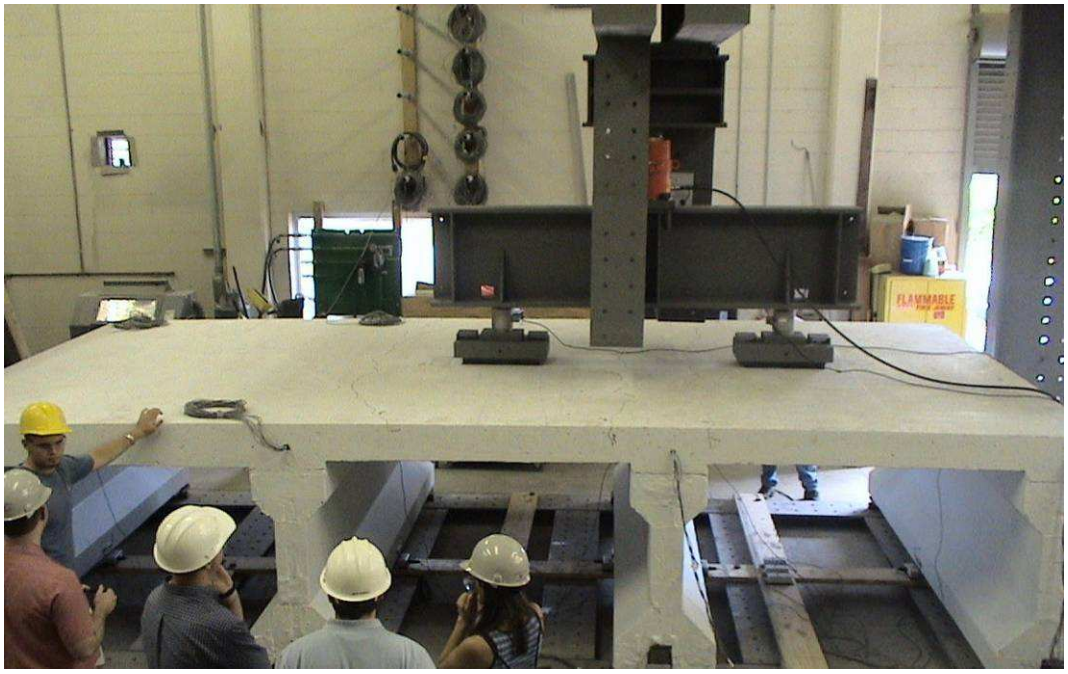

Figure 4.15 General View of the TEST 1 Loading Setup

Figure 4.16 Punching Through the Concrete Deck – Top of the Deck (Bay 1)

Figure 4.17 Punching Through the Concrete Deck – Bottom of the Deck (Bay 1)

Figure 4.18 shows a comparison of the deck's global displacements under the loading area, in Bays 1 and 2. The variation of the displacement from under the loading area to the free edge of the Lab model is presented in Figures 4.19 and 4.20.

As it can be seen the displacements in the two bays, Bays 1and 2, follow the same load-deformation curve, and they are about the same magnitude. Moreover, the deformation in each bay varies in the longitudinal direction, from the area under the load to the free edge of the Lab model.

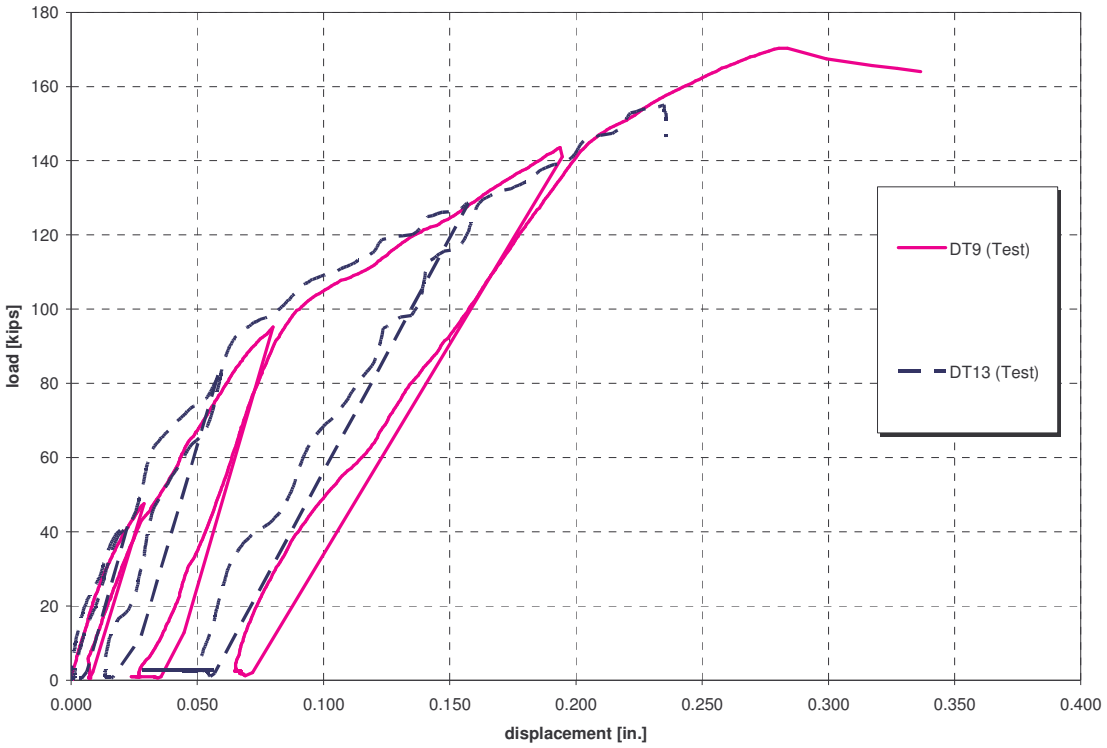

Figure 4.18 Comparison of the Displacements Under the Loading Area - Bays 1 and 2 (TEST 1)

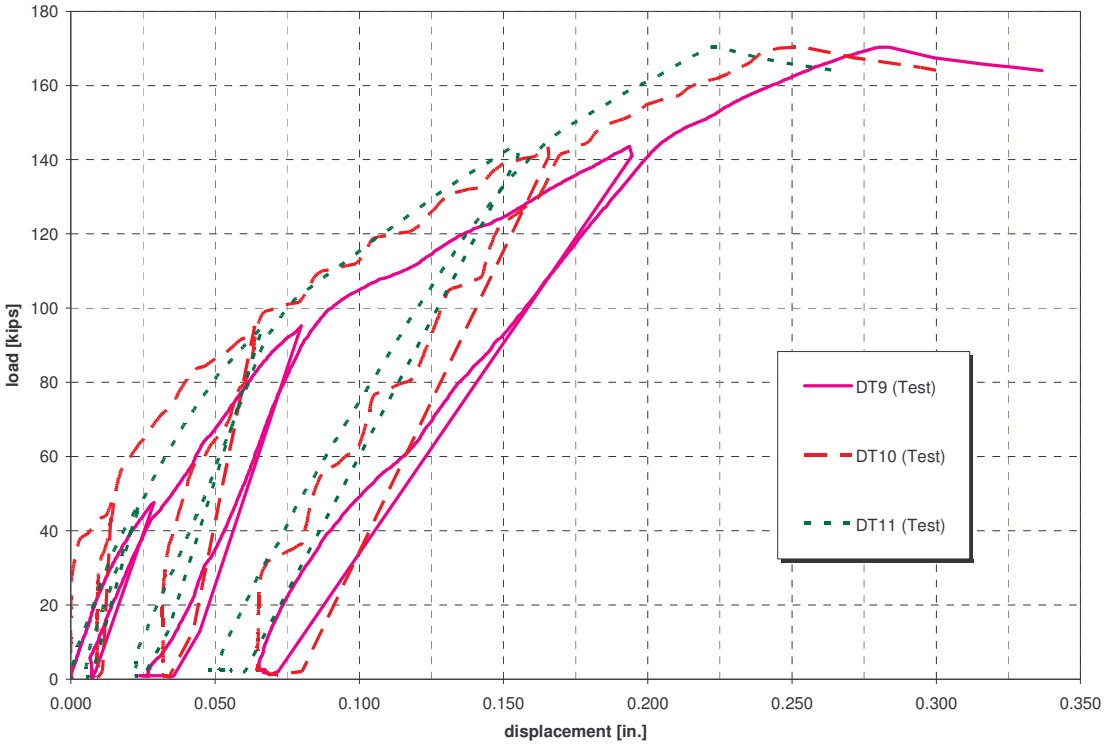

Figure 4.19 Displacements in Bay 1 (TEST 1)

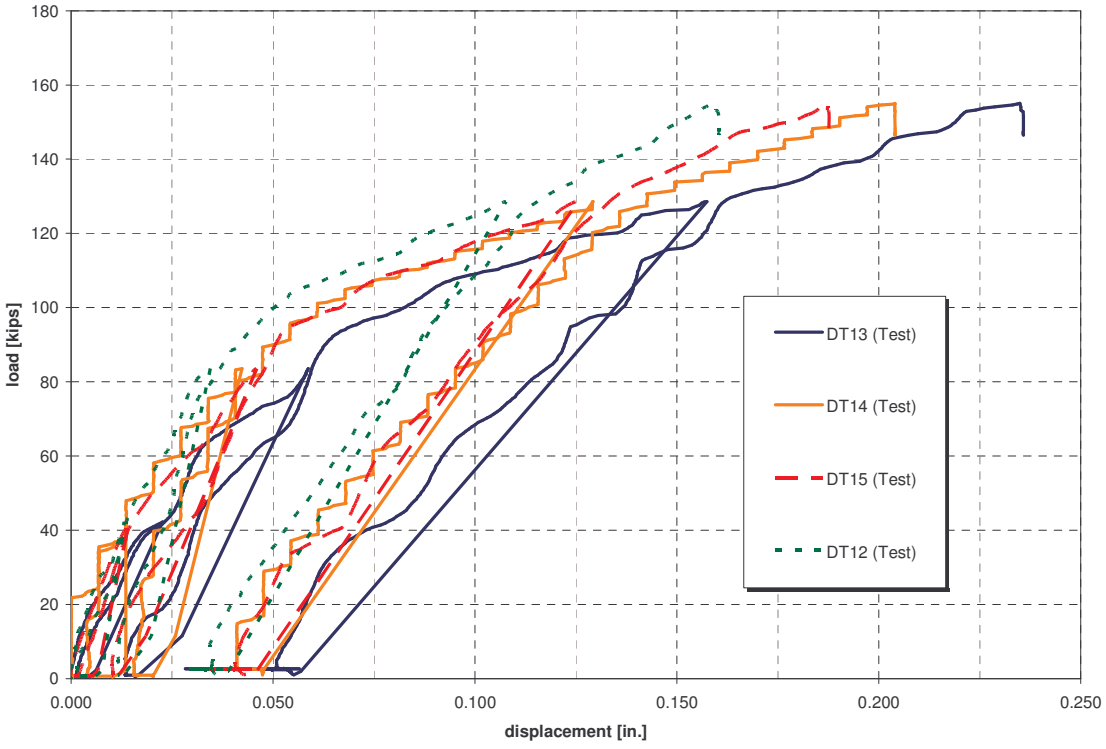

Figure 4.20 Displacements in Bay 2 (TEST 1)

The strain levels in the top reinforcement layer over the girder, under the loading area and bottom reinforcement layer are presented in Figures 4.21 to 4.24. As it can be seen from the above mentioned figures, the recorded strains were at the same level in both bays, and did not exceed 0.35% in the GFRP rebars.

The deformation was not restricted in the longitudinal direction. As a result, small tension was developed in the top reinforcement rebars (see Figure 4.21). However, in the transverse direction, the prestressed girders act like a support for the deck developing the arching effect. Consequently, compression strains are present in the top reinforcement rebars, as it can be seen from Figure 4.22. But this compression strain turns to tension after the crushing of the concrete under the loaded area and development of cracks over the girders. Tension strain is present in the bottom reinforcement layer in both directions (see Figures 4.23 and 4.24), also in the top reinforcement layer over the prestressed girders (see Figure 4.25).

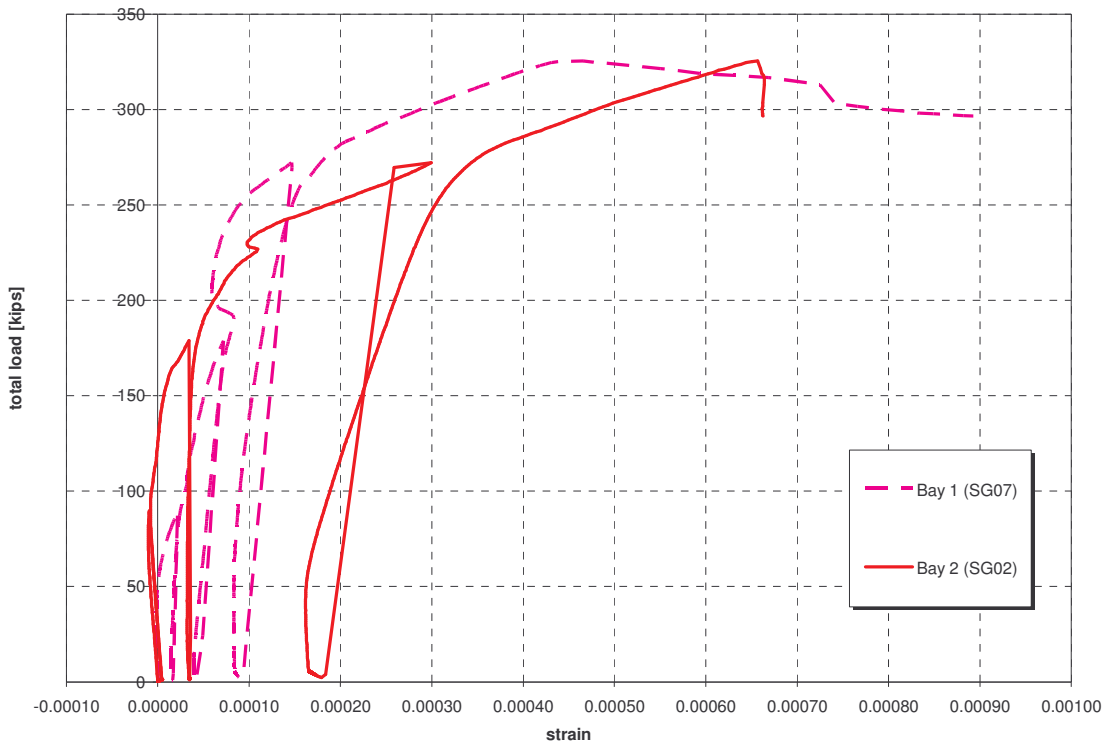

Figure 4.21 Longitudinal Strain in Top Reinforcement for Bays 1 and 2 (TEST 1)

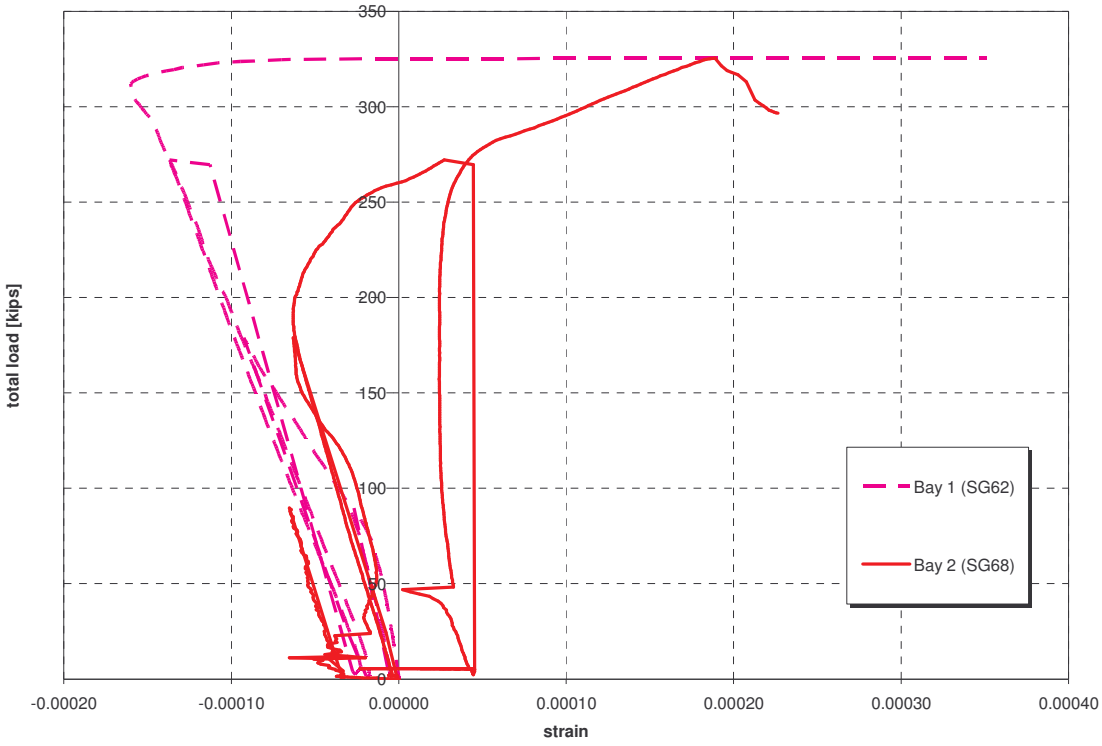

Figure 4.22 Transverse Strain in Top Reinforcement for Bays 1 and 2 (TEST 1)

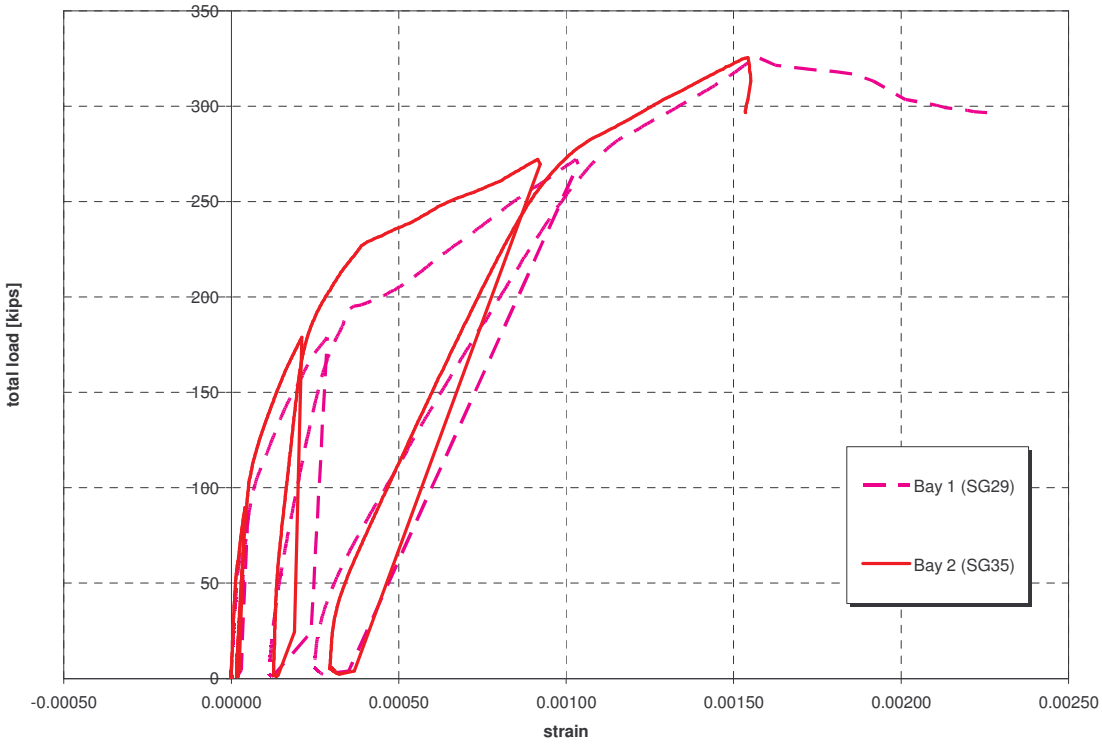

Figure 4.23 Longitudinal Strain in Bottom Reinforcement for Bays 1 and 2 (TEST 1)

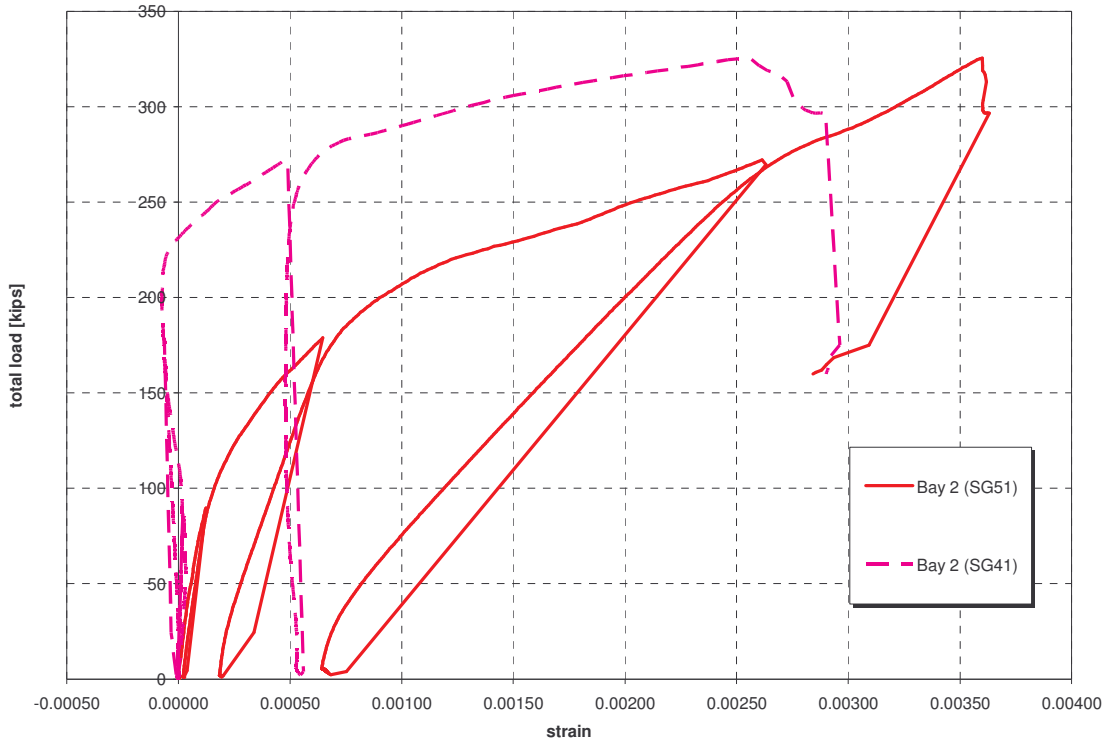

Figure 4.24 Transverse Strain in Bottom Reinforcement for Bay 2 (TEST 1)

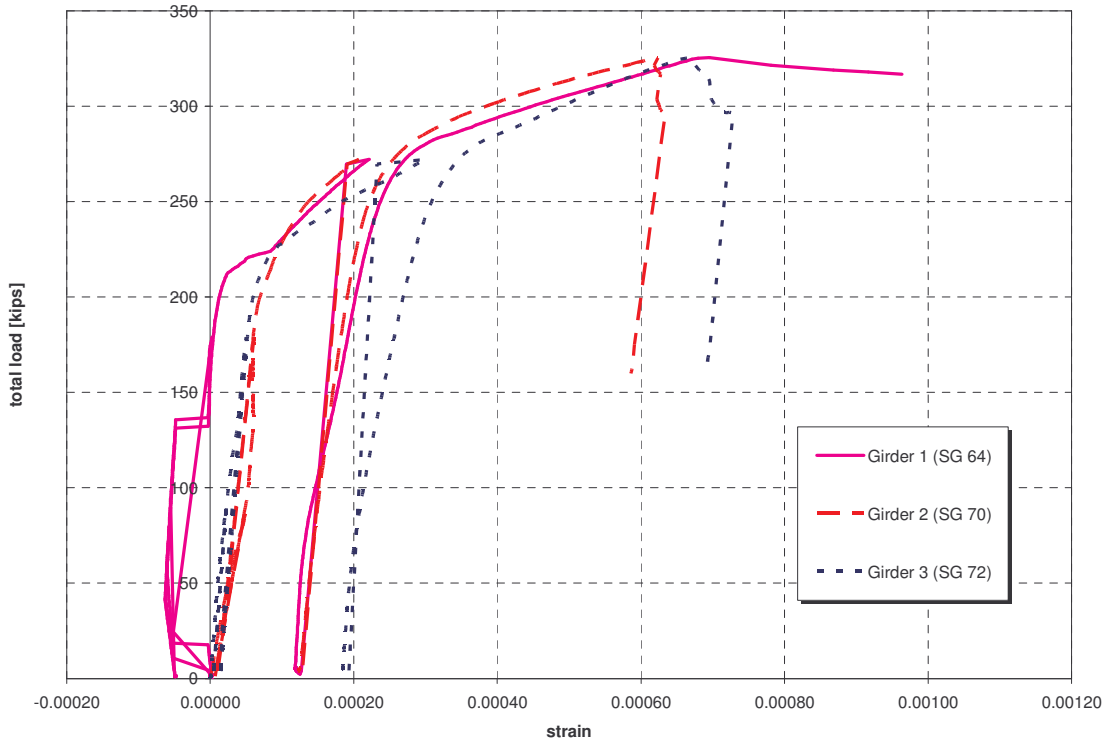

Figure 4.25 Strain Level in Top Reinforcement Over the Middle of the Girders (TEST 1)

4.2.2 Experimental Results – TEST 2

During TEST 1, only the slab in Bay 1 failed. This provided the opportunity to run an extra test, not requested in the research proposal. During the TEST 2, only the second bay was loaded in the same location as in the TEST 1. But in this case, the specimen was loaded only in one point as it can see from the Figure 4.26.

The instrumentation was modified for this loading case. The strain transducers were left in the same position. The displacement transducers were re-positioned according to Figure A.6. Again, 38 strain gage readings were registered. See Figures A.1 and A.2 for strain gage positions and numbering.

In this case the load was applied monotonically, and the ultimate load reached was 245 Kips. The failure mode was punching shear in this case as well. The variation of the global displacement of the deck, from under the loading area to the free edge of the Lab model, is presented in Figure 4.27.

The strain levels in the top reinforcement layer over the girder, under the load area and bottom reinforcement layer are presented in Figures 4.28 through 4.30. Even if the Lab model had cracks and permanent deformations, the same remarks can be made about the resulting deformations and strain as for TEST 1. However, during TEST 2 higher strain readings were recorded, up to 0.64% in the bottom reinforcement layer.

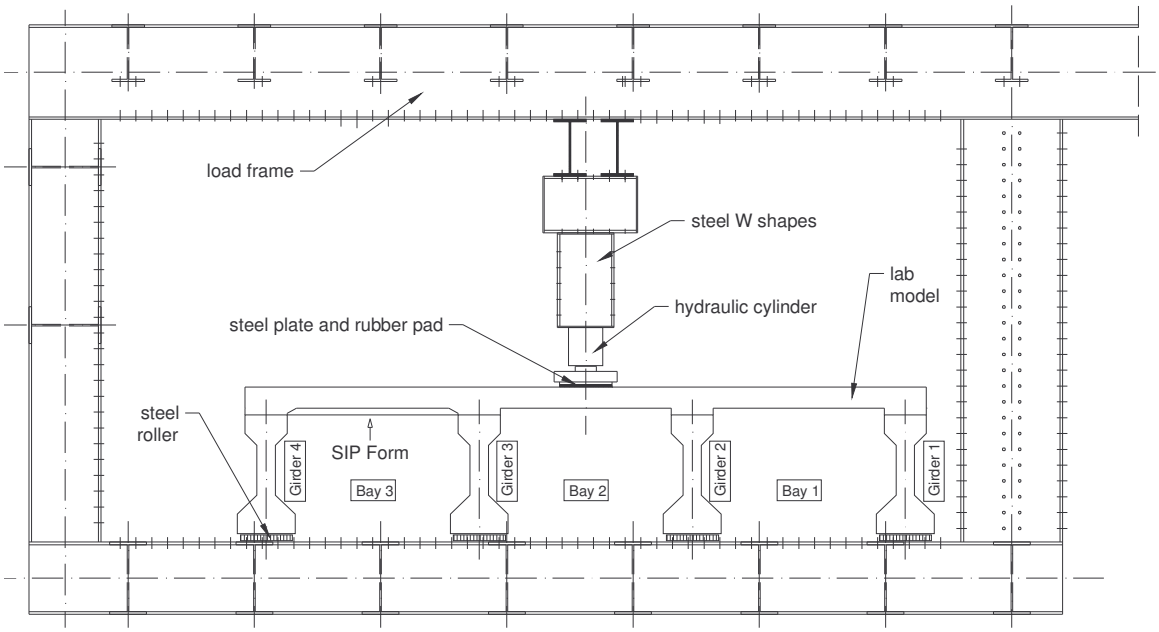

Figure 4.26 Experimental Setup for TEST 2

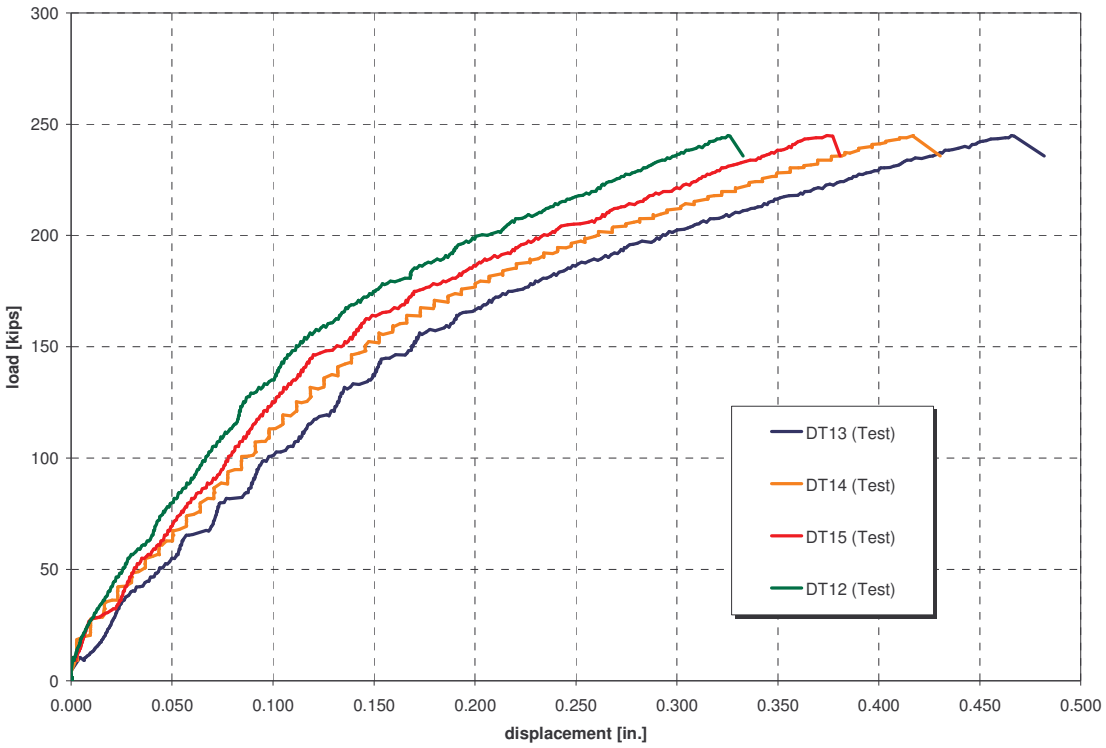

Figure 4.27 Displacements in Bay 2 (TEST 2)

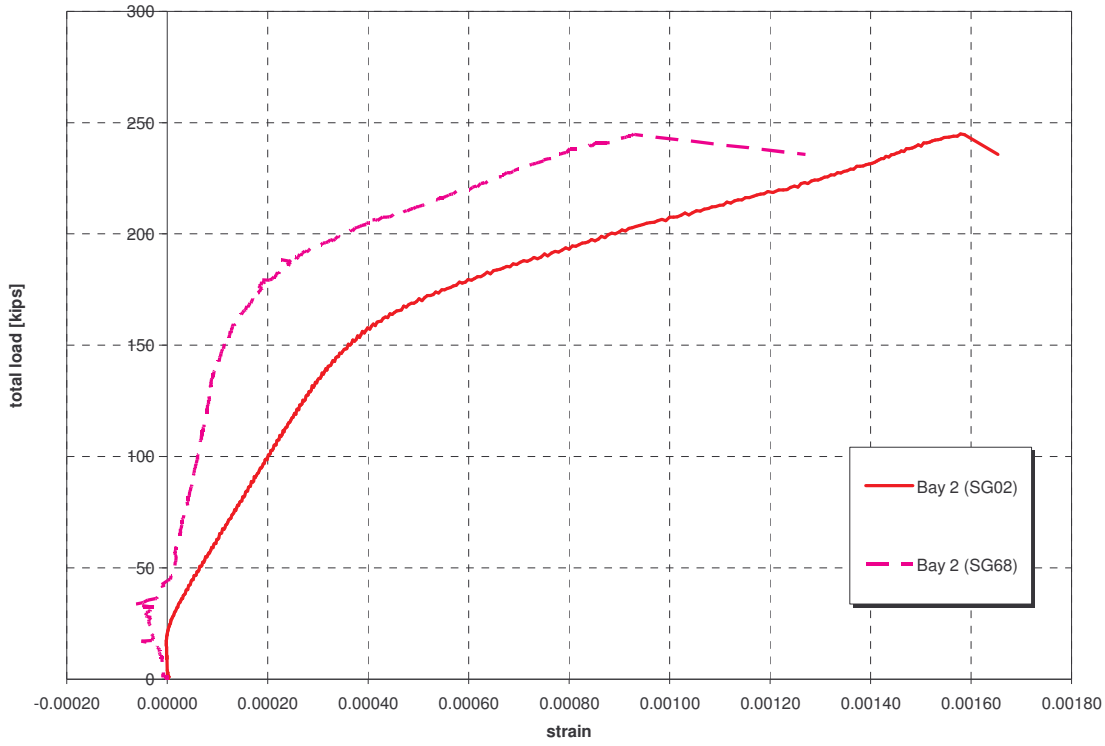

Figure 4.28 Transverse and Longitudinal Strain in Top Reinforcement (TEST 2)

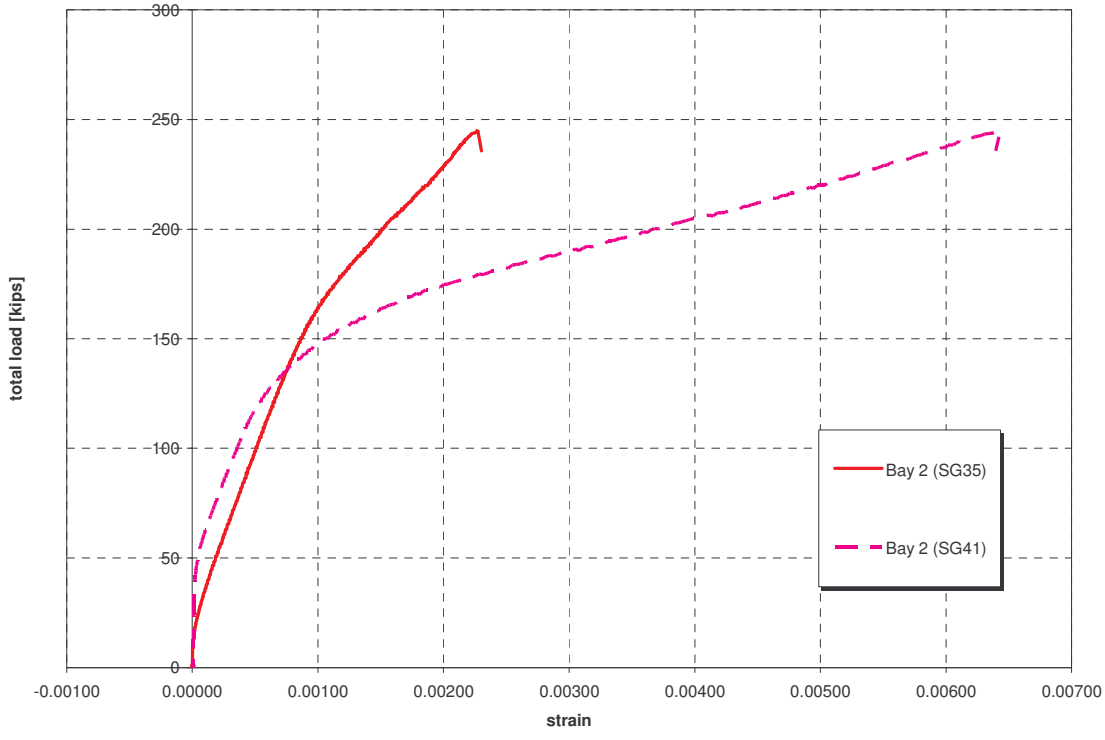

Figure 4.29 Transverse and Longitudinal Strain in Bottom Reinforcement (TEST 2)

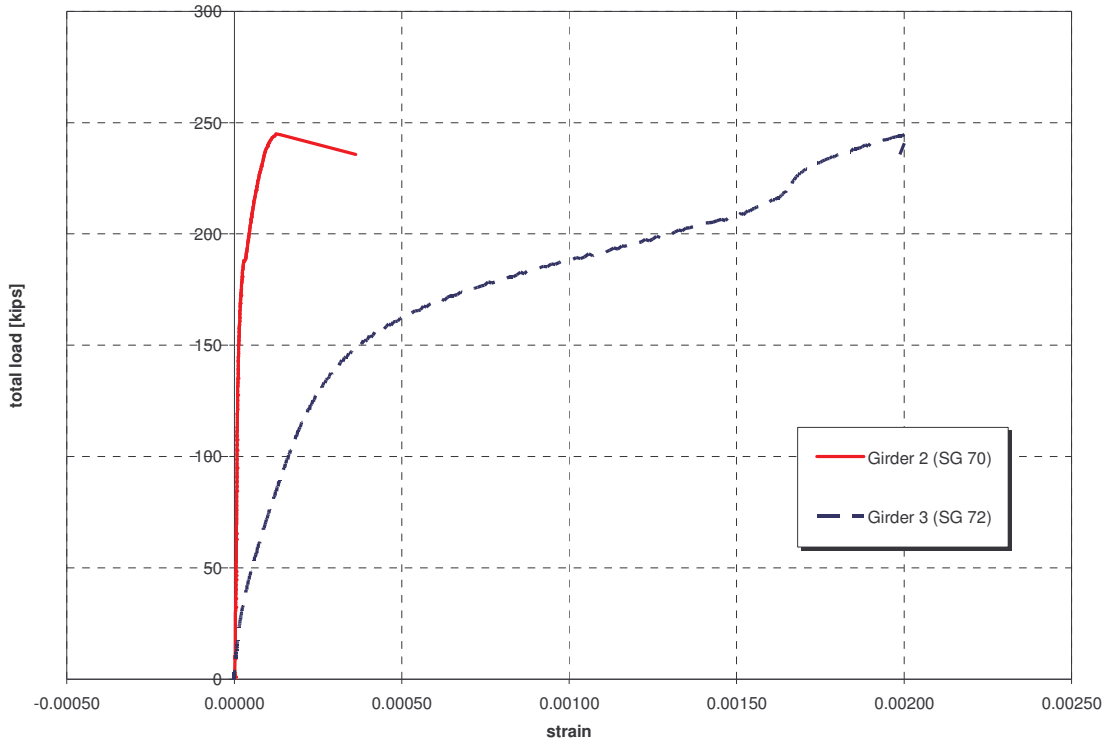

Figure 4.30 Strain Level in Top Reinforcement Over the Middle of Girders 2 and 3 (TEST 2)

4.2.3 Experimental Results – TEST 3

As it was described earlier, a third test (TEST 3) was decided to be done. In this case, the loaded bay (Bay 3) had stay-in-place (SIP) metal forms and loaded with a single concentrated force (see Figure 4.31). The load was applied with 50 Kips loading steps until failure, and released to 0 Kips after each load step. The instrumentation was the same as for TEST 2, except the displacement transducers were repositioned, as it can be see in the Figure A.7 (Appendix A).

The ultimate failure load was 232 Kips, and the failure mode was punching shear again. The variation of the global displacement of the deck, from under the loading area to the free edge of the Lab model is presented in Figure 4.32. As it can be seen, the displacements were about the same magnitude as in the two earlier test setups.

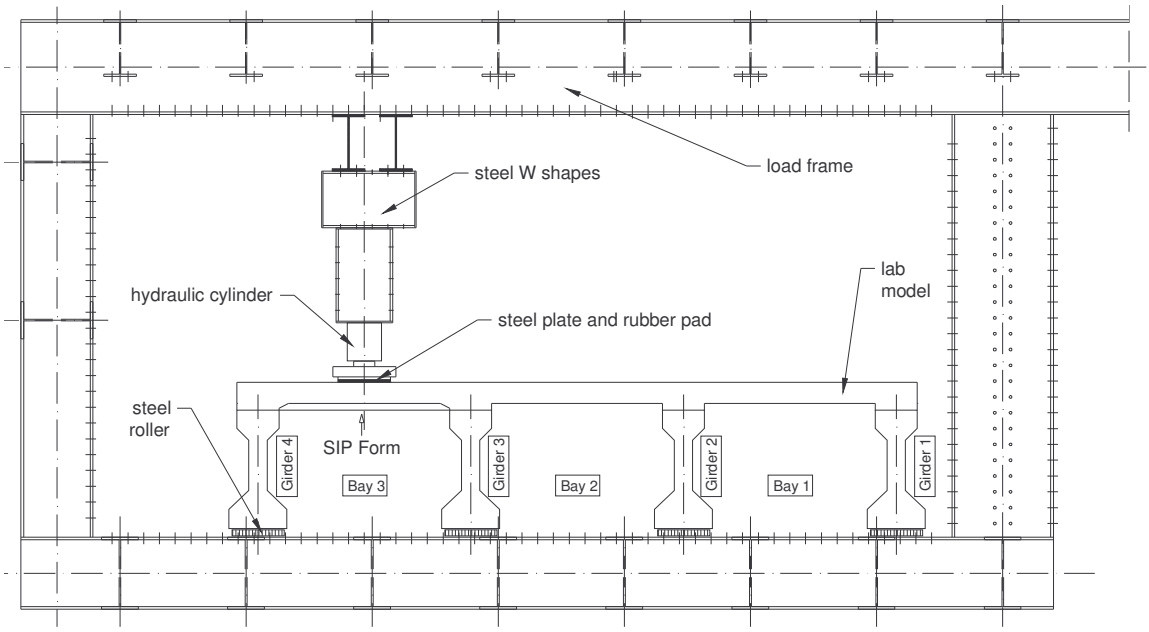

Figure 4.31 Experimental Setup for TEST 3

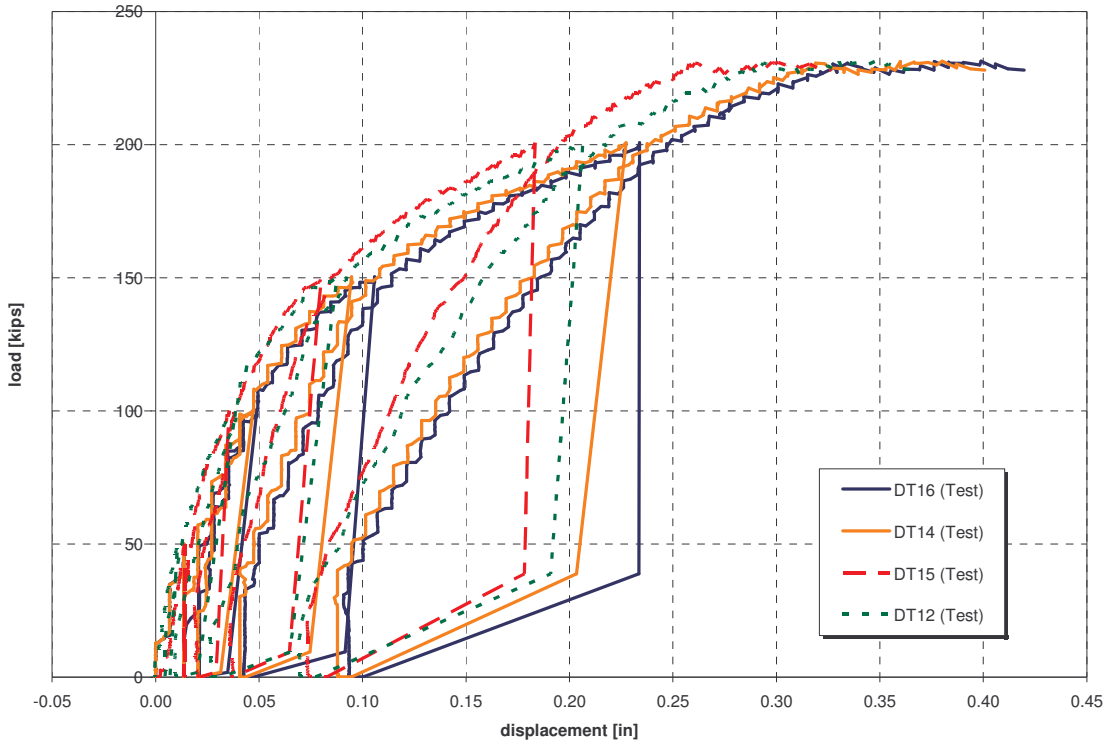

Figure 4.32 Displacements in Bay 3 (TEST 3)

The strain levels in the top reinforcement layer over the girder, under the load area and bottom reinforcement layer are presented in Figures 4.33 through 4.35. It can be seen from Figure 4.33 that in this case the SIP form increased the arching effect. In the transverse direction the strain in the top reinforcement layer was higher then in the case of TEST 2. However, this didn't lead to an increase in the ultimate load. As it was mentioned earlier, punching shear governed the failure again.

The tension strain, in both transverse and longitudinal direction, in the bottom reinforcement layer was smaller then in the other two load cases. This occurred due to the presence of the SIP that acted as an extra reinforcement in the tension zone. The strain over the prestressed girders was at about the same level as in the two earlier test setups.

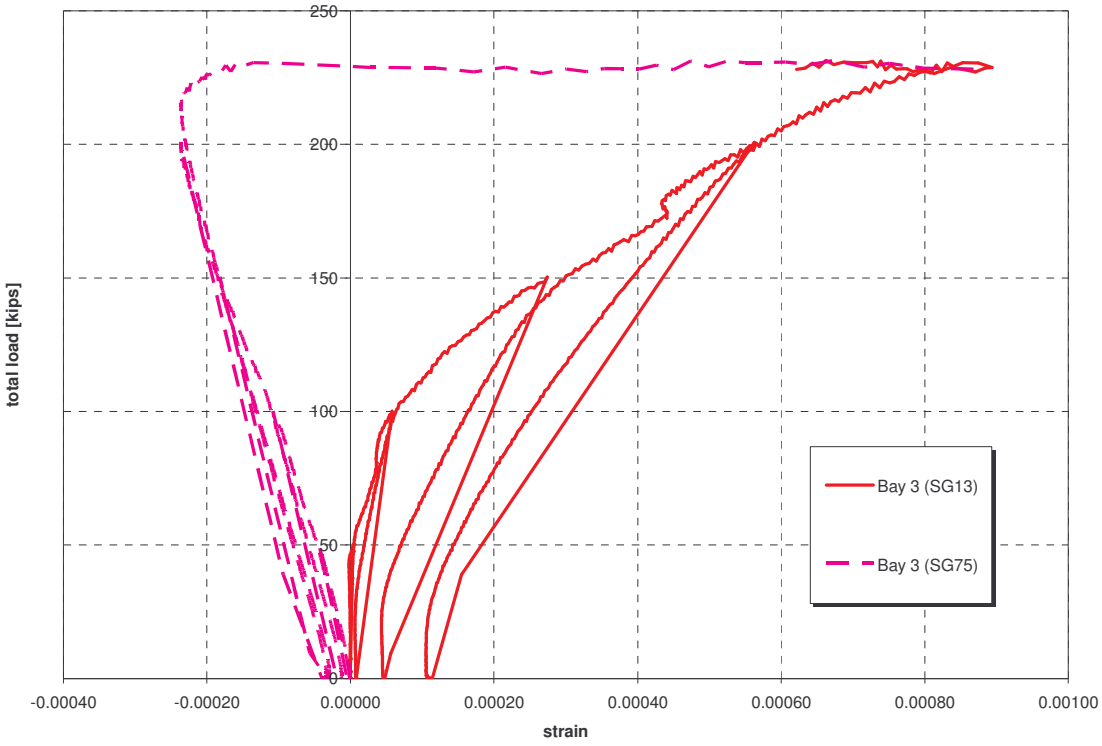

Figure 4.33 Transverse and Longitudinal Strain in Top Reinforcement (TEST 3)

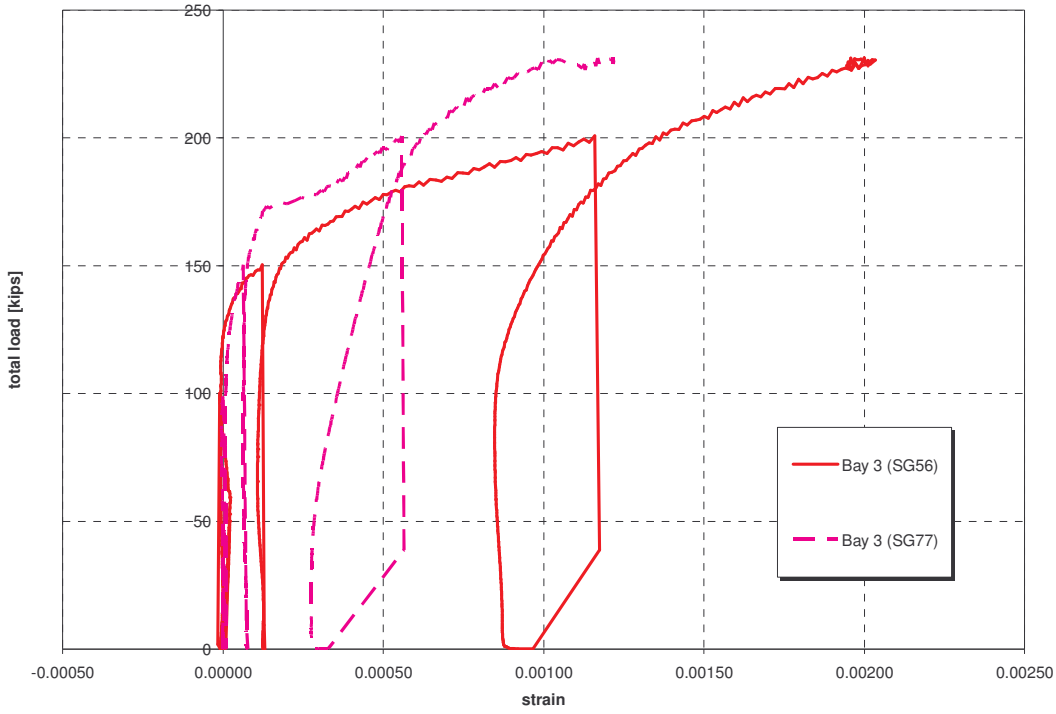

Figure 4.34 Transverse and Longitudinal Strain in Bottom Reinforcement (TEST 3)

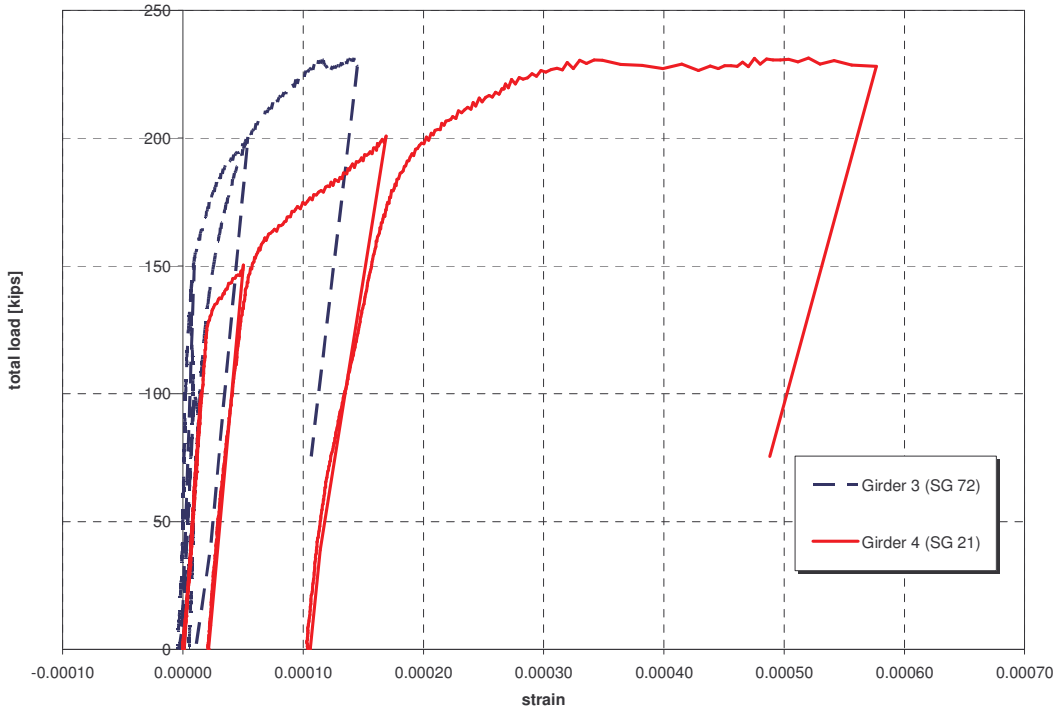

Figure 4.35 Strain Level in Top Reinforcement Over the Middle of Girders 3 and 4 (TEST 3)

4.3 Comparison of Numerical versus Laboratory Test Results

As it was described earlier, the TEST 1 Lab model testing was modeled numerically using the actual specimen dimensions and material characteristics. Originally, the same model was investigated with two options, namely allowing and restraining the cracking of the concrete in the prestressed girders. The results are shown in Figure 4.36 on the relative deformation of the concrete deck in Bay 1. It can be noted that there were no differences in deformation, but there is a difference in the ultimate load.

Analyzing the two models it was found that the same principle may be applied, as described in earlier sections, to stop the numerical analysis when the strain reaches the 0.0019 in/in value at a predefined section. Using this assumption, both numerical models resulted in the same ultimate failure load. This load can be considered as the ultimate failure load for the case when the cracking was allowed in the prestressed concrete girders.

Figures 4.37 and 4.38 show a comparison between the experimental and numerical results of the relative deck deformation under the applied wheel load. As it can be seen, in both cases the numerical model is more flexible than the actual Lab model. However, in both cases the load deformation curves have the same slope.

Figure 4.39 shows a screen capture from the ANSYS FE program, representing the strain level in the general area of the loaded surface. SG27 to SG30 represent the equivalent position of strain gages in the actual Lab model. Comparison between the experimental strain readings and the numerical results, at the correspondent locations, are presented in Figures 4.40 to 4.43. As it can be seen, the numerical results follow the same path as the experimental ones. Moreover, the magnitude of the numerical values is comparable.

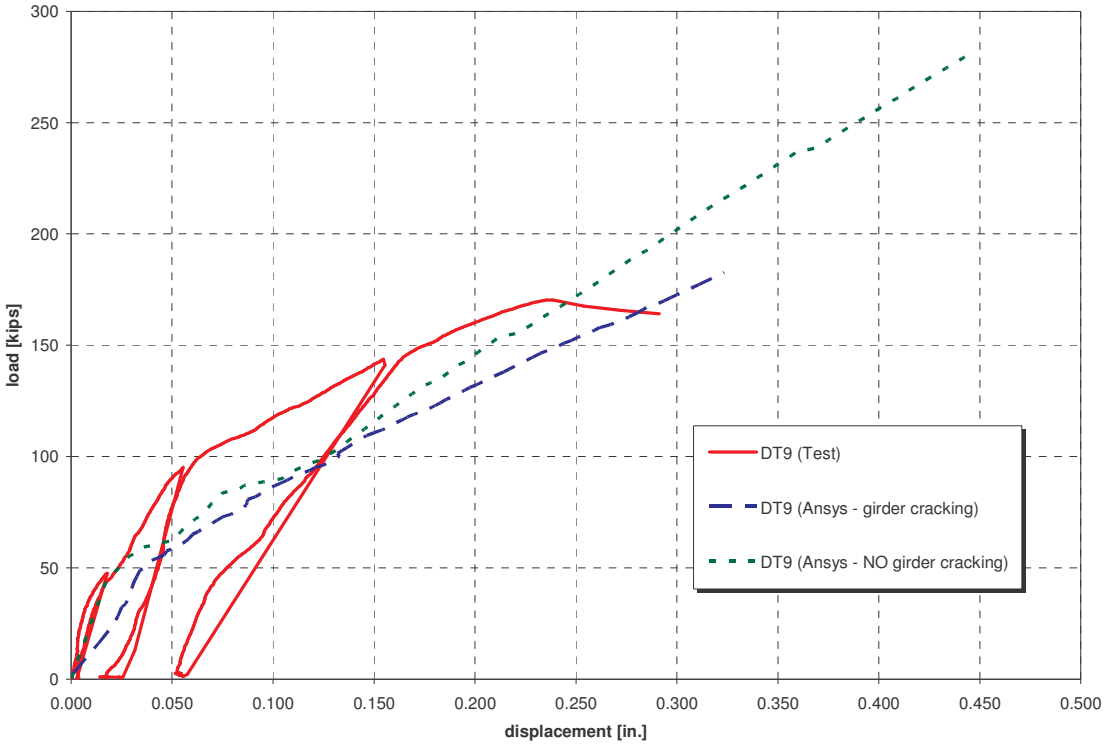

Figure 4.36 Effect of Allowing Cracking in the Prestressed Girders

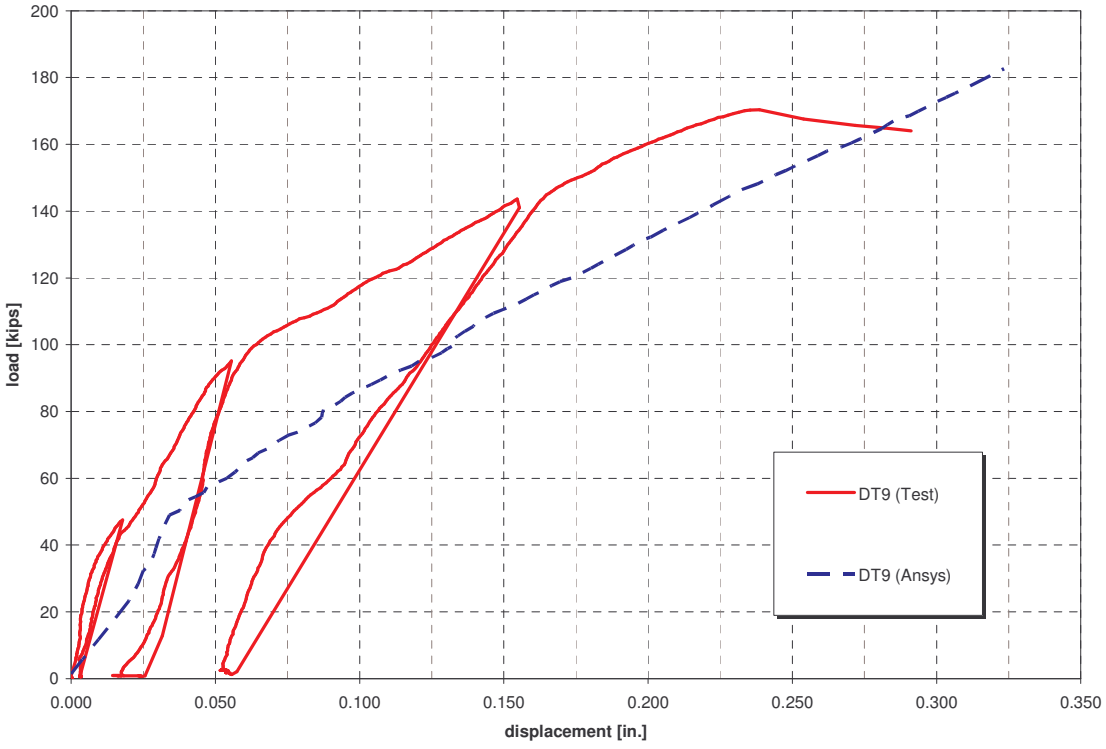

Figure 4.37 Test vs. Numerical Results for Deformation at Bay 1

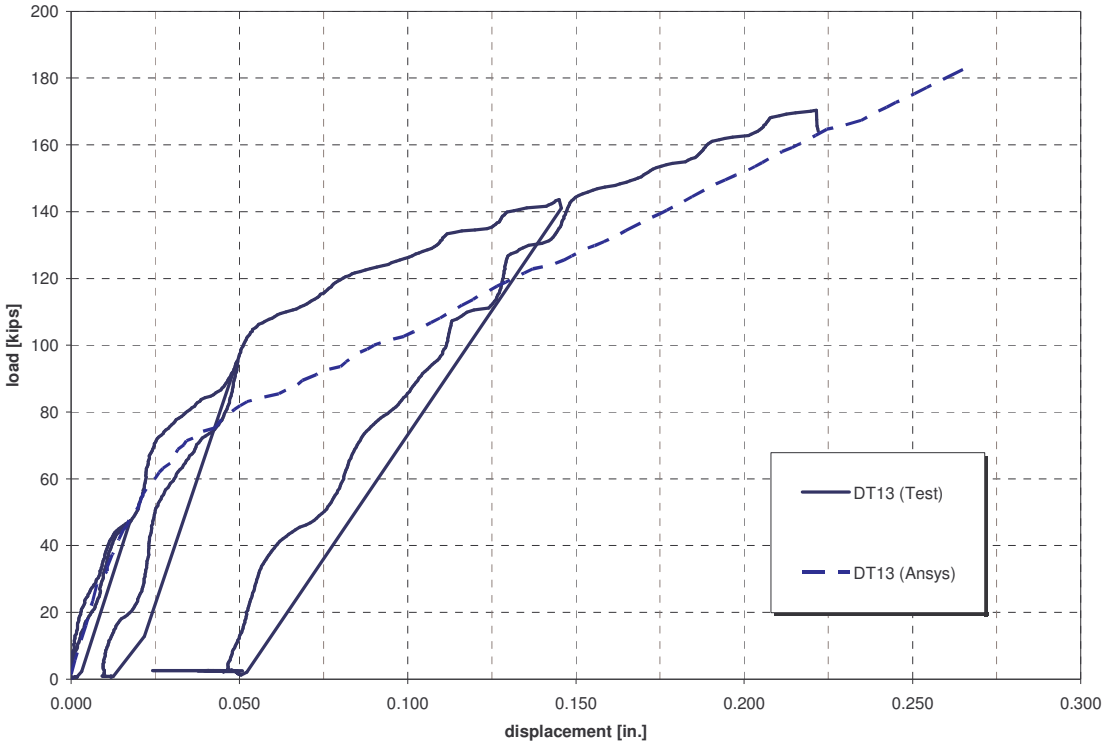

Figure 4.38 Test vs. Numerical Results for Deformation at Bay 2

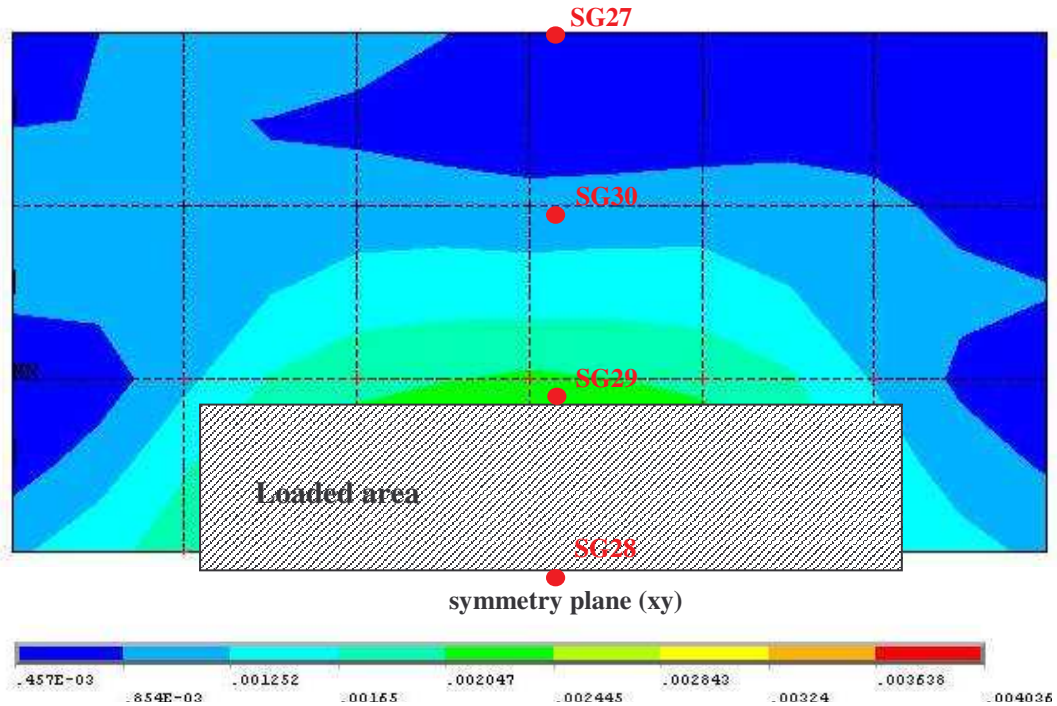

Figure 4.39 Strain Level in the Bottom Reinforcement Under the Loading Area in Bay 1

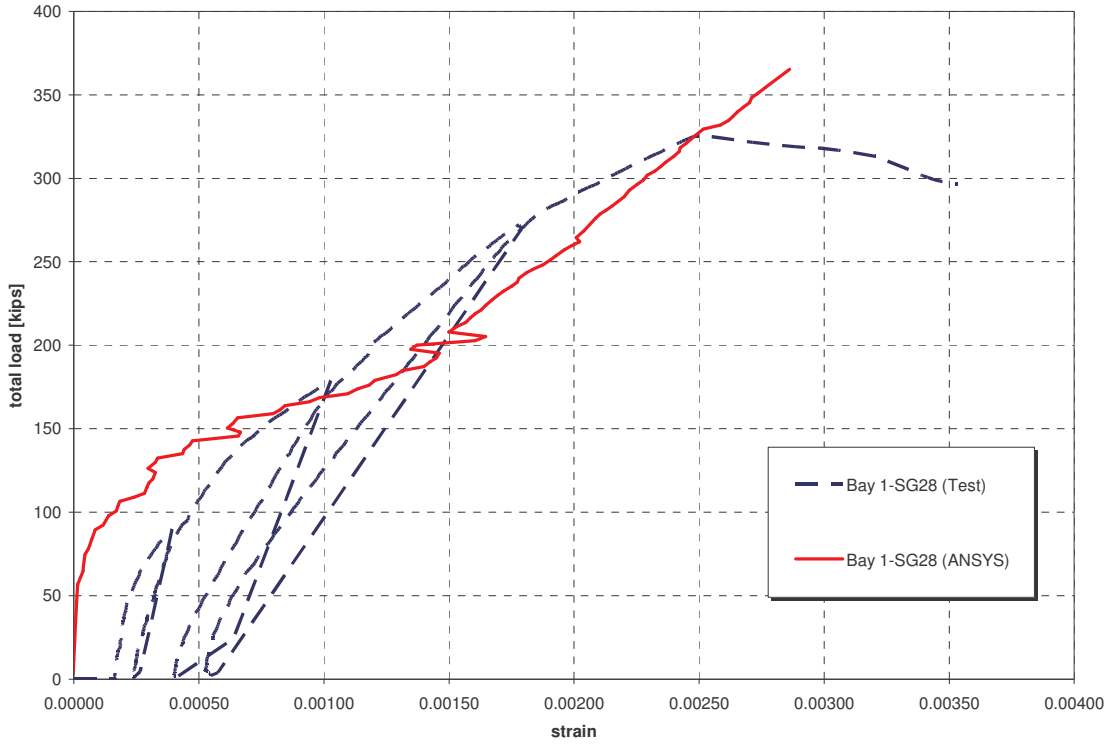

Figure 4.40 Test vs. Numerical Results for Strain at the Approximate Position of SG28

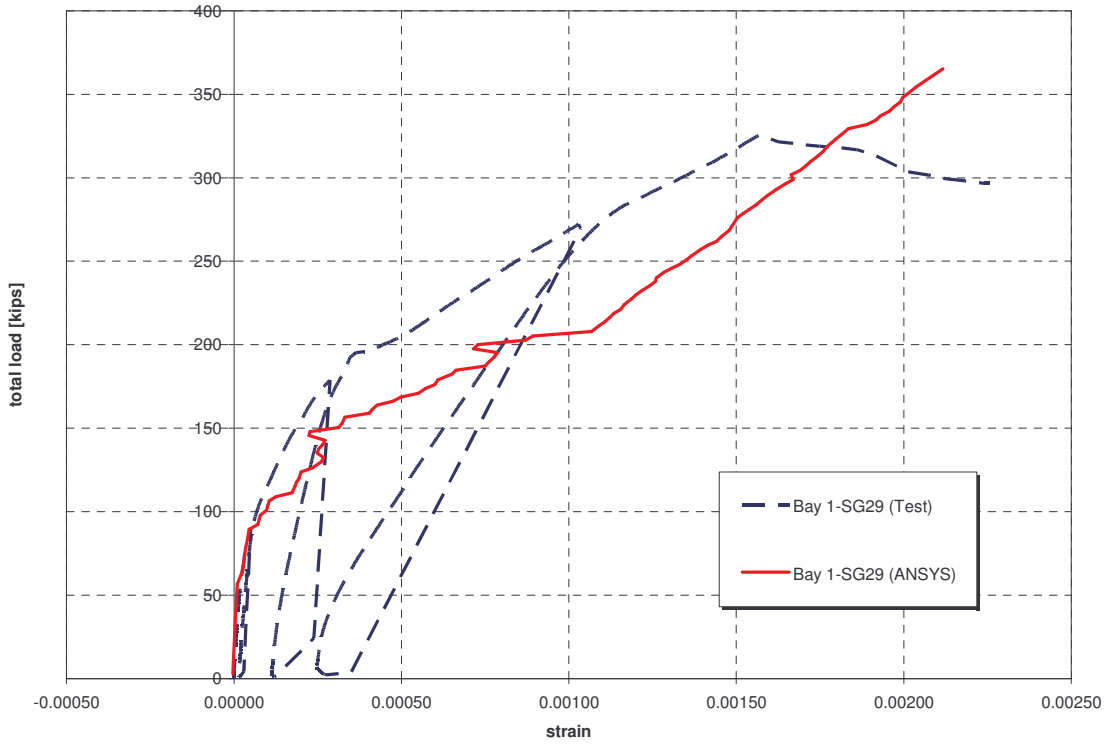

Figure 4.41 Test vs. Numerical Results for Strain at the Approximate Position of SG29

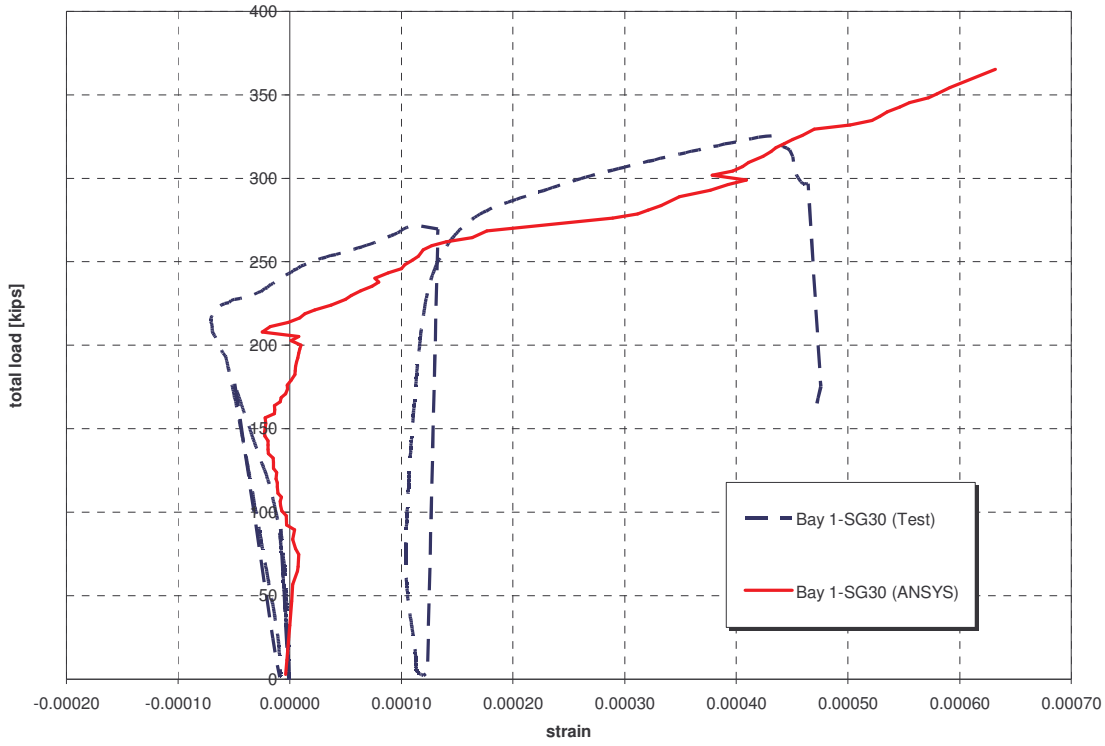

Figure 4.42 Test vs. Numerical Results for Strain at the Approximate Position of SG30

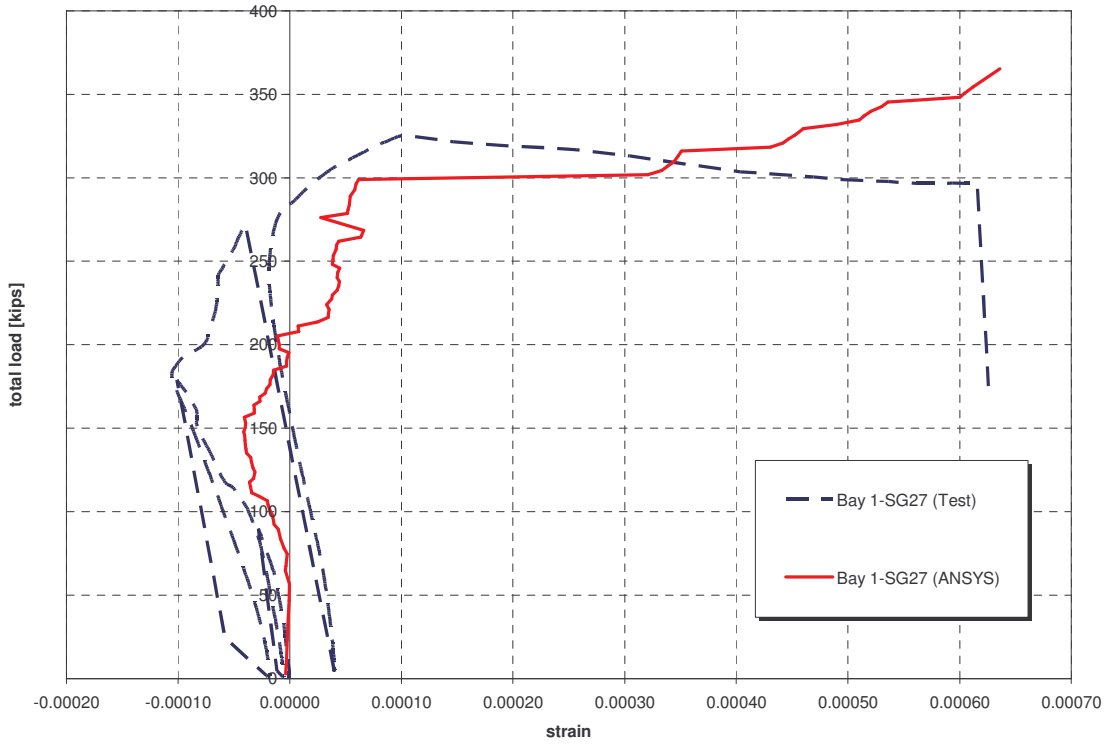

Figure 4.43 Test vs. Numerical Results for Strain at the Approximate Position of SG27

4.4 Bridge Load Testing

4.4.1 Instrumentation and Testing Protocol

The UNC Charlotte research team monitored the bridge construction during the September-November 2005 period, and a detailed report is included in Appendix C. This activity allowed the installation of 36 strain gages directly on the GFRP rebars, before the concrete was placed in the bridge deck (during which a number of these instruments were damaged). The location of these gages is shown in Figure 4.44. As it can be seen, the gages were installed on the GFRP rebars in the deck, directly above the AASHTO Type III girders, concentrated in Spans B and C (as the length of the two outside spans was equal, only Span C was heavily instrumented, in addition to the center span).

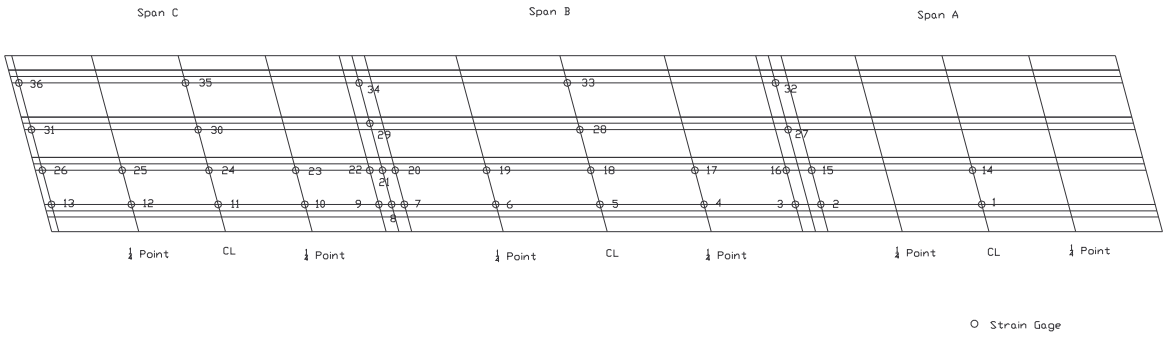

Figure 4.44 Bridge Instrumentation – Strain Gage Location

In addition to strain gages, 20 strain transducers were also installed on the Type III girders (location shown in Figure 4.45). These were positioned mainly along 2 girders to capture the continuous-for-live-load response of the bridge, and at the centerline of Spans B and C to monitor the transverse distribution of the truck loads between the 4 girders. In addition, based on their reliability, these strain transducers were also used during the bridge dynamic tests. Similarly, 16 displacement transducers were used in Spans B and C to record the peak vertical deformation of bridge superstructure.

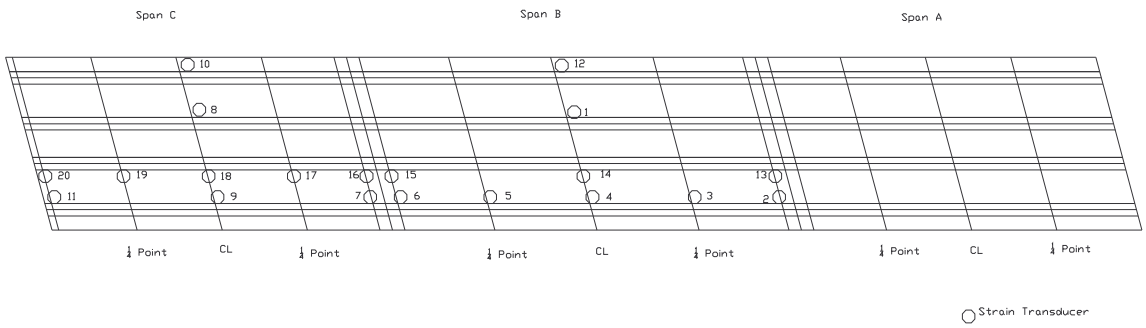

Figure 4.45 Bridge Instrumentation – Strain Transducer Location

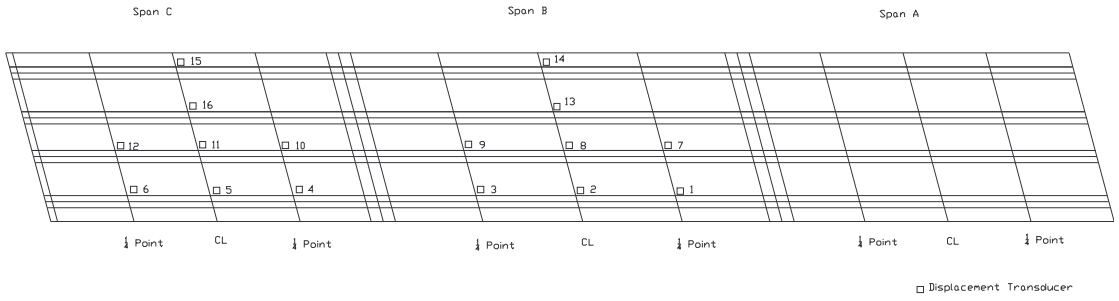

Figure 4.46 Bridge Instrumentation – Displacement Transducer Location

The bridge was designed based on an HS-20 live load. To simulate approximately 75% of this load, two fully loaded tandem trucks were provided by the Division Engineer, and used to load the bridge (see Figure 4.47). In order to provide adequate loading data, each truck axle was weighed by a DMV officer at the bridge site, resulting in 51,460 and 54,520 lbs truck weights.

Previous research performed by the UNC Charlotte team proved that there were no significant differences in bridge response to a slow moving truck (quasi-static loading), as compared to a truck stopped at certain locations on the bridge. Therefore, this bridge was tested with the two trucks following very closely, and moving at a speed less than 5 mph along 7 different load paths (see Figure 4.48), considering both East- and West-bound directions. As it can be seen, these load paths were selected to result in maximum interior/exterior girder stresses, and to follow the traffic lanes, and the centerline of the bridge.

Figure 4.47 Bridge Load Testing

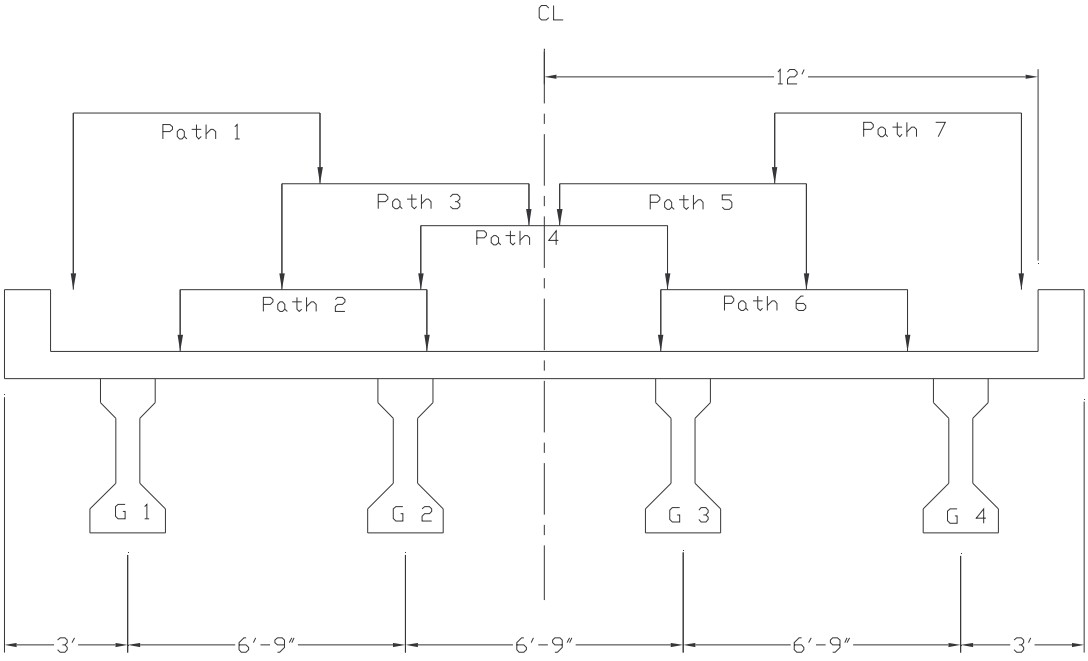

Figure 4.48 Quasi-static Load Paths

In order to provide information on the effect of vehicles traveling on the bridge at the speed limit, considered in design through the impact factor, dynamic tests were also performed on the bridge using one truck moving at 40 mph. Due to safety reasons, only one truck was used in the dynamic tests; prior to which, the same truck was used for additional quasi-static tests to provide the baseline readings for comparison. Only load paths 2, 4 and 6 (in both directions) were considered for the impact analysis, as these cover the most frequently used load paths on a two-lane bridge.

It has been proven by several studies that in order to capture the dynamic response of a bridge, the sampling rate of the data acquisition system must record data at a considerable rate. In this project, strain transducer readings were taken 250 times a second, significantly faster, than the rate of one reading every 3 seconds used during the quasi-static loading phase. It will be shown later that this dynamic sampling rate was more than adequate to determine the impact factor of the selected truck.

4.4.2 Load Test Results

As it was mentioned earlier, 72 instruments were used to record the bridge response to dozens of loading paths, resulting in a large number of data files. However, in this report only the most important findings will be included, as related to GFRP rebar strain, girder strain and vertical deformation, transverse load distribution, and live load impact factor.

Figure 4.49 (horizontal axis refers to DAQ readings, from vehicle start to stop) shows selected displacement transducer (DT) readings for quasi-static load path 1, East Bound (traveling from Span C towards Span A). Instrument DT2 located at center of Span 2 – girder 1 (also shown in Figure 4.45) recorded the largest vertical deformation of all the tests, approximately 0.05 in., representing a significantly smaller deformation than the AASHTO-specified limit of L/800. It is interesting to note that while the trucks were positioned over Span C, the instruments in that span (e.g. DT6 or DT 12) recorded downward deformation, but a slight uplift was recorded in Span B (e.g. DT2 or DT9), proving a superstructure continuity for live loads.

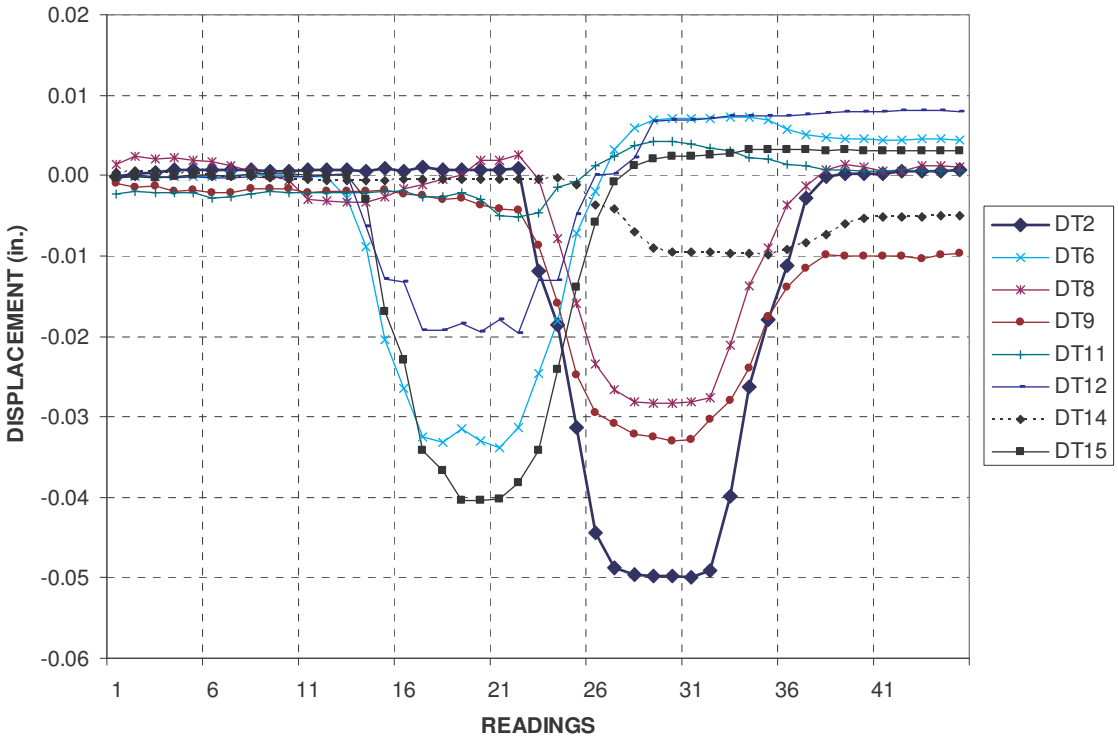

Figure 4.49 Quasi-static Loading: Path 1, East Bound – Girder Deformation

Although the graph in Figure 4.50 will only be meaningful in color, it shows similar trend as the previous figure: compression at the bottom of girders in Span B while the trucks are positioned on Span C. The peak tension strain level of 45 με was recorded by instrument ST4, on girder 1 in Span B, and the peak compression strain of 26 με was recorded by ST7 on the same girder at the first interior support.

With respect to GFRP rebar strain levels, 241 με was recorded by gage SG27 (shown in Figure 4.51), located on the deck reinforcement along girder line 3, above the second interior support. Although it seams like a significant strain level, this value is far from the composite rebar ultimate strain of 12,000 με (or 1.2%).

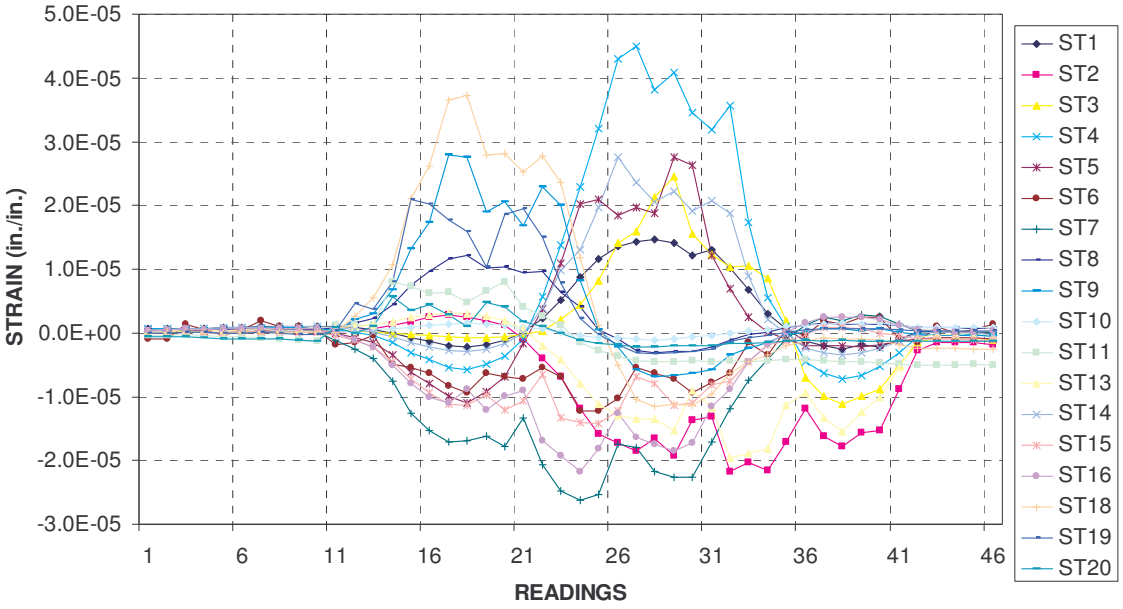

Figure 4.50 Quasi-static Loading: Path 1, East Bound – Girder Strain Level

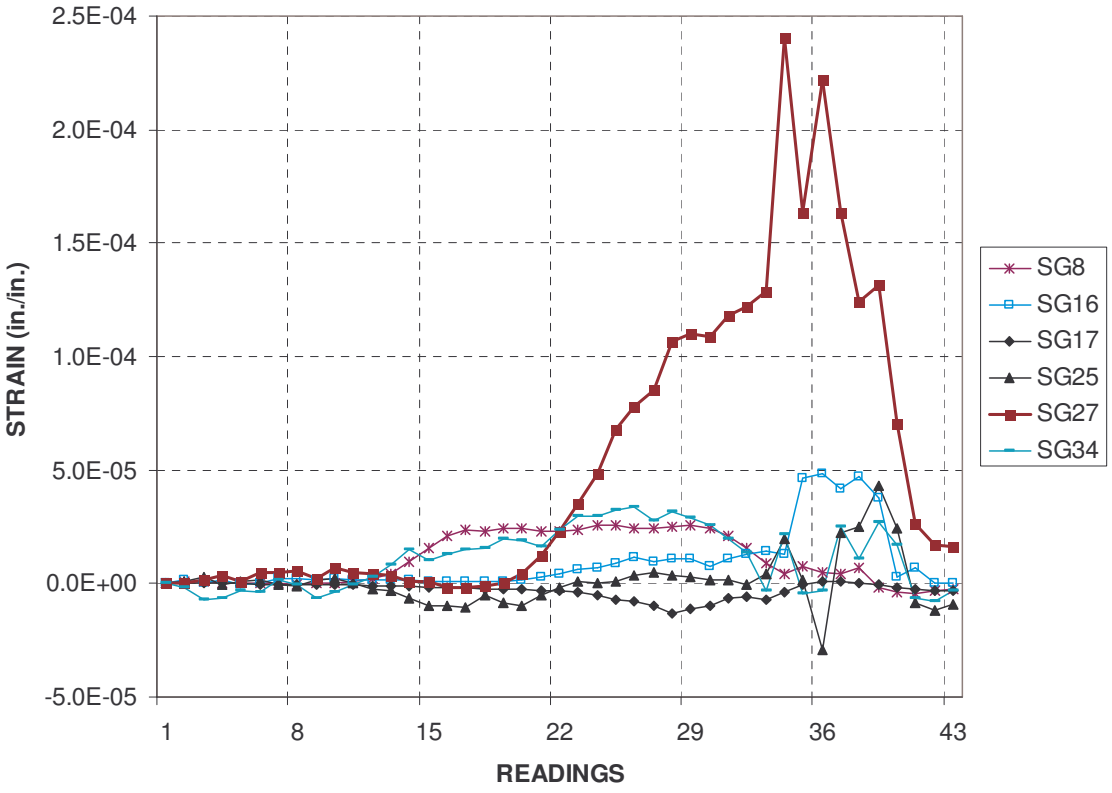

Figure 4.51 Quasi-static Loading: Path 4, East Bound – GFRP Rebar Strain

A live load distribution factor is used in design of bridge girders, which considers the amount of vehicular load distributed to each girder, taking into consideration girder spacing, girder and deck geometric properties, superstructure materials, etc... To determine this distribution factor through load testing, girder strain and/or deformation levels are being compared in the transverse direction.

As an example, Figure 4.52 shows the girder strain history throughout the 7 load paths (LP1-LP7), while the trucks were traveling West Bound. In this case, Span B is being investigated, where ST4, ST 14 and ST1 are located. However, the strain transducer ST12 located on girder 4 did not work properly, and its readings were substituted with the readings of ST10, as these were comparable (although somewhat smaller due to the shorter exterior spans) throughout the entire testing protocol. It is clear from this figure that during LP1, trucks traveling on top of girder 1, ST4 recorded the highest strain levels. On the other hand, during LP7 girder 4 was located directly under the truck loads, and ST10 recorded the highest strains.

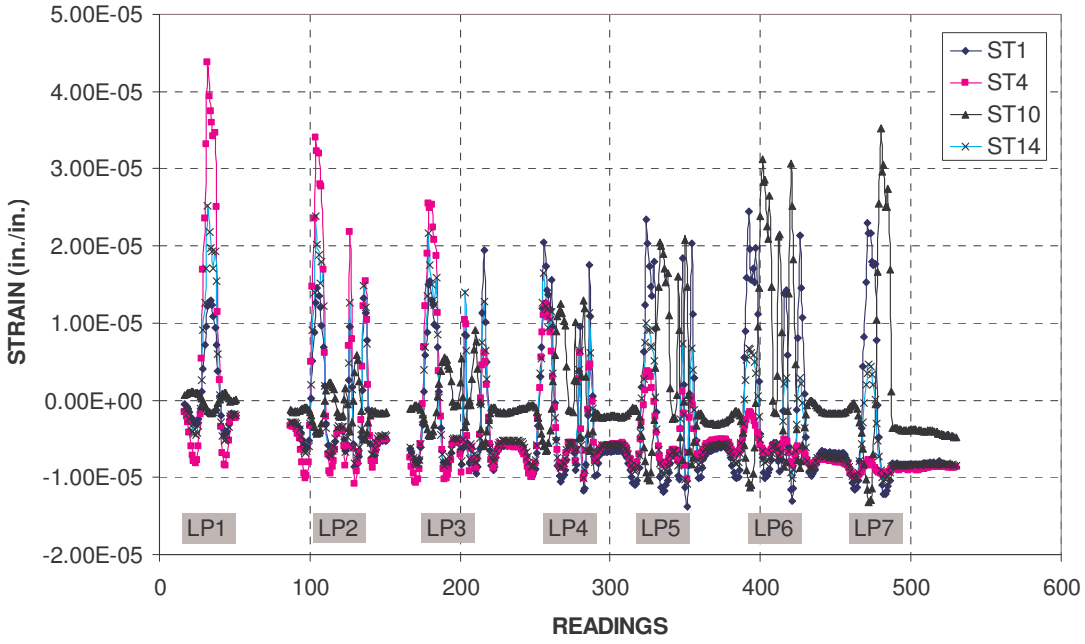

Figure 4.52 Quasi-static Loading: Paths 1-7, West Bound – Girder Strain

The peak strain values from Figure 4.52 were then used to determine the experimental distribution factors, with the aid of the equations developed by Stallings and Yoo (1999), and modified by Gergely et al. (2006) to account for only 2 wheel lines (i.e. one traffic lane occupied, instead of both). Table 4.1 summarizes the results of these calculations. As expected, the two exterior girders have higher distribution factors than the interior girders, and the values are comparable with the anticipated design distribution factors.

The same calculations were made using strain gage readings for the East Bound tests at the exterior spans, and as it can be seen from Table 4.2, the results are comparable with the previous table. During these analyses it was also clear that the displacement transducers did not produce accurate enough readings to perform meaningful calculations. Due to very low deformation levels, some of these transducers operated within the instrument's noise range.

Table 4.1 Distribution Factors – Strain Transducers (West Bound)

Load Path	Strain Readings (με)				Distribution Factors			
	ST4/G1	ST14/G2	ST1/G3	ST10/G4	G1	G2	G3	G4
1	44	25	12	-2	1.11	0.63	0.30	-0.05
2	37	27	19	7	0.82	0.60	0.42	0.16
3	32	28	21	10	0.70	0.62	0.46	0.22
4	18	20	27	14	0.46	0.51	0.68	0.35
5	10	16	30	23	0.25	0.41	0.76	0.58
6	3	14	31	34	0.07	0.34	0.76	0.83
7	-1	11	30	37	-0.03	0.26	0.78	0.96

Table 4.2 Distribution Factors – Strain Gages (East Bound)

Load Path	Strain Readings (με)				Distribution Factors			
	SG1/G1	SG14/G2	SG30/G3	SG35/G4	G1	G2	G3	G4
1	-24	-14	-9	-4	0.94	0.55	0.35	0.16
2	-17	-14	-9	-3	0.79	0.65	0.42	0.14
3	-15	-13	-13	-8	0.61	0.53	0.53	0.33
4	-10	-12	-14	-11	0.43	0.51	0.60	0.47
5	-7	-10	-13	-13	0.33	0.47	0.60	0.60
6	-2	-7	-15	-15	0.10	0.36	0.77	0.77
7	-1	-6	-14	-16	0.05	0.32	0.76	0.86

Current bridge design procedures require the use of an impact factor to account for the dynamic effects of vehicles traveling at the posted speed limit. This impact factor allows for a live load increase of up to 30%. Research showed that this value will depend on the many factors, among others: superstructure system and component material, wearing surface and approach slab condition, vertical and horizontal geometry of the bridge and connecting roadway. In addition to these factors, the dynamic effects determined through load testing will also be a function of the test vehicle's physical and geometric properties, such as axle and wheel base, load distribution, suspension stiffness, etc...

As it was mentioned earlier, in order to experimentally determine the impact factor, one fully loaded truck was used, first traveling at slow speed (to establish a baseline level), then at the legal speed limit. Table 4.3 summarizes the findings of the dynamic tests, using 7 strain transducers (ST1-ST7), 3 load paths (2, 4 and 6), and both East and West Bound directions. To capture peak effects, both compression and tension strain readings were considered. The largest impact factor was found to be 1.33 (or 33% increase), just over the design limit of 30%. However, it is clear from this table that the largest impact values were recorded mostly for smaller strain levels. When considering only the higher strain values, the impact factor decreases to 1.09, representing a 9% increase in live load effects.

Figures 4.53 and 4.54 show the strain readings for Load Path 6, West Bound, slow and dynamic loading: designated in Table 4.3 as LP6WS and LP6WD, respectively. Some of the readings are within the instruments noise level (about 2-3 με), however, the majority of the readings are at an expected strain level. It is also clear from these figures that 4 of the strain transducers were positioned at the interior span, the other three instruments were located at the exterior span.

Table 4.3 Impact Factors – Strain Transducers

Load Path	ST1		ST2		ST3		ST4		ST5		ST6		ST7	
	max	min	max	min	max	min	max	min	max	min	max	min	max	min
LP2ES	9	-25	12	-22	10	-15	8	-7	5	-27	4	-25	4	-18
LP2ED	7	-25	9	-24	8	-17	7	-8	6	-23	5	-19	4	-15
IMPACT	**0.78**	**1.00**	**0.75**	**1.09**	**0.80**	**1.13**	**0.88**	**1.14**	**1.20**	**0.85**	**1.25**	**0.76**	**1.00**	**0.83**
LP2WS	9	-23	10	-29	10	-14	9	-6	6	-33	5	-24	4	-14
LP2WD	6	-15	10	-16	8	-12	6	-8	7	-28	4	-23	4	-16
IMPACT	**0.67**	**0.65**	**1.00**	**0.55**	**0.80**	**0.86**	**0.67**	**1.33**	**1.17**	**0.85**	**0.80**	**0.96**	**1.00**	**1.14**
LP4ES	8	-23	10	-16	12	-24	11	-16	4	-16	4	-22	4	-26
LP4ED	8	-20	7	-14	9	-22	9	-17	4	-13	4	-18	5	-26
IMPACT	**1.00**	**0.87**	**0.70**	**0.88**	**0.75**	**0.92**	**0.82**	**1.06**	**1.00**	**0.81**	**1.00**	**0.82**	**1.25**	**1.00**
LP4WS	8	-21	8	-15	11	-21	10	-13	4	-15	5	-20	5	-24
LP4WD	8	-19	8	-12	11	-19	13	-14	4	-14	4	-20	5	-25
IMPACT	**1.00**	**0.90**	**1.00**	**0.80**	**1.00**	**0.90**	**1.30**	**1.08**	**1.00**	**0.93**	**0.80**	**1.00**	**1.00**	**1.04**
LP6ES	6	-14	6	-6	10	-25	11	-32	3	-5	4	-12	5	-28
LP6ED	5	-12	5	-7	8	-18	10	-21	3	-5	3	-12	4	-29
IMPACT	**0.83**	**0.86**	**0.83**	**1.17**	**0.80**	**0.72**	**0.91**	**0.66**	**1.00**	**1.00**	**0.75**	**1.00**	**0.80**	**1.04**
LP6WS	7	-15	7	-9	12	-24	13	-28	3	-6	4	-13	5	-28
LP6WD	6	-14	6	-6	10	-25	9	-29	3	-5	4	-11	6	-26
IMPACT	**0.86**	**0.93**	**0.86**	**0.67**	**0.83**	**1.04**	**0.69**	**1.04**	**1.00**	**0.83**	**1.00**	**0.85**	**1.20**	**0.93**

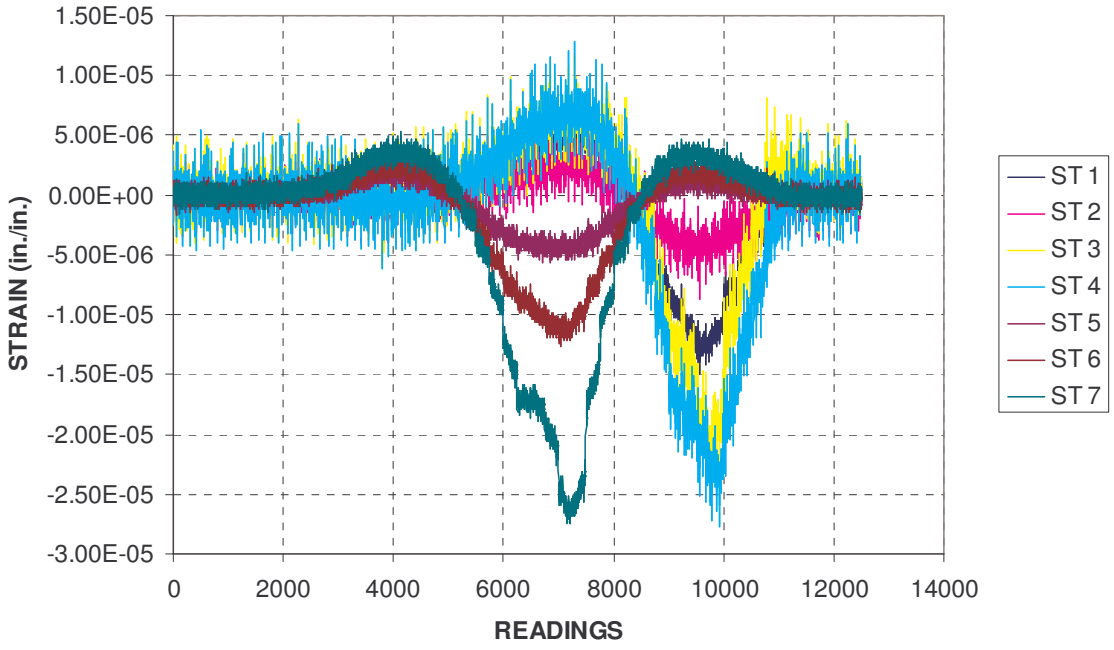

Figure 4.53 Dynamic Loading: Load Path 6, West Bound – Slow Speed

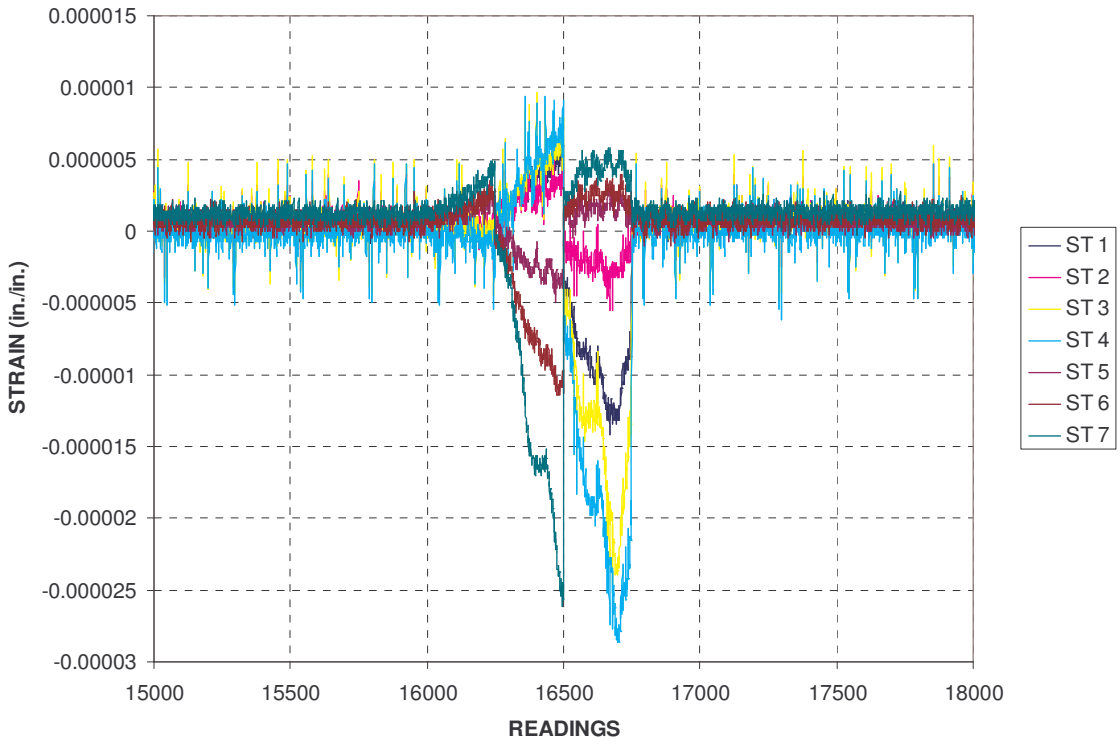

Figure 4.54 Dynamic Loading: Load Path 6, West Bound – High Speed

5. Durability Testing Materials

5.1 Concrete Mix Design

The design criterion of the concrete mix was to have a compressive strength of 5000 psi (34.5 MPa) with a desired water-to-cement ratio of 0.49 and a slump of 4″ (101.6 mm) (Ray, 2005). This ratio ensures that proper hydration can still occur (Somayaji, 2001) which is important for the chemical reaction needed in hydraulic cement. It was recommended by Ray (2005) that the w/c ratio be less than the 0.50 but higher than 0.45 to maintain a compressive design strength of 3500 to 4500 psi (Somayaji, 2001). The final mix design required 0.676 oz. (20 ml) of air entrainment of Master Builders, AE-90, for 2.0 ft^3 (0.074 yd^3) batch of concrete. Each mix was tested following ASTM guidelines (ASTM C231, 1999) utilizing a Type-B air meter before any specimens were created to ensure an air content of 6% ± 1%. The coarse aggregate was specified as a #78 pea gravel that has a maximum aggregate size of 3/8″ (9.525 mm). The fine aggregate was supplied by the rock quarry as being suitable for use in concrete and was termed as "screen washings." Both aggregates are granite in nature, thus accounting for the same specific gravity value of 2.8. These values along with the grain distribution for the fine aggregate are presented in Figure 5.1. The aggregates were oven-dried for 24 hours prior to the mix and then allowed to return to room temperature for at least one day to eliminate the need to measure moisture contents and adjust the required water for each mix.

Table 5.1 Material Properties of Coarse and Fine Aggregates

Coarse Aggregate		**Fine Aggregate**	
Max Size (in):	0.375	Fineness Modulus:	2.9
Specific Gravity:	2.8	Specific Gravity:	2.8
Absorption:	0.5%	Absorption:	0.9%
Moisture Content:	0.00%	Moisture Content:	0.00%

Concrete mixing followed ASTM guidelines (ASTM C192, 1999), in which the order of material placement is (1) the coarse aggregate and half of the water together with the air-

entraining admixture, (2) the fine aggregate, (3) the cement, and (4) the remaining water. The procedure used in determining the concrete mixing proportions is shown in Appendix D, where the final mixing ratio is 1C:1.16FA:1.13CA:0.49W.

Compressive concrete cylinder tests were conducted following ASTM guidelines to ensure that each batch maintained the desired uniformity in performances (ASTM C39, 1999).

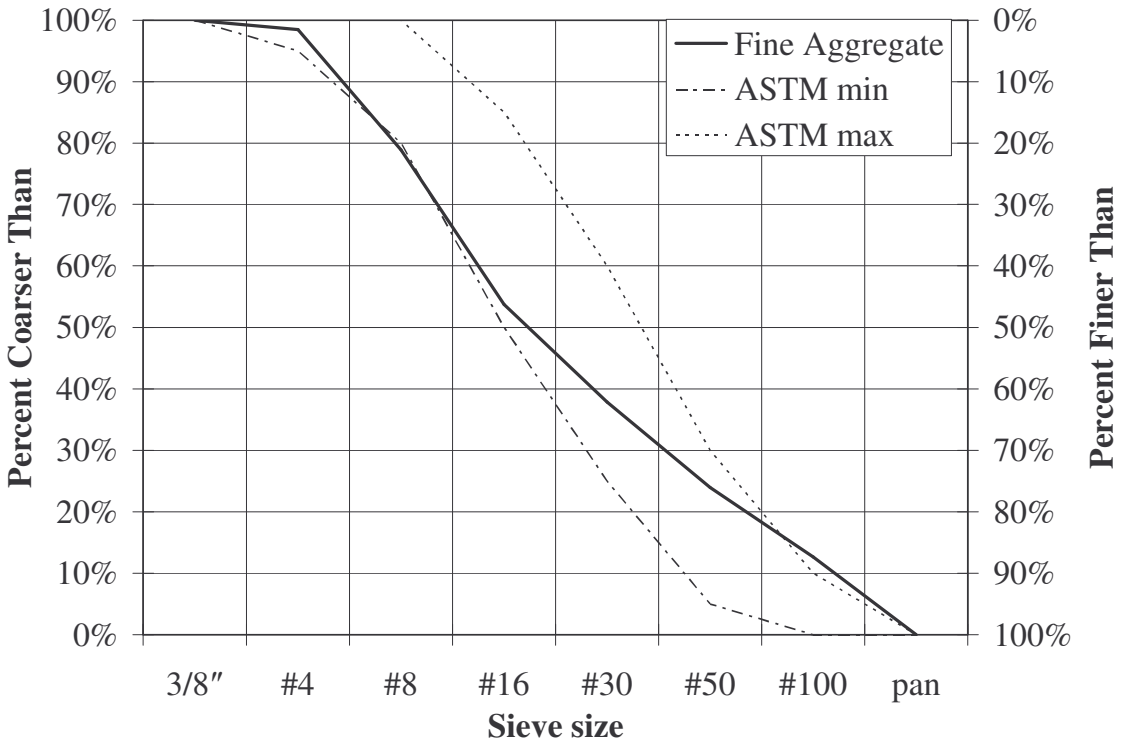

Figure 5.1 Grain Distribution of Fine Aggregate

The 4″ × 8″ (101.6 mm × 203.2 mm) tests cylinders have been shown to yield higher values than the standard 6″ × 12″ (152.4 mm × 304.8 mm) cylinders (Somayaji, 2001). The cylinder tests used for this research program confirmed slightly higher average compressive strengths as expected –24% higher relative to a target value of 5000 psi (34.5 MPa) at 6200 psi (42.75 MPa) (Somayaji, 2001).

5.2 Bond-Slip Test Specimens

The concrete samples made with the designed mix were utilized as the substrate in the bond-slip specimens. The substrate has a cylindrical cross-section of a standard 6″ × 12″ (152.4 mm × 304.8 mm) compression test specimen. This substrate specimen was recommended by NCDOT officials and is similar to that seen in the research conducted by Tastani and Pantazopoulou (2002) and Vijay (1999). While ACI 440 (2004) recommends the bond-slip specimens to be of a rectangular prism with dimensions of 7.875″ × 7.875″ × 7.875″ (200 mm × 200 mm × 200 mm), due to simplicity, and with the number of specimens to be tested, a cylindrical cross section specimen was selected.

5.2.1 Un-reinforced Pullout Specimen

Figure 5.2 shows a representation of the un-reinforced pullout specimen, where the anchorage system is an 8″ (203.2 mm) steel pipe with expansive grout as the filler; the remaining 19″ (483 mm) being exposed with no additional confinement around the GFRP bar. This test setup was used for the non-exposed specimens (dry conditions). The following section discusses the reasoning behind use of the reinforced specimen and the procedure implemented.

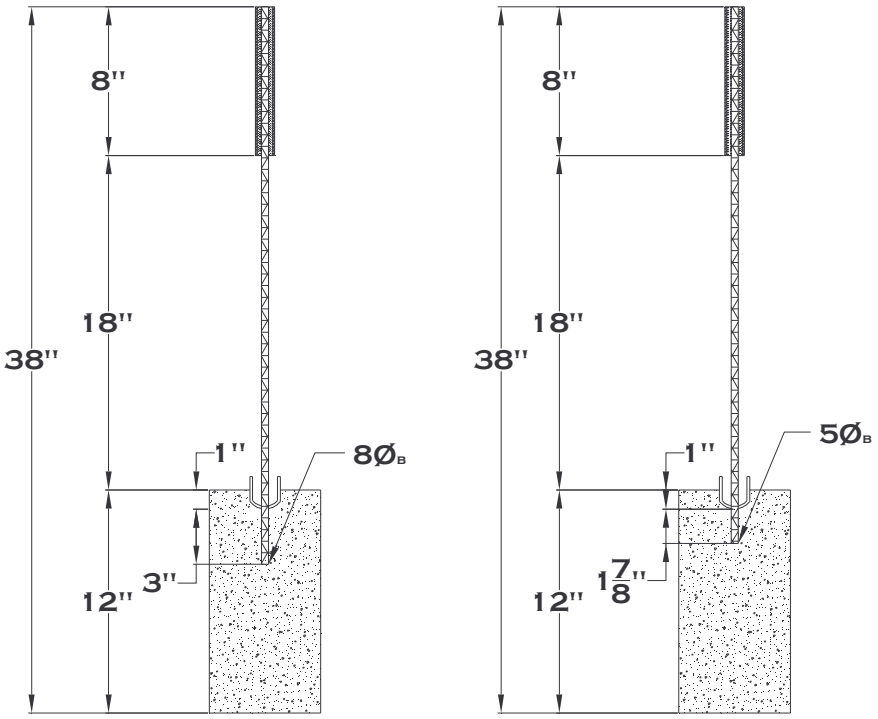

Figure 5.2 Bond-Slip Substrate Dimensions

5.2.2 Reinforced Pullout Specimen

Upon removal of the pullout specimens from the processing tanks at the 6 month duration period, it was noticed that the exposed segment of rebars had themselves degraded due to exposure to the harsh environments. A method was therefore conceived to preserve the rebars for pullout testing in order to prevent failure from occurring within the exposed segment of the rebar itself. In this procedure, a steel pipe protectant sleeve was fitted over the entire length of the expose rebar with an epoxy filler within the PVC cap to prevent any bearing stress on the GFRP member during loading. Then a grout filler, similar to that as used for the preparation of the tensile specimens, was used to create a bond between the steel pipe and the exposed segment of rebar (see Figure 5.3).

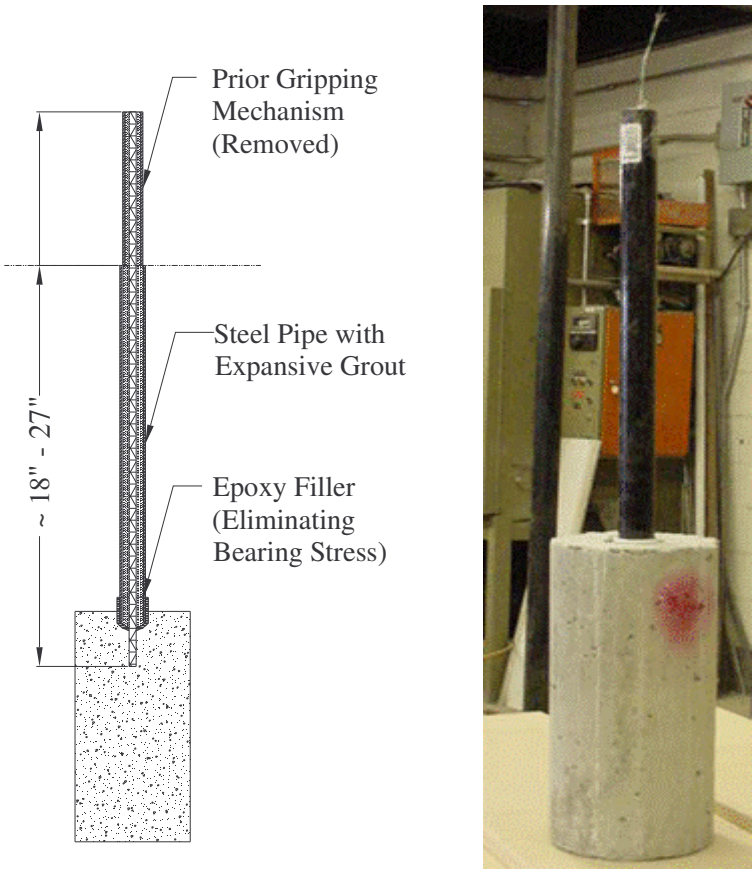

Figure 5.3 Bond-Slip Reinforced Substrate

In order to measure the elongation of the rod, a strain gage was attached at approximately the mid section of the GFRP rebar. The procedure used in the application of the strain gage can be found in Appendix E. The test setup that was used in measuring the slip of the GFRP bar during the pullout tests can be seen in Figures 5.4 to Figure 5.5.

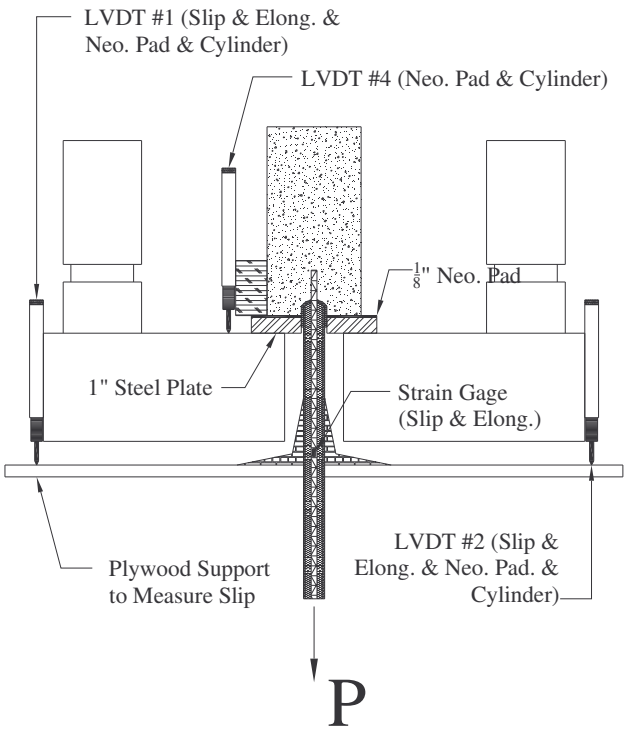

Figure 5.4 AutoCAD Drawing Representation of Pullout Test Setup

Figure 5.5 Actual Pullout Test Setup within UTM at UNC Charlotte

5.3 Glass Fiber Reinforced Polymer (GFRP) Rebar Material Properties

The GFRP rebar used in the testing of absorption, tensile, and bond-slip specimens were supplied by four different manufactures. Currently, Concrete Protection Products Inc. (Pultrall) and Hughes Brothers are nationally known for their research and consequent GFRP application in concrete decks and reinforced masonry walls. At the time of this project, Hughes Brothers donated rebar for the laboratory testing of a small span bridge deck and supplied the reinforcement for the concrete bridge deck constructed in Macon County. Other rebar manufacturers, Kodiak and Tillco, also supplied materials to support this project.

5.3.1 Concrete Protection Products Inc. (Pultrall)

Concrete Protection Products, Inc. (CPPI) is a concrete rebar fabricator/distributor specializing in glass and carbon fiber reinforced polymer (FRP) composite rebars for reinforcing concrete structures. They are well known for GFRP research and applications to reinforce concrete decks and masonry walls.

CPPI operates out of their sales office in Dallas, Texas, and currently has a fabrication/ distribution facility in Greensboro, North Carolina. CPPI also offers the following assistance to designers and contractors interested in using composite rebars in their projects:

- Large Inventory of Material
- Custom Lengths & Shapes of FRP Rebar
- Application Assistance
- Design Assistance
- Detailed Quotations
- Ship Anywhere in the World

CPPI exclusively represents the V-ROD® composite rebar product line manufactured by Pultrall, Division of ADS Composites Group, Inc. Rebars are currently available in the

following sizes and dimensions: #2 (1/4 inch), #3 (3/8 inch), #4 (1/2 inch), #5 (5/8 inch), #6 (3/4 inch) and #8 (1 inch). The rebar is available either straight or in factory bent configurations. CPPI's rebars come in standard lengths of 10 and 20 feet, although custom lengths from 1 to 50 feet are available. All normal and custom bent shapes are available in all bar diameters. CPPI donated 13 #3 bars in 20 foot lengths for this project.

V-ROD® rebars are composed of a state-of-the-art urethane modified vinylester resin reinforced with specially developed corrosion resistant glass fibers. All products are produced in an ISO 9002 certified production facility. Table 5.2 displays the physical and mechanical properties of these GFRP rebar sizes #2 through #8 (CPPI, 2005). The #3 GFRP rebar was used on this project.

Table 5.2 Physical and Mechanical Properties of CPPI (Pultrall) GFRP Bars

PHYSICAL PROPERTY		#2	#3	#4	#5	#6	#8
Nominal Size		1/4	3/8	1/2	5/8	3/4	1
	mm	#6	#10	#13	#16	#19	#25
Nominal Diameter	in	0.25	0.375	0.5	0.625	0.75	1
	mm	6.35	9.53	12.7	15.88	19.05	25.4
Cross-sectional Area	in^2	0.049	0.11	0.196	0.307	0.442	0.785
	mm^2	31.7	71.3	126.7	197.9	285.1	506.7
Weight	lb/lin ft	0.052	0.113	0.182	0.286	0.413	0.733
	g/m	77.4	168.4	271.4	425	614.4	1090.1
Glass Content	% wt	77.1	77.4	77.9	77.8	78.3	78.2
	% vol	59.1	59.6	60.3	60.1	60.8	60.7
MECHANICAL ROPERTY		#2	#3	#4	#5	#6	#8
Nominal tensile strength	MPa	873	852	788	761	730	665
	ksi	127	123	114	110	106	96
Guaranteed Design Tensile Strength[1]	MPa	784	765	708	683	656	597
	ksi	114	111	103	99	95	87
Nominal Tensile Modulus	GPa	46.5	43.2	43.9	46.7	46.1	41.9
	ksi	6739	6261	6362	6768	6681	6073
Tensile Strain	%	1.88	1.97	1.79	1.63	1.58	1.59
Poisson's Ratio[2]	---	0.25	0.21	0.26	0.25	0.25	0.28
Development Length	mm	226	298	369	443	511	655
	inch	8.9	11.7	14.5	17.5	20.1	25.8
Ratio of Modulus of Elasticity to Strength	---	53.3	50.7	55.7	61.4	63.2	63
Nominal Compressive Strength	MPa	553	538	463	443	528	505
	ksi	80	78	67	64	77	73
Nominal Flexural Strength	MPa	996	929	842	784	707	655
	ksi	144	135	122	114	102	95
Nominal Flexural Modulus	GPa	52.9	49.5	44.5	41.9	47.3	46.7
	ksi	7667	7174	6449	6072	6855	6768
Flexural Strain	%	1.88	1.88	1.89	1.87	1.49	1.4
Nominal Shear Strength	MPa	225	183	220	199	204	206
	ksi	33	27	32	29	30	30
Bond Stress	MPa	14.8	15.1	14.1	15.2	14.8	14.8
	psi	2145	2188	2043	2203	2145	2145
Longitudinal Coefficient of Thermal Expansion	per $^{\circ}$C	5.9×10^{-6}	5.5×10^{-6}	5.5×10^{-6}	6.4×10^{-6}	6×10^{-6}	6.1×10^{-6}
	per $^{\circ}$F	3.2×10^{-6}	3×10^{-6}	3×10^{-6}	3.5×10^{-6}	3.3×10^{-6}	3.4×10^{-6}
Transverse Coefficient of Thermal Expansion	per $^{\circ}$C	36.1×10^{-6}	37×10^{-6}	36×10^{-6}	35×10^{-6}	37×10^{-6}	35.4×10^{-6}
	per $^{\circ}$F	20×10^{-6}	20.5×10^{-6}	20×10^{-6}	19.4×10^{-6}	20.5×10^{-6}	19.7×10^{-6}
Moisture Absorption	%	0.65	0.47	0.38	0.42	0.21	0.17

5.3.2 Hughes Brothers

Hughes Brothers is located in Seward, Nebraska and was founded in 1921. The focus of their production centers around wood products such as crossarms, braces, wood guy guards, and ground wire molding. In the 1940's, Hughes Brothers expanded into developing pole line hardware and custom manufactured metal fittings and parts. Today, they manufacture wood, metal and fiberglass products and are also well known for their GFRP research and applications in reinforcing concrete decks and masonry walls. Table 5.3 displays the physical and mechanical properties of these GFRP bars ranging from #2 to #10 (Hughes Brothers – 2005). Hughes Brothers donated 20 #3 bars at 13 foot lengths to this project along with the required reinforcement for the testing of the full-scale bridge deck, in the lateral direction, conducted in the UNC Charlotte structures laboratory.

Table 5.3 Physical and Mechanical Properties of Hughes Brothers GFRP Bars

Bar Size		Cross Sectional Area		Nominal Diameter		Guaranteed Tensile Strength		Tensile Modulus of Elasticity	
(mm)	(in)	(mm^2)	(in^2)	(mm)	(in)	(MPa)	(ksi)	(GPa)	(psi × 10^6)
6	#2	33.23	0.0515	6.35	0.250	825	120	40.8	5.92
9	#3	84.32	0.1307	9.53	0.375	760	110	40.8	5.92
13	#4	144.85	0.2245	12.70	0.500	690	100	40.8	5.92
16	#5	217.56	0.3372	15.88	0.625	655	95	40.8	5.92
19	#6	295.50	0.4580	19.05	0.750	620	90	40.8	5.92
22	#7	382.73	0.5932	22.23	0.875	586	85	40.8	5.92
25	#8	537.90	0.8337	25.40	1.000	550	80	40.8	5.92
29	#9	645.00	1.0000	28.65	1.230	517	75	40.8	5.92
32	#10	807.34	1.2513	31.75	1.250	480	70	40.8	5.92

5.3.3 Kodiak

International Grating, Inc. (trade name Kodiak) GFRP rebar is made by the pultrusion process where the strands are soaked in resin and pulled through a die that removes the excess resin. To produce the deformed surface that is similar to that found on the traditional steel reinforcement rods, additional bands of glass fibers are wrapped around the strands. The final procedure is to heat cure the rebar and cut it to length (Boyd, 1997).

The material properties of Kodiak's GFRP #3 rebar are 77 ksi (530.9 MPa) for yield strength, 100 ksi (689.5 MPa) for ultimate strength, and a modulus of elasticity of 6.7×10^6 psi (46.2 GPa) (Boyd, 1997). Kodiak donated 20 #3 bars at 13 foot lengths to this project.

5.3.4 Tillco

Tillco is located in Marshall, Arkansas and was established in 1984. Tillco operates as a producer of fiberglass reinforced plastics with three specific forms of FRP rebar manufacturing:

- Open mold lay-up - for highly corrosive environments
- Pultrusion - for higher strength applications
- Fabrication - using pultrusions to customer specifications

The open mold lay-up rebar used to be their sole product, with pultrusion capabilities added afterwards. In 1996, Tillco purchased Marshall Vega Corporation, who had begun manufacturing FRP rebar in 1974.

The Tillco FRP material is a composite consisting of a cross-linking polymer resin matrix reinforced by continuous glass filaments in a reinforcement-to-matrix ratio of 70:30 percent by weight. Fiberglass roving is drawn into a tank of thermosetting plastic resin where saturation takes place. The roving is then drawn through an orifice equal in diameter to the glass-to-resin ratio of 70:30. A spiral winding is applied to the member which is cured continuously, producing a void-free, corrosion-resistant matrix that bonds and protects the glass fibers (Tillco, 2005).

From Tillco's website, the minimum tensile strength of the FRP bars is listed as 140 ksi (965.3 MPa), with a tensile modulus of 7.86×10^6 psi (54.2 GPa) and a coefficient of thermal expansion of 5.5×10^{-6} per °F (3.0×10^{-6} per °C). Tillco donated 28 #3 bars at 13 foot lengths to this project.

5.4 Steel-Grouted Tabs

For the gripping mechanism for the tensile and bond-slip specimens, an 8″ to 10″, ¾″ diameter steel pipe (outside diameter 1.005″) was used with an expansive grout (see next subsection) as the bond mechanism.

5.4.1 Expansive Grout

A grouting system, Bristar 100, was used to form a bond between the steel tabs and the rebars to serve as a grip-mechanism for tensile testing in the UTM. Bristar 100 is primarily used as a destructive agent in the demolition of rock and reinforced concrete. Bristar is a powder consisting of silicate type inorganic compound and an organic compound. When Bristar 100 is mixed with the appropriate quantity of water and poured into a cylindrical hole that is drilled into either the rock or concrete, the grout hardens and consequently expands, thus initiating fracture of the rock or concrete for easy removal. Bristar 100 has an expansive stress of more than 8530 psi (6000 t/m^2); however, DTI (Demolition Technologies Inc.) states that there is little change in the stress when the water ratio is ± 30%, but it decreases as the water ratio is either increased or decreased. The recommendation to use Bristar 100 was made by Mr. Gremmel of Hughes Brothers, who has specialized in the testing of GFRP rebars. Based on DTI supplied information, once Bristar 100 is poured into a hole, the Bristar expands and thus exerts its strength (in approximately six hours) creating a high degree of frictional resistance to the inner surface of the hole. The expansive stress along the hole depth is almost constant except near its entrance due to contact with air (DTI, 2005).

5.4.2 Epoxy Resin

The Sikadur 300 is a two-component high strength, and high modulus epoxy used as an impregnating resin to bond the SikaWrap composite Structural Strengthening System for horizontal and vertical applications (Sikadur 300 Handout, 2006). The two parts of the Sikadur 300 consists of: Component A – epoxy resin, and Component B – amines. The

Component A : Component B ratio of the system is 1:3.14; material properties of the epoxy resin are presented in Table 5.4.

Table 5.4 Material Properties of Sikadur 300 Impregnating Resin

Viscosity	Elongation at Break	Tensile Strength		Tensile Modulus		Flexural Strength		Flexural Modulus	
		(MPa)	(ksi)	(MPa)	(ksi)	(MPa)	(ksi)	(MPa)	(ksi)
500 cps	3 %	55	8	1,724	250	79	11.5	3,450	500

5.4.3 Schedule 40 Steel Pipe

During initial testing, it was determined that the PVC pipe would not be adequate to sustain the expansive strength of the Bristar 100 grout. Therefore, after consulting Mr. Gremmel's anchorage potting procedure for #3 GFRP rebar, it was determined that schedule 40 steel pipe could be used as the anchorage system. Two different sizes were used: ¾″ diameter for the tensile testing of GFRP rebar and 1″ diameter for the bond-slip structural strengthening method. The properties of the schedule 40 steel pipe is shown in Table 5.5.

Table 5.5 Material Properties of Schedule 40 Steel Pipe

Pipe Diameter (inches)	Diameter		Nominal Thickness (in)	Transverse Areas (in^2)			Weight	
	External	Internal		External	Internal	Steel	(lb/ft)	(kg/m)
¾	1.05	0.82	0.11	0.87	0.53	0.33	1.13	1.68
1	1.32	1.05	0.13	1.36	0.86	0.49	1.68	2.5

5.5 Measuring Devices

Elongations and strains within the GFRP were measured through the use of an extensometer and strategically placed strain gages. The extensometer was used to measure the strain in the longitudinal direction of the tensile test specimens. The strain

gages were used on the pullout tests to determine any elongation of the bar that would be taken into account for the measuring of the slippage of the rebar embedded in the concrete.

5.5.1 Model 3543 Long Gage Length Extensometer

The model 3543 long gage length extensometer was used to be within the specifications that the gage length should not be less than eight times the diameter of the FRP rebar and the distance from the anchorage should be at least eight times the diameter (ACI 440.3R, 2004), which is approximately 3″ (76.2 mm) in this case. A gage length of 8″ was used during tensile testing within the UTM (4″ (101.6 mm) from the center of the specimen and 3.5″ (88.9 mm) from the anchorage as shown in Figure 5.6).

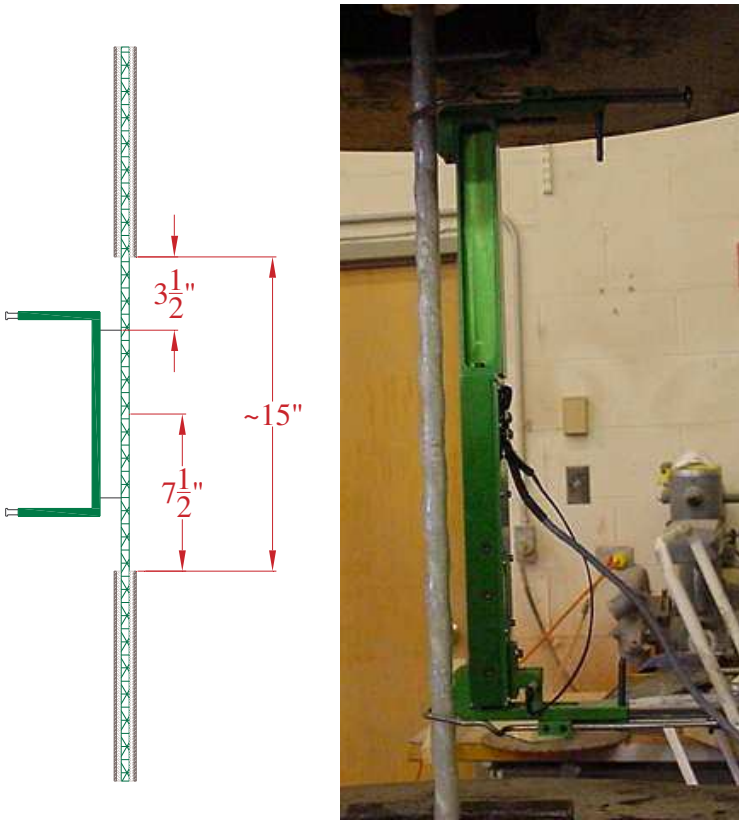

Figure 5.6 Schematic and Picture of Specimen with Actual Tensile Test Setup

The extensometers used are 350 ohm strain gages which are compatible with nearly any test system meeting ASTM Class B-2 requirements for accuracy and are ideal for the testing of steel rebars and GFRP rebars.

5.5.2 Vishay Micro-Measurements 250BG General Purpose Strain Gage

The strain gage that was used in determining the elongation of the bond-slip specimen was a Vishay Micro-Measurements 250G general purpose strain gage in the gage series of EA. The strain gage has a resistance of 120 ± 0.3% Ohms, with a gage length of 0.25″ (6.35 mm) and an overall width of 0.125″ (3.175 mm). Further details regarding the application of the strain gage are given in Appendix F. Figure 5.7 shows a representation of the strain gages used during application.

Figure 5.7 Strain Gages used to measure elongation of GFRP Rebar

6. Durability Testing Procedures

6.1 pH Calibration & Data

A pH range of between of 12.5 to 13.2 (with practical concentration being between 12.8 to 13.0) was requested in order to simulate the alkalinity of the concrete environment. The recommended starting ratio for sodium hydroxide (NaOH), potassium hydroxide (KOH), and calcium hydroxide ($Ca(OH)_2$) was 0.5 NaOH, 1.0 KOH, and 0.03 $Ca(OH)_2$.

Previous research produced a pH chemical ratio that was used for an alkaline environment in the testing of GFRP rebar, as stated earlier by Dr. Ray (2005). To determine the amounts of NaOH, KOH, and $Ca(OH)_2$ that would be needed for the 100 gallon processing tanks, smaller tests were conducted in the UNC Charlotte Environmental Lab. Upon completion of the tests, a new ratio was determined to be: 0.5 NaOH, 1.0 KOH, and 0.04 $Ca(OH)_2$.

Before the chemicals were placed into the tanks, the chambers were first filled with water and then brought up to their specified temperatures. To ensure that the pH level was within the requested range, chemicals were added proportionately to obtain a new chemical ratio of: 0.6 NaOH, 1.0 KOH, and 0.1 $Ca(OH)_2$. This provided a pH environment of 12.8 to 12.9 within the tanks.

The absorption, tensile, and bond-slip specimens were distributed into their corresponding chambers as requested by the NCDOT. Readings of pH and temperature were then taken on a daily basis in the initial stages to ensure the proper pH level. During the first 22.5 days, the pH level was observed to fluctuate. To determine the cause of this change in the tanks, temperature readings were taken at Day 25.5 to see if a change in tank temperature might cause differences in the pH levels. Figures showing the monitoring of pH and temperature levels can be found in Appendix F. This late development explains why the temperature is not plotted in Figures F.1, F.2, and F.3.

It should be noted that for the 100 and 130 durability chambers, at the 180 and 365 day duration, one chamber from each chart is not shown because these chambers were turned off in order to optimize the space and chambers being used. During testing, several of the heaters had either over heated or were no longer functional. Therefore, the pullout specimens were moved into operating chambers and the non-functional chambers were no longer monitored.

Table 6.1 Average Temperature & pH Level over 540 Days

Chamber Description (°F)	Chamber No.	Average Temp.	Average pH
74	#1	72.3	13.0
74	#2	72.7	12.9
100	#3	99.0	12.5
100	#4	103.3	12.4
100	#5	105.8	12.4
100	#6	106.4	12.3
130	#7	133.4	11.9
130	#8	134.3	11.9
130	#9	135.7	12.0
130	#10	129.5	12.2

As Table 6.1 shows, the average temperatures are within the targeted values; the same is true of the pH levels with the exception of the 130°F durability chambers. For this reason, a mixer was used to agitate the settled $Ca(OH)_2$ crystals to determine if this would bring up the pH level. The mixing produced the same results as with no mixing.

7. Durability Testing of GFRP Bars

Three series of tests were conducted on two scenarios of GFRP rebar under four different environments (Dry, Alkaline at Room Temperature, Alkaline at 100°F, and Alkaline at 130°F). Two absorption tests were conducted (initial and general) on 2″ (50.8 mm) specimens exposed to the four simulated environments. The reasoning behind the two absorptions tests is during the initial testing, the method of measuring was changed in the middle of testing, therefore altering the results. A more defined method of taking measurements was determined, providing a more "general" result in the absorption results. Tensile testing was conducted on 35″ (889 mm), two unscathed specimens and one nicked sample, which were exposed to the same environments as the initial absorption specimens. Bond-stress testing was conducted on specimens with 1.875″ and 3.0″ (47.625 mm and 76.2 mm) development lengths, which were exposed to similar environments as the absorption and tensile specimens. After completing the bond-stress tests, compressive and modulus testing was conducted on the concrete cylinders. Although this was not asked for by the NCDOT, the results are furnished as additional information.

7.1 Absorption Testing – Initial Findings

The absorption specimens were placed in the same tanks that contained the tensile specimens. This placement allowed for a correlation to be made between these two types of specimens. A description of the preparation of the absorption specimens, unscathed and nicked, is presented in Section 7.1.1 of this report.

7.1.1 Preparation of Absorption Specimens

The procedure for the preparation of the absorption specimens was a novel concept as was the procedure to "nick" the GFRP rebar specimens for placement into the durability chambers, as described below.

Two types of specimens were selected for the absorption studies: nicked and unscathed GFRP rebars. The unscathed specimens were selected to determine the durability of the rebar having the full benefit of the epoxy coating on the surface and at the ends while being subjected to an alkaline solution at different temperature environments. The nicked specimens, on the other hand, were considered to evaluate the potential durability of these rebars under conditions similar to those encountered in the field in which a defect arising from the construction site might compromise the integrity of these reinforcing elements.

The rebars with the imposed artificial defect were nicked at the approximate midlength of the test specimen and at a depth ranging between .0625″ to .1250″ (1.588 mm to 3.175 mm) from the surface. The rebar was nicked by using an air-compressed grinder wheel that was approximately .045″ (1.143 mm) in thickness. A micrometer was used to ensure that a proper depth was maintained during the nicking process. The absorption test specimens were prepared at nominal two inch lengths, with a range between 1.875″ to 2.25″ (47.625 mm to 57.15 mm). The ends of the rebars were coated with epoxy in order to gage absorption through the rebar surface alone, similar to that of Vijay's dissertation (1999).

7.1.2 Changes in Length

Original length measurements were taken prior to placing the specimens in the chamber. This established a baseline for the moisture uptake in the rebar with respect to time. During the initial findings for change in length, it should be noted that only one initial length measurement was taken from Day 0.0 to 28.0. After Day 28.0, three length measurements were taken and averaged. Any negative values resulting from measurement discrepancies were excluded from the averaging and subsequent reporting. Also noteworthy is the fact that the dry specimens did not show any change in length or weight (length change and moisture content figures for the dry specimens have not been included in this report). The results of these measurements are shown for unscathed and nicked specimens in Figures 7.1 to 7.6. Table 7.1 summarizes and compares results from

unscathed and nicked samples.

Table 7.1 Average % Length Changes for Unscathed & Nicked Specimens

Samples	Temperature	Duration							
		3 Days	5 Days	10 Days	45 Days	90 Days	180 Days	365 Days	540 Days
Unscathed	RT	2.9	2.9	3.2	4.2	4.2	4.5	4.4	4.6
	100°F	2.8	2.6	2.4	3.0	3.2	3.6	3.2	3.4
	130°F	2.2	2.2	2.5	3.0	3.0	2.9	2.7	2.7
Nicked	RT	0.8	0.8	0.7	0.6	0.7	0.8	0.5	0.5
	100°F	0.9	0.7	0.8	0.7	0.8	0.8	0.5	0.5
	130°F	1.2	1.0	0.9	0.9	0.9	0.7	0.7	0.6

For both unscathed and nicked samples at all temperatures, the largest length gains occur initially at up to 3 days, and then decreased to ~ 10 days, and then increased again, slowly and steadily, up to 180 days, expect for the nicked specimens which show a very significant decrease to 90 days. After 90 days, the nicked specimens experienced a slight increase. At 365 days, the nicked samples experienced a noteworthy decrease. This was likely been due to a change in material properties of the specimens during the duration in the tanks along with a deterioration of the epoxy ends of the specimens while in the alkaline solution, as also corroborated from the visual observations of the specimens.

From the following figures, one common trend that can be recognized is that all the specimens encountered a dramatic spike in moisture uptake. The most likely reason for this sudden increase could be due to the sudden placement of the specimens into the designated tanks for which the material properties of the glass fibers and resin matrix encountered and had to adapt to the new environment. After a duration of approximately 30 days or less, the samples were then able to adjust to the new conditions and the moisture uptake was found to stabilize. From Figures 7.1 and 7.3 it can be assumed from the trends of the Kodiak bars than an inferior surface coating was applied to these specimens based on these rebars having the highest moisture uptake as compared to those from the other vendors. In this manner, the Tillco rebars, although not as high as those of the Kodiak rebars, demonstrated still a higher moisture uptake as compared to the rebars furnished from Hughes Bros. and Pultrall, both of which seemed to have similar

moisture uptake characteristics. The reason for some of the dramatic decreases in length changes could be due tin part to the epoxy coating deteriorating at the ends. The other possibility could be due to the change and loss of material properties; this was especially true for the Kodiak rebars as further elaborated on in the following subsection.

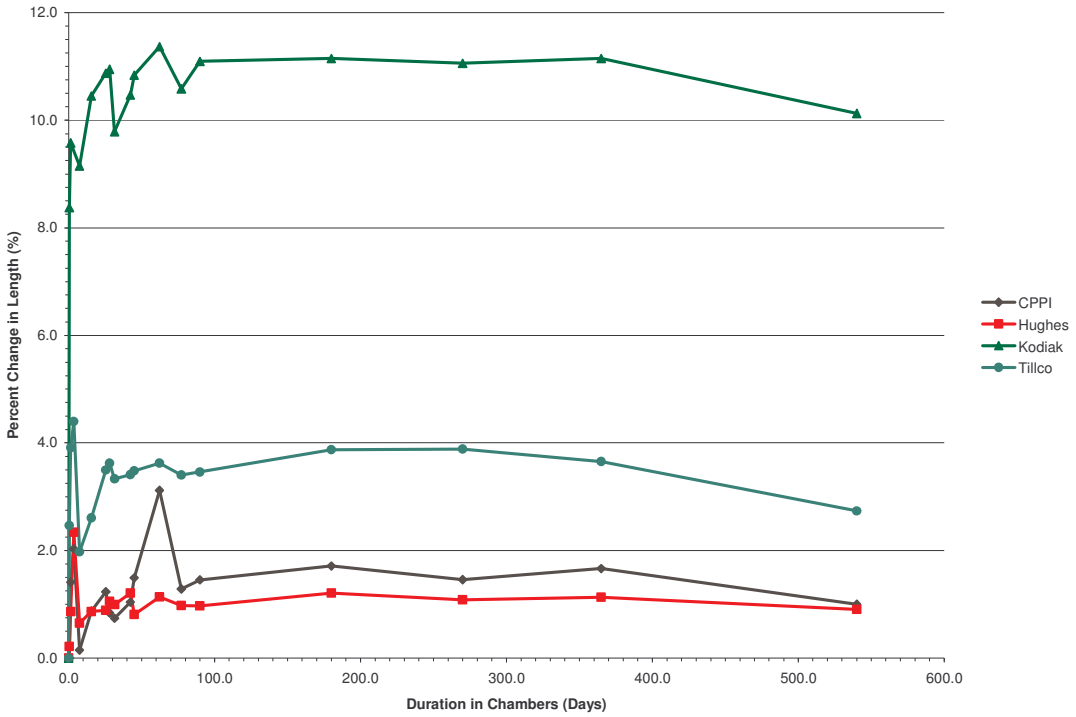

Figure 7.1 Extensional Effects Due to Moisture Uptake of Unscathed Specimens at Room Temperature

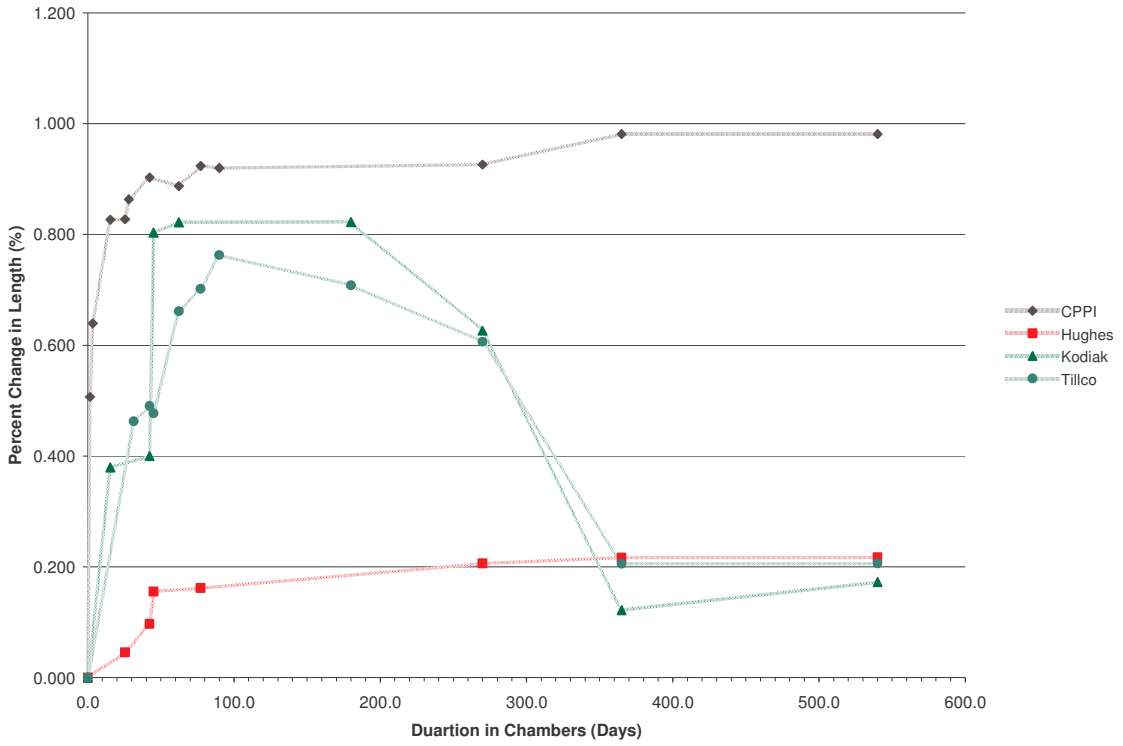

Figure 7.2 Extensional Effects Due to Moisture Uptake of Nicked Specimens at Room Temperature

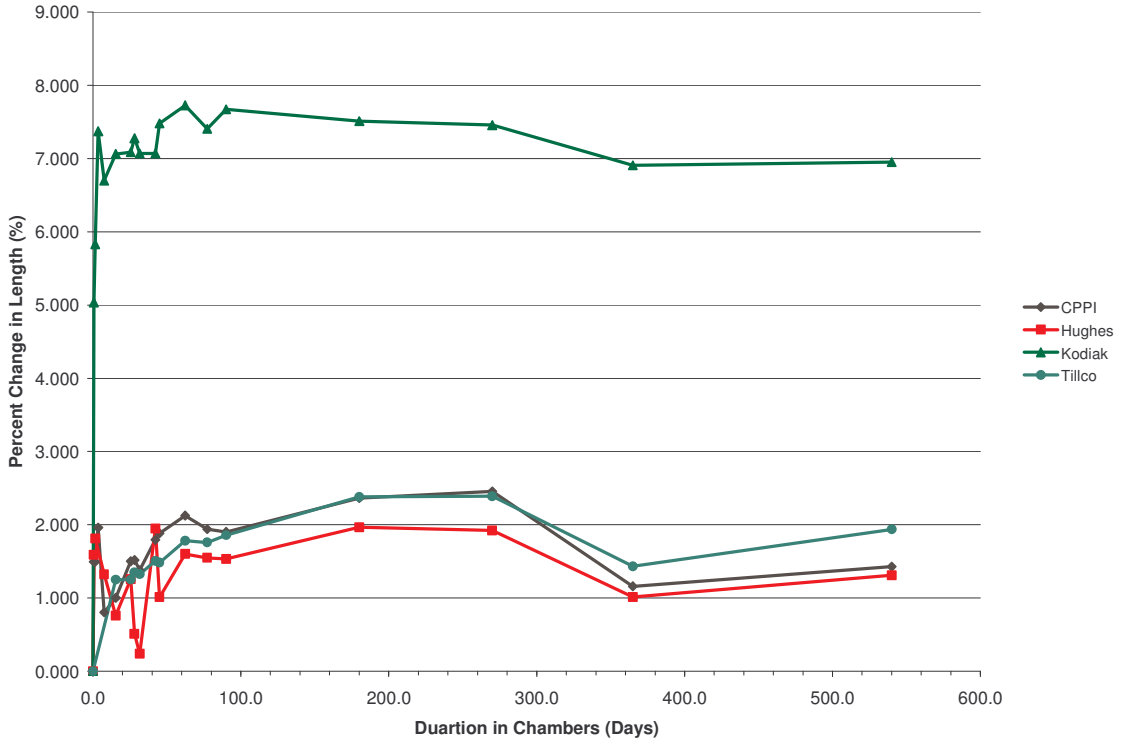

Figure 7.3 Extensional Effects Due to Moisture Uptake of Unscathed Specimens at 100°F

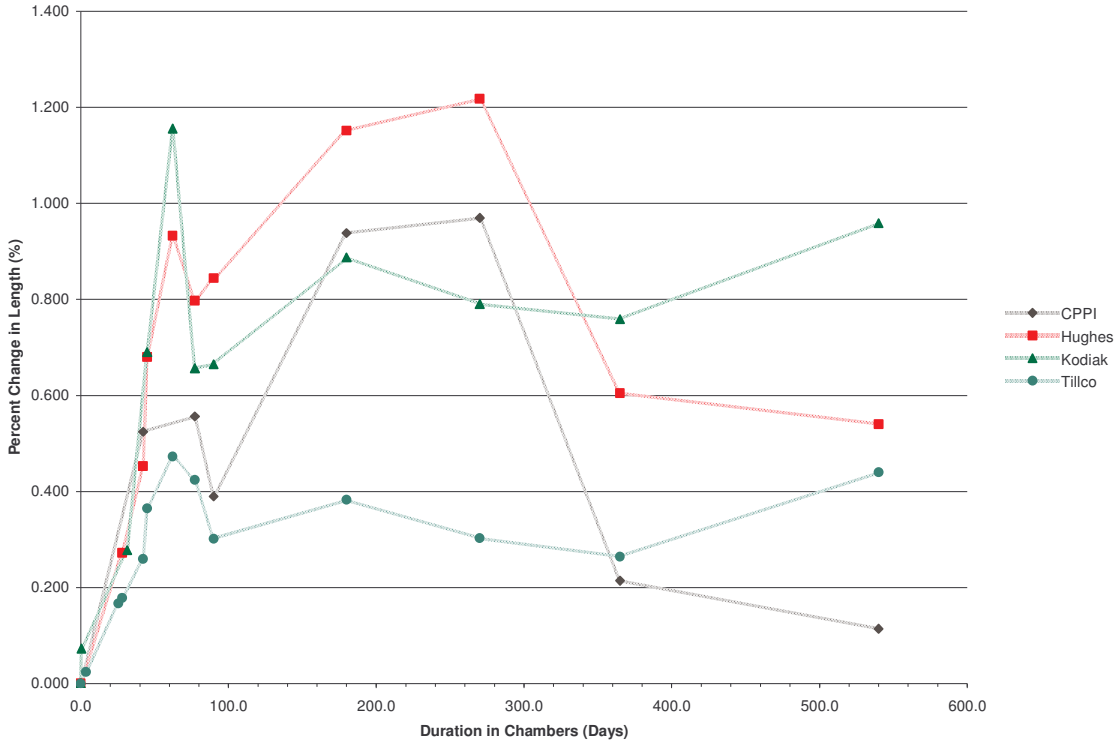

Figure 7.4 Extensional Effects Due to Moisture Uptake of Nicked Specimens at 100°F

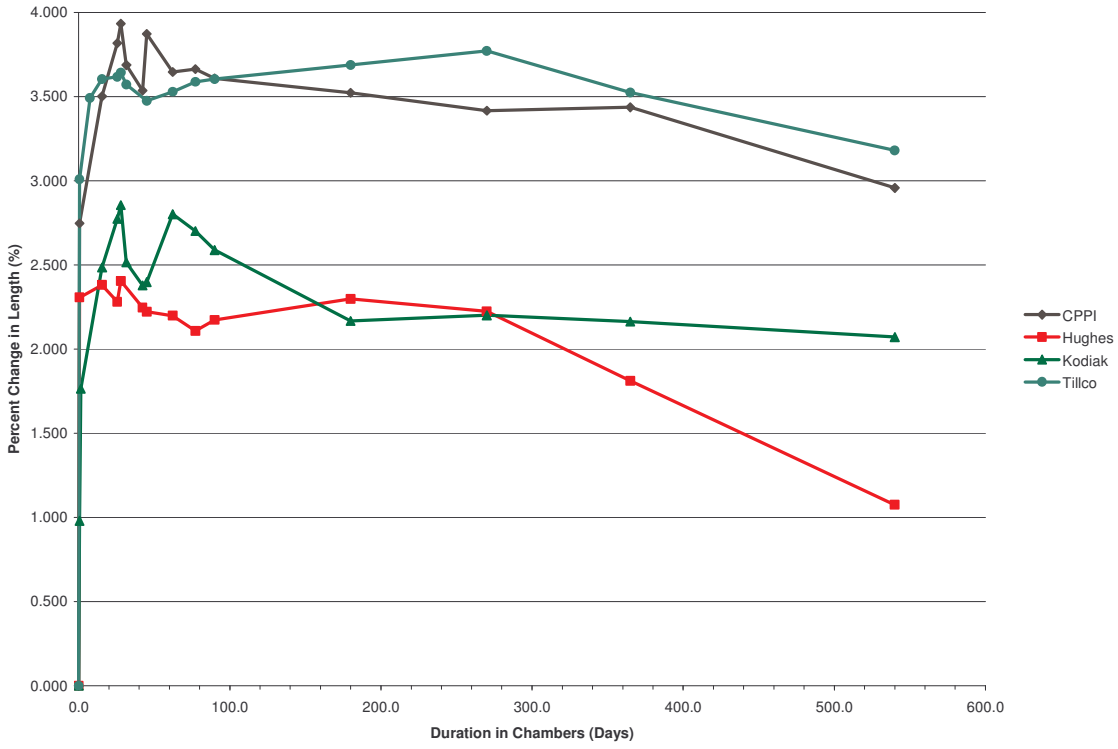

Figure 7.5 Extensional Effects Due to Moisture Uptake of Unscathed Specimens at 130°F

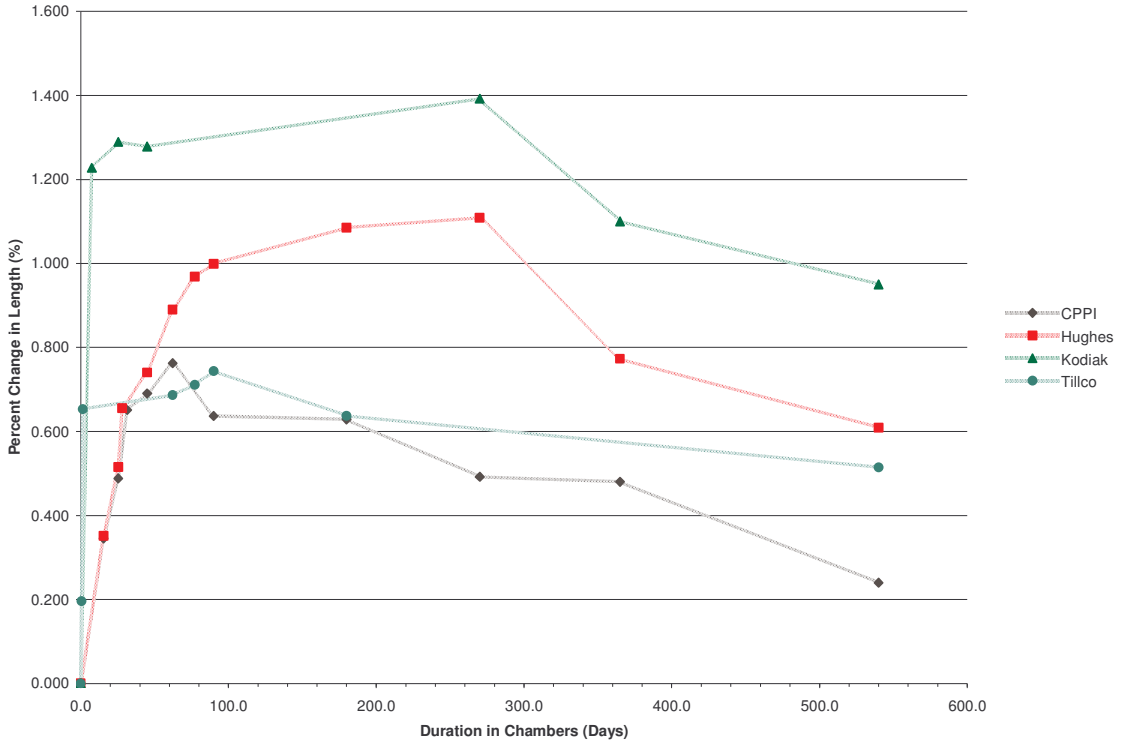

Figure 7.6 Extensional Effects Due to Moisture Uptake of Nicked Specimens at 130°F

7.1.3 Moisture Content

Changes in moisture content were investigated in a manner similar to that for lengths. The varying moisture contents of the specimens are presented in Figures 7.7 to 7.12 with respect to duration of exposure. Table 7.2 summarizes and compares results from unscathed and nicked samples.

Table 7.2 Average % Moisture Content for Unscathed & Nicked Specimens

Samples	Temperature	Duration							
		3 Days	5 Days	10 Days	45 Days	90 Days	180 Days	365 Days	540 Days
Unscathed	RT	5.5	4.2	4.2	3.8	3.6	4.0	3.9	4.0
	100°F	3.1	2.9	3.3	3.8	4.0	4.2	4.4	4.2
	130°F	3.3	3.3	3.4	3.4	3.7	4.5	6.8	4.8
Nicked	RT	0.9	0.9	1.0	1.2	1.4	1.3	1.4	1.7
	100°F	1.2	1.2	1.4	2.0	2.0	2.5	2.7	2.8
	130°F	2.0	1.9	2.0	0.8	0.9	2.5	4.7	2.4

For both unscathed and nicked samples at all temperatures, the largest moisture content occurs initially at up to 3 days, and then steadily increases to ~ 10 days, and then, either increases or decreases again, slowly and steadily up to 45 days, except for 130℉ nicked. For the room temperature and 100℉ specimens, the percent change stays steady and level; however, for the 130℉ there is a slow increase from 45 days to 90 days, then a dramatic increase up to 365 days.

A similar observation can be said for the change in moisture to that of the change in length, for which a sudden spike in moisture uptake is exhibited with a slight decrease or stabilization that ensures after adjustment to the new environment; a slow and steady increase follows thereafter. Once again, the Kodiak rebars seem to have an inferior protective surface while the Pultrall rebars seem to have the best outer coating. According to Pultrall's information for their #3 rebars (Table 5.2) the stated percentage of absorption of 0.47% corroborates closely with the findings of this study for which the percentage absorption for room temperature and at 100℉ were found to be 0.31% and 0.45%, respectively.

In Figures 7.12 and 7.13, there is a dramatic increase in moisture absorption after the 90 day duration period. From observations at the 90 day duration, the Kodiak glass fibers were found to have debonded from the resin matrix allowing moisture to be absorbed in the exposed pores. The change in diameters is also accounted for because of the separation of the fibers from the resin, as compared to the dry samples. This observation is seen in Figure 7.7 correspondingly, as longitudinal cracks and failure of the helical wrap within the Kodiak specimen together with fiber debonding at the specimen ends.

Figure 7.7 Kodiak 130°F Absorption Specimens at 9 Month Duration

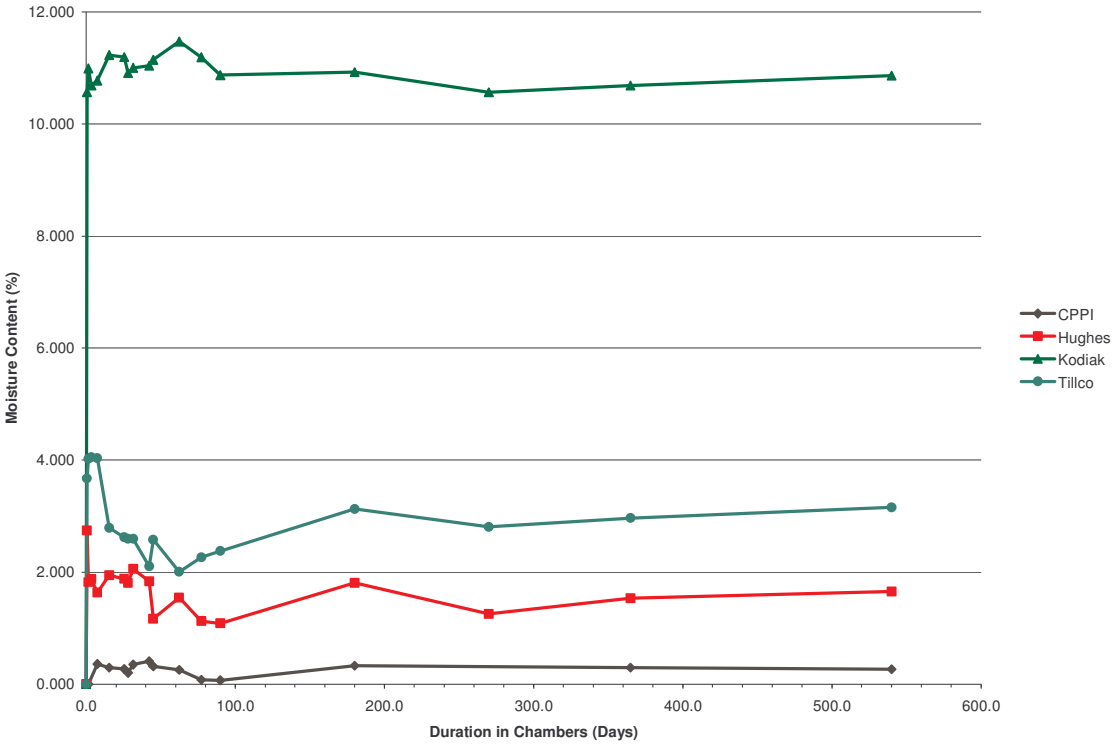

Figure 7.8 Weight-Based Effects Due to Moisture Uptake of Unscathed Specimens at Room Temperature

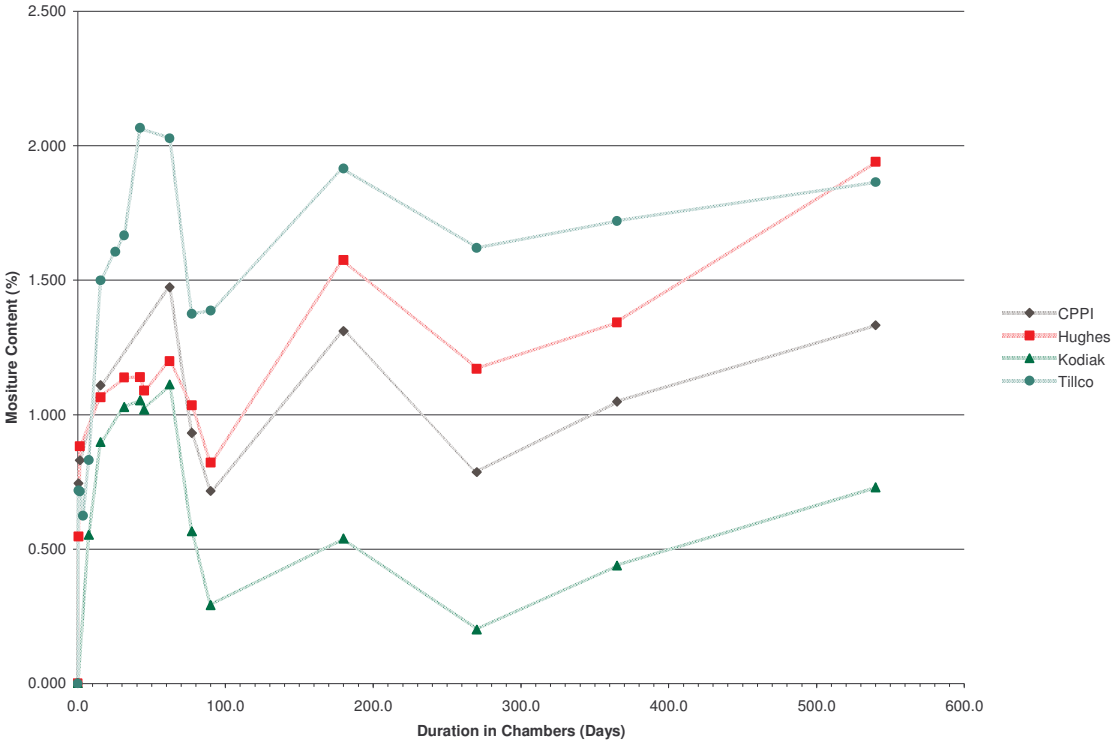

Figure 7.9 Weight-Based Effects Due to Moisture Uptake of Nicked Specimens at Room Temperature

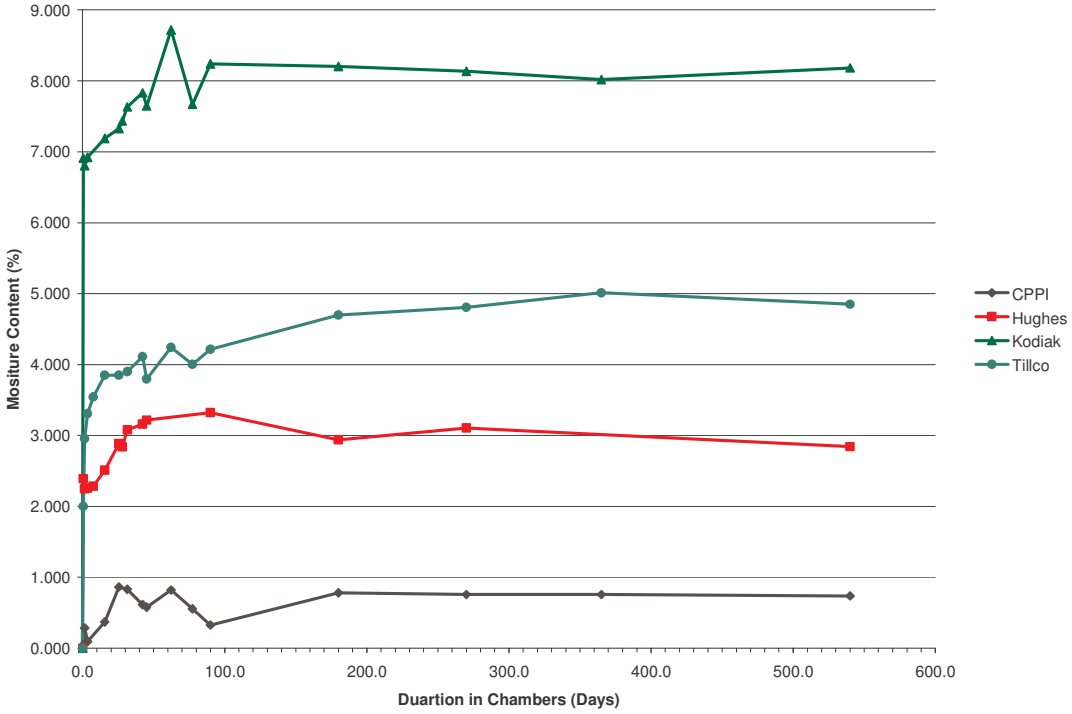

Figure 7.10 Weight-Based Effects Due to Moisture Uptake of Unscathed Specimens at 100°F

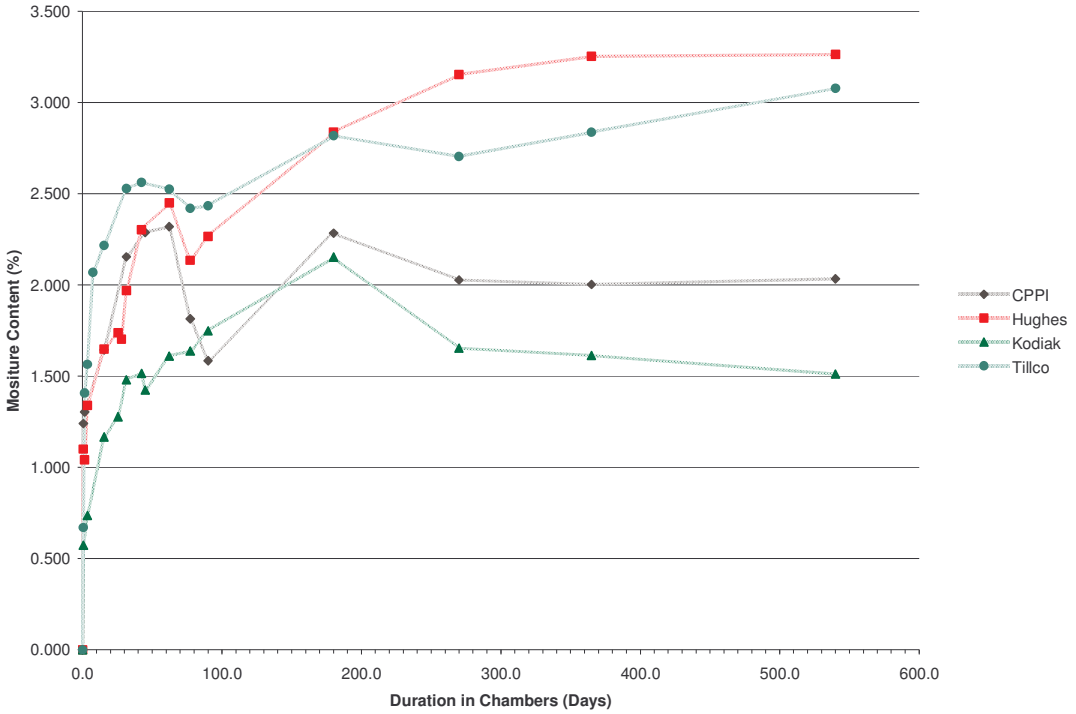

Figure 7.11 Weight-Based Effects Due to Moisture Uptake of Nicked Specimens at 100°F

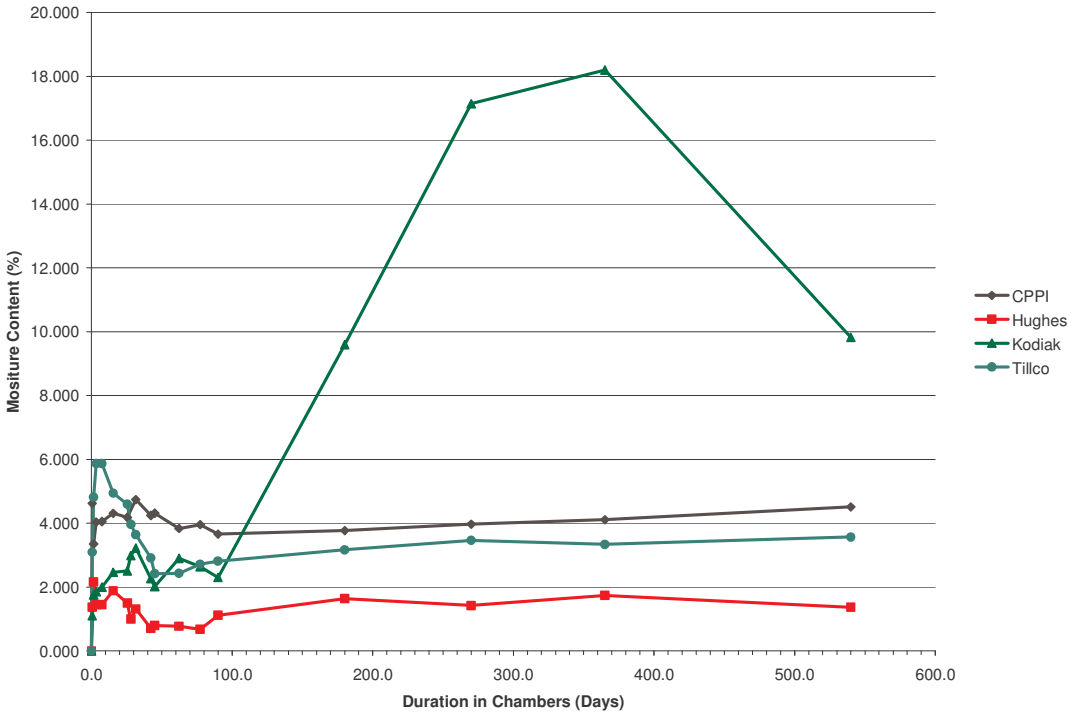

Figure 7.12 Weight-Based Effects Due to Moisture Uptake of Unscathed Specimens at 130°F

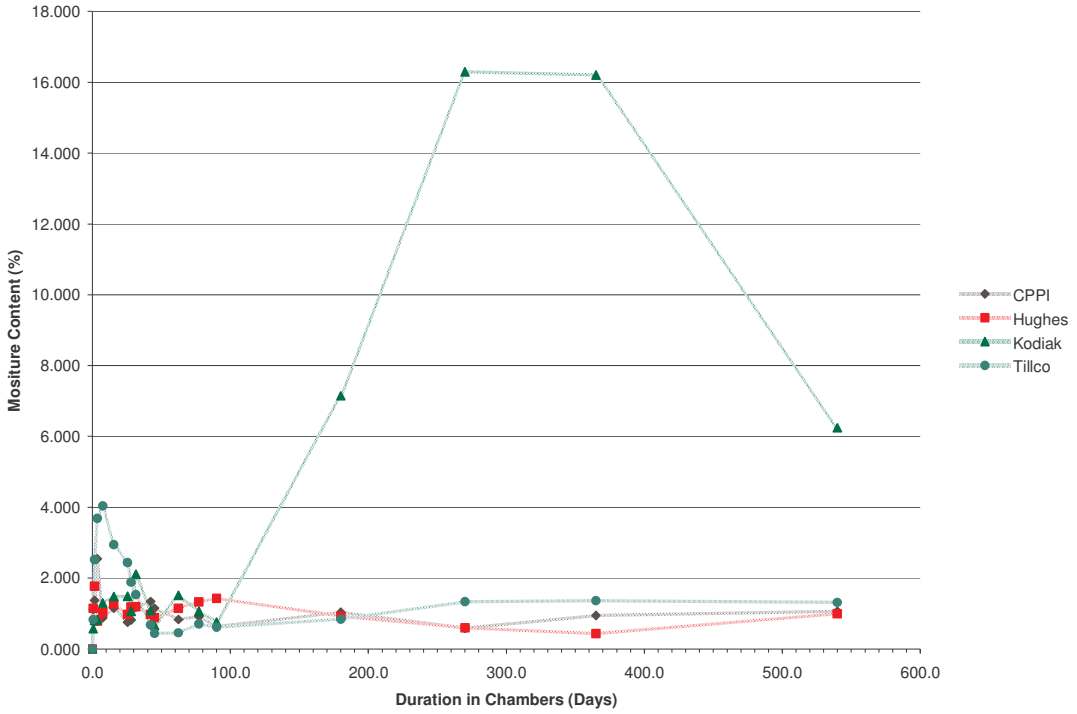

Figure 7.13 Weight-Based Effects Due to Moisture Uptake of Nicked Specimens at 130°F

7.1.4 Overall Initial Analysis

For the purpose of verification, another 60 day testing period protocol on the absorption specimens was conduced in two temperature/humidity chambers, wherein the temperature and humidity were closely controlled. In this case, three specimens of each rebar for each condition were monitored for changes in length, diameter, and weight under a dry and again an alkaline environment at 74°F, 100°F, and 130°F.

7.2 Absorption Testing – 2nd Iteration

During conditioning of the absorption specimens in the temperature/humidity chambers, between the days of June 24 – 26, 2006, UNC Charlotte experienced a campus-wide outage; the results for these days there could have been altered slightly due to the specimens having been exposed to elevated temperatures. Data for the length and diameter specimens was collected for 30 days and found not to have a major deviation

from previously collected data.

7.2.1 Change in Length

Three original length measurements were taken prior to the placement of the specimens in their respected chambers in order to establish a baseline for the moisture uptake in the rebar with respect to time. The results of these measurements are shown for unscathed and nicked specimens in Figures 7.14 to 7.19. Table 7.3 summarizes and compares results from unscathed and nicked samples.

Table 7.3 Average % Length Changes for Unscathed & Nicked Specimens

Samples	Temperature	Duration				
		2.5 Days	5 Days	13 Days	19 Days	30 Days
Unscathed	RT	0.5	0.7	0.4	0.4	0.1
	100°F	0.6	0.7	0.8	0.5	0.3
	130°F	0.9	1.0	1.0	0.9	0.5
Nicked	RT	0.5	0.8	0.6	0.5	0.3
	100°F	0.8	1.0	1.1	0.8	0.3
	130°F	1.4	1.4	2.0	1.3	0.9

After 2.5 days, all the specimens except for those soaking in the 130°F bath experienced a slight increase over the duration of 2.5 days; however at 13 days the room temperature samples experienced a decrease up to the 30 day mark. At the 19 day mark, the higher temperature specimens started experiencing the same decrease. From looking at the data and figures, it is expected that there should have been a decrease in the higher temperature specimens at 13 days, but this was seen only in the room temperature specimens. The decrease in percent change at the 13 and 19 day marks could be due to the changes in the GFRP material properties.

From the figures, the data is much closer from a trend-wise standpoint than the results from the previous investigation. In Figures 7.14, 7.15, 7.16, and 7.17, the trend of Kodiak and Tillco being the inferior rebars is verified with the moisture uptake being higher as compared to the results of Pultrall and Hughes Bros. These figures, however,

corroborate the observations that were made from the previous investigation.

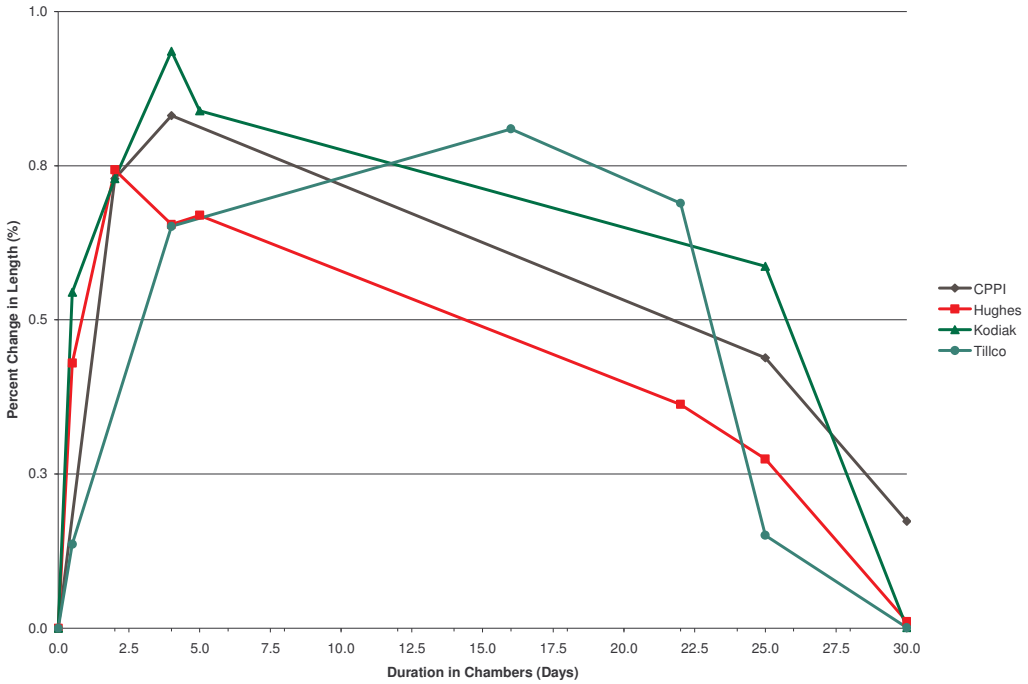

Figure 7.14 Extensional Effects Due to Moisture Uptake of Unscathed Specimens at Room Temperature

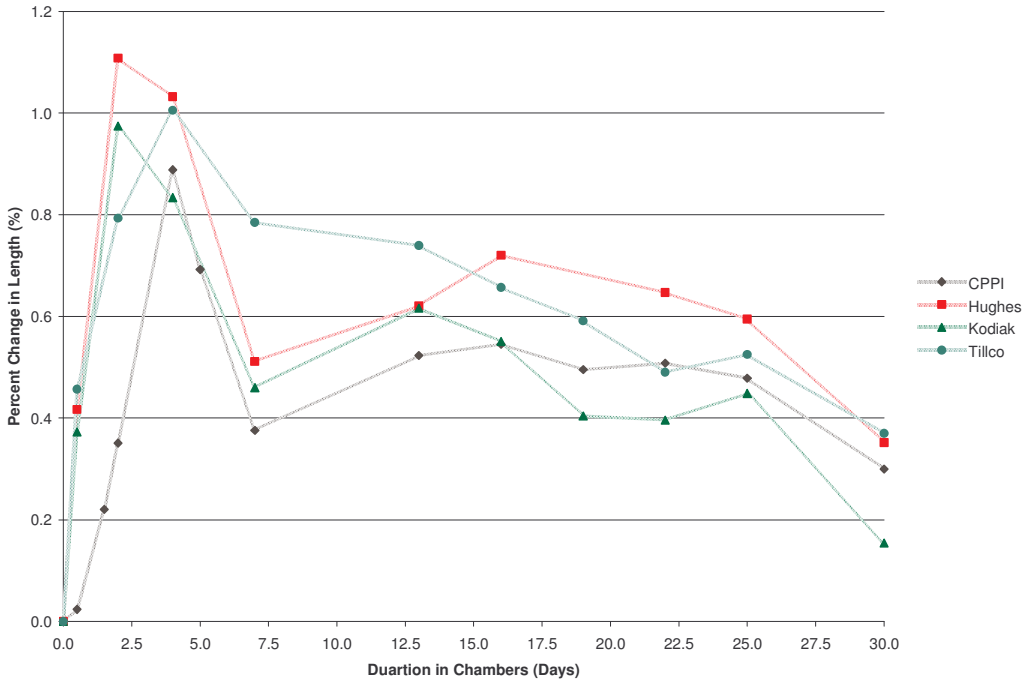

Figure 7.15 Extensional Effects Due to Moisture Uptake of Nicked Specimens at Room Temperature

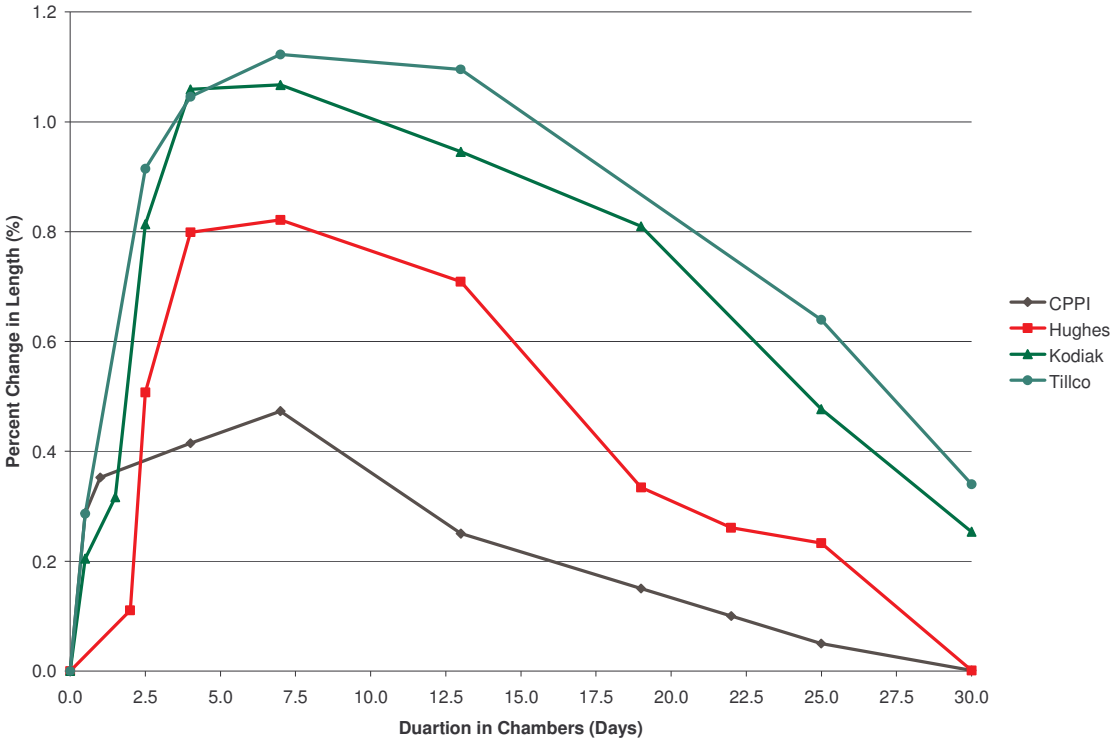

Figure 7.16 Extensional Effects Due to Moisture Uptake of Unscathed Specimens at 100°F

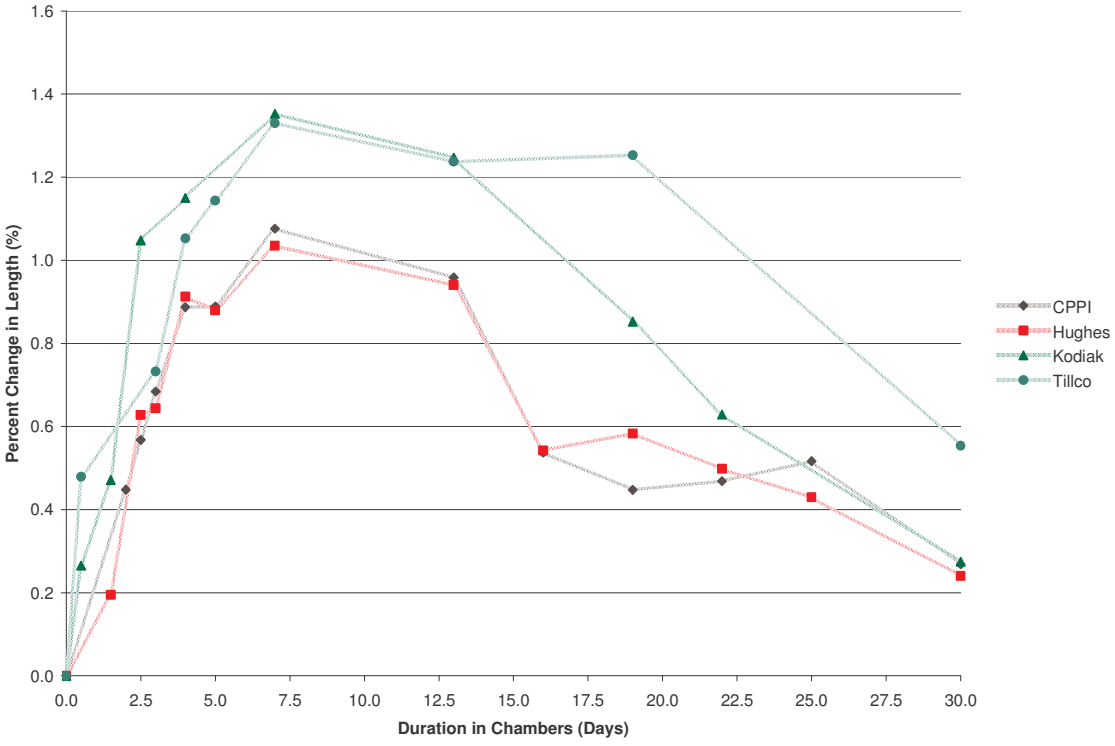

Figure 7.17 Extensional Effects Due to Moisture Uptake of Nicked Specimens at 100°F

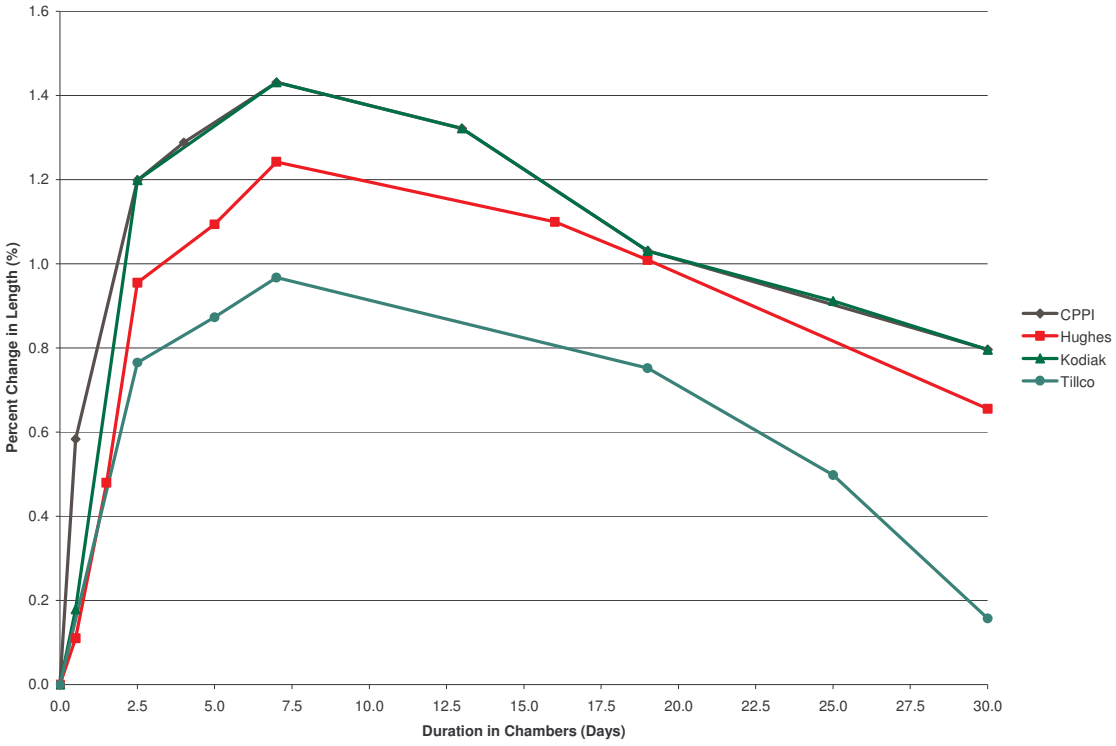

Figure 7.18 Extensional Effects Due to Moisture Uptake of Unscathed Specimens at 130°F

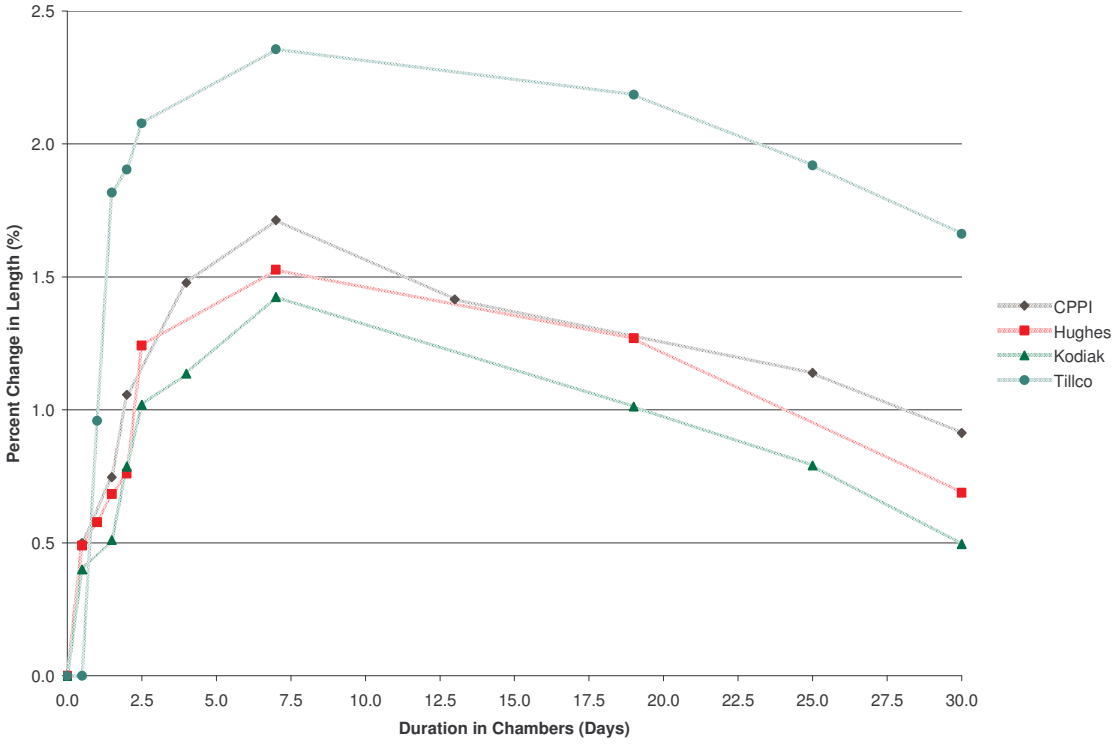

Figure 7.19 Extensional Effects Due to Moisture Uptake of Nicked Specimens at 130°F

7.2.2 Change in Diameter

As was conducted for the change in length specimens, three original diameter measurements were taken prior to placing the specimens in their respected chamber. This established a baseline for the moisture uptake in the rebar with respect to time. The results of these measurements are shown for unscathed and nicked specimens in Appendix G. The reason being, from observing the data collected, no true trend could be established due to inconsistencies in the way the diameter was being measured. This is due to the fact that the rebar encounters bulges during the pultrusion process or change in diameter along the length of the rebar. Therefore, the measurements taken one day are not going to be the same measurements that are taken the next day. Table 7.4 summarizes and compares results from unscathed and nicked samples.

Table 7.4 Average % Diameter Changes for Unscathed & Nicked Specimens

Samples	Temperature	Duration				
		2.5 Days	5 Days	13 Days	19 Days	30 Days
Unscathed	RT	1.2	1.6	0.0	-1.2	0.4
	100°F	1.0	1.6	3.4	-0.1	-0.5
	130°F	1.4	1.9	2.4	-0.2	-0.2
Nicked	RT	-0.3	0.3	0.0	-1.4	-0.3
	100°F	1.8	1.4	3.8	0.2	0.0
	130°F	1.9	1.9	3.3	1.0	-0.6

7.2.3 Moisture Content

Changes in moisture content were investigated in a manner similar to that as was done for weights. The varying moisture contents of the specimens are presented in Figures 7.20 to 7.25 with respect to exposure durations. Table 7.5 summarizes and compares results from the unscathed and nicked samples.

Table 7.5 Average % Moisture Content for Unscathed & Nicked Specimens

Samples	Temperature	Duration							
		1 Days	2.5 Days	5 Days	13 Days	25 Days	35 Days	45 Days	60 Days
Unscathed	RT	1.0	0.4	0.3	0.6	0.4	0.6	0.7	0.8
	100°F	1.2	0.7	0.3	0.6	0.4	0.8	0.8	0.7
	130°F	1.3	0.9	0.5	0.4	0.6	0.7	1.0	1.5
Nicked	RT	1.1	0.3	0.3	0.7	0.3	0.6	0.6	0.6
	100°F	1.1	0.7	0.3	0.5	0.6	0.8	0.8	0.7
	130°F	1.1	0.9	0.5	0.5	0.5	0.7	0.8	1.2

There is a dramatic increase in weight observed at the first day for the unscathed specimens, whereas the nicked samples experienced changes more uniformly. This spike in moisture uptake was also observed during the initial findings. The one key observation is that after the campus-wide power outage (see Section 7.2), the specimens experienced an increase in absorption at 13 days. From the figures, the trend appears to be that after the first stages of being exposed to the alkaline solution, there is a dramatic spike in moisture uptake. During the next 20 to 30 days, there is a stabilization observed at around 0.50%. After a duration of 30 days, there is a slight increase to about 0.70% and again stabilizes for period of 30 days. An explanation for the spike at the first day is likely due to the specimens having adapted to the new environment. This could also explain why there is a slight increase at 13 days due to the power being turned on and off.

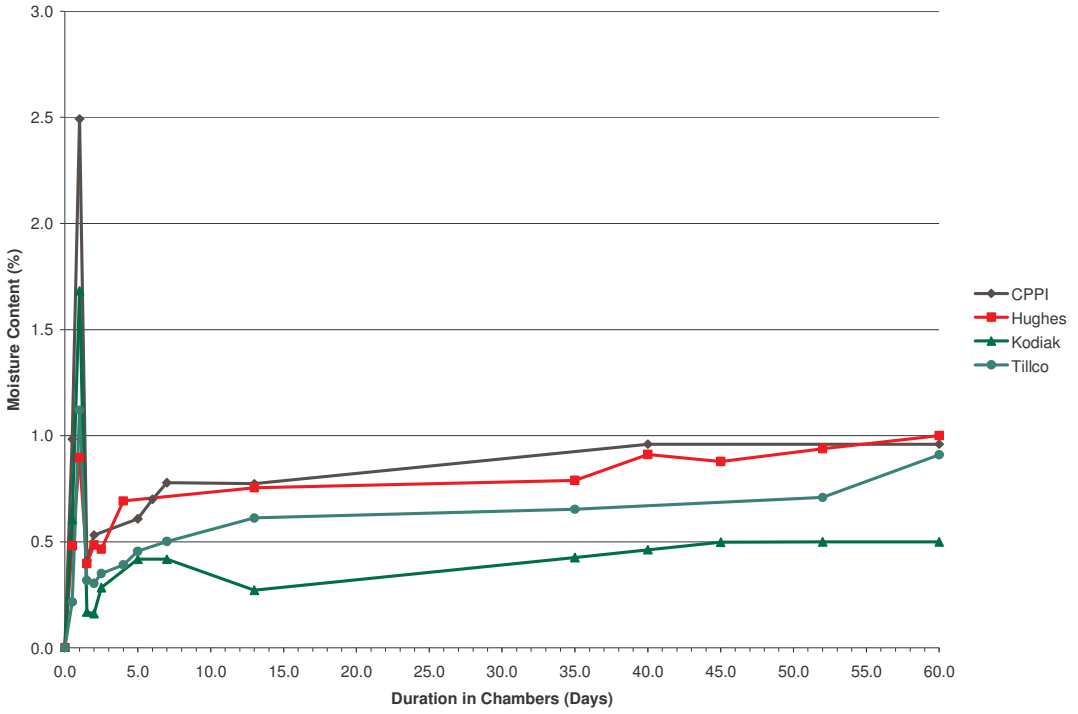

Figure 7.20 Weight-Based Effects Due to Moisture Uptake of Unscathed Specimens at Room Temperature

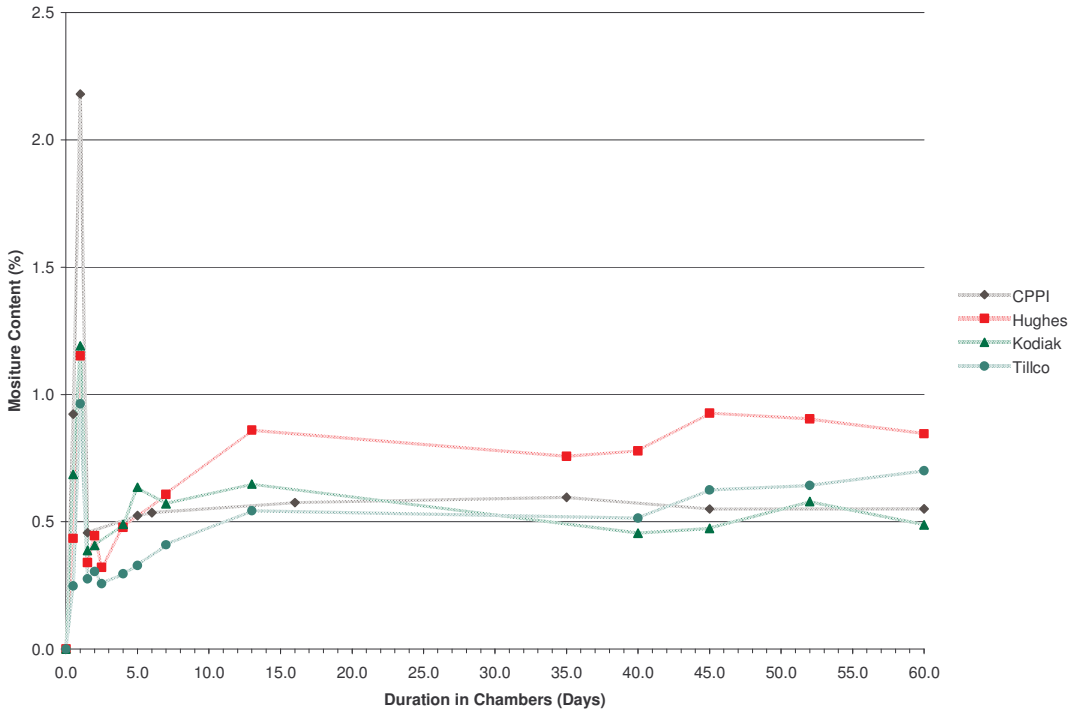

Figure 7.21 Weight-Based Effects Due to Moisture Uptake of Nicked Specimens at Room Temperature

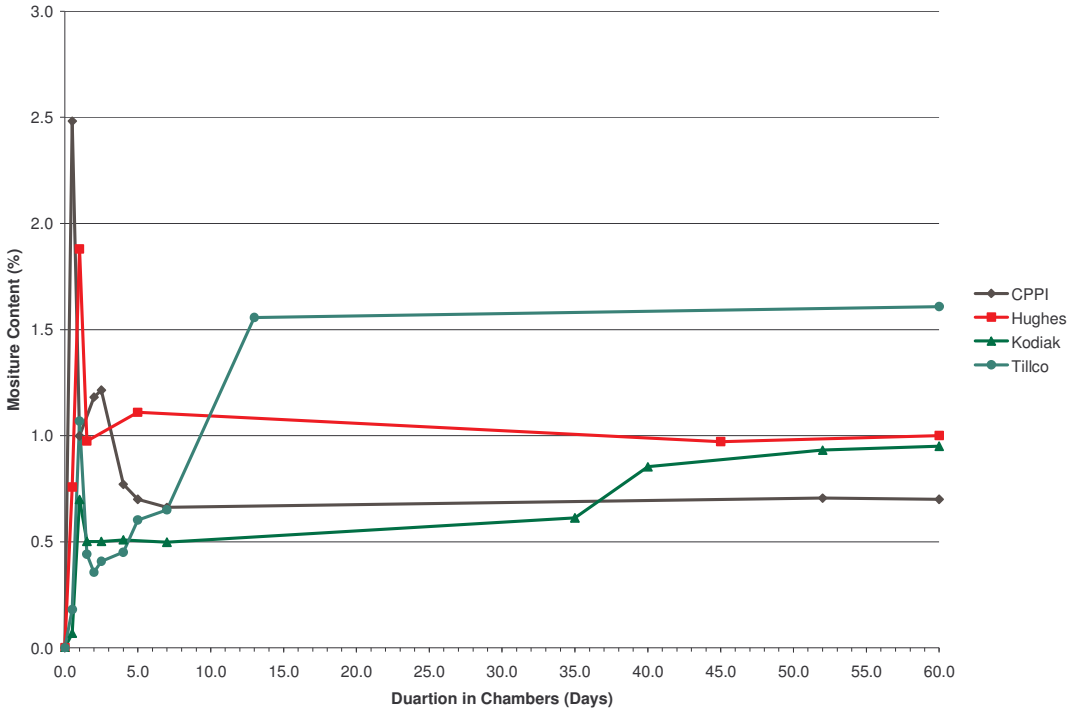

Figure 7.22 Weight-Based Effects Due to Moisture Uptake of Unscathed Specimens at 100°F

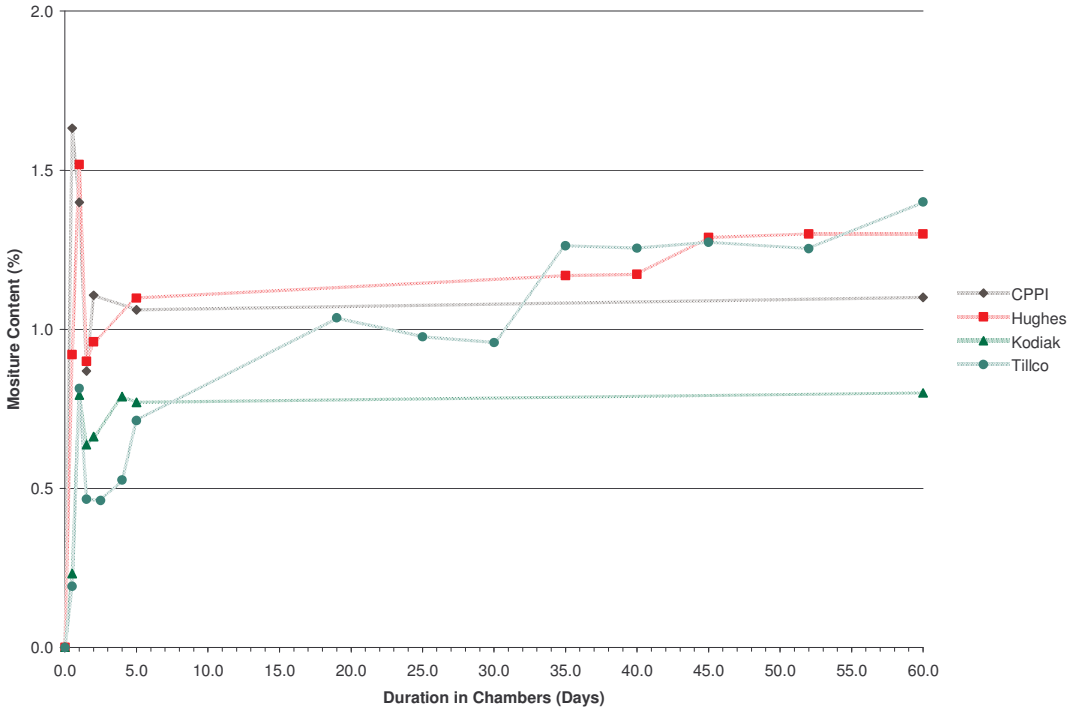

Figure 7.23 Weight-Based Effects Due to Moisture Uptake of Nicked Specimens at 100°F

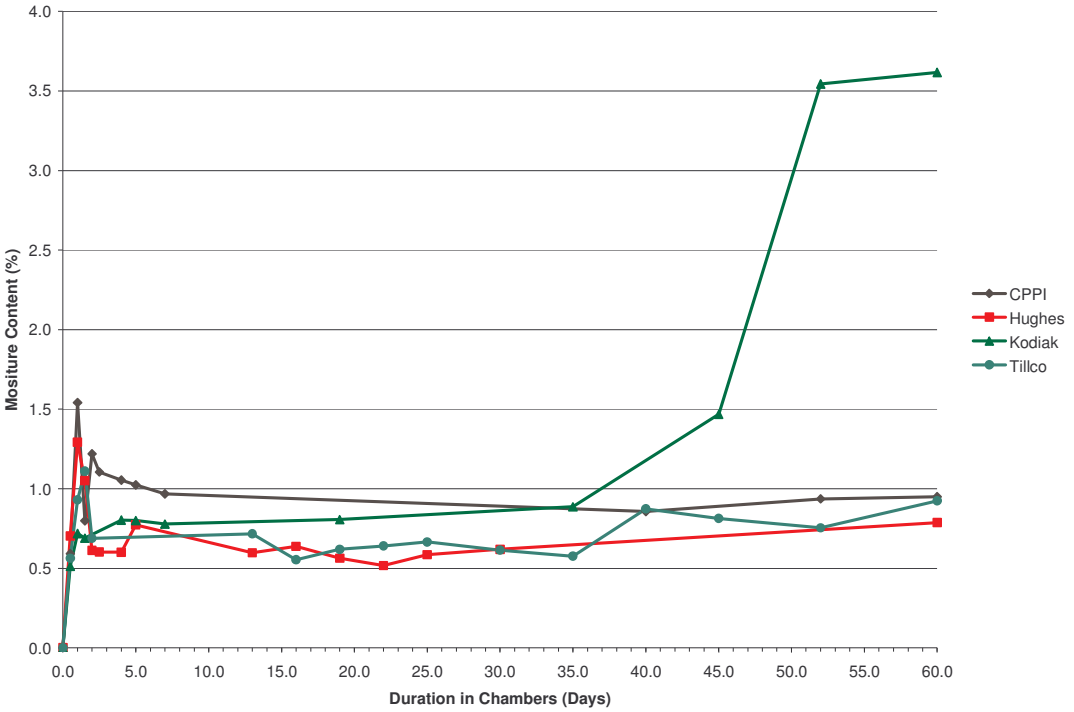

Figure 7.24 Weight-Based Effects Due to Moisture Uptake of Unscathed Specimens at 130°F

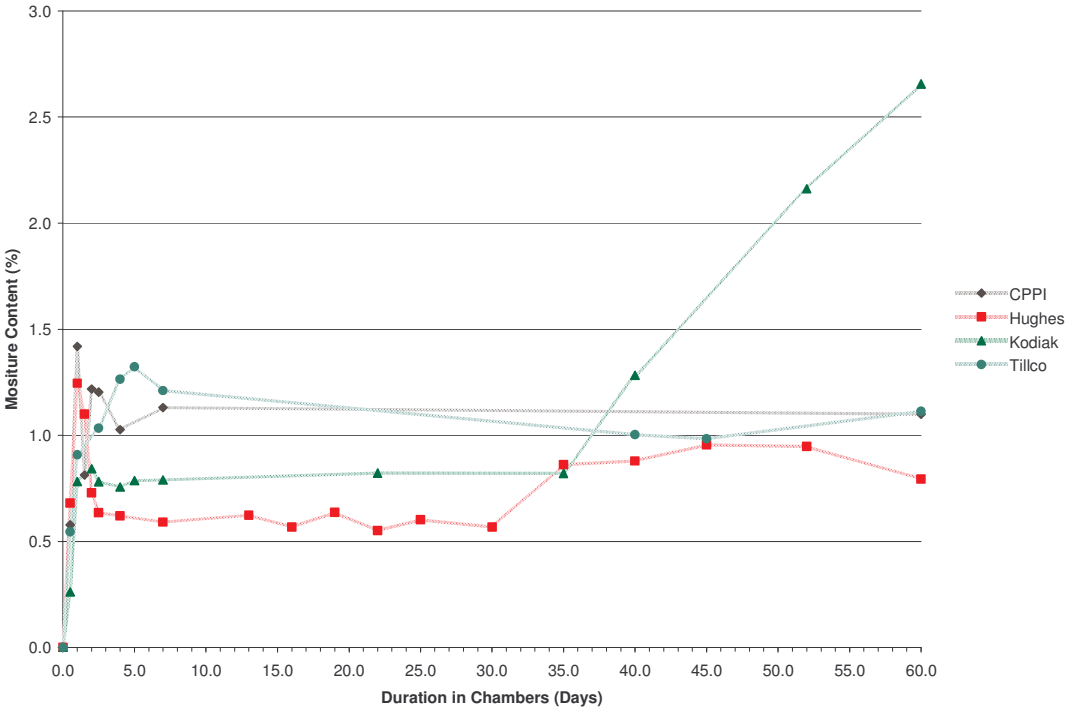

Figure 7.25 Weight-Based Effects Due to Moisture Uptake of Nicked Specimens at 130°F

7.2.4 Overall Analysis

CPPI (Pultrall) is the only rebar furnished that states the absorption uptake of #3 rebar (Table 5.2). For the unscathed results at room temperature, the average moisture uptake was 0.50% which is within 6% of the data stated by CPPI at 0.47%.

7.3 Tensile Testing Results

The tensile specimens were tested at 3 Month, 6 Month, and 12 Month durations within the four different environments. An extensometer was used to measure strain in the longitudinal direction in order to determine the stiffness of the GFRP rebars; stress versus strain diagrams are provided in Appendix G.

7.3.1 Tensile Stress Analysis

The following table is a representation of the decrease in strength during the duration of the specimens as subjected to the alkaline environments. The decrease in tensile stress is based on the overall average of the control samples under dry conditions. A percentage decrease is based on the average of all four vendor GFRP rebars as shown in Table 7.6. It should be noted that since the Kodiak specimens completely degraded at the 12 month duration, it was assumed that the bar had lost 100 % of its ultimate tensile strength, and this value was used in calculating the average decrease of tensile strength.

Table 7.6 Average % Decrease of Tensile Strength for Unscathed & Nicked Specimens

Samples	Temperature	Duration			
		3 Months	6 Months	12 Months	18 Months
Unscathed	RT	14.8%	18.1%	31.7%	38.7%
	100°F	20.7%	38.0%	43.1%	56.8%
	130°F	45.7%	61.1%	74.6%	76.1%
Nicked	RT	12.6%	20.2%	32.6%	41.0%
	100°F	19.6%	28.7%	38.0%	60.8%
	130°F	45.4%	61.7%	68.3%	75.2%

From the trend lines it was observed that the rebars from Pultrall and Hughes Bros. experienced only a small decrease in tensile strength with the exception of the test samples exposed to 130℉ being due most likely to the protective coatings furnished to these specimens and absent from the Kodiak and Tillco rebars. Without a protective outer coating, the degradation process seems to be accelerated, as especially seen in the case of the Kodiak rebars where by 6 Months the test samples became so embrittled for which testing was no longer possible.

Also, the control nicked specimens experienced a 22.9% decrease in strength compared to the unscathed samples. It can be assumed that slightly damaging the glass fiber/resin matrix by approximately a tenth of an inch decreases the overall tensile strength by 25% for #3 GFRP rebar.

The following figures are representations of the tensile strength for the unscathed and nicked specimens for 3 months, 6 months, and 12 months.

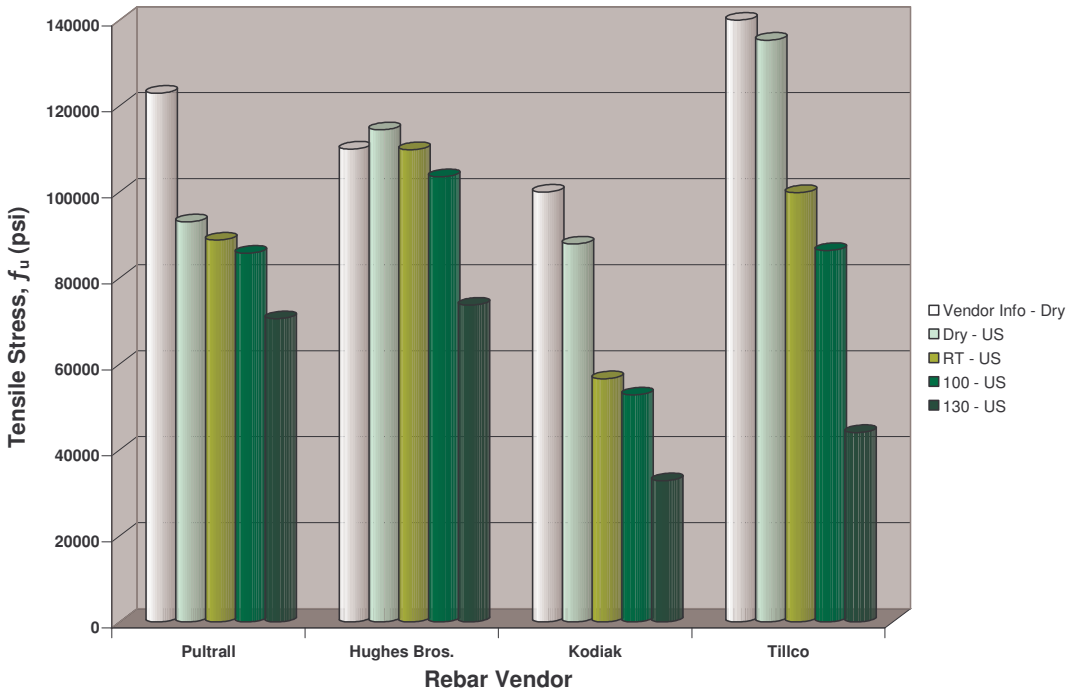

Figure 7.26 Average Tensile Strength for Unscathed at 3 Months

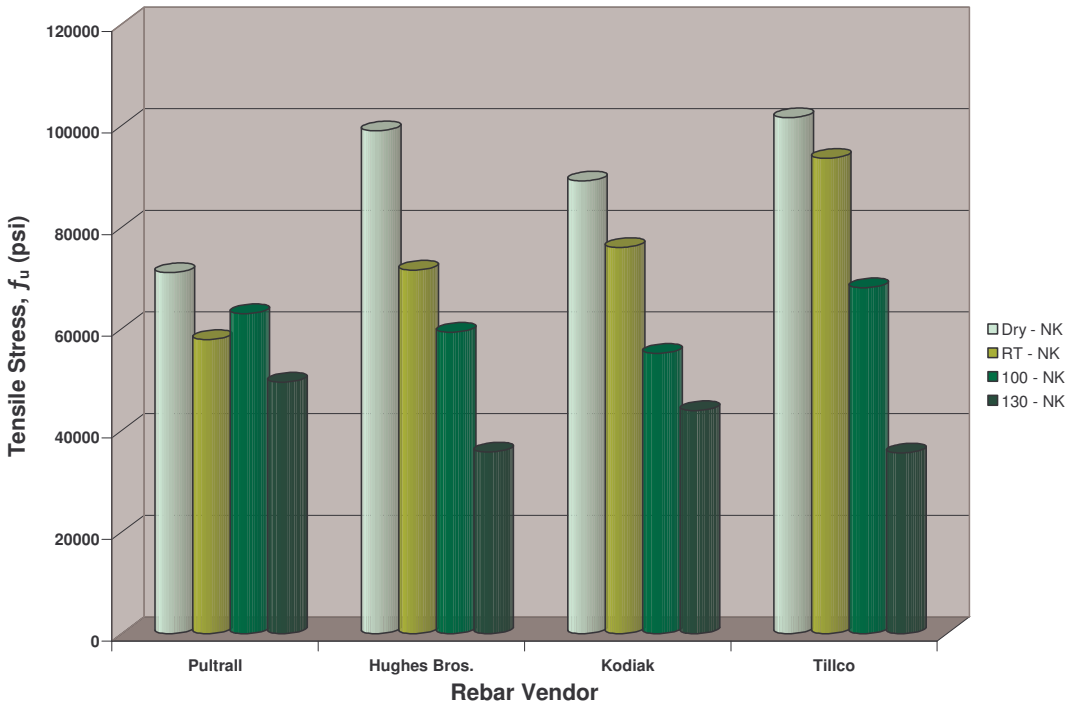

Figure 7.27 Tensile Strength for Nicked at 3 Months

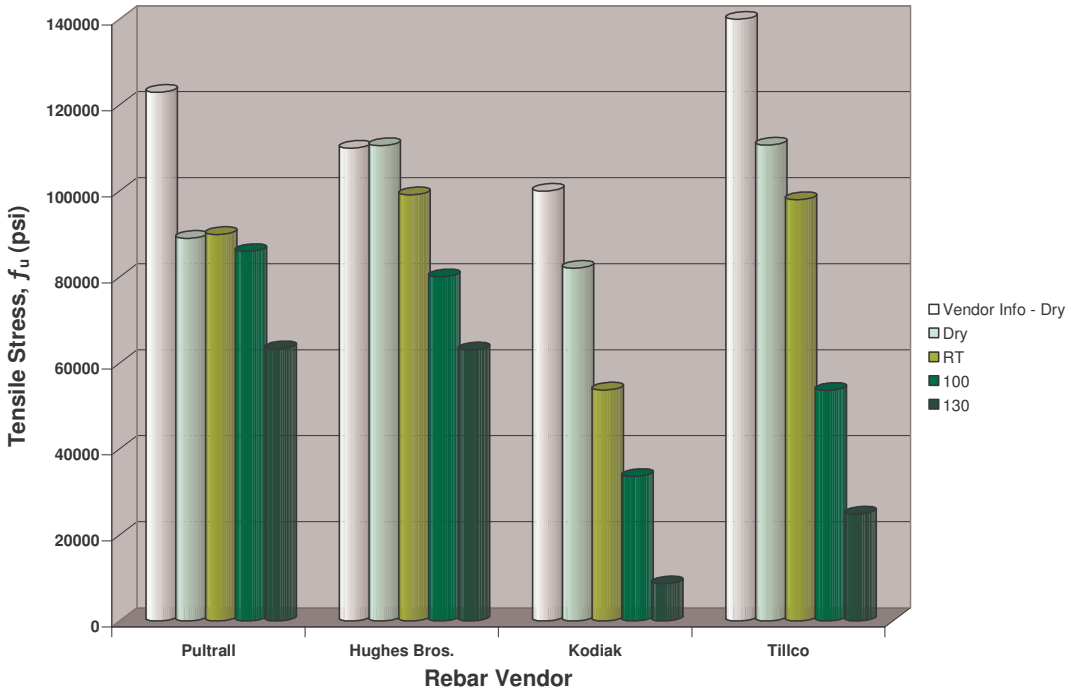

Figure 7.28 Average Tensile Strength for Unscathed at 6 Months

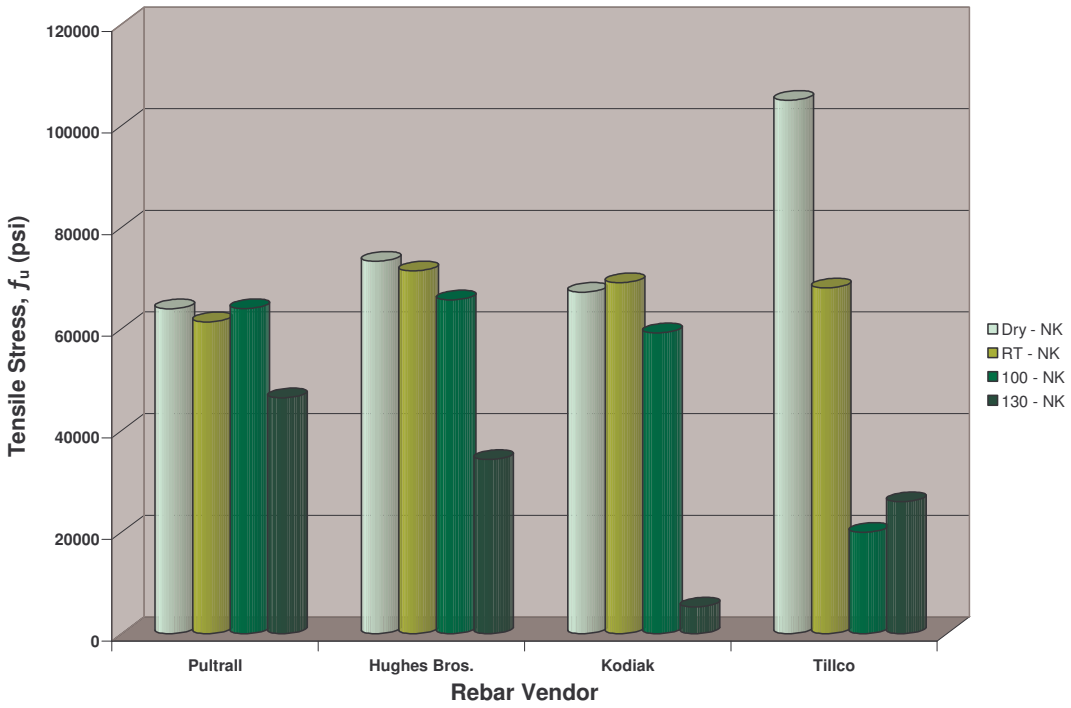

Figure 7.29 Tensile Strength for Nicked at 6 Months

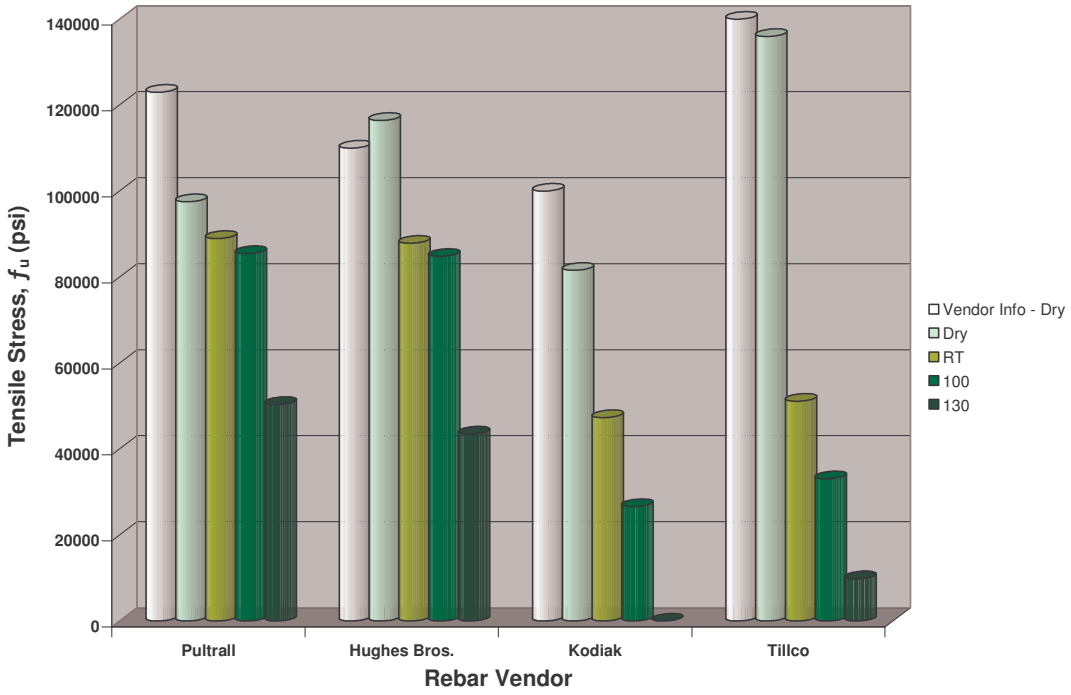

Figure 7.30 Average Tensile Strength for Unscathed at 12 Months

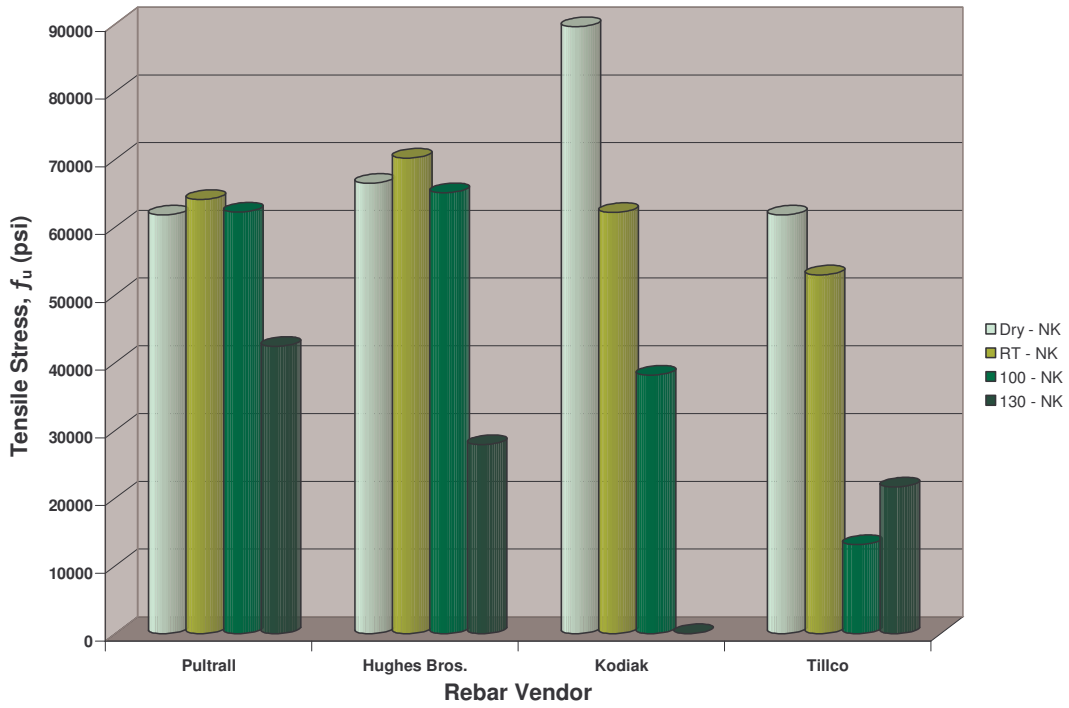

Figure 7.31 Tensile Strength for Nicked at 12 Months

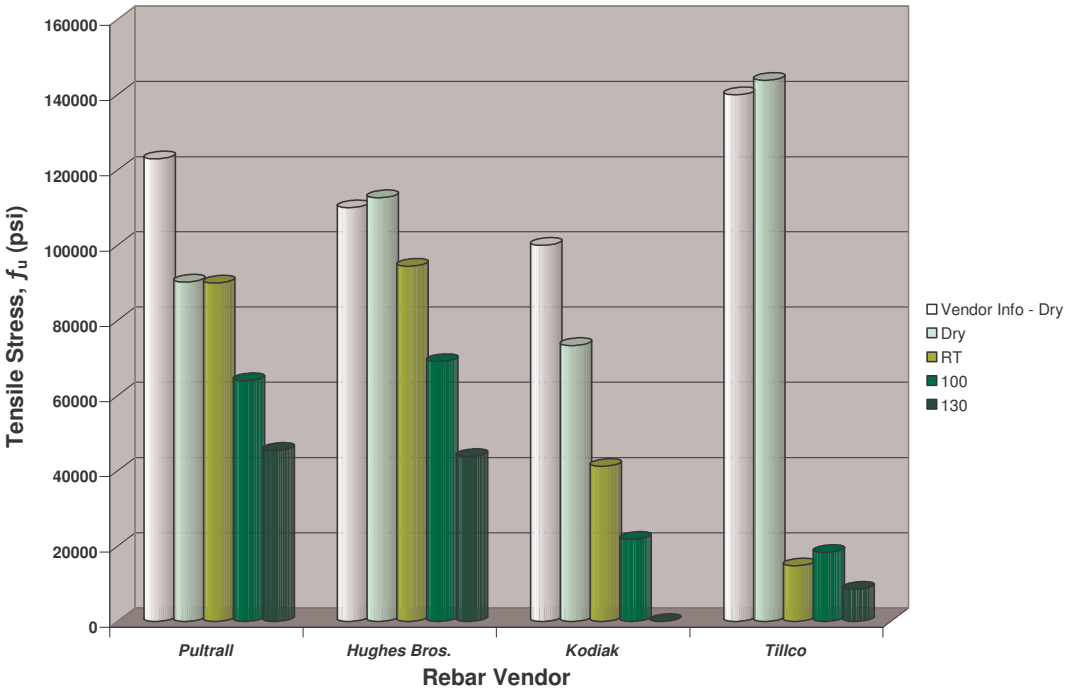

Figure 7.32 Average Tensile Strength for Unscathed at 18 Months

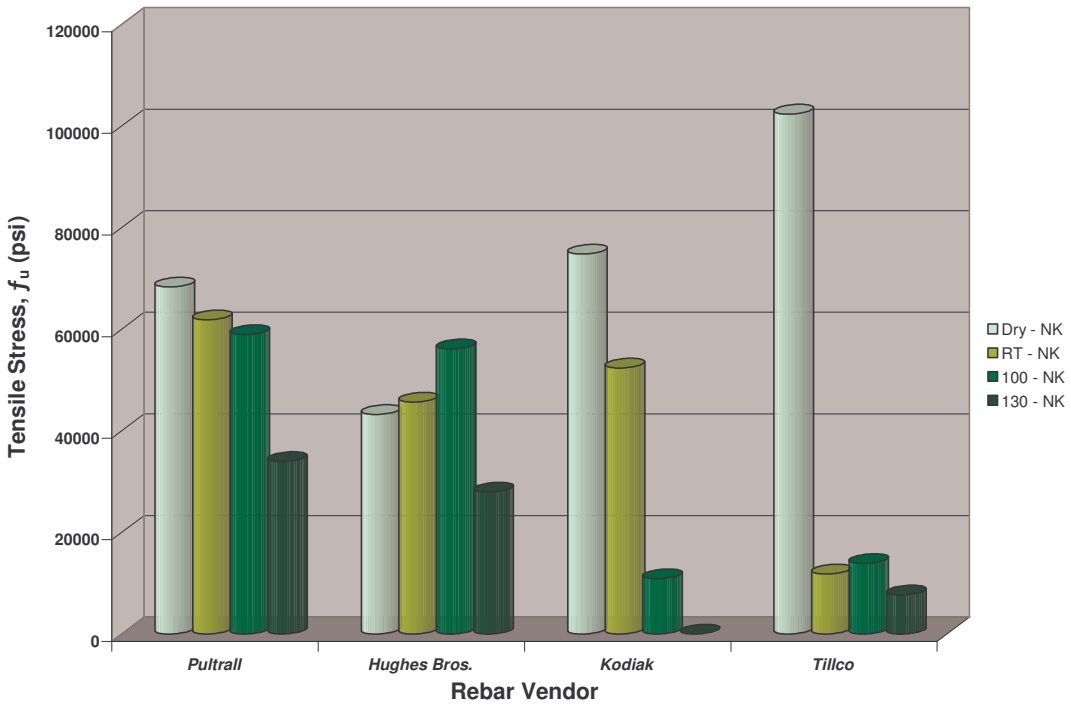

Figure 7.33 Tensile Strength for Nicked at 18 Months

7.3.2 Tensile Stiffness Analysis

The following table is a representation of the decrease in stiffness during the duration of the specimens as subjected to the alkaline environments. The decrease in stiffness is based on the overall average of the control samples under dry conditions, where the modulus of elasticity was calculated using the following equation (ACI 440.3R, 2004):

$$E_L = \frac{F_1 - F_2}{(\varepsilon_1 - \varepsilon_2)A}$$

where, E_1 = axial (longitudinal) modulus of elasticity, F_1 and ε_1 = load and corresponding strain, respectively, at approximately 50% of the ultimate tensile capacity or guaranteed tensile capacity, F_2 and ε_2 = load and corresponding strain, respectively, at approximately 20% of the ultimate tensile capacity or guaranteed tensile capacity, and A = cross-sectional area.

A percentage decrease is based on the average of all four vendor GFRP rebars as shown in Table 7.7. It should be noted that since the Kodiak specimens completely degraded at the 12 month duration, it was assumed that the bar had lost 100% of its stiffness, and this value was used in calculating the average decrease of modulus of elasticity. Also, during the testing of the 12 month specimens, the extensometer was not properly calibrated prior the testing of the tensile specimens. Therefore, a trend was established for the 12 month period based on the observations saw during the 6 month and 18 month testing periods.

Table 7.7 Average % Decrease of Tensile Stiffness for Unscathed & Nicked Specimens

Sample	Temperature	Duration			
		3 Months	6 Months	12 Months	18 Months
Unscathed	RT	6.5%	8.1%	10.9%	13.6%
	100°F	9.7%	14.7%	18.8%	22.9%
	130°F	11.4%	20.8%	26.5%	32.1%
Nicked	RT	10.8%	13.6%	16.8%	20.1%
	100°F	14.7%	25.5%	35.2%	44.8%
	130°F	21.3%	34.5%	49.8%	65.1%

The same observations noted for the tensile specimens hold for the stiffness of the GFRP rebar as well.

The control nicked specimens experienced a 23.9% decrease in stiffness compared to the unscathed samples. As stated for the tensile strength reduction, it can be assumed that slightly damaging the glass fiber/resin matrix by approximately a tenth of an inch decreases the overall modulus of elasticity by 25% for #3 GFRP rebar.

The following figures show of the effects on the modulus of elasticity for the unscathed and nicked specimens for 3, 6, and 18 months. It should be noted that the results for the 12 month duration are not shown due to inaccurate readings from the extensometer during testing, and stress versus strain relationships are shown in Appendix H.

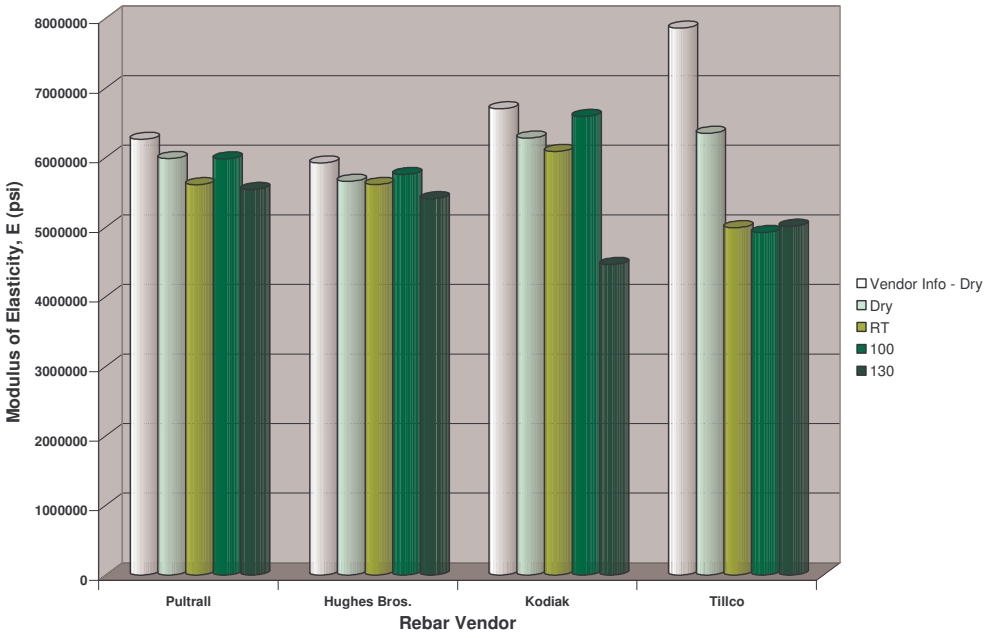

Figure 7.34 Average Modulus of Elasticity for Unscathed at 3 Months

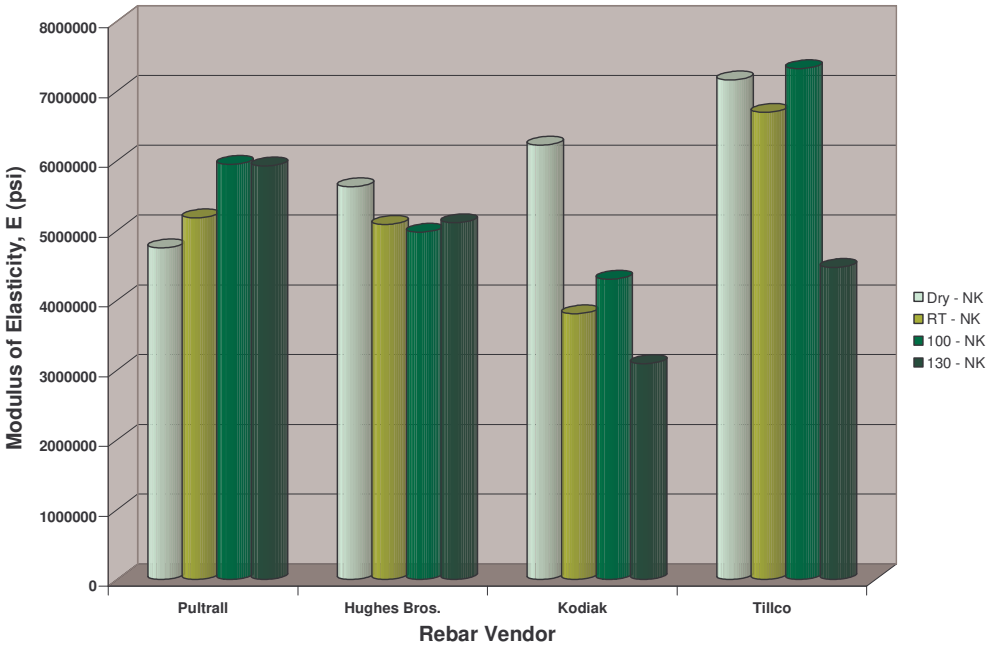

Figure 7.35 Modulus of Elasticity for Nicked at 3 Months

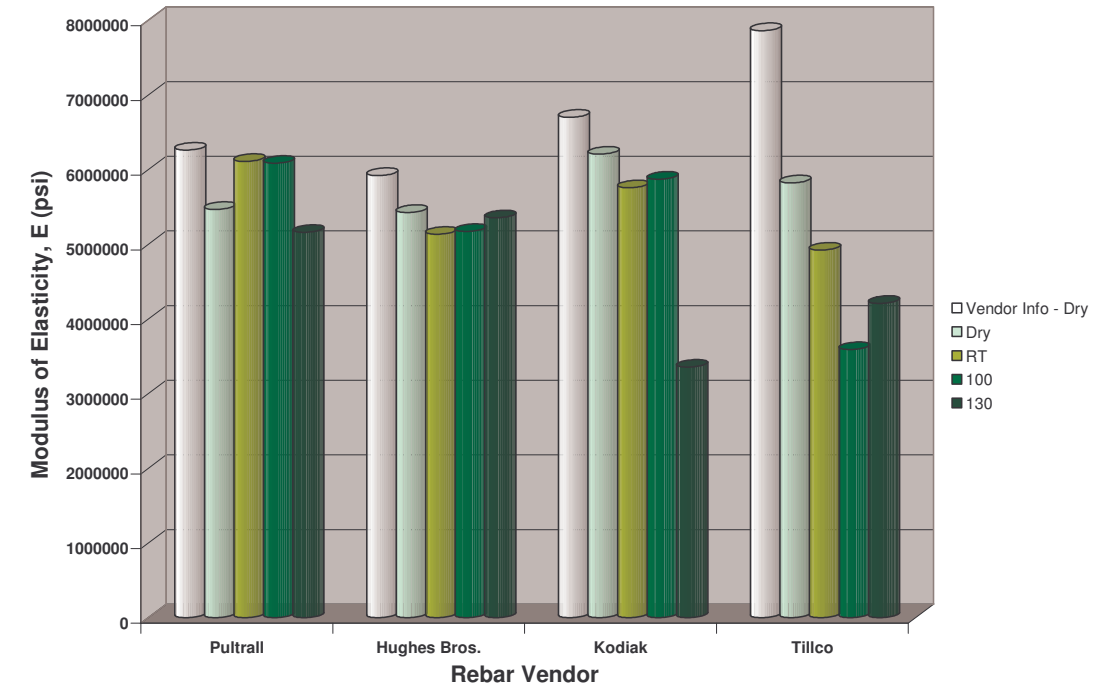

Figure 7.36 Average Modulus of Elasticity for Unscathed at 6 Months

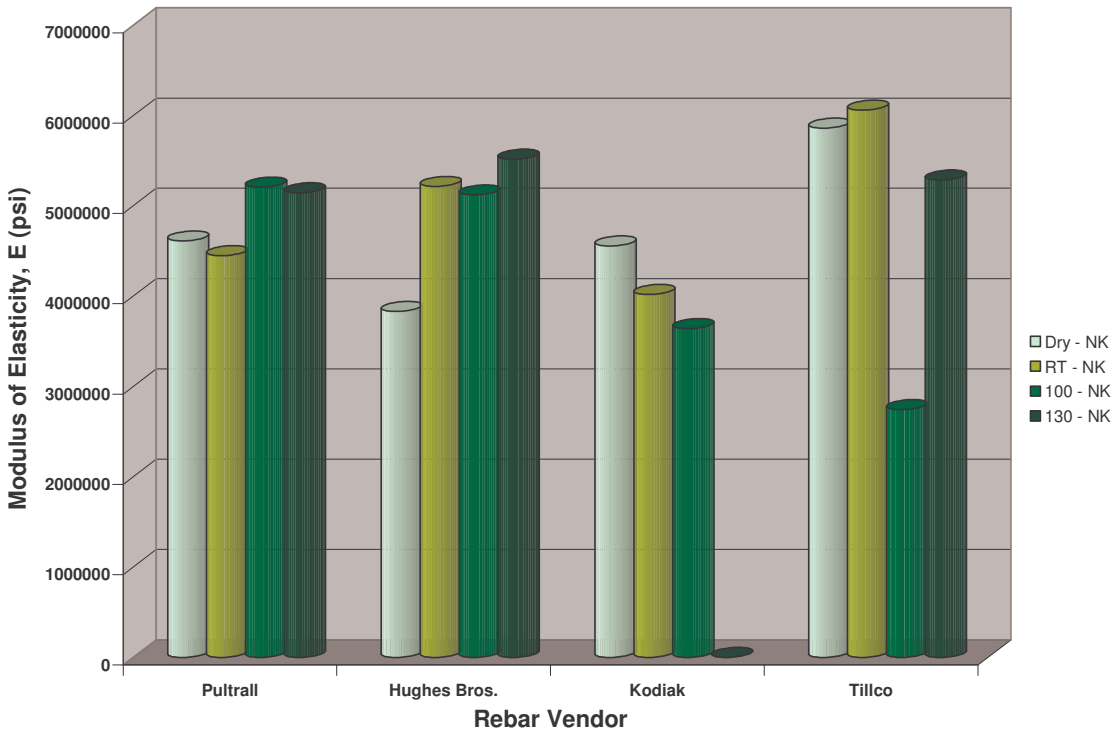

Figure 7.37 Modulus of Elasticity for Nicked AT 6 Months

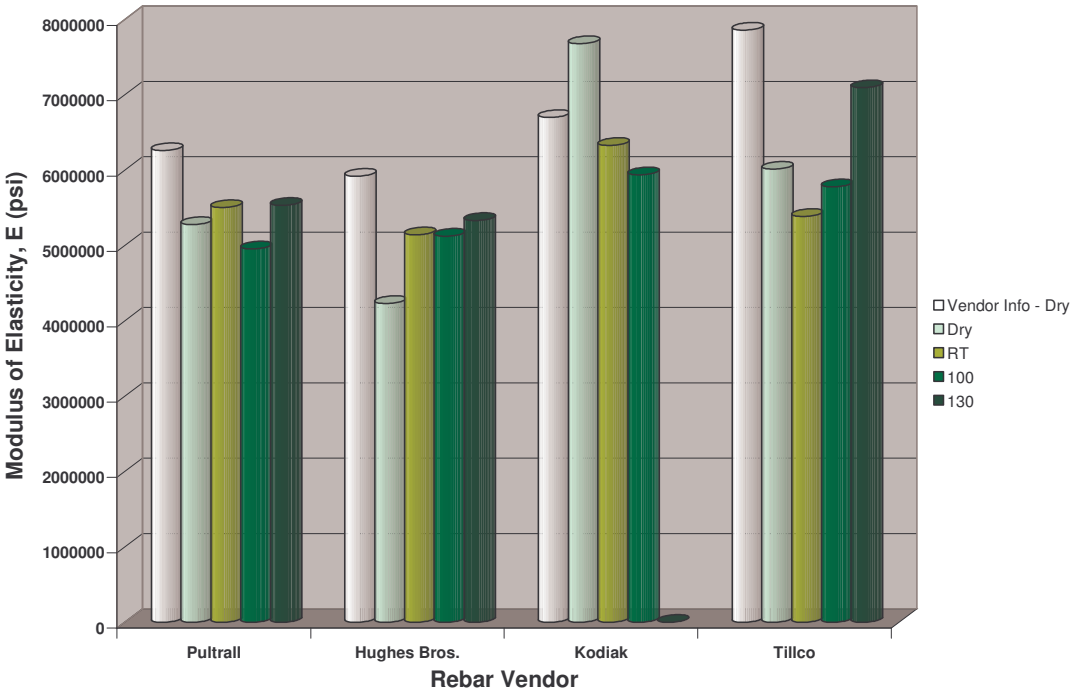

Figure 7.38 Average Modulus of Elasticity for Unscathed at 18 Months

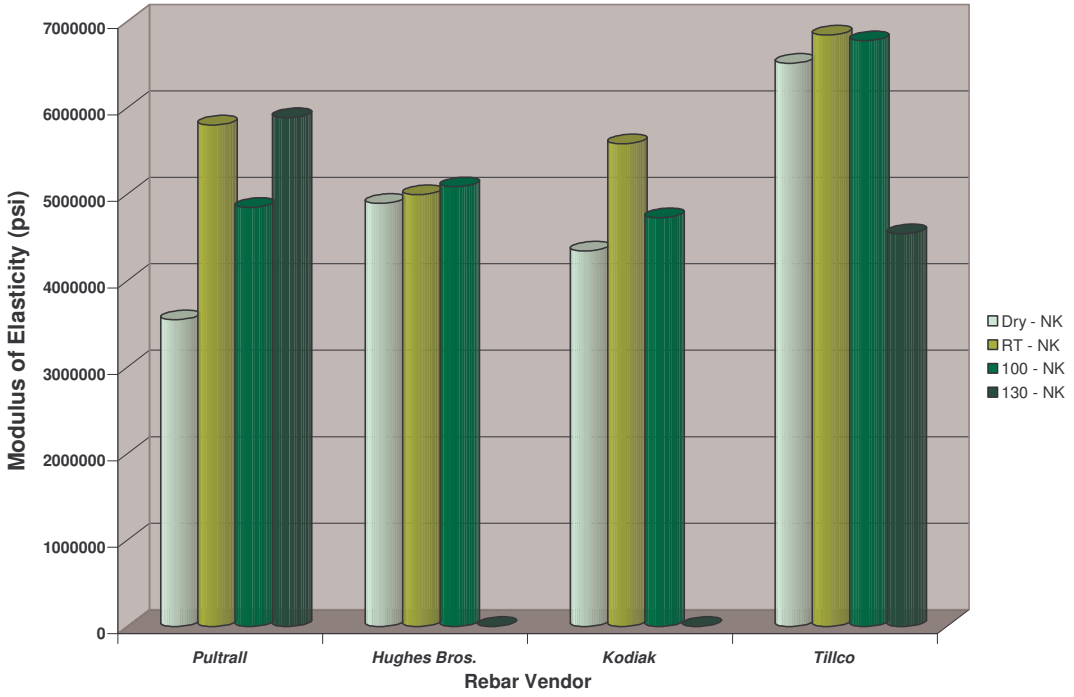

Figure 7.39 Modulus of Elasticity for Nicked at 18 Months

7.3.3 Overall Analysis

A common trend between all figures is the fact that the tensile strength decreases with increase in temperature, with the exception of some cases during the nicked specimens (i.e. Figure 53 for Pultrall and Hughes Bros.) The reasoning behind this difference in results is possibly due to there only being one sample for testing. If more samples had been tested, erroneous results could have been more readily recognized and, consequently, distended. Other possibilities of errors being introduced include: consistency in nicking the GFRP rebars, the positioning of the specimens within the testing machine to ensure loading aligned with the longitudinal axis, or slippage within the gripping mechanisms. Further research of the nicking of the fibers should be conducted with a larger testing sample.

A common trend between all figures is the fact that the stiffness measures are stable for all environments between Pultrall and Hughes Bros. rebars at 3 months, 6 months and 18 months (within 10% of the stated stiffness); however, Kodiak and Tillco rebars both experienced a decline in moduli relative to harsh environment exposures and long durations. The nicked specimens, on the other hand, seem to vary in stiffness. As stated, during the investigation of the rebar tensile strength, the difference may be due to only having one sample available for testing.

7.4 Bond-Stress Results

The bond-stress specimens were tested at 6 Month, 12 Month, and 18 Month durations within the four different environments (i.e. dry conditions, room temperature, 100°F, and 130°F). The dry conditions, 100°F, and 130°F environments had two specimens at each embedment length for each rebar vendor. The three duration periods of the control test samples (dry conditions) were averaged. Three LVDTs and a strain gage were used to monitored slippage of the bar, crushing of the concrete, and elongation of the rebar. Through this data, slippage could be accurately calculated in order to plot bond-stress versus slippage diagrams, which are presented in Appendix E. Upon completion of the

pullout test samples, the concrete cylinders were smoothed and capped so as to test the concrete for stiffness and compressive strength in accordance to ASTM C496 and ASTM C39/C39M, respectively.

7.4.1 Bond Stress Analysis

The following table is a representation of the decrease in strength throughout the duration in the alkaline environments. The decrease in bond stress is based on the overall average of the control samples under dry conditions. The percentage decrease is based on the average of all four vendors GFRP bars.

Table 7.8 Average Bond Stress (psi) for Two Different Development Lengths

Development Length	Temperature	Duration		
		6 Months	12 Months	18 Months
5Øb	DRY	2407	1976	1689
	RT	2405	2098	1796
	100°F	2125	1857	1601
	130°F	1690	1252	1004
8Øb	DRY	2615	2474	2248
	RT	2132	1754	1564
	100°F	2307	1655	1260
	130°F	1967	1292	1127

From Table 7.8, the rebars were found to lose bond strengths over long exposure periods to the harsh aging exposures and elevated temperatures. Again, the results presented have several factors that could not be eliminated during testing: eccentricity of the specimen during loading, inadequate sample size for testing (i.e. one sample for room temperature), and the degradation of the rebars during exposures to the alkaline environment and elevated temperatures. From the test results, it was found that the protective coating along with bulges throughout the longitudinal length of the rebars increased the bond strength of the GFRP rebar.

In the following figures representing the average bond stress of the test specimens, those bars that are discolored represent the expected trend, though not achieved experimentally,

as based on other similar experimental trends.

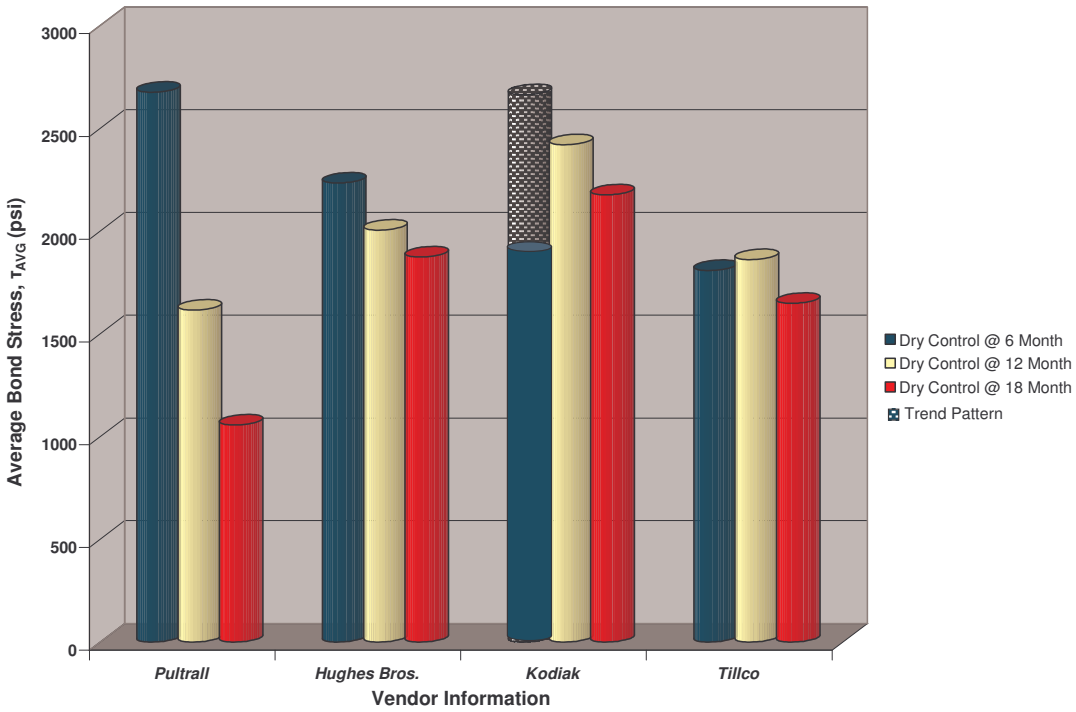

Figure 7.40 Average Bond Stress for $5Ø_b$ for Dry Conditions

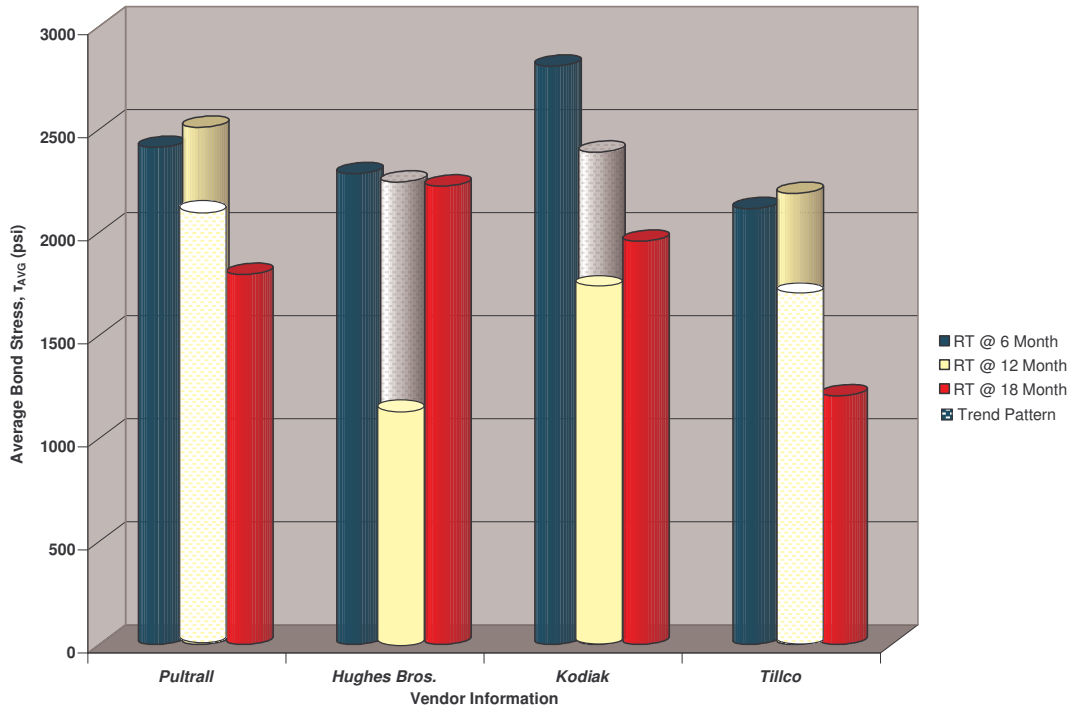

Figure 7.41 Bond Stress for $5Ø_b$ for Room Temperature

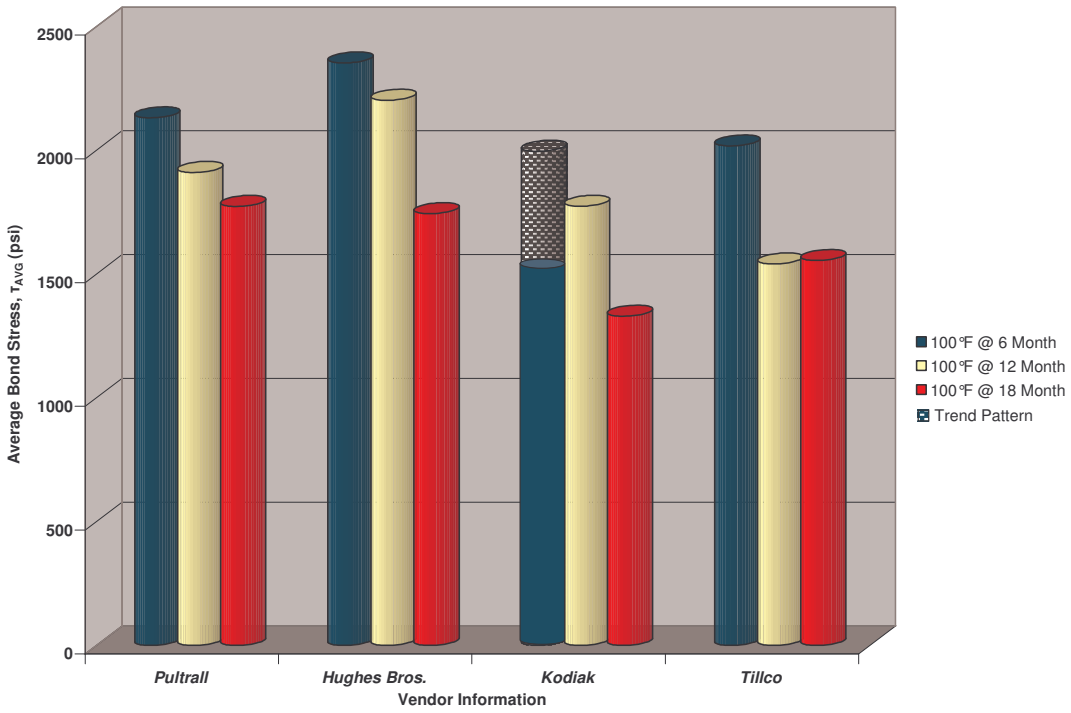

Figure 7.42 Average Bond Stress for 5$Ø_b$ for 100 ℉

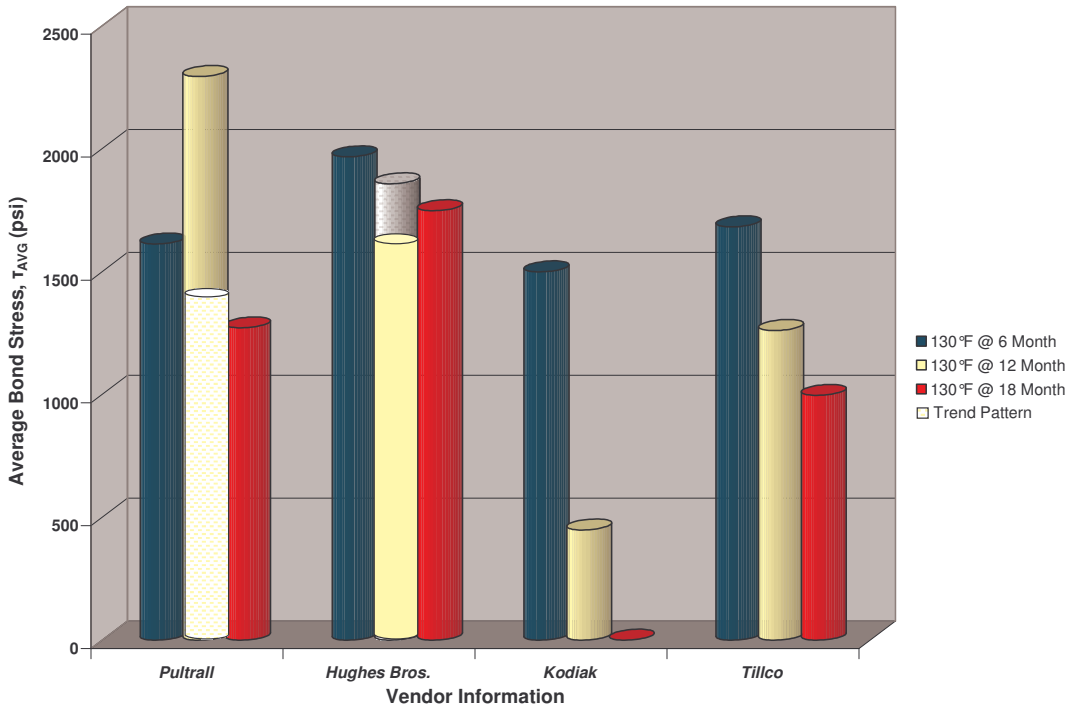

Figure 7.43 Average Bond Stress for 5$Ø_b$ for 130 ℉

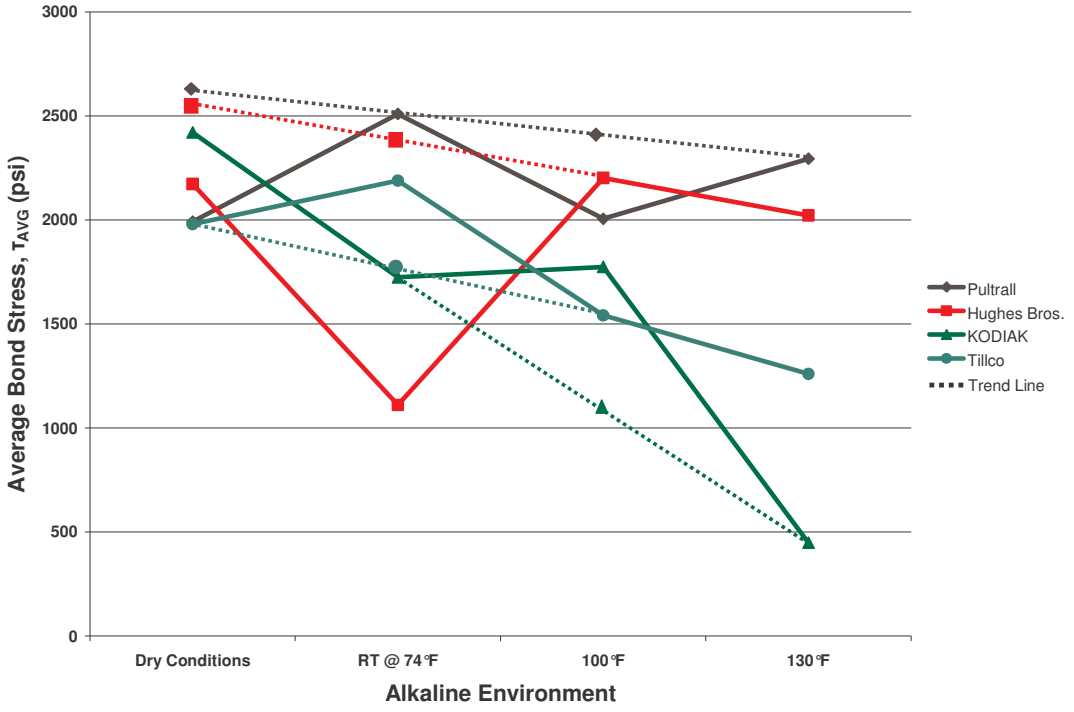

Figure 7.44 Trend Line of Bond Stress for $5Ø_b$ at 6 Months

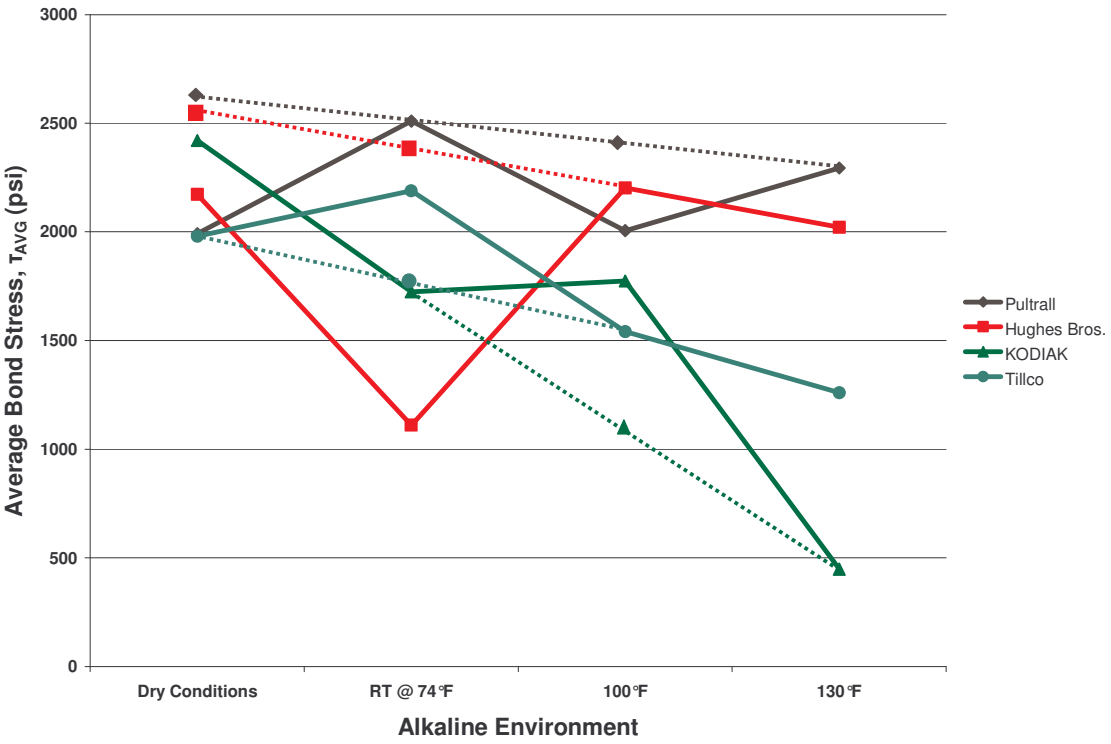

Figure 7.45 Trend Line of Bond Stress for $5Ø_b$ at 12 Months

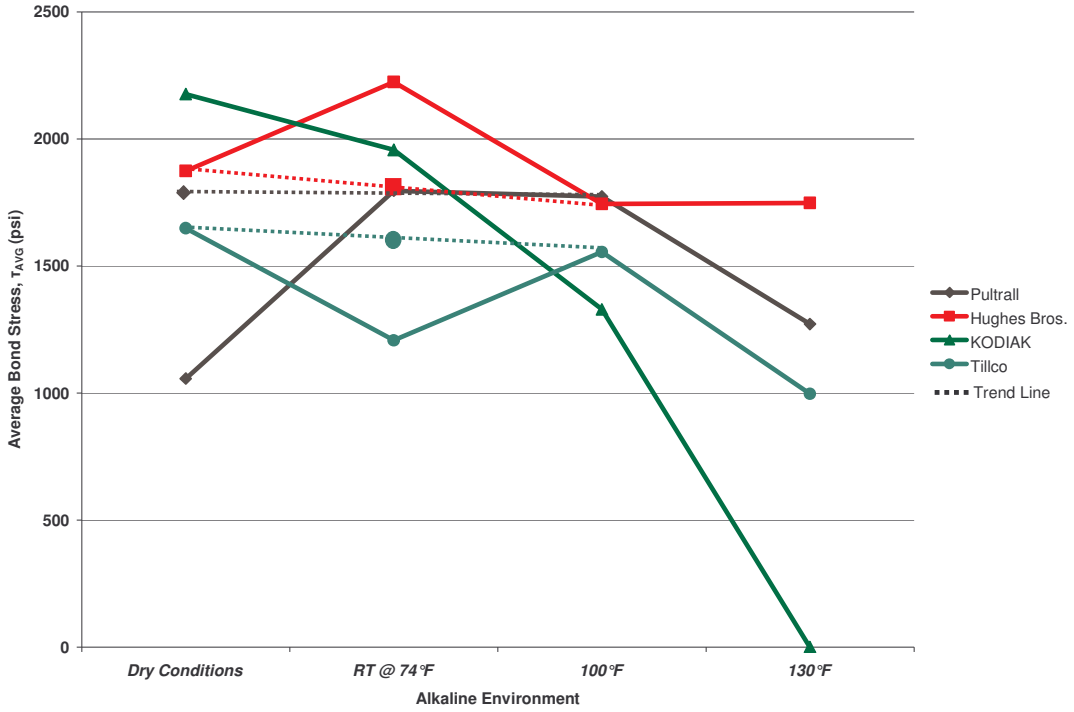

Figure 7.46 Trend Line of Bond Stress for 5$\varnothing_b$ at 18 Months

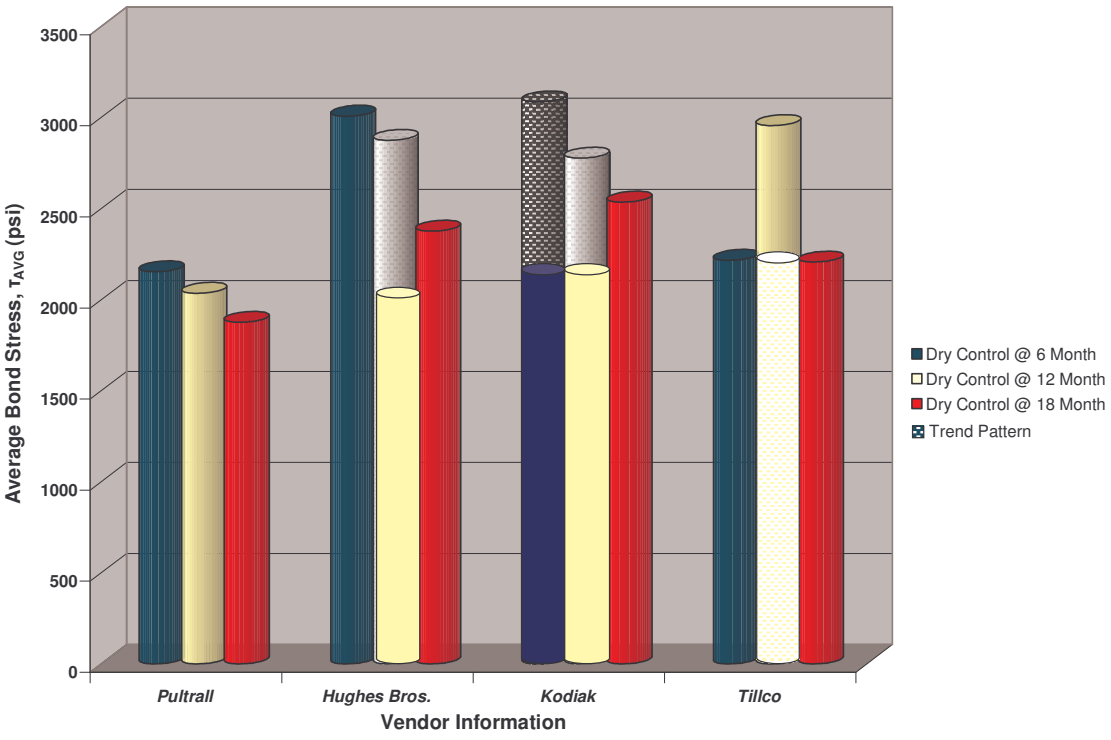

Figure 7.47 Average Bond Stress for 8$\varnothing_b$ for Dry Conditions

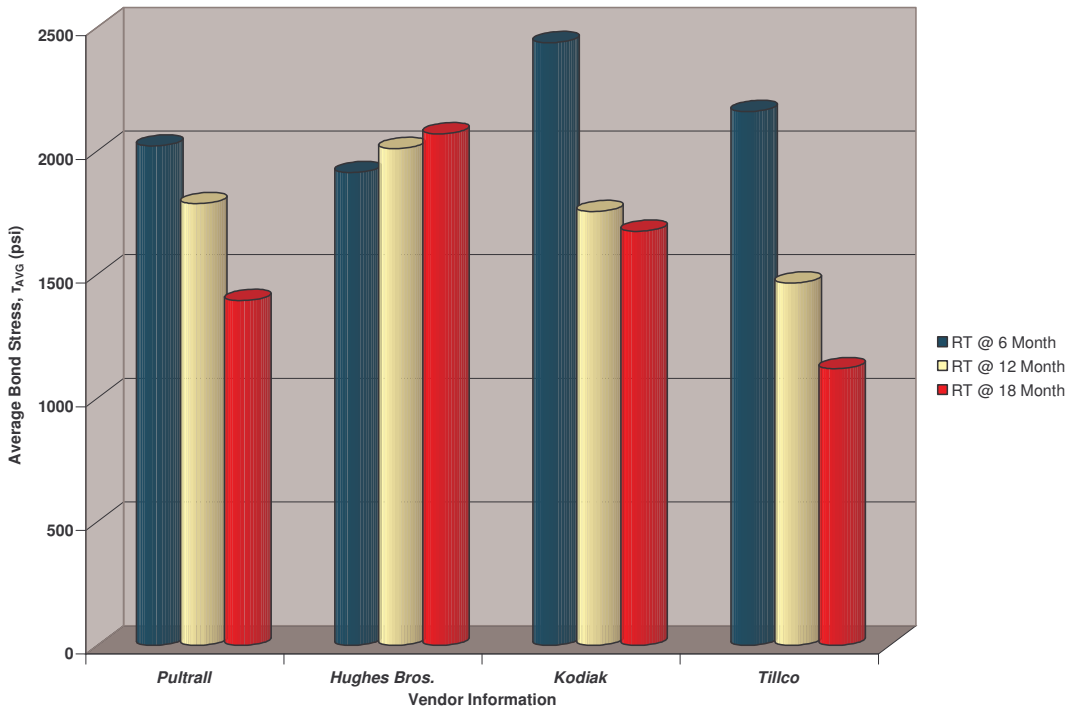

Figure 7.48 Bond Stress for $8\varnothing_b$ for Room Temperature

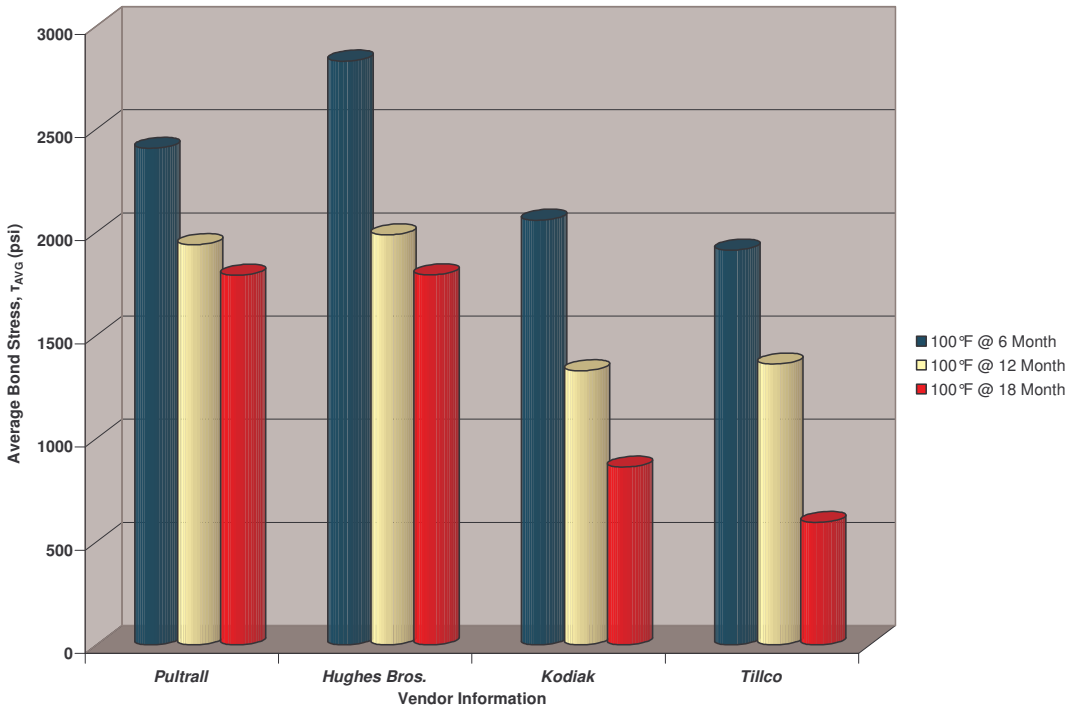

Figure 7.49 Average Bond Stress for $8\varnothing_b$ for 100℉

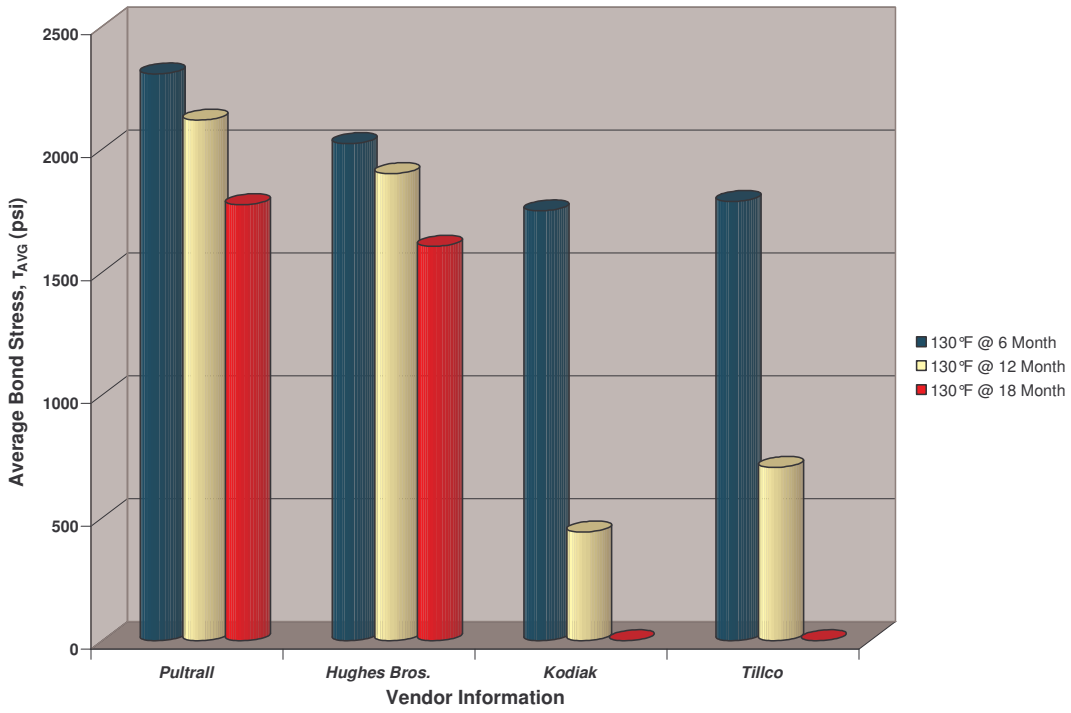

Figure 7.50 Average Bond Stress for 8$\emptyset_b$ for 130℉

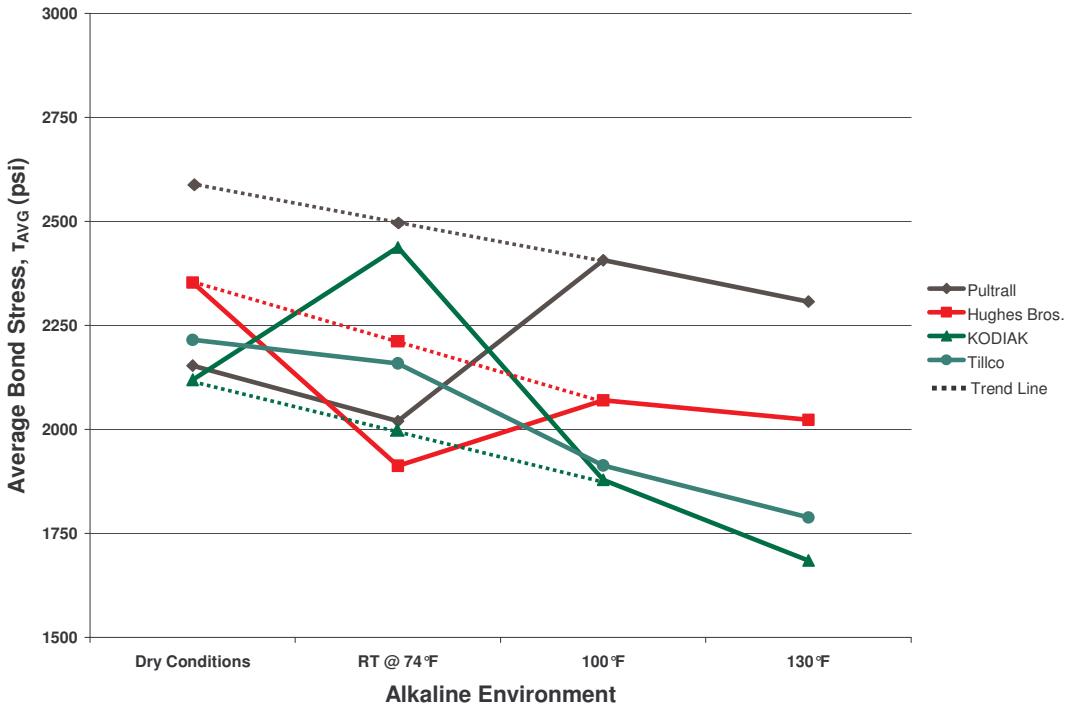

Figure 7.51 Trend Line of Bond Stress for 8$\emptyset_b$ at 6 Months

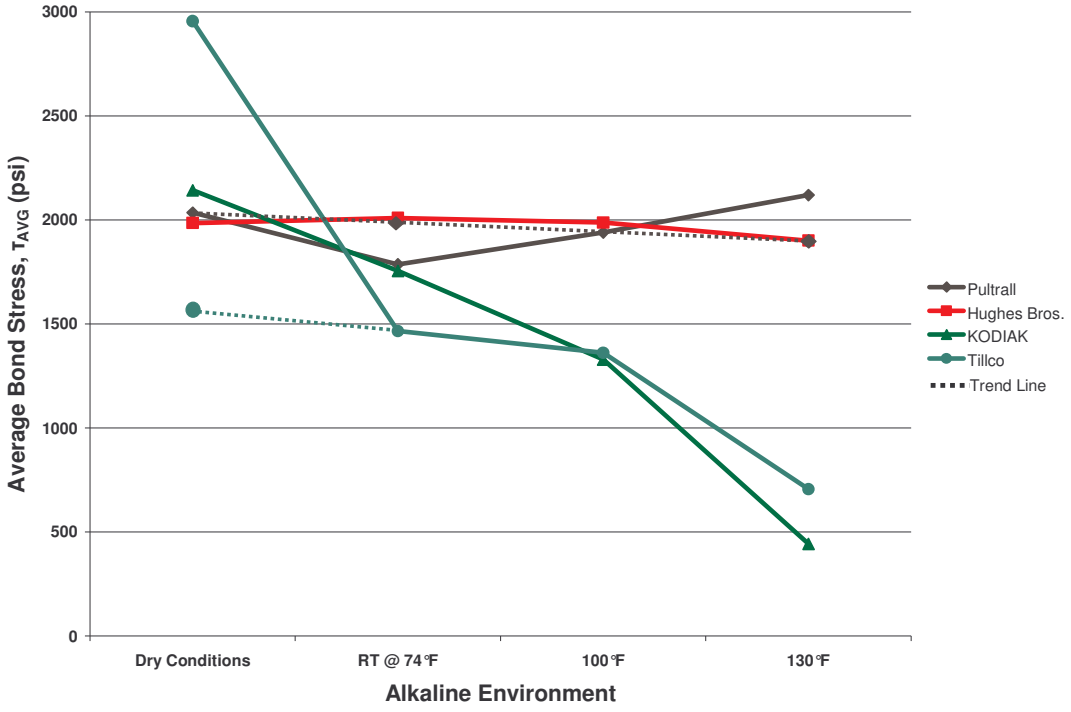

Figure 7.52 Trend Line of Bond Stress for 8$\emptyset_b$ at 12 Months

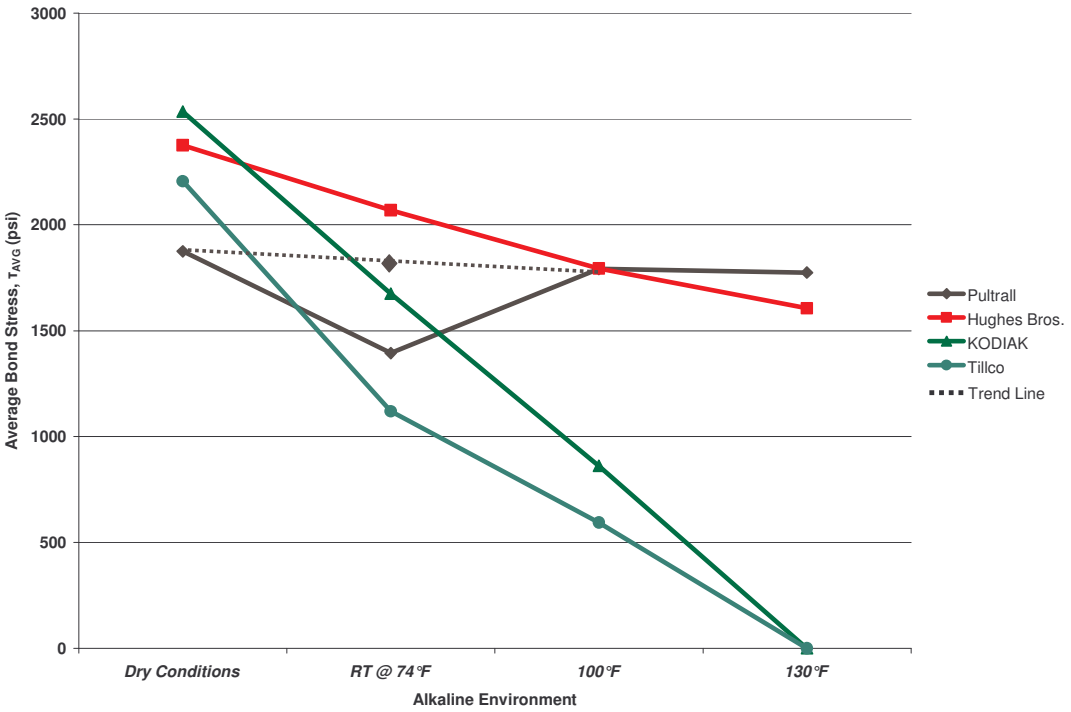

Figure 7.53 Trend Line of Bond Stress for 8$\emptyset_b$ at 18 Months

Figures 7.44, 7.45, 7.46, 7.51, 7.52 and 7.53 show overall trend lines, although there are some instances that a data point seems to not follow expected behavior, i.e. room temperature results in Figure 7.43 for Pultrall, Hughes Bros. and Kodiak, where a proper trend point along with a proposed trend line are placed within the figure. Again, these trend lines are based on an overall analysis of the data collected during testing. Therefore, the researchers proposed these trend lines with the intent to interpret such characteristic behavior – further testing should be conducted on a larger sampling size to verify such conclusions from this study. Bond stress as a function of slippage displacement results collected from the DAQ system is represented in Appendix I.

8. Conclusions and Recommendations

8.1 Structural Analysis and Test Conclusions

Extensive numerical analyses were performed on the actual bridge deck, on the prestressed girders, and on the lab model. Furthermore, a large-scale laboratory model was also built with the same cross-section (except the parapet portion) as the actual bridge deck. All of these analyses and tests proved that the governing failure mode for these bridge decks (similarly to traditional steel-reinforced bridge decks) is punching shear, as anticipated. It was also proved that the failure loads well exceed the design vehicular load levels, and occurred at GFRP rebar strain levels far below the ultimate values. This suggests that in future GFRP rebar applications the reinforcement ration could be further reduced, making composite reinforcements a more economical alternative from the structural/construction point of view.

Once completed, the bridge located in Macon Co. was instrumented and load tested using two fully loaded tandem trucks. Strain and displacement measurements were taken by 72 instruments installed throughout the 3-span bridge. Both quasi-static and dynamic tests were performed following 7 and 3 load paths, respectively. The results indicate that the applied dynamic load did not increase the live load impact factor by more than 9%, when the larger strain readings were considered. Furthermore, the recorded maximum girder deformations were well below the limits specified by AASHTO. Finally, the measured distribution factors for both exterior and interior girders were within the expected range.

8.2 Durability Absorption Test Conclusions

Several tests were conducted during the 18 Month period ranging from the testing of GFRP rebars for moisture uptake relative to changes in lengths, diameters, and weights, to the percentage degradations of tensile and stiffness properties of specimens along with simple pullout tests to observe changes in the bond strengths of the various types of the GFRP rebars based on differing reinforcements, outer surface coatings, and exposure to

alkalinity at different temperatures. From the test results, several conclusions can be drawn to aid in the implementation of these composite rebars in design applications to highway structures.

From the absorption tests, it was found that the GFRP rebars incurred sizable strains in the longitudinal and, even more noticeably, in the hoop directions. It must be stated, however, that this was the case for the bare rebars, and in order to fully qualify this assertion for embedded rebars within concrete structures having adequate cover, additional tests would have to be performed to ascertain differential strain readings. Other concerns related to temperature effects particularly with reference to differing coefficients of thermal expansions (CTEs) between the composite and concrete materials, were concluded not to play a major role; longitudinally, the CTEs between the rebar ($\approx 3.3 \times 10^{-6}$ 1/F - 5.6×10^{-6} 1/F) and the concrete ($\approx 4 \times 10^{-6}$ 1/F - 6×10^{-6} 1/F) are very similar; transversely, the CTE of the rebar ($\approx 12 \times 10^{-6}$ 1/F) is slightly greater than double that of the concrete ($\approx 5 \times 10^{-6}$ 1/F), though, for the extreme temperatures considered in this project with a temperature differential of nearly 60 F, the imparted strains were only found to be around 700 με, which is considerably less than the threshold strain-level of concrete acting in compression.

The tensile and stiffness properties were found to decrease during increased exposures to the alkaline environment and elevated temperatures. There was approximately a 25% decrease in the tensile strengths of the nicked specimens as compared to their control counterparts. As observed during the absorption testing, the tensile and stiffness properties greatly decreased during the accelerated aging processes for the Kodiak and Tillco rebars, whereas the Pultrall and Hughes Bros. only showed a decrease in material properties, such as degradation of protective coating, tensile strength and overall stiffness. After the 6 month duration period, the Kodiak samples had degraded to such an extent that it was impossible to continue testing for these specimens (see Figure 7.7); after the 12 month period, the same could also be said for the Tillco rebars. The nicked specimens experienced similar losses in strength and stiffness as did the unscathed specimens. In conclusion, some surface protective coating such as the fine silica sand

coating as furnished to the Pultrall and Hughes Bros. rebars were found to retard the deterioration of the GFRP material properties.

For the pullout specimens, the degradation surface of the protective coating along with the hoop expansion (i.e. bulging) of the rebars during the pultrusion process is thought to have enhanced the bond strength of the GFRP rebars. During testing, all rebars experienced a pullout failure as originally designed for testing purposes. The theoretical relationship is for the bond stress (τ) is:

$$\tau = \frac{P}{\pi d_b \ell_d}$$

where P is the applied load, d_b is the bar diameter, and ℓ_d is the development length.

The empirical development length as dictated by ACI 440.1R-06, Eq. (11-2) is given as:

$$\frac{\tau}{\sqrt{f_c'}} = 4.0 + 0.3\frac{C}{d_b} + 100\frac{d_b}{\ell_d}$$

where the code restricts the C/d_b to a maximum value of 3.5. Using, then, a conservative value obtained for the average bond stress from among the testing-dataset of: $\tau \approx 700$ psi, a concrete strength, $f'_c \approx 6000$ psi, and a $d_b = 0.375$", the value of the development length for a #3 GFRP was found to be:

$\ell_d \approx 9.4$"

which, when divided by d_b, gives the following ratio:

$\ell_d/d_b \approx 25$

This is in line with the minimum requirements recommended by ACI 440.1R-06 of $20d_b$, though, some manufacturers, e.g. Mr. Doug Gremmel of Hughes Bros., recommends using an $\ell_d \approx 40d_b$.

Such values of ℓ_d are considerably larger than what governs for regular steel rebars, the #3 value being:

$\ell_d/d_b \approx 9$

which is less than half.

Overall, the chloride durability of the GFRP rebars is much better than that as exhibited by the Epoxy Coated Rebars (ECR) because the latter is still susceptible to corrosion should the epoxy coating become compromised for any reason. The major durability problem with the GFRP rebars, however, is exposure to alkaline environments, as present naturally in the environment of normal Portland cement mixes. Suggestions to mitigate these effects include using concretes with fly ash (see ASTM C618) and silica fume (see ASTM C1240) thus resulting in lowered pH values (i.e. high-performance concretes (HPCs); use of low-alkali cements (if available) is also recommended, though this will likely increase construction-costs.

To give an idea of present costs, Hughes Bros. charges ≈44¢/ft for the straight #3 rebars. Tillco charges ≈39¢/ft for the straight #3 rebars. Contrast this with straight #3 steel rebars which cost around ≈12¢/ft, i.e. about 1/4 - 1/3 the cost.

Generally speaking, GFRP rebars offer the following advantages:

-Densities ranging between $1/6^{th}$ - $1/4^{th}$ (i.e. 80 - 130 pcf) that of steel rebars, they offer a reduction in weight that leads to lowered transportation costs and easier handling on the project site.

-Resistance to corrosion

-Higher tensile strengths (≈30% - 50% higher than steel)

-FRP rebars are electrically and thermally nonconductive

So, GFRP rebars are well-suited alternatives in bridge decks where de-icing salts are used, and a for in/near marine structure use.

From the findings of this research undertaking, it is recommended that the GFRP rebars provided by Pultrall and Hughes Bros. be used.

9. Implementation and Technology Transfer Plan

9.1 Durability Implementation and Technology Transfer Plan

Research Product: Concrete Protection Products Inc. (Pultrall)

Suggested User: NCDOT, Bridge Designers

Recommended Use: bridge deck applications, i.e. NCDOT Bridge in Macon County, for which corrosive environments, i.e. marine and de-icing agents, may be present.

Recommended Training: application and procedure of GFRP rebar placement within bridge decks.

Research Product: Hughes Bros.

Suggested User: NCDOT, Bridge Designers

Recommended Use: bridge deck applications, i.e. NCDOT Bridge in Macon County, for which corrosive environments, i.e. marine and de-icing agents, may be present.

Recommended Training: application and procedure of GFRP rebar placement within bridge decks.

Research Product: Kodiak

Suggested User: Materials and Test

Recommended Use: should be further researched and tested due to the high degradation rate within a simulated concrete environment; recommendations are that a protective coating similar to those as furnished by the Pultrall and Hughes Bros. rebars be applied to increase the durability of this rebar.

Recommended Training: none

Research Product: Tillco

Suggested User: Materials and Test

Recommended Use: should be further researched and tested due to the high degradation rate within a simulated concrete environment; recommendations are that a protective coating similar to those as furnished by the Pultrall and Hughes Bros. rebars be applied to increase the durability of this rebar.

Recommended Training: none.

OVERALL RECOMMENDATION

Research Product: Various GFRP Rebar Vendors

Suggested User: NCDOT Highway Department, Consultant Bridge Designers

Recommended Use: taking the protective coating of Pultrall and Hughes Brothers, and the increased deformities in the bars produce in Kodiak, combining the two strengths of the rebar vendors to create a bar that will have a protective coating against an alkali attack along with an increased in bond strength for bridge deck applications, i.e. NCDOT Bridge in Macon Bridge, where corrosive environment, i.e. saltwater, marine, and de-icing, are severe; an approximate life expectancy was determined for the four rebars based on previous analytical models (Nkurunziza et al., 2002), (Vijay, 1999); the life expectancy of Pultrall and Hughes Bros. is projected to be approximately 60 to 90 years, Tillco is projected to have a life expectancy of 40 to 60 years, while Kodiak had the shortest life expectancy of 20 to 30 years.

Recommended Training: application and procedure of GFRP within bridge decks.

9.2 Structural Implementation and Technology Transfer Plan

Research Product: GFRP deck reinforcement performance

Suggested User: bridge designers

Recommended Use: considering the fact that both analytical and experimental results yielded GFRP rebar strains and stresses well below its design limits, it is suggested to use a smaller deck reinforcement ratio in both top and bottom mats (both directions).

Recommended Training: none

Research Product: developed FE model

Suggested User: bridge designers

Recommended Use: the attached FE batch file can be used, with reasonable confidence, in future GFRP deck reinforcement parametric studies and initial design calculations.

Recommended Training: some minor modifications to this batch file would be required to tailor the model to actual bridge parameters of future design and construction projects.

10. References

AASHTO Standard Specifications for Highway Bridges (1998), American Association of the State Highway and Transportation Officials.

AASHTO LRFD Bridge Design Specifications (2004), U.S. Customary Units, third Edition. American Association of the State Highway and Transportation Officials.

ACI 440.3R-04 Guide Test Methods for Fiber-Reinforced Polymers (FRPs) for Reinforcing or Strengthening Concrete Structures, American Concrete Institute, 2004.

Advantages of Bristar (2005), Technical Data Sheet/Product Sheet, Demolition Technologies Inc., June 2005.

ANSYS (2002), ANSYS University Advanced User's Manual Release 8.0, ANSYS Inc.

ASTM C 39/C 39M, Standard Test Method for Compressive Strength of Cylindrical Concrete Specimens, American Society for Testing and Materials.

ASTM C 192, Standard Practice for Making and Curing Concrete Test Specimens in the Laboratory, American Society for Testing and Materials.

ASTM C 231, Standard Test Method for Air Content of Freshly Mixed Concrete by the Pressure Method, American Society for Testing Materials.

ASTM C 496, Standard Test Method for Splitting Tensile Strength of Cylindrical Concrete Specimens, American Society for Testing and Materials.

Benmokrane, B., Tighiouart, B., Challal, O. (1996), Bond Strength and Load Distribution of Composite GFRP Reinforcing Bars in Concrete, Title No. 93-M28, ACI Materials Journal, May-June 1996, pp. 246-253.

Bristar Technical Information, Technical Data Sheet, Demolition Technologies Incorporated, Greenville, AL, 2005.

Boyd, Curtis Barton (1997), A Load-Deflection Study of Fiber Reinforced Plastics as Reinforcement in Concrete Bridge Decks, Master Thesis, Department of Civil Engineering at Virginia Polytechnic Institute & State University, May 1997.

Calcium Chloride Ice Melting, (1992), Technical Data Sheet, Scotwood Industries.

Cusson, R. and Xi, Y., The Behavior of Fiber-Reinforced Polymer Reinforcement in Low Temperature Environmental Climates, Report No. CDOT-DTD-R-2003-4, Department of Civil, Environmental & Architectural Engineering, University of Colorado, Boulder, CO, 2002.

Fiberglass Rebar Material Properties, (2005), Technical Data Sheet, Concrete Protection Products, Inc. (CPPI), June 2005.

General Purpose Strain Gages – Linear Pattern, Technical Data Sheet, Vishay Intertechnology, Inc., Malvern, PA, 2005.

Hassan, T.K., Rizkalla, S.H. (2003), Design Consideration for Continuous Bridge Deck Slabs (Project No. B-3485), Technical Report CFL-RD-2003/09, Constructed Facilities Laboratory, NC State University, Raleigh, North Carolina, September 2003.

Hassan, T.K., Rizkalla, S.H., Rochelle, R. (2004), Punching shear Strength of GFRP Reinforced Deck Slabs in Slab-Girder Bridges, 4th International Conference on Advanced Composite Materials in Bridges and Structures, Calgary, July 2004, pp. 1-8.

Ice-Stop Ice Control Agent, (1992), Product Data, Reilly Wendover, Division of Reilly Industries.

Kachlakev, D., Miller, T., Yim, S., Chansawat; K., Potisuk., T.(2001), Finite Element Modeling of Reinforced Concrete Structures Strengthened with FRP Laminates, Final Report SPR 316, Oregon Department of Transportation, Salem, Oregon, May 2001.

Kadioglu, Fethi, Pidaparti, Ramana M. (2004), Composite Rebars Shape Effect in Reinforced Structures, Composite Structures 67 (2005), March 2004, pp. 19-26.

Kinnunen, S., Nylander, H. (1960), Punching of Concrete Slab without Shear Reinforcement, Transactions of the Royal Institute of Technology, Stockholm, Sweden, No. 158.

Malvar, L. J., Tensile and Bond Properties of GFRP Reinforcing Bars, ACI Materials Journal, V. 92, No. 3, 1995, pp. 276-285.

MB-AE™ Air Entraining Admixture, Technical Data Sheet, Master Builders, Inc., BASF Admixtures, Inc., Ludwigshafen, Germany, 2005.

Model 3543 Long Gage Length Extensometer, Technical Data Sheet, Epsilon Technologies, Inc., Jackson, WY, 2005.

Muruts, M., and Nad, L., Laminated Glass Fiber Reinforced Plastic (GFRP) Bars in Concrete Structures, 2nd Int. PhD Symposium in Civil Engineering, Budapest, Slovakia, 1998.

Physical Data (2005), Technical Data Sheet, Tillco, June 2005.

Physical Properties – Aslan 100, 101 GFRP Rebar (2005), Technical Data Sheet, Hughes Brothers, June 2005.

Ray, Indrajit (2005), Assistant Professor, Civil Engineering Department, University of West Virginia, West Virginia, April 2005.

Sikadur® 300 High Modulus, High Strength, Impregnating Resin, Technical Data Sheet, Wetherill Park, New South Wales, 2005.

Somayaji, Shan (2001), Civil Engineering Materials – 2nd Edition, Prentice Hall, Upper Saddle River, New Jersey, 2001.

Tannous, Fares E., Saadatmanesh, Hamid (1999), Durability of AR Glass Fiber Reinforced Plastic Bars, Journal of Composites for Construction, February 1999, pp. 12-19.

Tastani, S. P., Pantazopoulou, S. J. (2002), Experimental Evaluation of the Direct Tension – Pullout Bond Test, Bond in Concrete – from research to standards, Department of Civil Engineering, Demokitus University of Thrace, Greece, 2002, pp. 1-8.

Vijay, P. V. (1999), Aging and Design of Concrete Members Reinforced with GFRP Bars, Ph.D. Dissertation, Department of Civil Engineering at West Virginia, West Virginia, 1999.

Appendixes

Appendix A – ANSYS calibration batch input file

```
/TITLE,Macon County Bridge - GFRP Deck
/PREP7
!*
!(03/01/05-FINAL)
!*
/PREP7
!*
ANTYPE,STATIC,NEW                !Suppresses the expanded interpreted input data listing
!*
ET,1,SOLID65                     !3-D Reinforced Concrete Solid
KEYOPT,1,1,0                     !Include extra displacement shapes
KEYOPT,1,5,1                     !Repeat solution at each integration point
KEYOPT,1,6,3                     !Print solution also at each integration point
KEYOPT,1,7,1                     !Include tensile stress relaxation after cracking to help convergence
!*
ET,2,LINK8                       !Link element for the pretensioning rebar
!*
MPTEMP,1,0
MPDATA,EX,1,,3370000             !Deck concrete
MPDATA,PRXY,1,,.2
TB,MISO,1,1,5,                   !Multilinear Isotropic Model
TBTEMP,0
TBPT,,0.00031,1044.7
TBPT,,.00068,2070
TBPT,,.00108,2865
TBPT,,.00148,3308
TBPT,,.00208,3500
TB,CONC,1,1,9,                   !'Concrete' model
TBTEMP,0
TBDATA,,.25,.25,444,-1,,
!*
MPTEMP,1,0
MPDATA,EX,2,,5900000             !GFRP rebar
MPDATA,PRXY,2,,.3
TB,BISO,2,1,2,                   !Bilinear isotropic Model
TBTEMP,0
TBDATA,,72000,,,,,
!*
MPTEMP,1,0
MPDATA,EX,3,,4030000             !Girder concrete
MPDATA,PRXY,3,,.2
TB,MISO,3,1,5,                   !Multilinear Isotropic Model
TBTEMP,0
TBPT,,.00037,1491.1
TBPT,,.00086,3094
TBPT,,.00139,4264
TBPT,,.00192,4840
TBPT,,.00248,5000
TB,CONC,3,1,9,                   !'Concrete' model
TBTEMP,0
TBDATA,,.25,.25,530,-1,,
!*
MPTEMP,1,0
MPDATA,EX,4,,29000000            !Steel rebar
MPDATA,PRXY,4,,.3
TB,BISO,4,1,2,                   !Bilinear isotropic Model
TBTEMP,0
TBDATA,,270000,,,,,
!*
R,1, , , , , , ,                 !Real constant-concrete (no rebar)
R,2,2,.03, ,90,2,.031,           !Real constant-top deck
```

```
R,3,2,.03, ,90,2,.04,                   !Real constant-bottom deck
!*
R,4,.153,0.0045,                        !Top-girder prestressing rebar
R,5,.306,0.0045,                        !Middle-girder prestressing rebar
R,6,.408,0.0045,                        !Bottom-girder prestressing rebar
!*
K,1,0,45,0,
K,2,0,47.5,0,
K,3,0,50.5,0,
K,4,0,53.,0,
!*
KGEN,4,1,4,1,5., , , ,0                 !deck keipont generation
KGEN,3,13,16,1,8.75,,,,0
KGEN,2,21,24,1,4.5, , , ,0
KGEN,3,25,28,1,3.5, , , ,0
KGEN,2,33,36,1,4.5, , , ,0
KGEN,2,37,40,1,8.5, , , ,0
KGEN,7,41,44,1,5., , , ,0
KGEN,4,65,68,1,8.8333, , , ,0
KGEN,2,77,80,1,4.5, , , ,0
KGEN,3,81,84,1,3.5, , , ,0
KGEN,2,89,92,1,4.5, , , ,0
!*
KGEN,2,21,37,4,,-2., , ,0               !1st girder keipoint generation
KGEN,2,97,101,1,,-7.7, , ,0
KGEN,3,103,105,1,,-12.5 , , ,0
KGEN,2,110,,,-7.5,, , ,0
KGEN,2,112,,,7.5,, , ,0
KGEN,2,110,114,1,,-8.3 , , ,0
KGEN,2,115,119,1,,-2. , , ,0
!*
KGEN,2,77,93,4,,-2., , ,0               !2nd girder keipoint generation
KGEN,2,125,129,1,,-7.7, , ,0
KGEN,3,131,133,1,,-12.5 , , ,0
KGEN,2,138,,,-7.5,, , ,0
KGEN,2,140,,,7.5,, , ,0
KGEN,2,138,142,1,,-8.3 , , ,0
KGEN,2,143,147,1,,-2. , , ,0
!*
A,1,2,6,5                               !Deck areas
A,2,3,7,6
A,3,4,8,7
!*
A,5,6,10,9
A,6,7,11,10
A,7,8,12,11
!*
A,9,10,14,13
A,10,11,15,14
A,11,12,16,15
!*
A,13,14,18,17
A,14,15,19,18
A,15,16,20,19
!*
A,17,18,22,21
A,18,19,23,22
A,19,20,24,23
!*
A,21,22,26,25
A,22,23,27,26
A,23,24,28,27
!*
A,25,26,30,29
A,26,27,31,30
A,27,28,32,31
!*
A,29,30,34,33
A,30,31,35,34
A,31,32,36,35
```

```
!*
A,33,34,38,37
A,34,35,39,38
A,35,36,40,39
!*
A,37,38,42,41
A,38,39,43,42
A,39,40,44,43
!*
A,41,42,46,45
A,42,43,47,46
A,43,44,48,47
!*
A,45,46,50,49
A,46,47,51,50
A,47,48,52,51
!*
A,49,50,54,53
A,50,51,55,54
A,51,52,56,55
!*
A,53,54,58,57
A,54,55,59,58
A,55,56,60,59
!*
A,57,58,62,61
A,58,59,63,62
A,59,60,64,63
!*
A,61,62,66,65
A,62,63,67,66
A,63,64,68,67
!*
A,65,66,70,69
A,66,67,71,70
A,67,68,72,71
!*
A,69,70,74,73
A,70,71,75,74
A,71,72,76,75
!*
A,73,74,78,77
A,74,75,79,78
A,75,76,80,79
!*
A,77,78,82,81
A,78,79,83,82
A,79,80,84,83
!*
A,81,82,86,85
A,82,83,87,86
A,83,84,88,87
!*
A,85,86,90,89
A,86,87,91,90
A,87,88,92,91
!*
A,89,90,94,93
A,90,91,95,94
A,91,92,96,95
!*
A,21,25,98,97                    !1st Girder's areas
A,25,29,99,98
A,29,33,100,99
A,33,37,101,100
!*
A,97,98,103,102
A,98,99,104,103
A,99,100,105,104
A,100,101,106,105
```

```
!*
A,103,104,108,107
A,104,105,109,108
!*
A,107,108,111,110
A,108,109,112,111
!*
A,113,110,115,118
A,110,111,116,115
A,111,112,117,116
A,112,114,119,117
!*
A,118,115,120,123
A,115,116,121,120
A,116,117,122,121
A,117,119,124,122
!*
A,77,81,126,125                 !2nd Girder's areas
A,81,85,127,126
A,85,89,128,127
A,89,93,129,128
!*
A,125,126,131,130
A,126,127,132,131
A,127,128,133,132
A,128,129,134,133
!*
A,131,132,136,135
A,132,133,137,136
A,135,136,139,138
A,136,137,140,139
!*
A,141,138,143,146
A,138,139,144,143
A,139,140,145,144
A,140,142,147,145
!*
A,146,143,148,151
A,143,144,149,148
A,144,145,150,149
A,145,147,152,150
!*
VEXT,1,109,1,,,5.,,,            !Volume extrusion (5 inches in the Z direction)
!*
VSEL,,,,2,68,3,                 !Middle layer in the deck
VATT,1,1,1,
!*
VSEL,,,,3,69,3,                 !Top layer in the deck
VATT,1,2,1,
!*
VSEL,,,,1,67,3,                 !Bottom layer in the deck
VATT,1,3,1,
!*
VSEL,,,,70,109,1,               !Girder
VATT,3,1,1,
!*
AGEN,2,1,109,1,,,20.,,,         !Copy the areas
!*
VEXT,479,587,1,,,14.,,,
!*
VSEL,,,,111,177,3,              !Middle layer in the deck
VATT,1,1,1,
!*
VSEL,,,,112,178,3,              !Top layer in the deck
VATT,1,2,1,
!*
VSEL,,,,110,176,3,              !Bottom layer in the deck
VATT,1,3,1,
!*
VSEL,,,,179,218,1,              !Girder
```

```
VATT,3,1,1,
!*
VSEL,ALL,,,,,                    !Select the volumes (to be active all)
VGEN,4,1,109,1,,,5.,,,           !Generates volumes
VGEN,10,110,218,1,,,14.,,,
VGEN,2,1,109,1,,,160.,,,
VGEN,8,1527,1635,1,,,5.,,,
VGEN,2,110,218,1,,,180.,,,
VGEN,10,2399,2507,1,,,14.,,,
VGEN,2,1,109,1,,,340.,,,
VGEN,4,3489,3597,1,,,5.,,,
!*
LSEL,S,LOC,Y,43.,                !Top-girder reinforcing rebar
LSEL,R,LOC,X,37.,
LATT,4,4,2,
!*
LSEL,S,LOC,Y,43.,
LSEL,R,LOC,X,44.,
LATT,4,4,2,
!*
LSEL,S,LOC,Y,43.,
LSEL,R,LOC,X,117.9999,
LATT,4,4,2,
!*
LSEL,S,LOC,Y,43.,
LSEL,R,LOC,X,124.9999,
LATT,4,4,2,
!*
LSEL,S,LOC,Y,22.8,               !Middle-girder reinforcing rebar
LSEL,R,LOC,X,40.5,
LATT,4,5,2,
!*
LSEL,S,LOC,Y,22.8,
LSEL,R,LOC,X,121.4999,
LATT,4,5,2,
!*
LSEL,S,LOC,Y,2.,                 !Bottom-girder reinforcing rebar
LSEL,R,LOC,X,37.,
LATT,4,6,2,
!*
LSEL,S,LOC,Y,2.,
LSEL,R,LOC,X,40.5,
LATT,4,6,2,
!*
LSEL,S,LOC,Y,2.,
LSEL,R,LOC,X,44.,
LATT,4,6,2,
!*
LSEL,S,LOC,Y,2.,
LSEL,R,LOC,X,117.9999,
LATT,4,6,2,
!*
LSEL,S,LOC,Y,2.,
LSEL,R,LOC,X,121.4999,
LATT,4,6,2,
!*
LSEL,S,LOC,Y,2.,
LSEL,R,LOC,X,124.9999,
LATT,4,6,2,
!*
LSEL,ALL,
!*
KGEN,2,41,73,4,,-2.,,,0          !Diaphragm keipont generation
KGEN,2,41,73,4,,-9.7,,,0
KGEN,3,10954,10962,1,,-12.5,,,0
KGEN,2,106,130,24,,-12.5,,,0
!*
KGEN,2,1,17,4,,-2.,,,0
KGEN,2,1,17,4,,-9.7,,,0
KGEN,3,10988,10992,1,,-12.5,,,0
```

```
KGEN,2,102,,,,-12.5,,,0
!*
!*
A,101,37,41,10945                    !Diaphragm areas
A,10945,41,45,10946
A,10946,45,49,10947
A,10947,49,53,10948
A,10948,53,57,10949
A,10949,57,61,10950
A,10950,61,65,10951
A,10951,65,69,10952
A,10952,69,73,10953
A,10953,73,77,125
A,106,101,10945,10954
A,10954,10945,10946,10955
A,10955,10946,10947,10956
A,10956,10947,10948,10957
A,10957,10948,10949,10958
A,10958,10949,10950,10959
A,10959,10950,10951,10960
A,10960,10951,10952,10961
A,10961,10952,10953,10962
A,10962,10953,125,130
A,109,105,106,10981,
A,10981,106,10954,10963
A,10963,10954,10955,10964
A,10964,10955,10956,10965
A,10965,10956,10957,10966
A,10966,10957,10958,10967
A,10967,10958,10959,10968
A,10968,10959,10960,10969
A,10969,10960,10961,10970
A,10970,10961,10962,10971
A,10971,10962,130,10982
A,10982,130,131,135
A,112,109,10981,114
A,114,10981,10963,10972
A,10972,10963,10964,10973
A,10973,10964,10965,10974
A,10974,10965,10966,10975
A,10975,10966,10967,10976
A,10976,10967,10968,10977
A,10977,10968,10969,10978
A,10978,10969,10970,10979
A,10979,10970,10971,10980
A,10980,10971,10982,141
A,141,10982,135,138
A,10983,1,5,10984
A,10984,5,9,10985
A,10985,9,13,10986
A,10986,13,17,10987
A,10987,17,21,97
A,10988,10983,10984,10989
A,10989,10984,10985,10990
A,10990,10985,10986,10991
A,10991,10986,10987,10992
A,10992,10987,97,102
A,10993,10988,10989,10994
A,10994,10989,10990,10995
A,10995,10990,10991,10996
A,10996,10991,10992,10997
A,10997,10992,102,11003
A,11003,102,103,107
A,10998,10993,10994,10999
A,10999,10994,10995,11000
A,11000,10995,10996,11001
A,11001,10996,10997,11002
A,11002,10997,11003,113
A,113,11003,107,110
!*
```

```
VEXT,17209,17274,1,,,5.,,,                !Diaphragm Volume extrusion (5 inches in the Z direction)
!*
VSEL,ALL,,,,,,                            !Copy diaphragm to the middle of the span
VGEN,2,3925,3990,1,,,355.,,,
!*
VSEL,,,,3925,4056,1,                      !Diaphragm concrete
VATT,3,1,1,
!*
LESIZE,ALL,,,1,,1,,,1,                    !Line mesh size is 1
!*
VSEL,ALL,,,,,,                            !Select the volumes
MSHAPE,0,3d                               !Element shape definition
MSHKEY,1                                          !Mapped meshing
VMESH,ALL                                 !Mesh all the volumes
!*
LSEL,S,REAL,,4,6,1
LMESH,ALL,
LSEL,ALL,
!*
!*
NUMMERG,ALL,,,,LOW                        !Merge numbers
NUMCMP,ALL                                !Compress numbers
!*
F,2591,FY,-3125,,2895,304                 !Applying the load
F,2743,FY,-6250,,,
F,2632,FY,-6250,,2648,16
F,2596,FY,-6250,,2900,304
F,2936,FY,-6250,,2952,16
F,2592,FY,-12500,,2896,304
F,2748,FY,-12500,,,
F,2636,FY,-12500,,2644,4
F,2784,FY,-12500,,2800,16
F,2940,FY,-12500,,2948,4
F,2744,FY,-25000,,,
F,2788,FY,-25000,,2796,4
!*
D,239,UY,0.0,,240,1,,,,,
D,243,UY,0.0,,247,2,,,,,
D,295,UY,0.0,,296,1,,,,,
D,299,UY,0.0,,303,2,,,,,
!*
ASEL,S,LOC,Z,360.
DA,ALL,SYMM
ASEL,ALL
!*
ASEL,S,LOC,X,0.
DA,ALL,SYMM
ASEL,ALL
!*
!*
FINISH
!*
SAVE                                      !Save the model
!*
/SOLU                                     !Solution
ANTYPE, STATIC
OUTPR,ALL,3,
OUTRES,ALL,3,
!*
AUTOTS,ON                                 !Program chosen
NSUBST,50,
SOLCONTROL,1.0,INCP
NCNV,0                                    !Don't stop the analysis if  not converging
SOLVE
!
FINISH
```

Appendix B – Laboratory test setup and instrumentation

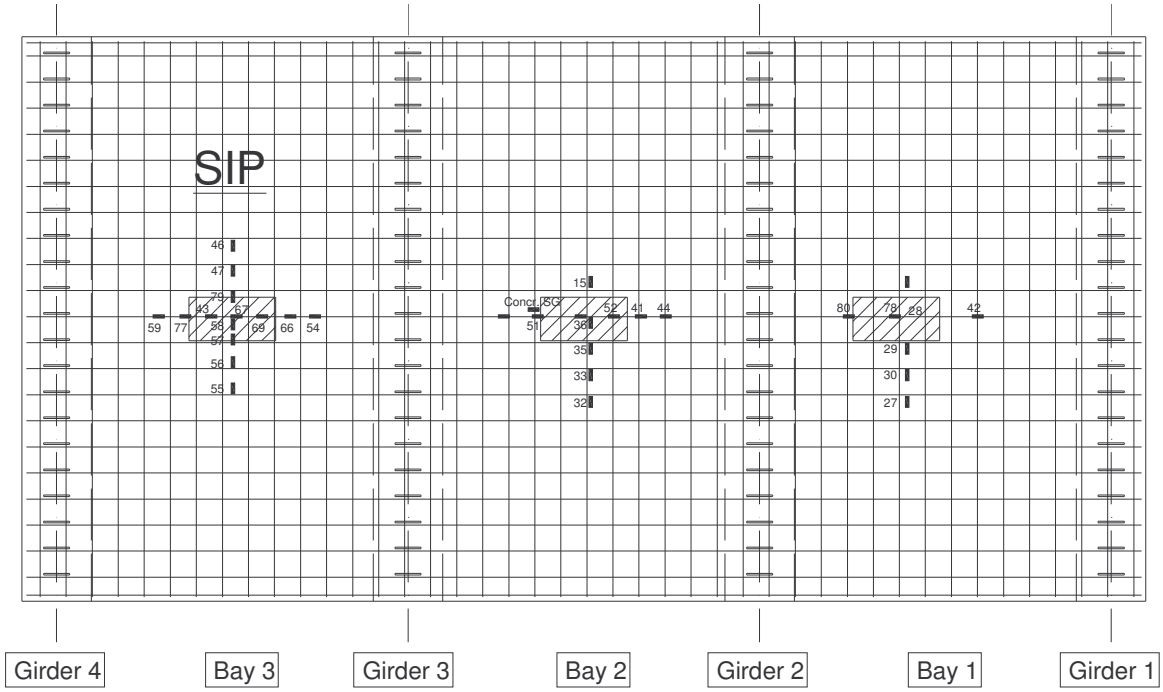

Figure B.1 Bottom layer reinforcing strain gages

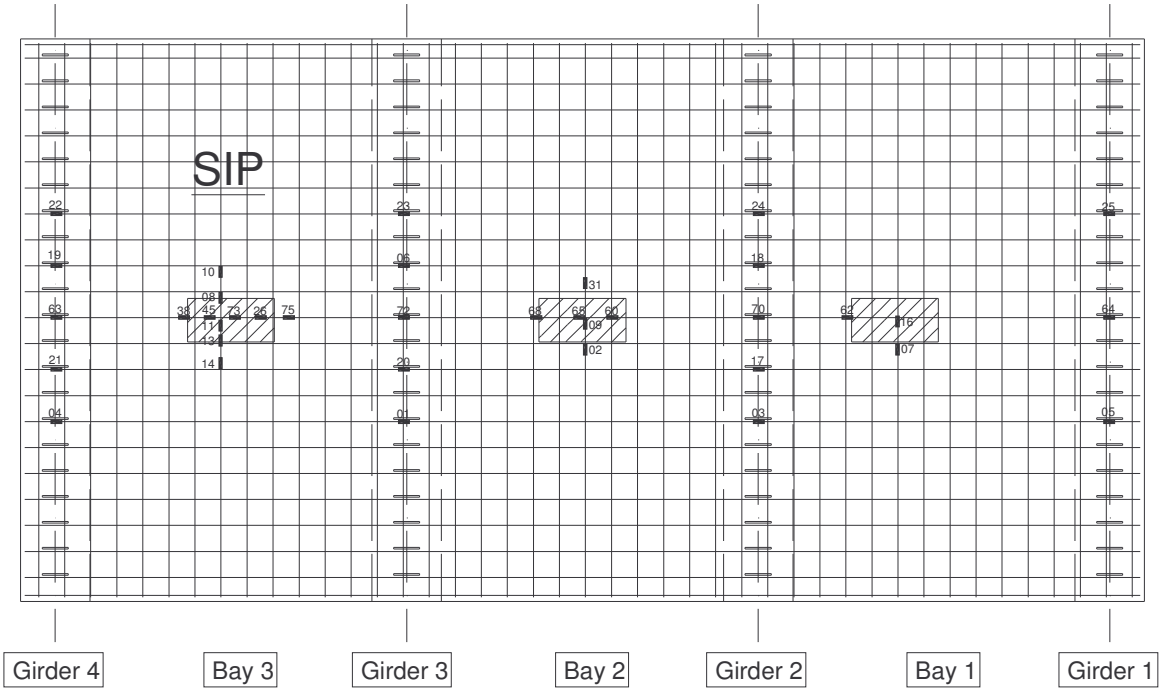

Figure B.2 Top layer reinforcing strain gages

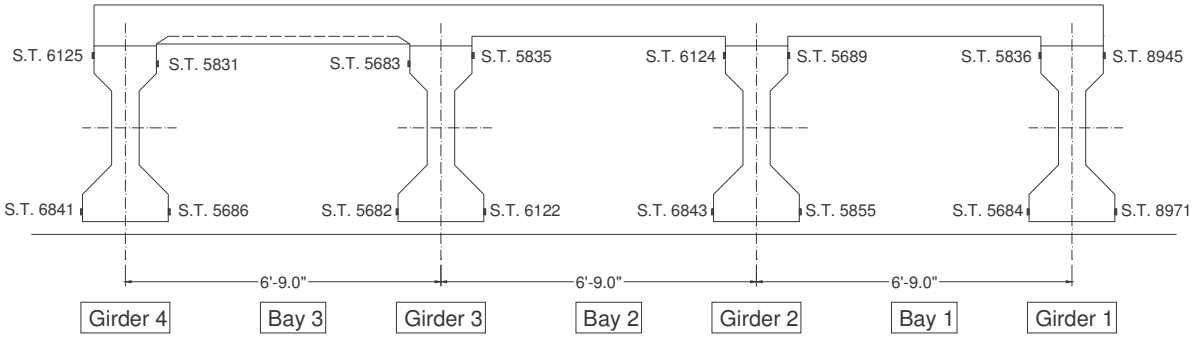

Figure B.3 Strain transducer positioning

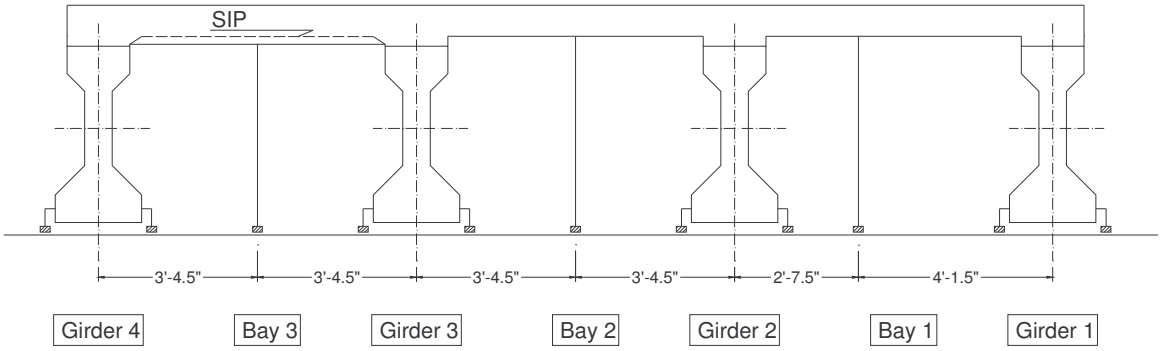

Figure B.4 Displacement transducer positioning

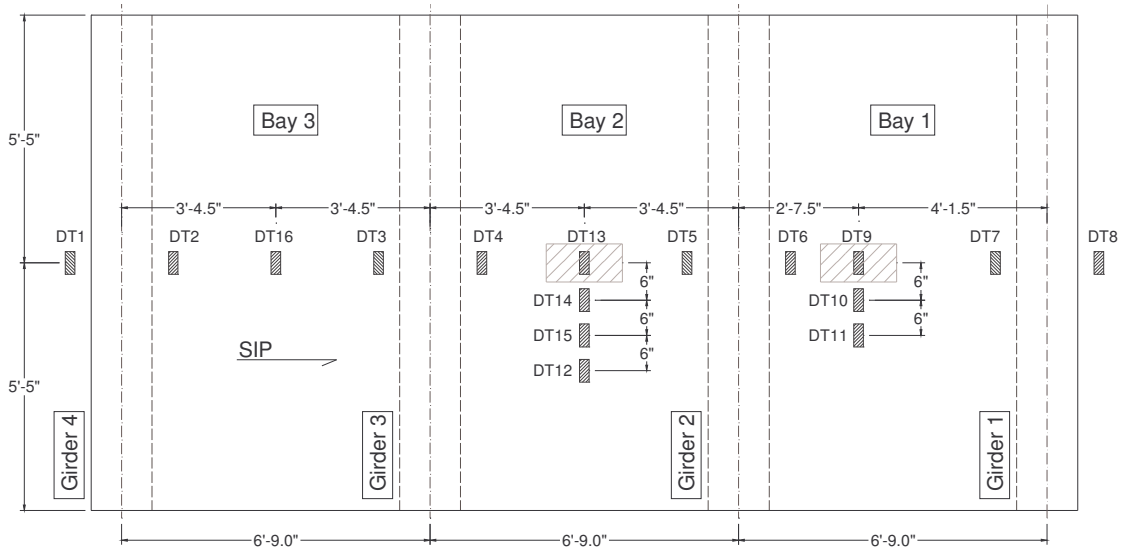

Figure B.5 Displacement transducers for TEST 1

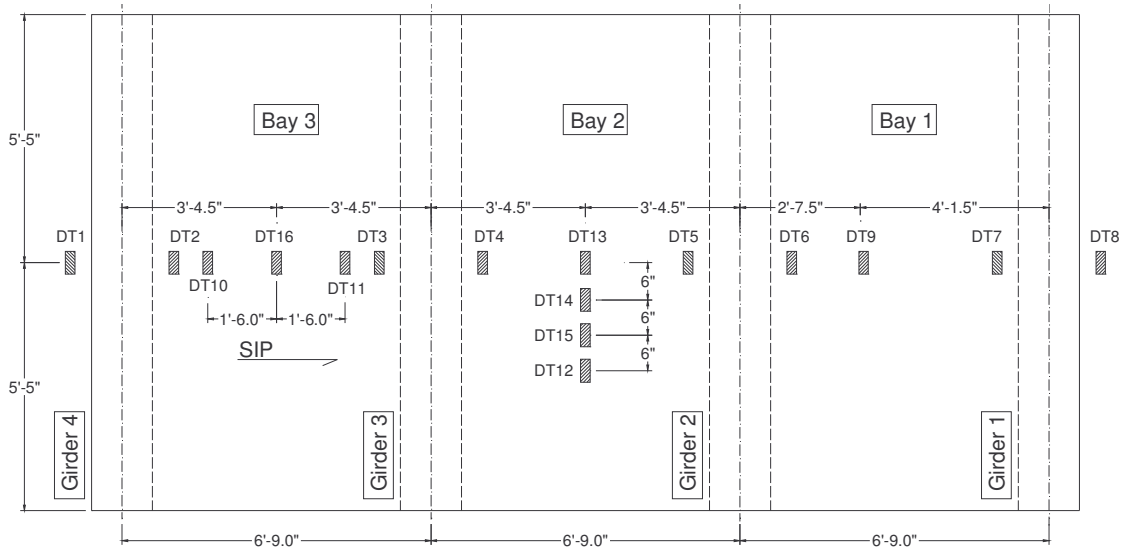

Figure B.6 Displacement transducers for TEST 2

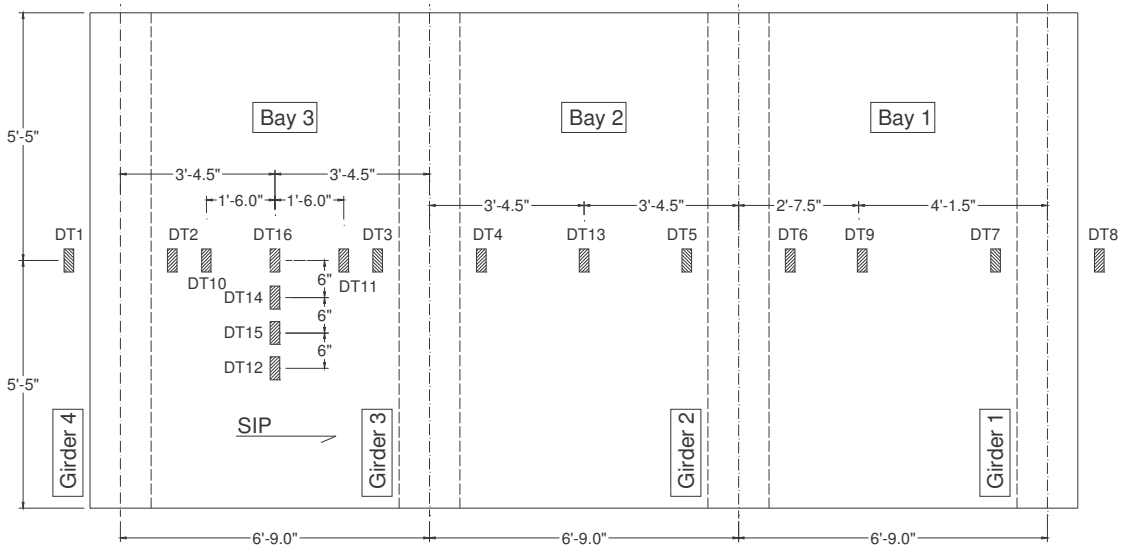

Figure B.7 Displacement transducers for TEST 3

Appendix C – Bridge construction report

As the single-span bridge No. 16 (shown in Figure C.1) on SR 1470 over Cartoogechaye Creek in Macon County, NC, no longer satisfied the need of the traveling public (posted below the legal load limit – as shown in Figure C.2), it was decided to replace it with a new 3-span bridge (NCDOT Project B-3485). The original structure consisted of timber piles, wooden abutments and steel girders.

In addition to a longer and wider new bridge, NCDOT decided to use glass fiber reinforced polymer (GFRP) rebars as deck reinforcement – a first in the state of North Carolina. Partial funding for the new construction, and for the related research project performed by UNC Charlotte, was provided by the Federal Highway Administration (FHWA) Innovative Bridge Research and Construction (IBRC) program.

Figure C.3 shows the layout of the new bridge and the existing structure (project drawings have been obtained from NCDOT's web page – public domain). As the new structure's length and width was significantly increased, new abutments and approach slabs were required, and the connecting pavement has been widened as well. In addition, to allow the construction of the two intermediate bents, a temporary causeway was built (see Figure C.4), which was completely removed before the end of the project. Figure C.5 shows the two completed reinforced concrete bents built on drilled piers.

Figure C.1 Original bridge site

Figure C.2 Original bridge posting

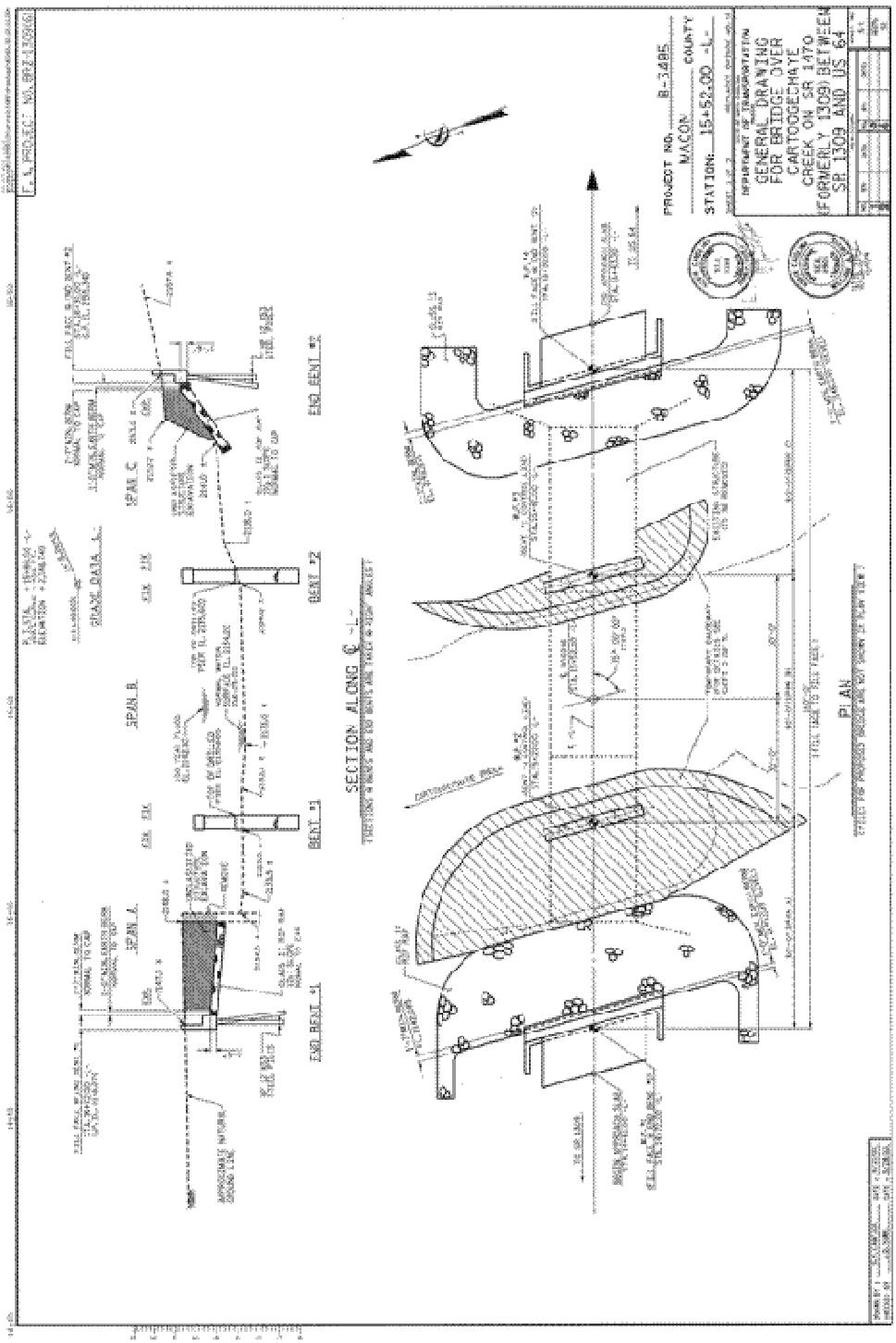

Figure C.3 General drawing of bridge replacement project

Figure C.4 Temporary causeway and site preparation

Figure C.5 Reinforced concrete bent construction

The new superstructure was designed as continuous for live load over three spans using an HS 20 design live load (i.e. continuous top reinforcement in the deck above the girder support). The outside spans are 50'-0" long, whereas the center span is 60'-0", each span designed with a 75^0 skew (see Figure C.6). Reinforced concrete end-bents, thru-bents, and intermediate diaphragms were specified.

The four, 3'-9" tall, AASHTO Type III prestressed concrete girders were positioned 6'-9" o.c. (see Figure C.7) on elastomeric bearing pads. The girders were reinforced with 7-wire ½" diameter low relaxation Grade 270 strands, 12 and 20 strands per girder, for the short and long girders, respectively.

In order to allow the construction of the deck, stay-in-place metal forms were used between the prestressed girders (see Figure C.8). Outside the exterior girders, temporary falsework was built to facilitate the construction of the 3'-0" deck overhang, as seen in Figure C.9.

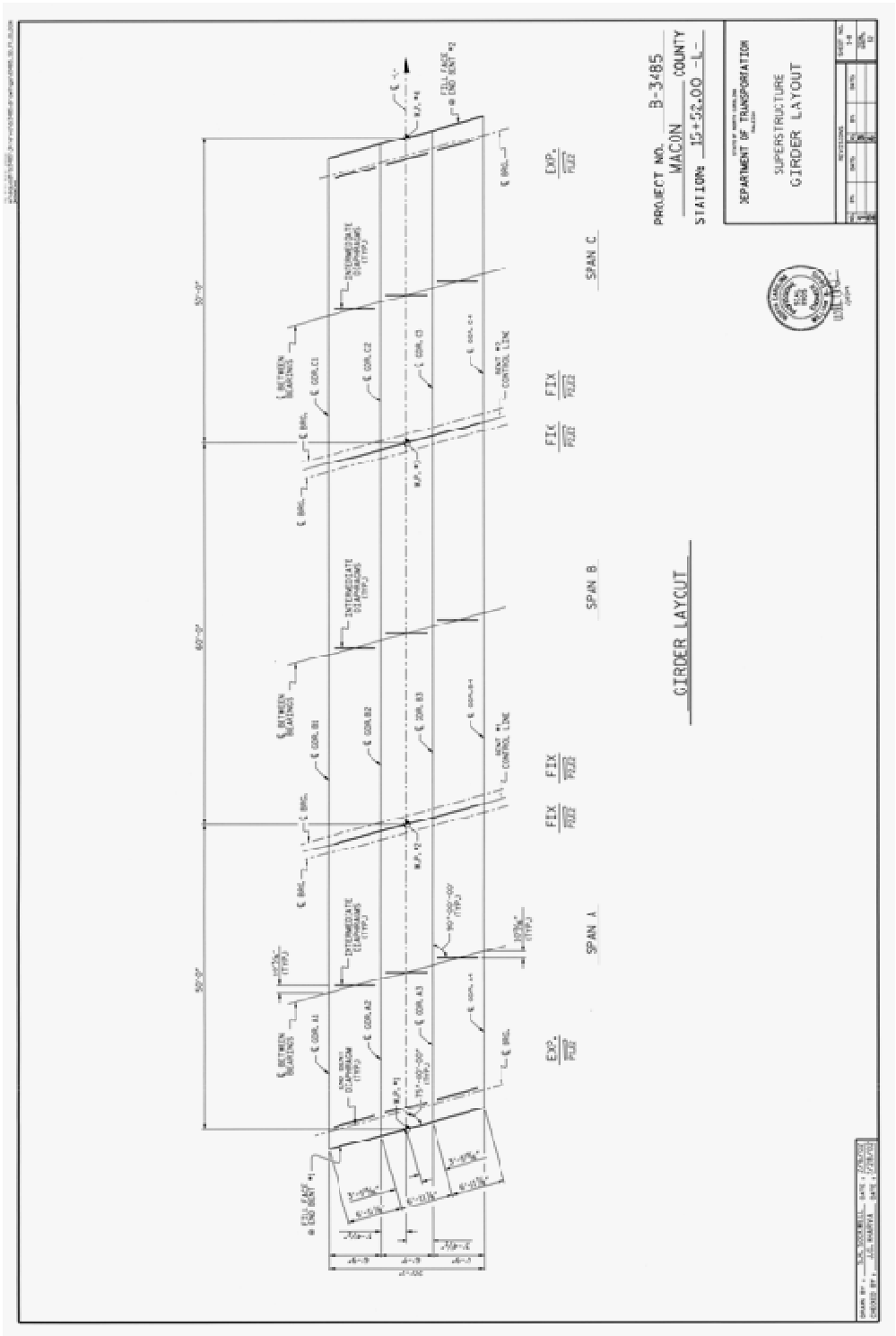

Figure C.6 Girder and diaphragm layout

Figure C.7 Superstructure detail

Figure C.8 Stay-in-place deck formwork

Figure C.9 Deck overhang support (falsework)

With small exception, the bridge deck contained only GFRP reinforcement in the form of deformed composite rebars of type ASLAN 100, manufactured by Hughes Brothers, Inc. As it can be seen from Figure C.10, all composite reinforcement was placed 6" o.c. #5 rebars were placed at the deck overhang area, #8 rebars were used in the top layer above the thru-bent diaphragms, #7 rebars were used at the bottom layer in the transverse direction, and finally, #6 rebars were used in every other position in the deck.

GFRP composite reinforcement placement requires special attention, with somewhat similar measures to epoxy coated rebar construction. Therefore, the general contractor closely followed the rebar manufacturer's specifications with respect to storage, handling and placement of rebars. Prior to placement, the rebars were stored covered to avoid excessive sunlight and moisture exposure. Only plastic chairs and spacers were used to place the rebar mats at the proper height. It is also clear from Figures C.11 and C.12 that the rebars were tied at every other bar intersection with plastic covered wires, avoiding contact with steel and other metal parts of the formwork.

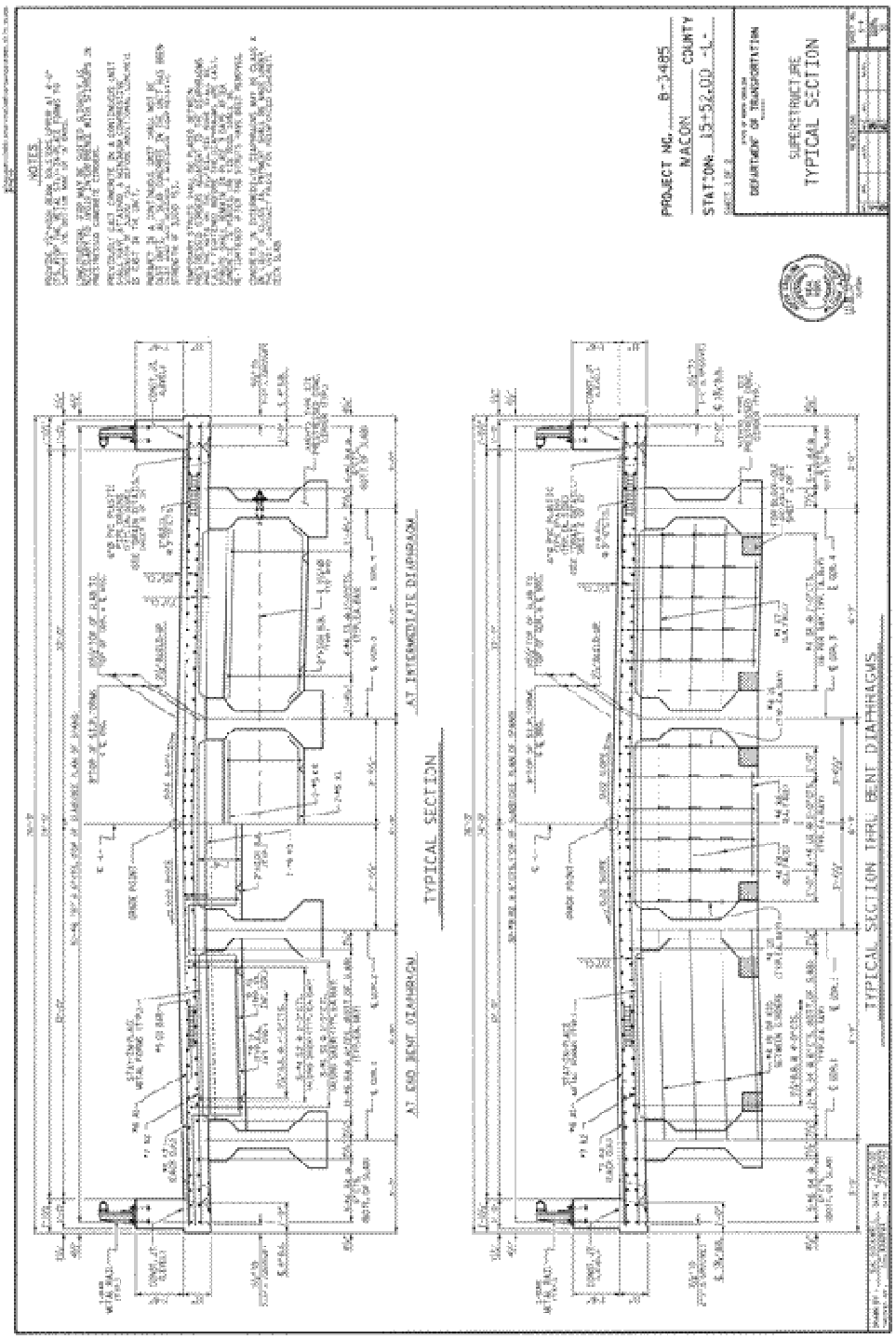

Figure C.10 GFRP deck reinforcement details

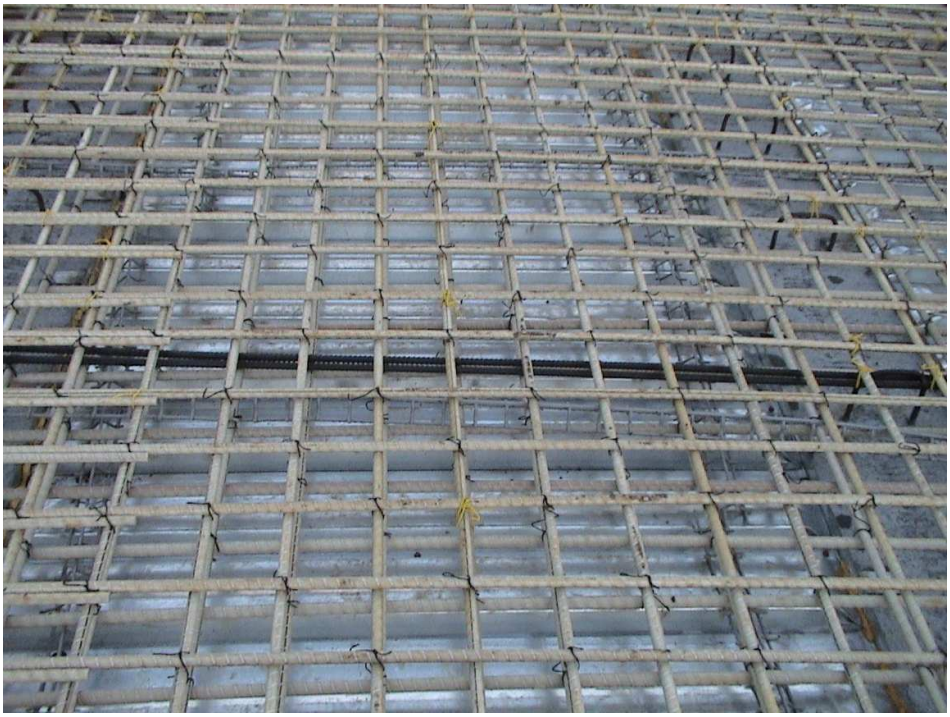

Figure C.11 Composite deck reinforcement

Figure C.12 Deck overhang reinforcement detail

Furthermore, it is also clear from these figures that the GFRP rebar mats were tied down to the formwork and prestressed girder stirrups, in order to avoid floating of these mats during concrete placement. This was necessary as these composite bars are significantly lighter than traditional steel reinforcement. The 6" diameter PVC pipe secured in placed by wires represented the deck drainage.

Figure C.13 shows the completed deck reinforcement, with the epoxy coated rebars used as reinforcement for the bridge rail. In the background, concrete was already placed in portions of the deck (using the equipment shown in Figure C.14), and covered to provide adequate protection from below-freezing temperatures and moisture evaporation. Class AA concrete was specified for the bridge deck, containing either fly ash or ground granulated blast furnace slag. Finally, Figure C.15 shows the construction of the reinforced concrete parapet using a sliding formwork.

Figure C.13 Completed deck reinforcement

Figure C. 14 Bridge deck concrete placement

Figure C.15 Bridge parapet construction

Figure C.16 shows the finished bridge structure with the completed approach slab and the connecting pavement. At the end bents, a 2" wide opening was saw cut between the approach slab and bridge deck. This allowed the placement of an evazote joints seal at both end bents providing an elastic seal. The bridge was finished with the installation of the guard rails outside the bridge deck area.

Finally, the bridge was instrumented using strain gages, strain transducers and displacement transducers, and with the help of two fully loaded tandem trucks (see Figure C.17), quasi-static and dynamic in-situ tests were performed to investigate the bridge's response to controlled live loads applied to the superstructure.

Figure C.16 Completed bridge structure

Figure C.17 In-situ bridge test

Appendix D – Concrete Mix Design for Pullout Specimens

Concrete Mix Proportioning & Design

Step 0 – Design Requirements

- Concrete Information
  - Type – Non-Air-Entrained
  - Compressive Strength of Concrete = 5000^{PSI}
  - Water-to-Cement Design Ratio = 0.49 (Ray, 2005)
  - Portland Cement Type I
- Coarse Aggregate Information
  - Maximum Size = ⅜″
  - Specific Gravity = 2.8
  - Absorption Capacity = 0.5 %
  - Moisture Content = 0.00 %
  - Unit Weight = 100 lbs/ft^3
- Fine Aggregate Information
  - Specific Gravity = 2.8
  - Absorption Capacity = 0.9 %
  - Moisture Content = 0.00%
  - Fineness Modulus = 2.9

Step 1 – Select Desired Slump

Recommend 4″ for Typical Design

Step 2 – Select the Maximum Aggregate Size

Specified in Design Requirements (Maximum Size = ⅜″)

Step 3 – Estimate the Mixing Water & Air Content

Water Requirement = 385 lb/yd^3
Range of Air Content = 4.5 – 7.5 % (Note: use 6 %)

Step 4 – Select w/c Ratio

Specified in Design Requirements (w/c = 0.49)

Step 5 – Calculate the Cement Content for 1 yd^3

$$cement\ required = \frac{340}{0.49} = 694\ lbs / yd^3$$

Step 6 – Estimate Coarse Aggregate Contents

From Table 3.12 for FM = 2.9
$V_{CA} = (0.45) \bullet (100) \bullet (27) = 1215$ lb/yd^3

Step 7 – Estimate the Fine Aggregate Content

$$Volume\,of\,Water = \frac{340}{62.4} = 5.45\ ft^3$$

$$Volume\,of\,Cement = \frac{694}{(62.4)(3.15)} = 3.53\ ft^3$$

$$Volume\,of\,CA = \frac{1215}{(62.4)(2.8)} = 6.95\ ft^3$$

$$Volume\,of\,Air = \frac{6 \bullet 27}{100} = 1.62\ ft^3$$

$$Volume\,of\,FA = 27 - 5.45 - 3.53 - 6.95 - 1.62 = 9.45\ ft^3$$

$$\therefore V_{FA} = (9.45)(2.8)(62.4) = 1651.1\ lb/yd^3$$

Step 8 – Absorption Correction for Aggregates & Water

Note: Aggregates are Oven-Dried for 24 ± 4 Hrs
Therefore: No Absorption Corrections Needed

Step 9 – Field Mix Proportions for 2 ft^3

Water = 28.5 lbs
Cement = 51.4 lbs
Coarse Aggregate = 90.0 lbs
Fine Aggregate = 122.3 lbs
AE-90 = 20 mL

Step 10 – Actual Mix Proportions for 2 ft^3 (through laboratory testing)

Water = 30.0 lbs
Cement = 60.8 lbs
Coarse Aggregate = 89.6 lbs
Fine Aggregate = 119.2 lbs
AE-90 = 18 mL

Field Mix Proportions = 1C:1.96:1.47CA:0.49W

Appendix E – Installation of Strain Gages

Installation Materials: gauze, Q-tips, grinder, sand paper, tweezers, cellophane tape, marker, degreaser, conditioner, neutralizer, adhesive, catalyst, and strain gage

1. Mark desired mounting position with marker.
2. Prepare surface of desired strain gage mounting location with grinder and sand paper as shown in Figure E.1.

Figure E.1 Roughed-up area on GFRP rebar specimen

3. Use degreaser to clean area, wiping in one directional strokes with gauze; continue to use a clean surface of gauze or a new piece of gauze until the gauze appears to remain clean after wiping the surface; apply additional degreaser as needed.
4. Apply conditioner to the surface and scrub area with Q-tip (see Figure E.2).

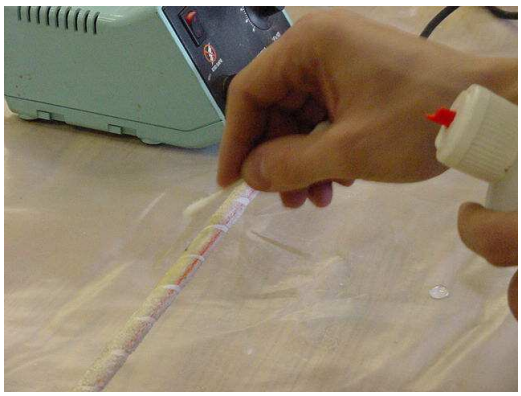

Figure E.2 Applying conditioner to specified area of application

5. Then wiping in one directional strokes with gauze, using a clean surface of gauze

or a new piece of gauze, until gauze remains clean after wiping and surface is dry.

6. Neutralize the surface by applying the neutralizer onto the surface and scrubbing with a Q-tip, dry by wiping with gauze.
7. Prep surface of gage box in similar fashion.
8. Remove gage from acetate cover with tweezers and lay on top of box.
9. Apply a piece of cellophane tape to gage that completely covers the gage.
10. Remove tape with gage from box and place in desired location, ensure proper orientation.
11. Peel back tape to remove gage from surface, maintain a shallow angle.
12. Apply catalyst to gage and surface and allow the surface to dry.
13. Apply one drop of adhesive to the gage.
14. Push gage back onto surface and apply pressure for one minute as shown in Figure E.3. Final product is present in Figure E.4.

Figure E.3 Applying pressure to strain gage

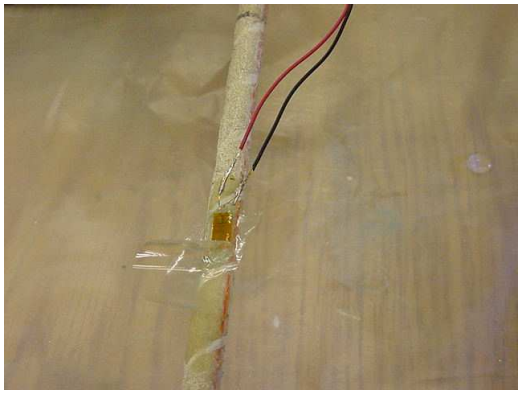

Figure E.4 Finished product

Appendix F – pH & Temperature Readings

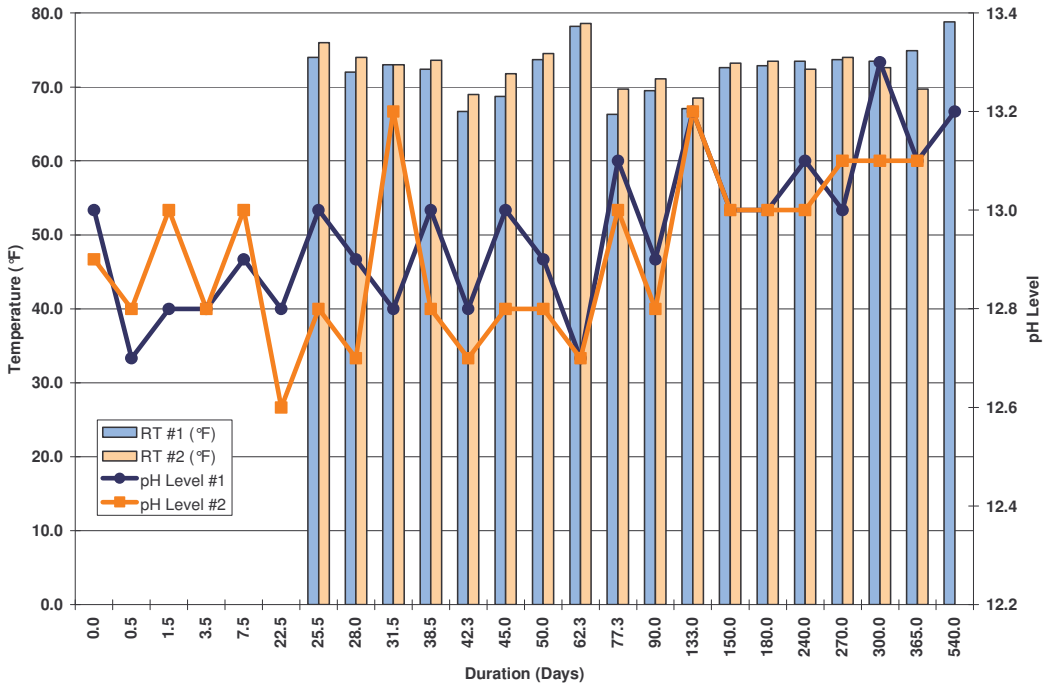

Figure F.1 pH & Temperature Readings at Room Temperature (Two Processing Tanks)

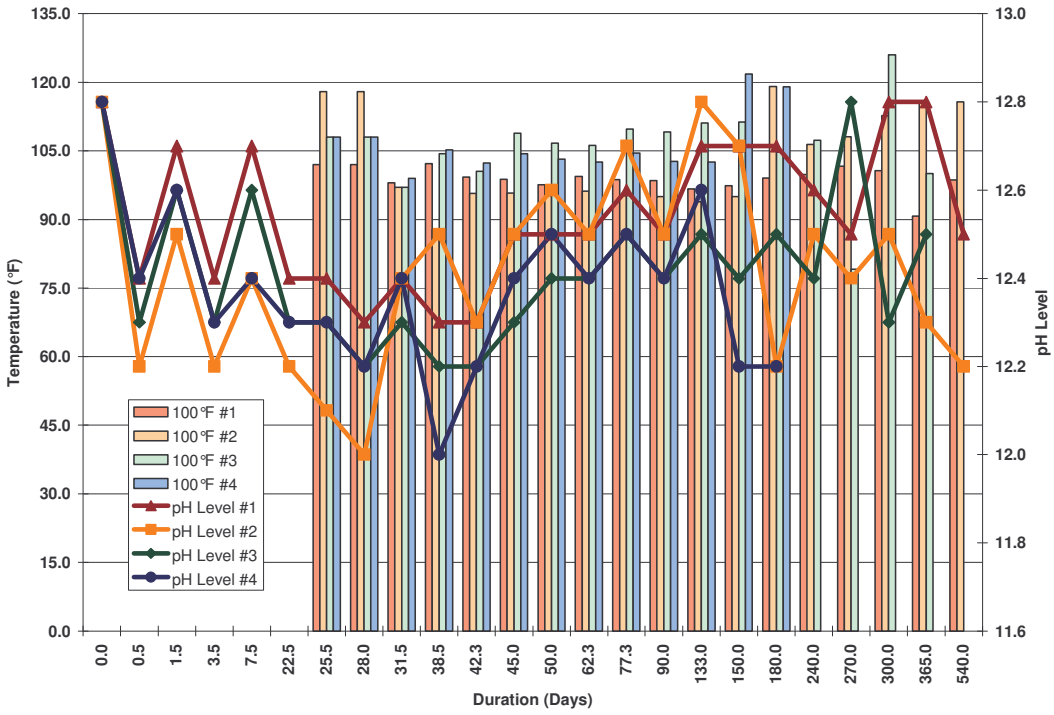

Figure F.2 pH & Temperature Readings at 100°F (Four Processing Tanks)

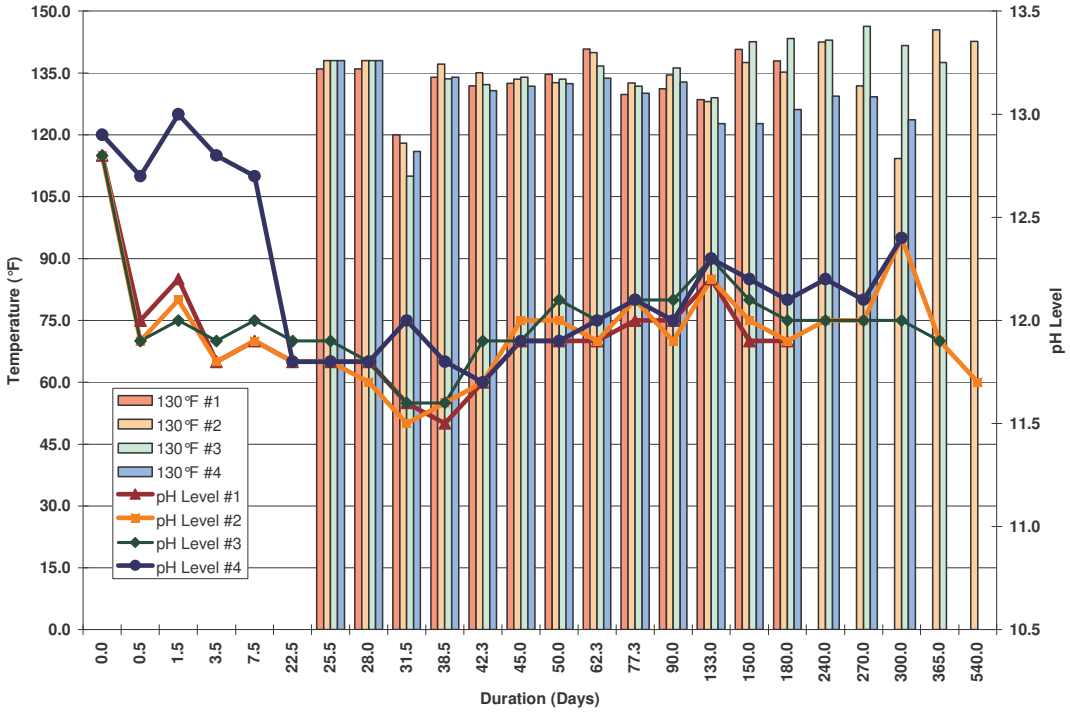

Figure F.3 pH & Temperature Readings at 130°F (Four Processing Tanks)

Appendix G – Change in Diameter Readings

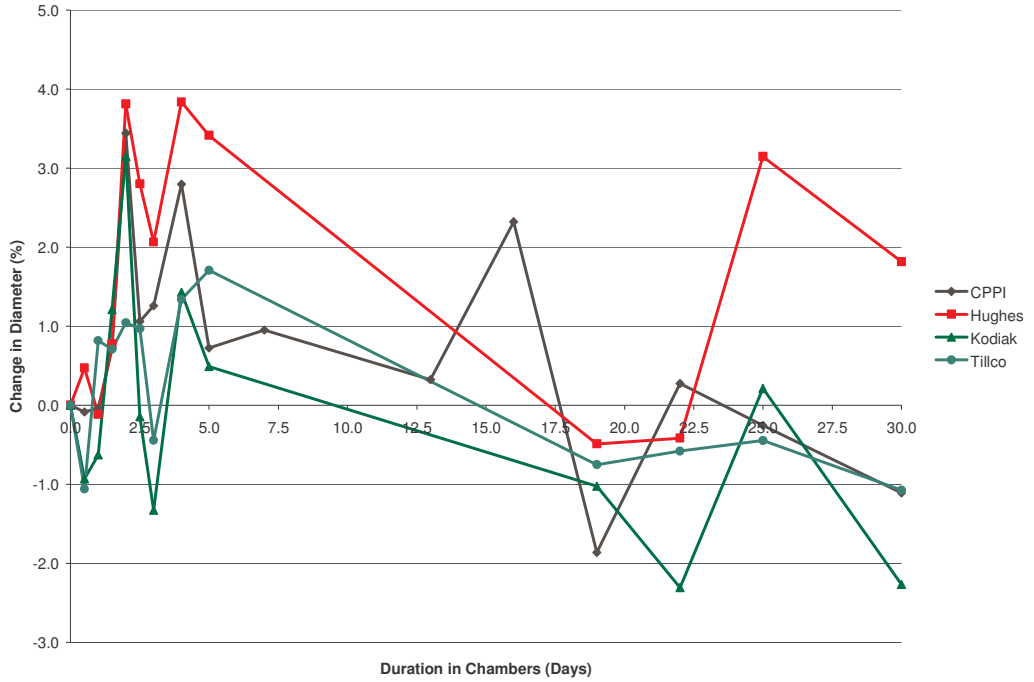

Figure G.1 Change in Diameter versus Duration for Unscathed Specimens at Room Temperature

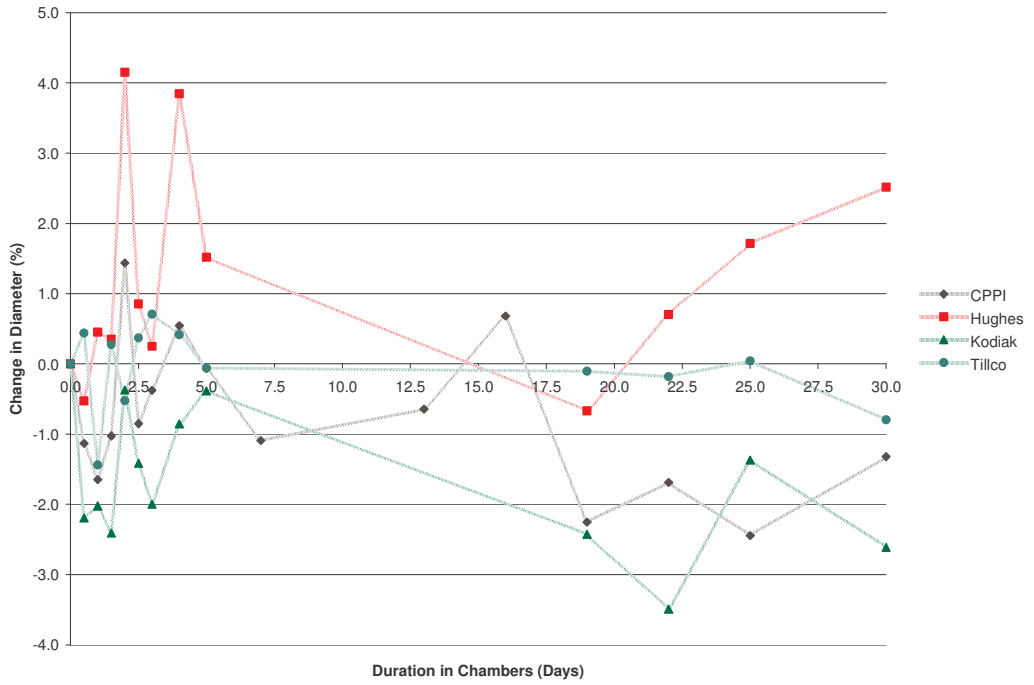

Figure G.2 Change in Diameter versus Duration for Nicked Specimens at Room Temperature

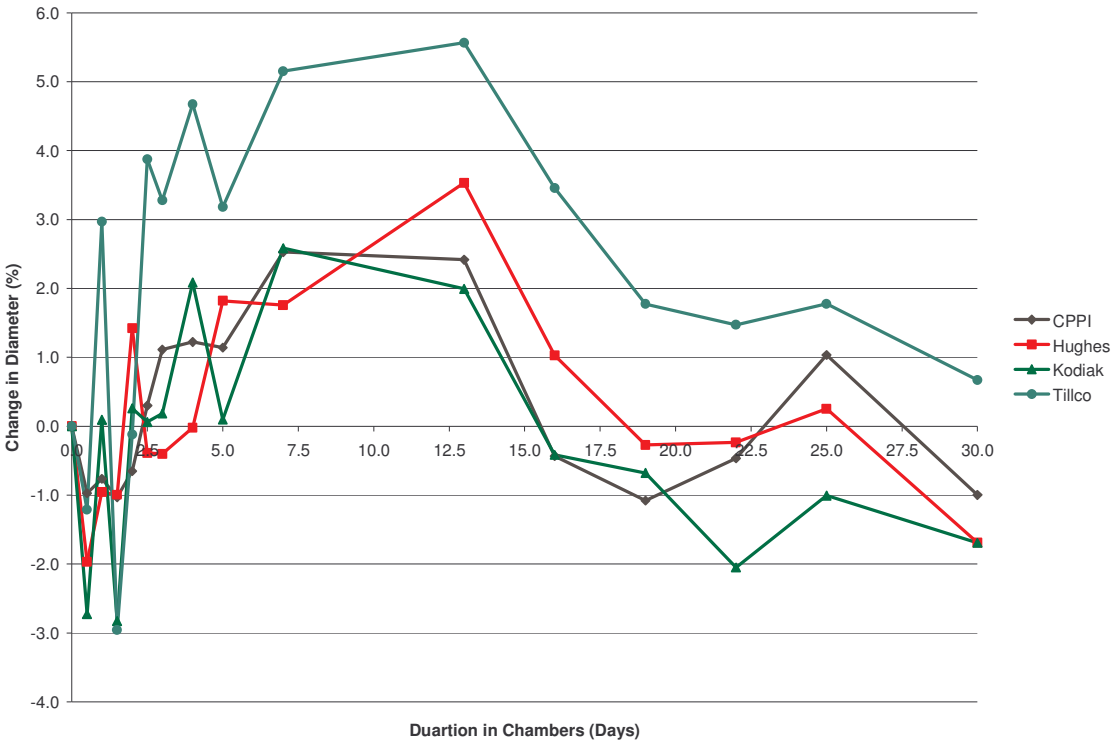

Figure G.3 Change in Diameter versus Duration for Unscathed Specimens at 100°F

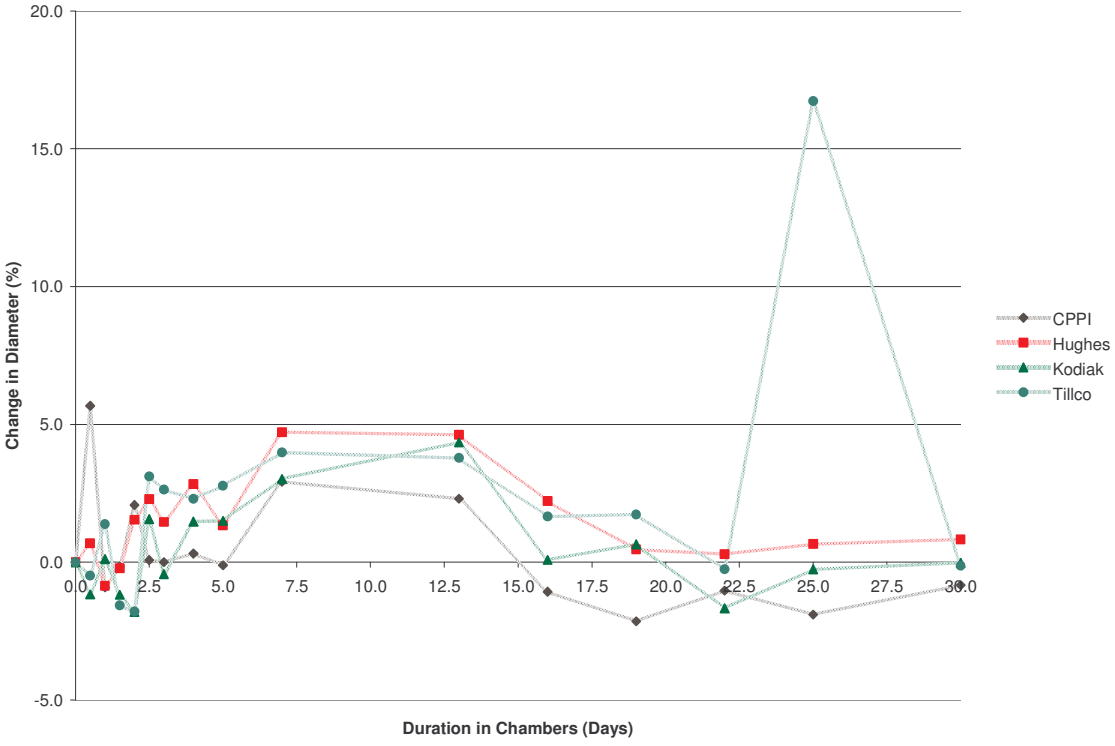

Figure G.4 Change in Diameter versus Duration for Nicked Specimens at 100°F

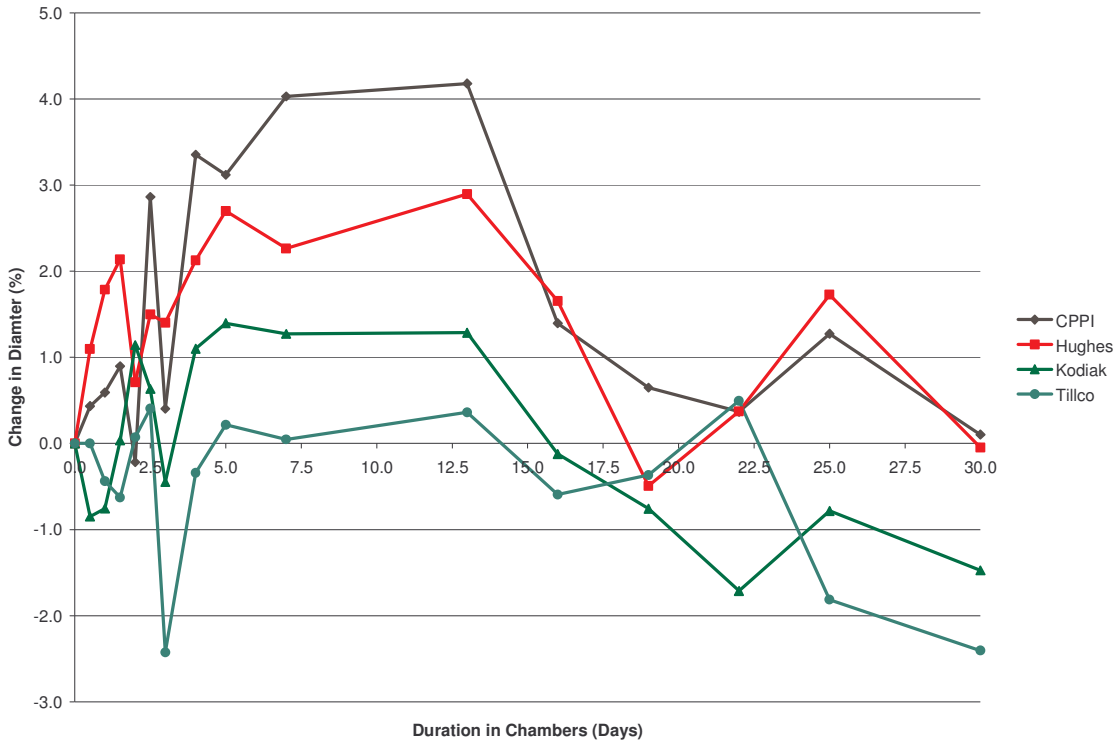

Figure G.5 Change in Diameter versus Duration for Unscathed Specimens at 130°F

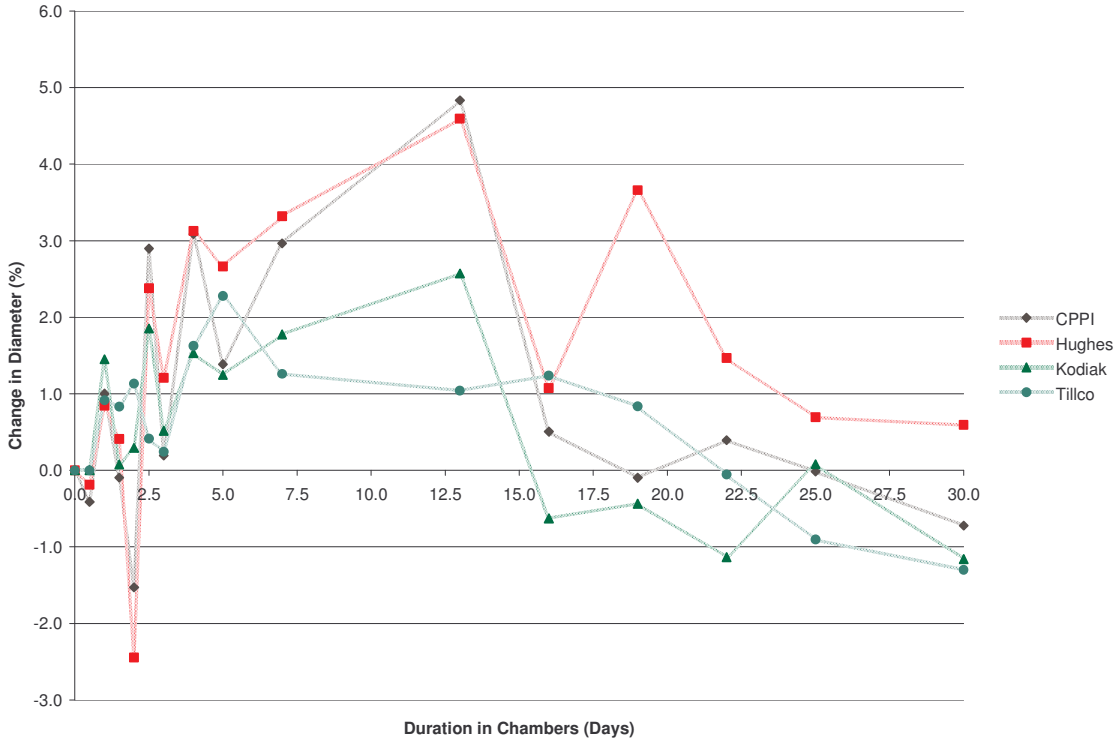

Figure G.6 Change in Diameter versus Duration for Nicked Specimens at 130°F

Appendix H – Tensile stress vs. strain diagrams

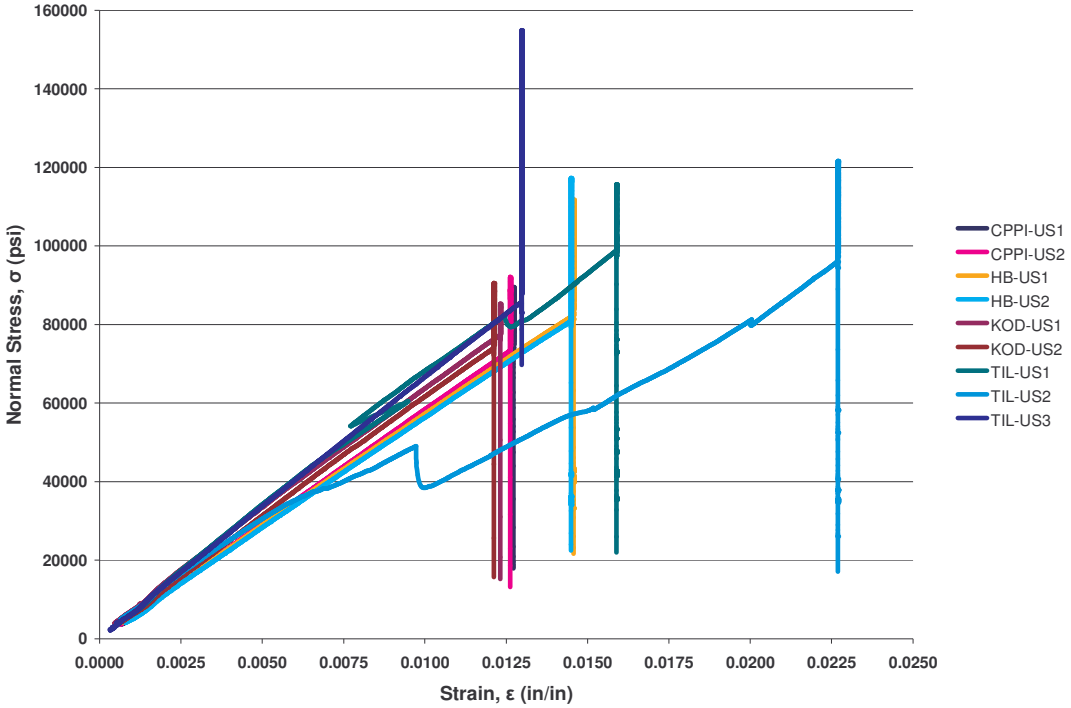

Figure H.1 Tensile Stress vs. Strain for Unscathed at Dry Conditions for 3 Months

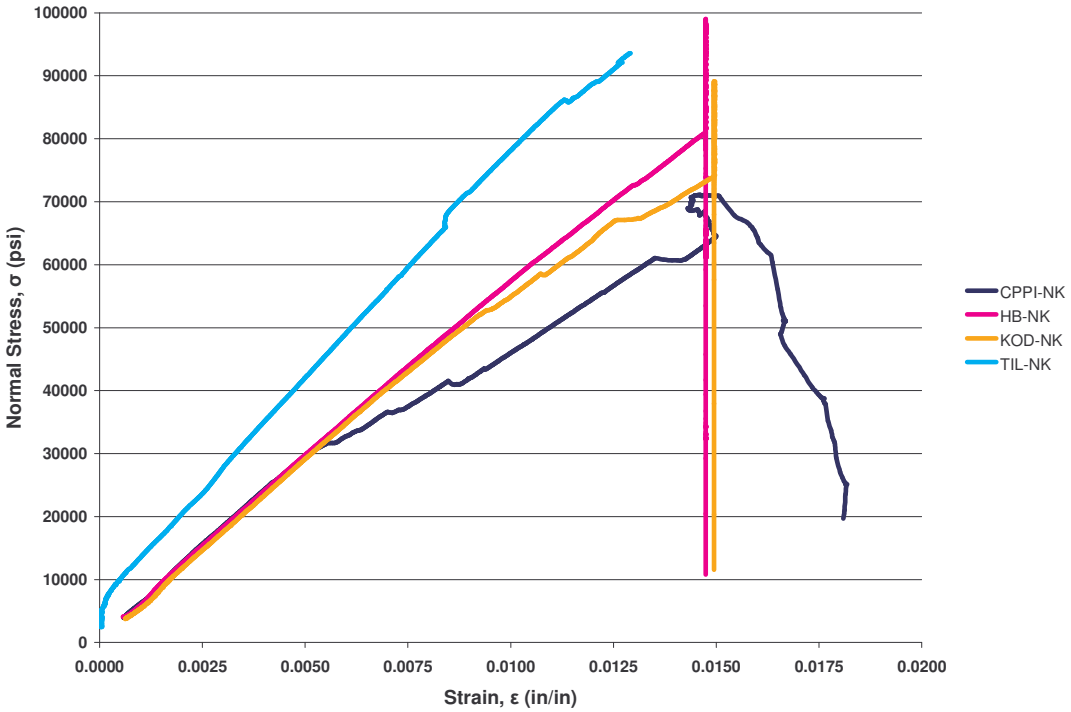

Figure H.2 Tensile Stress vs. Strain for Nicked at Dry Conditions for 3 Months

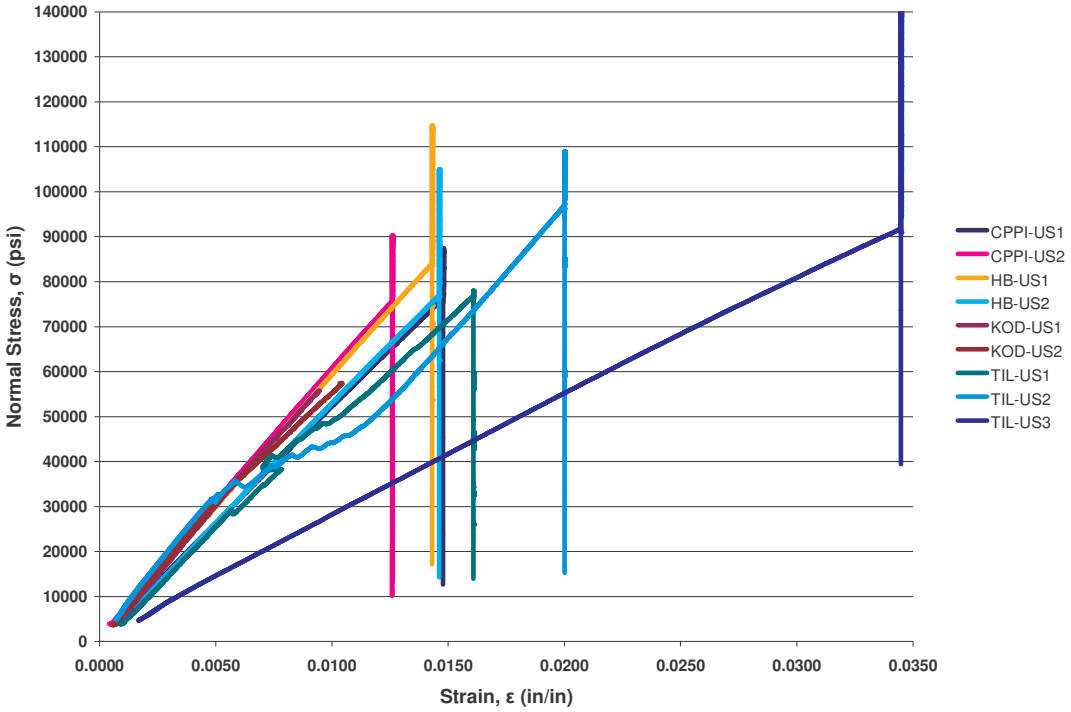

Figure H.3 Tensile Stress vs. Strain for Unscathed at Room Temperature for 3 Months

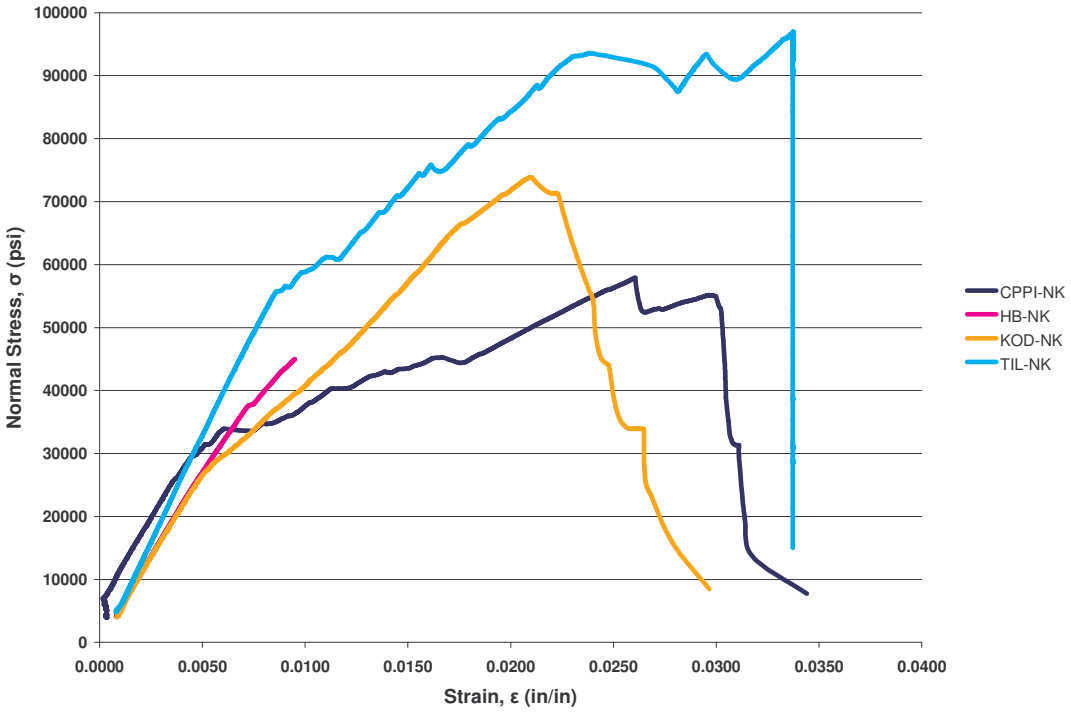

Figure H.4 Tensile Stress vs. Strain for Nicked at Room Temperature for 3 Months

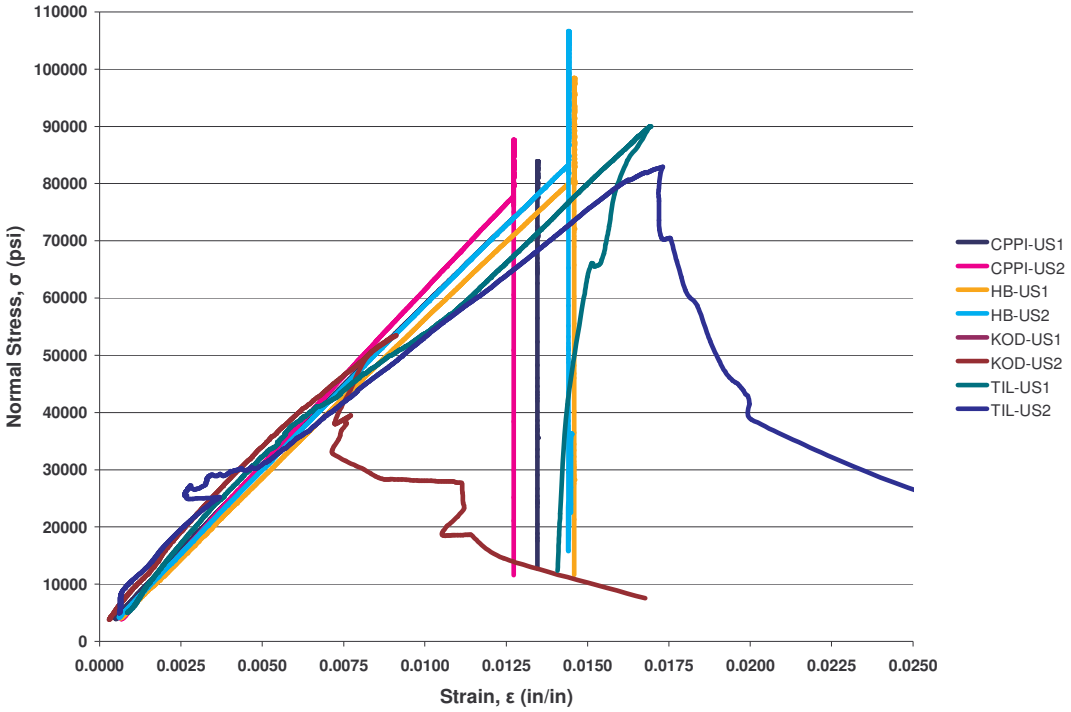

Figure H.5 Tensile Stress vs. Strain for Unscathed at 100℉ for 3 Months

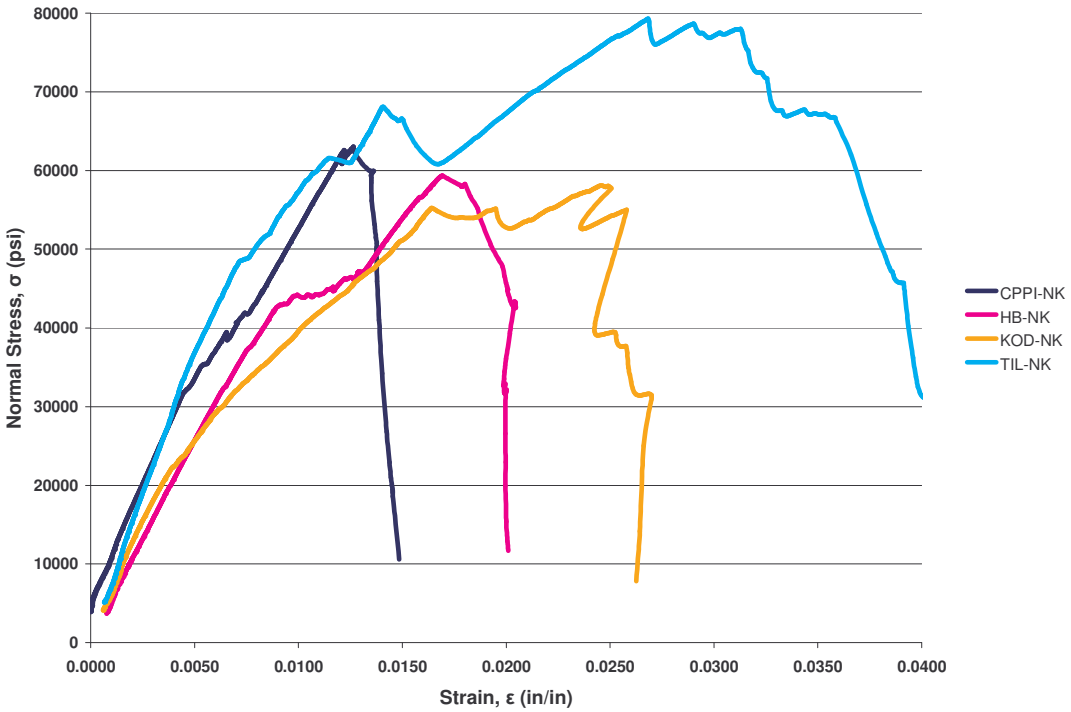

Figure H.6 Tensile Stress vs. Strain for Nicked at 100℉ for 3 Months

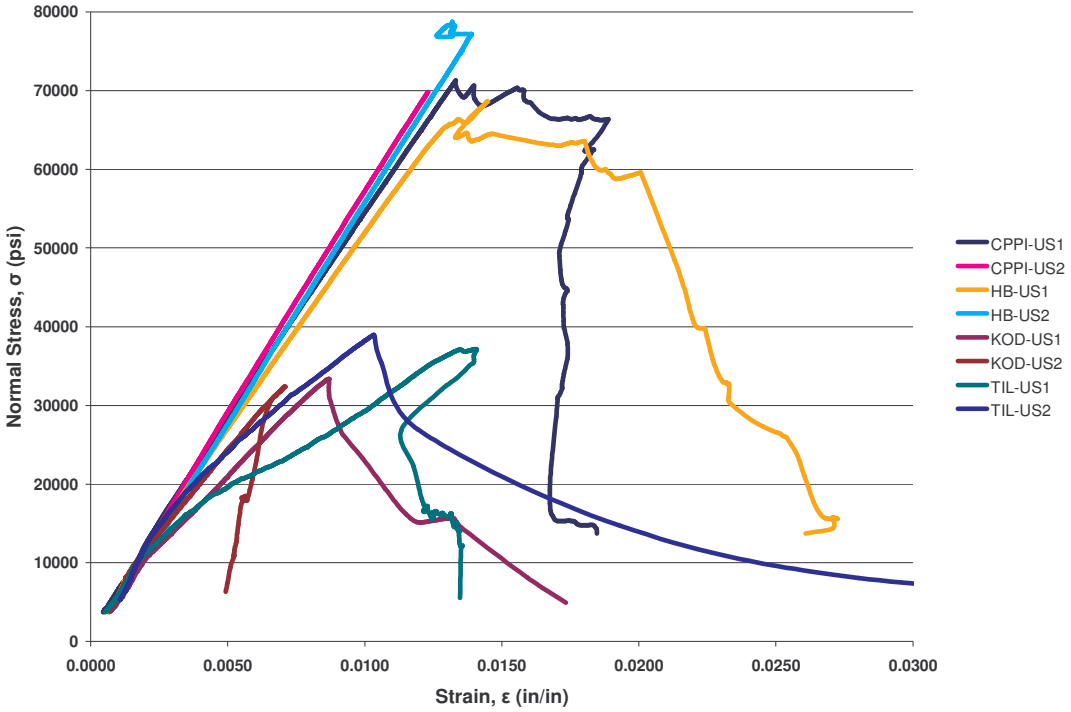

Figure H.7 Tensile Stress vs. Strain for Unscathed at 130℉ for 3 Months

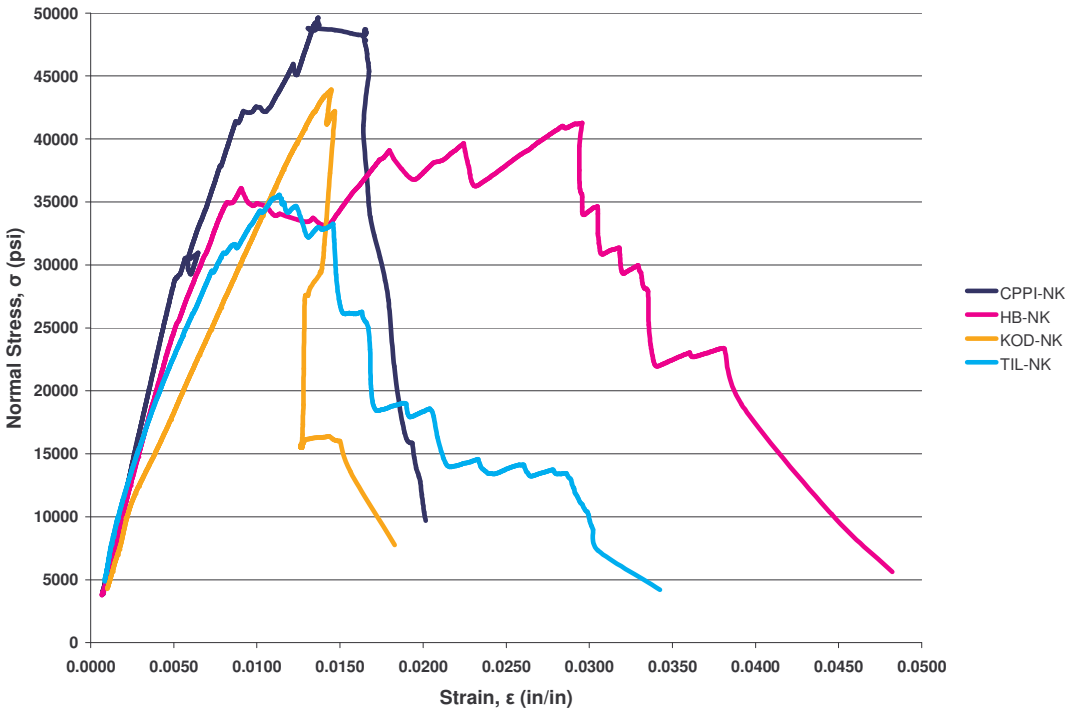

Figure H.8 Tensile Stress vs. Strain for Nicked at 130℉ for 3 Months

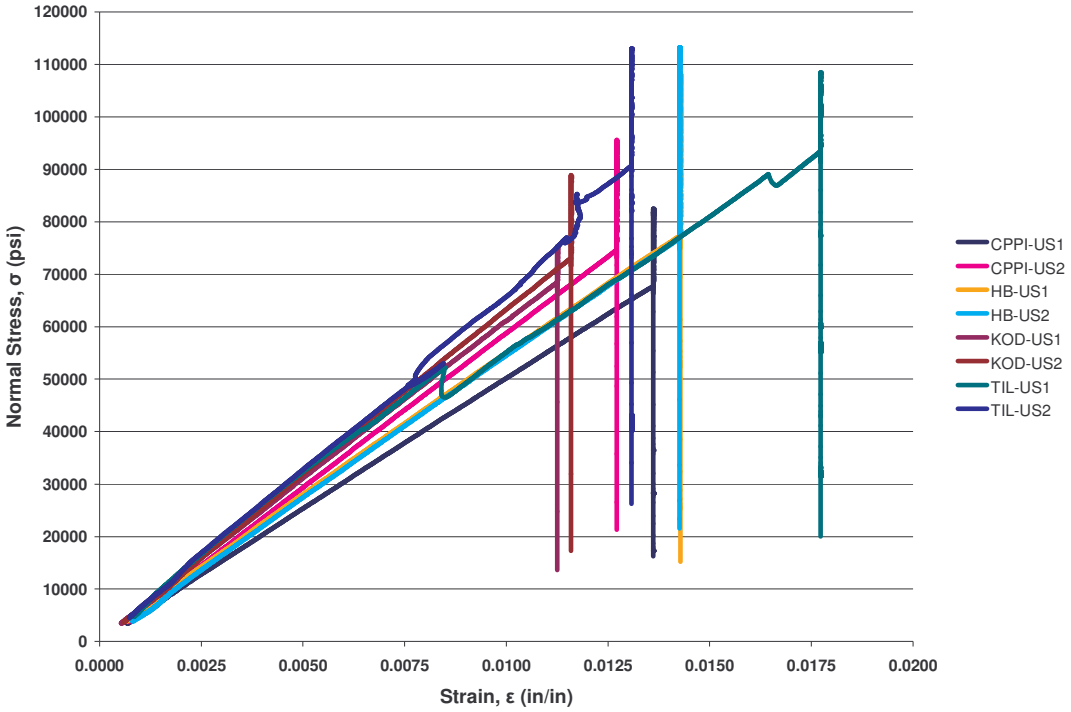

Figure H.9 Tensile Stress vs. Strain for Unscathed at Dry Conditions for 6 Months

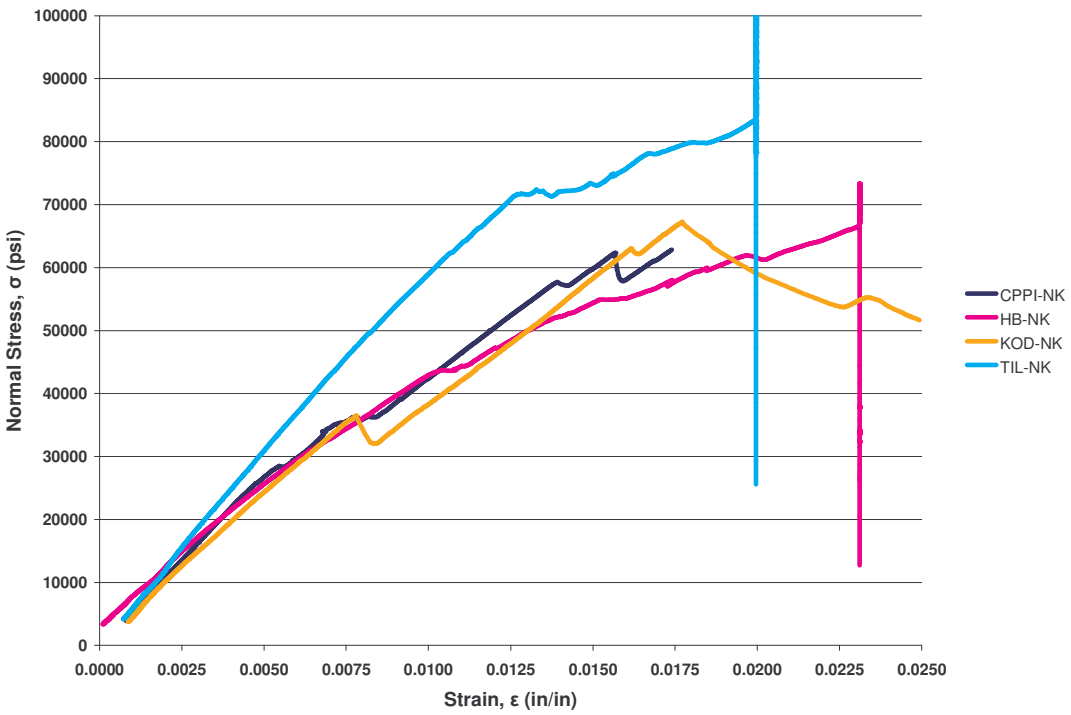

Figure H.10 Tensile Stress vs. Strain for Nicked at Dry Conditions for 6 Months

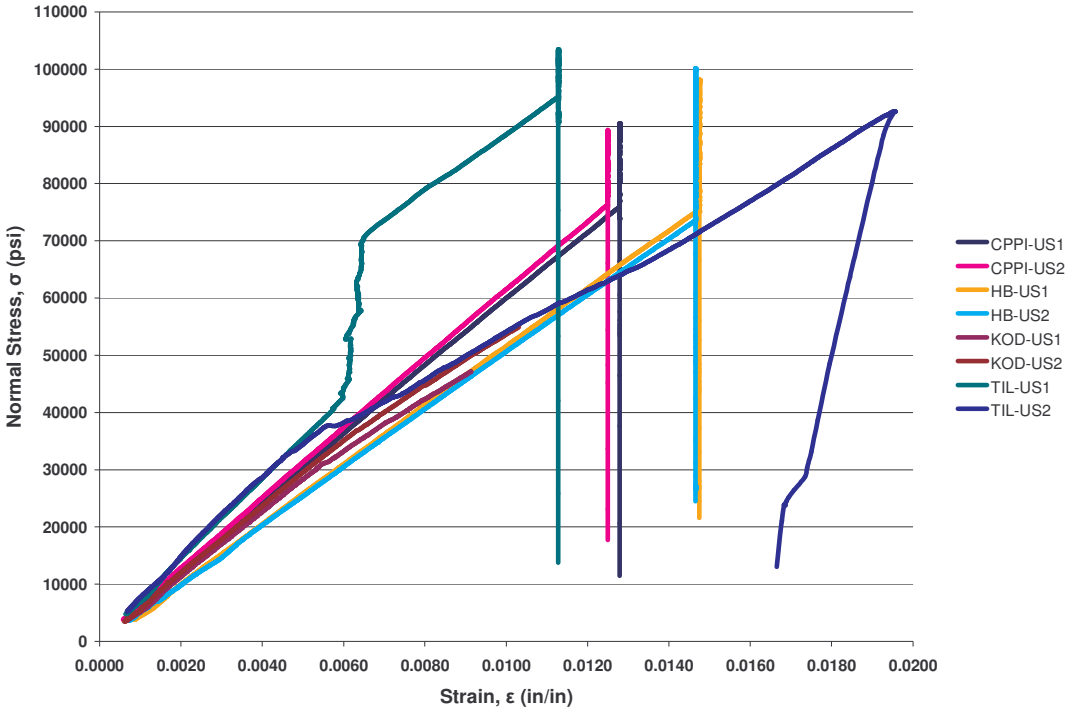

Figure H.11 Tensile Stress vs. Strain for Unscathed at Room Temperature at 6 Months

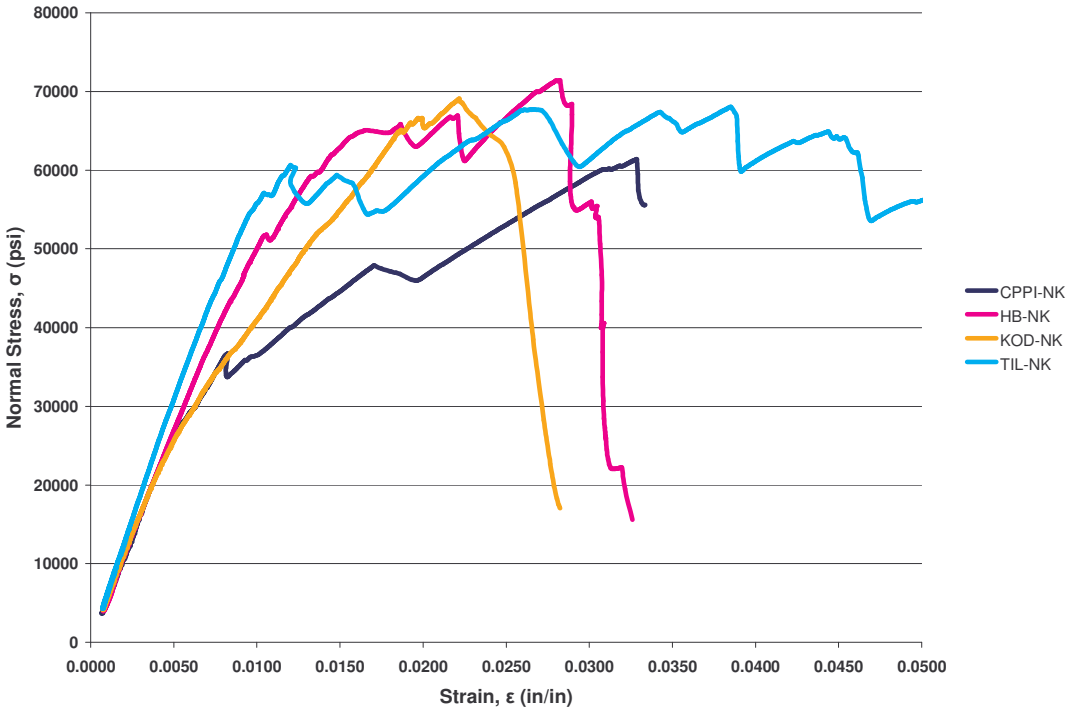

Figure H.12 Tensile Stress vs. Strain for Nicked at Room Temperature at 6 Months

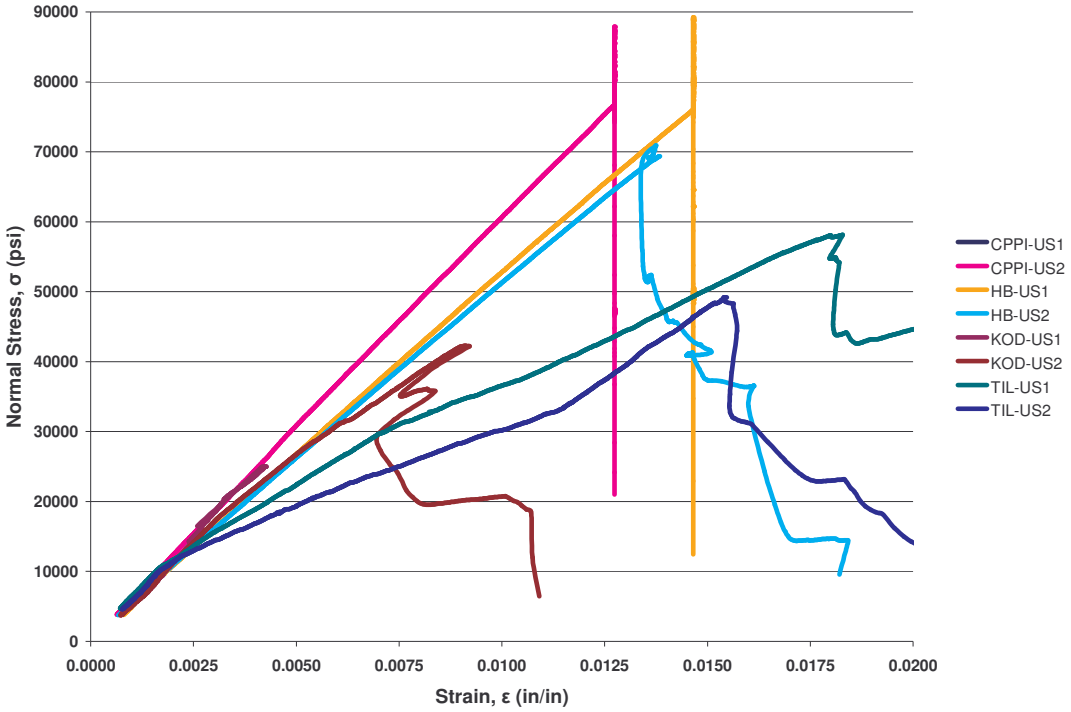

Figure H.13 Tensile Stress vs. Strain for Unscathed at 100℉ for 6 Months

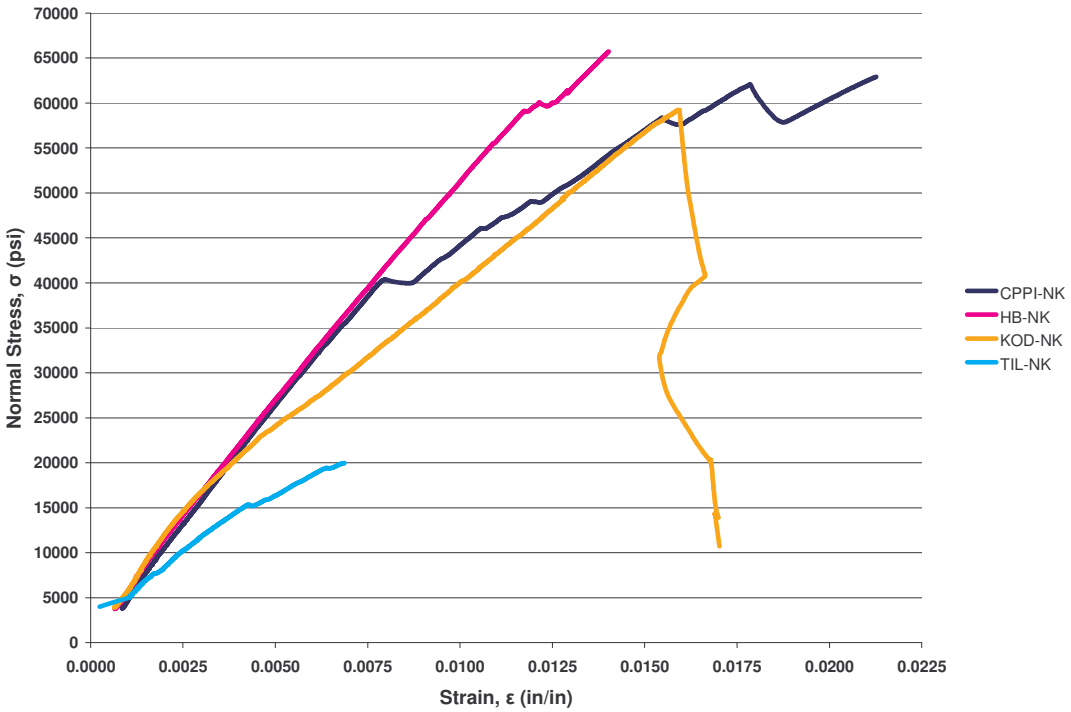

Figure H.14 Tensile Stress vs. Strain for Nicked at 100℉ for 6 Months

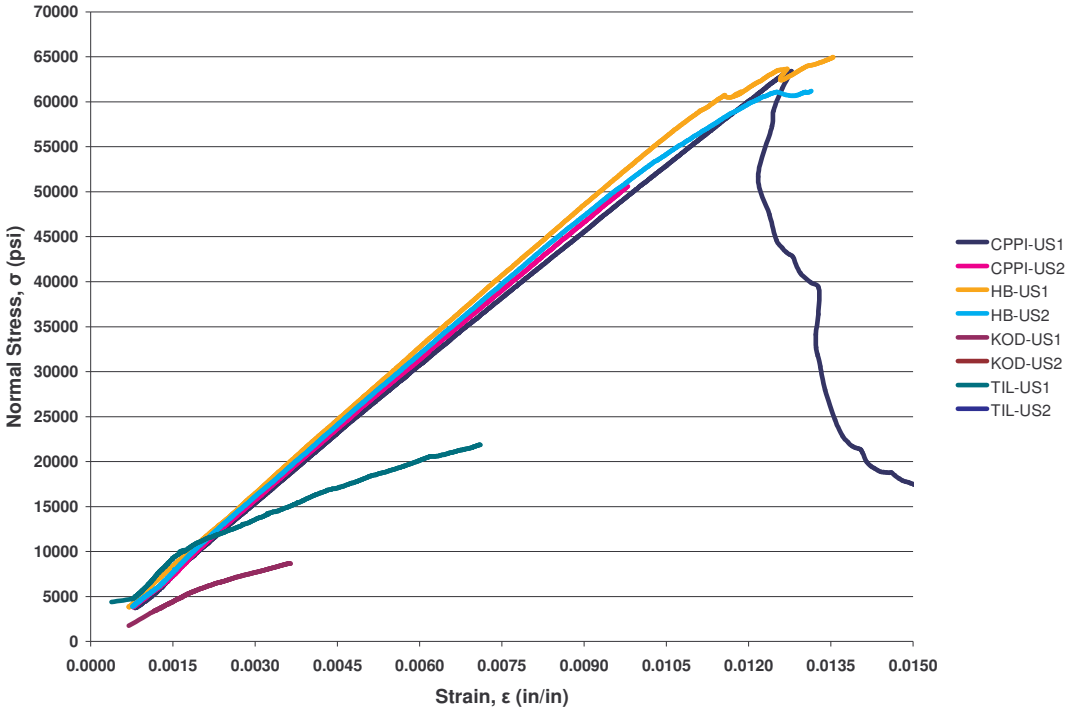

Figure H.15 Tensile Stress vs. Strain for Unscathed at 130℉ for 6 Months

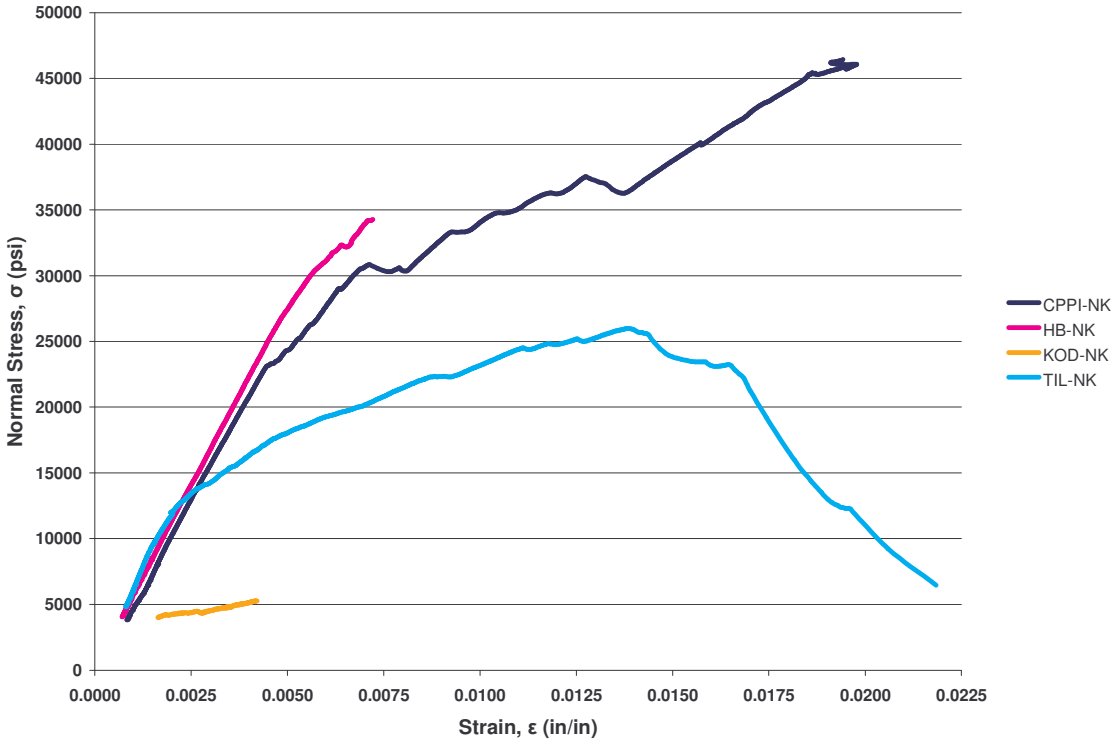

Figure H.16 Tensile Stress vs. Strain for Nicked at 130℉ for 6 Months

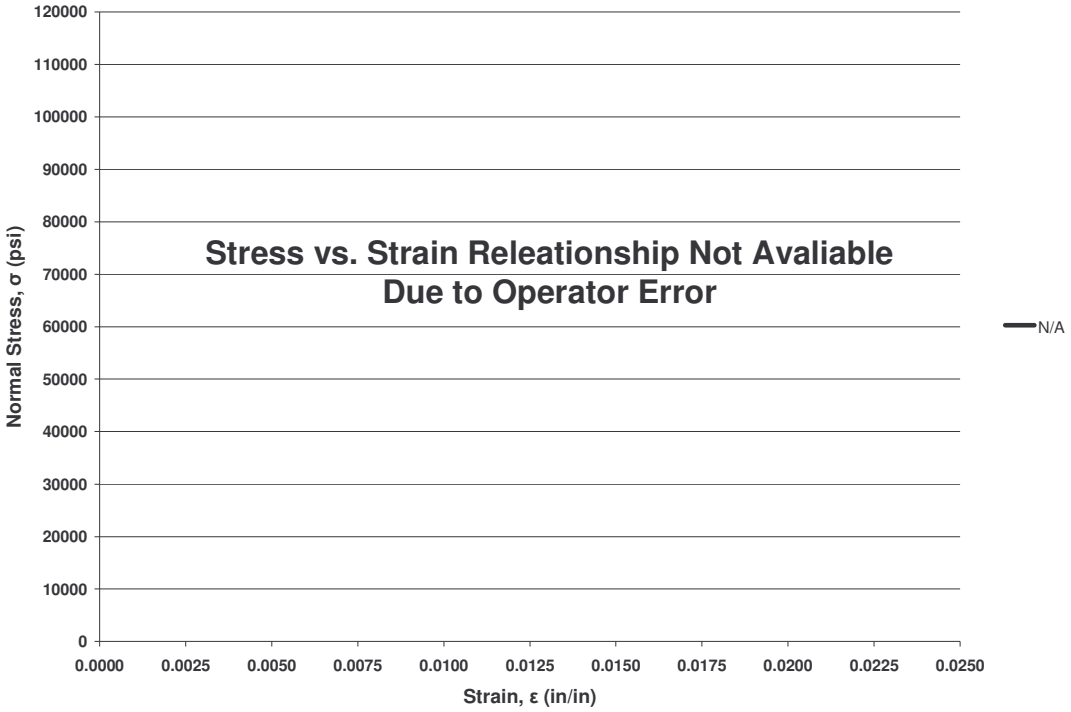

Figure H.17 Tensile Stress vs. Strain for All Environments for 12 Months

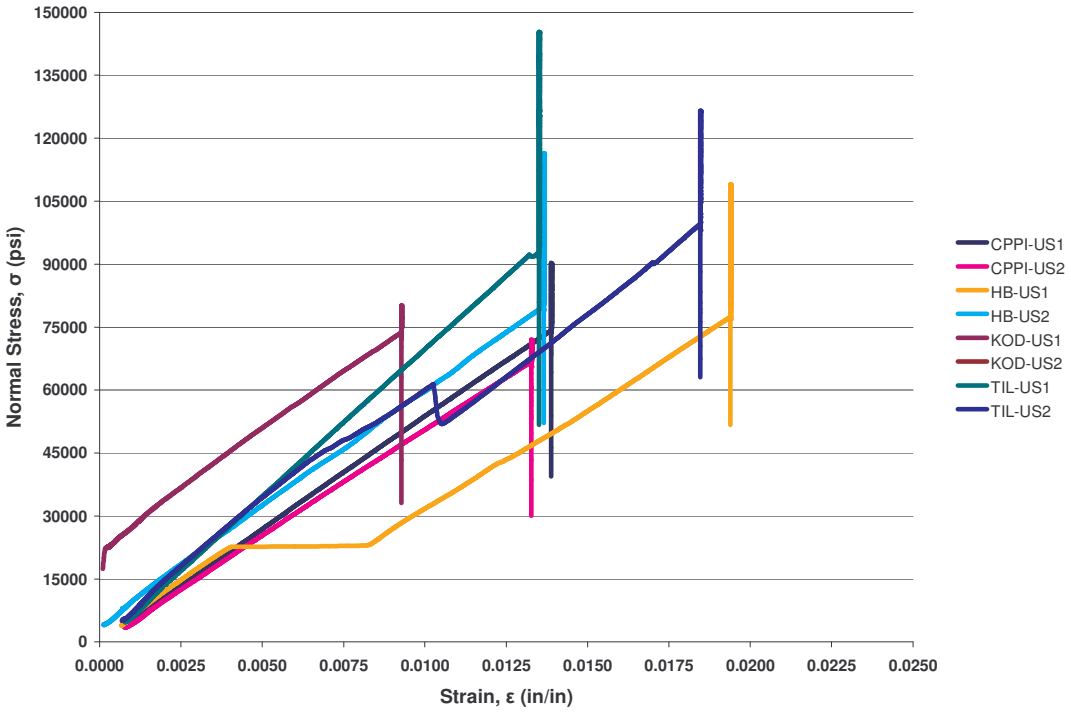

Figure H.18 Tensile Stress vs. Strain for Unscathed at Dry Conditions for 18 Months

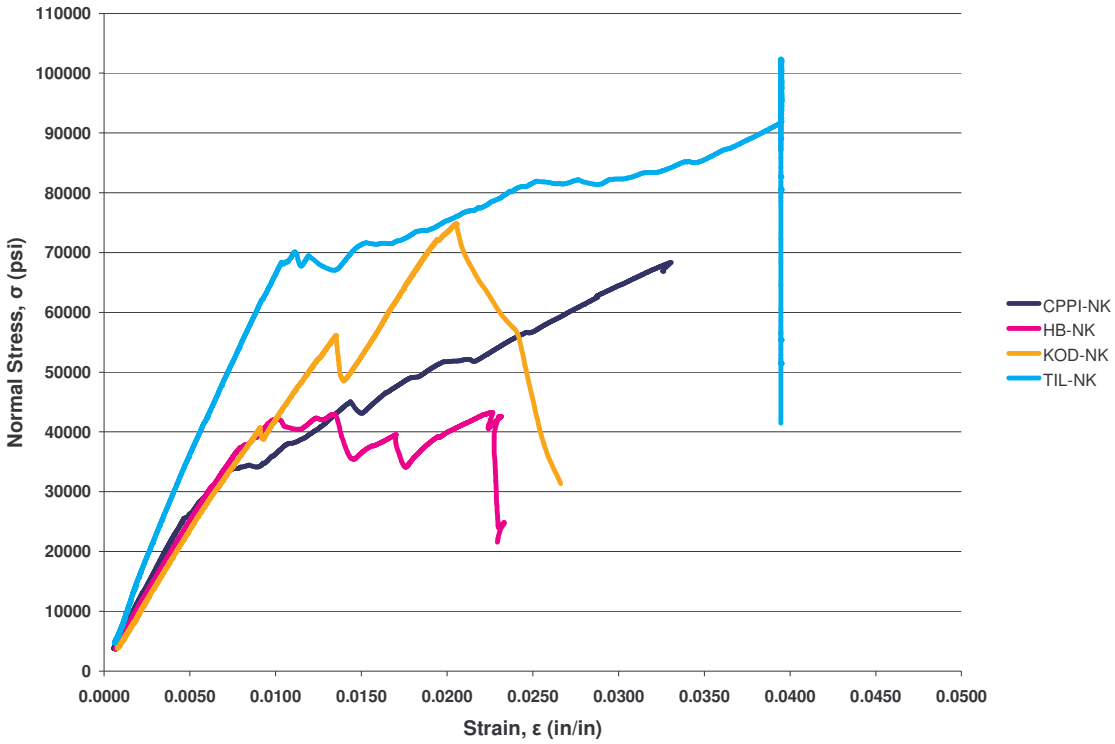

Figure H.19 Tensile Stress vs. Strain for Nicked at Dry Conditions for 18 Months

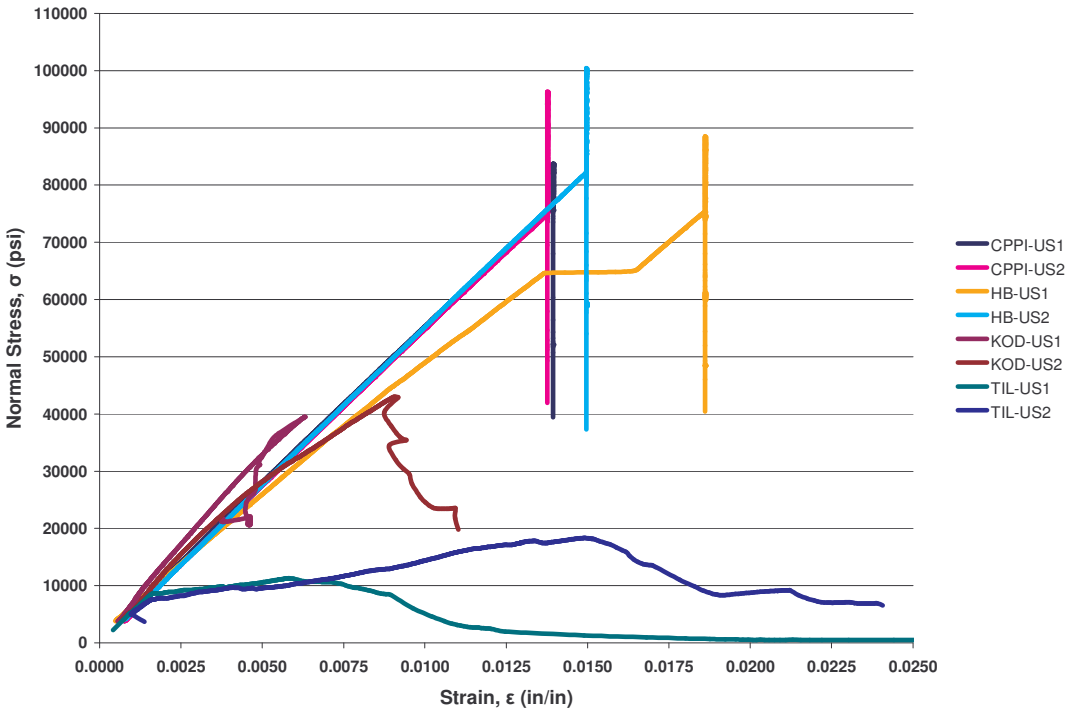

Figure H.20 Tensile Stress vs. Strain for Unscathed at Room Temperature for 18 Months

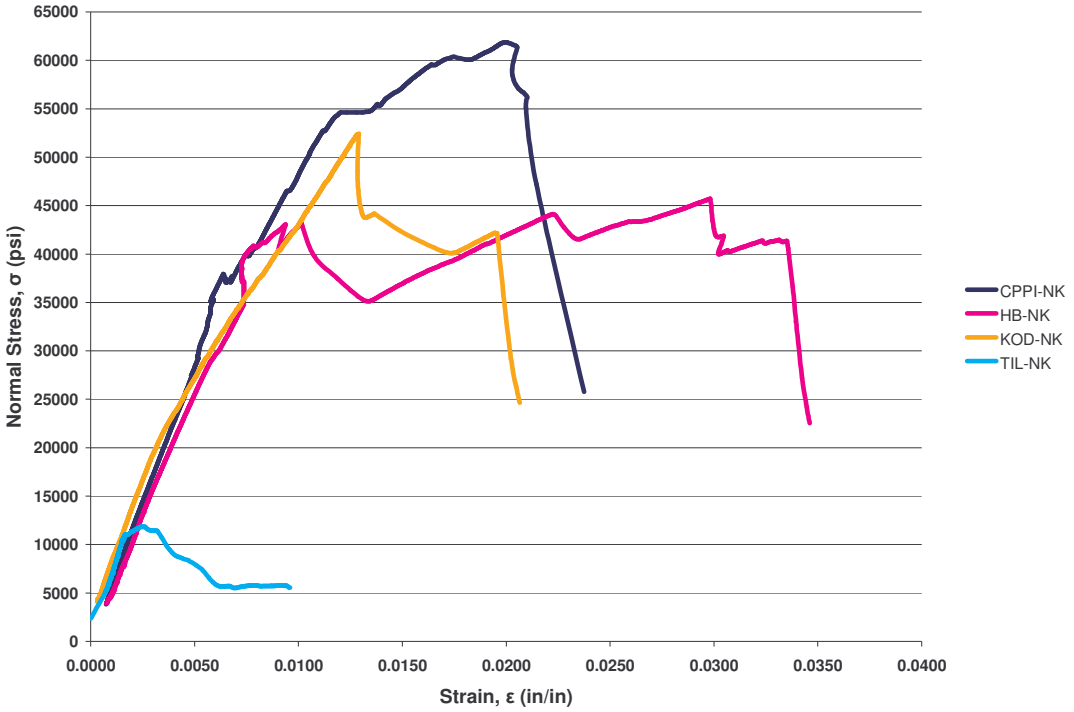

Figure H.21 Tensile Stress vs. Strain for Nicked at Room Temperature for 18 Months

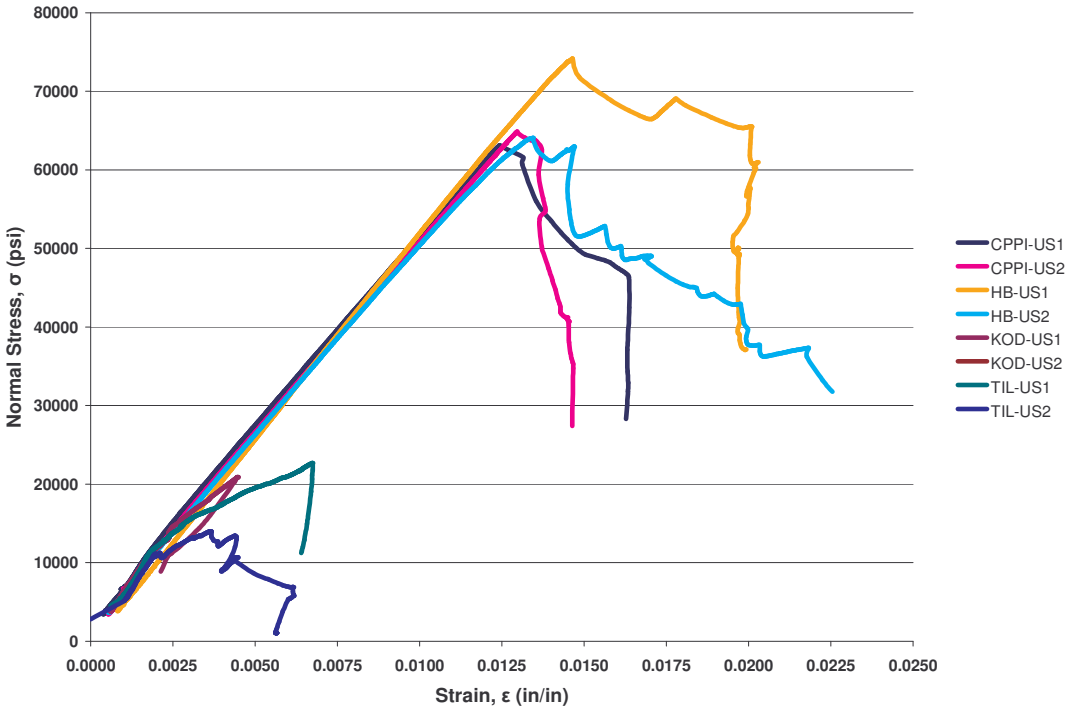

Figure H.22 Tensile Stress vs. Strain for Unscathed at 100℉ for 18 Months

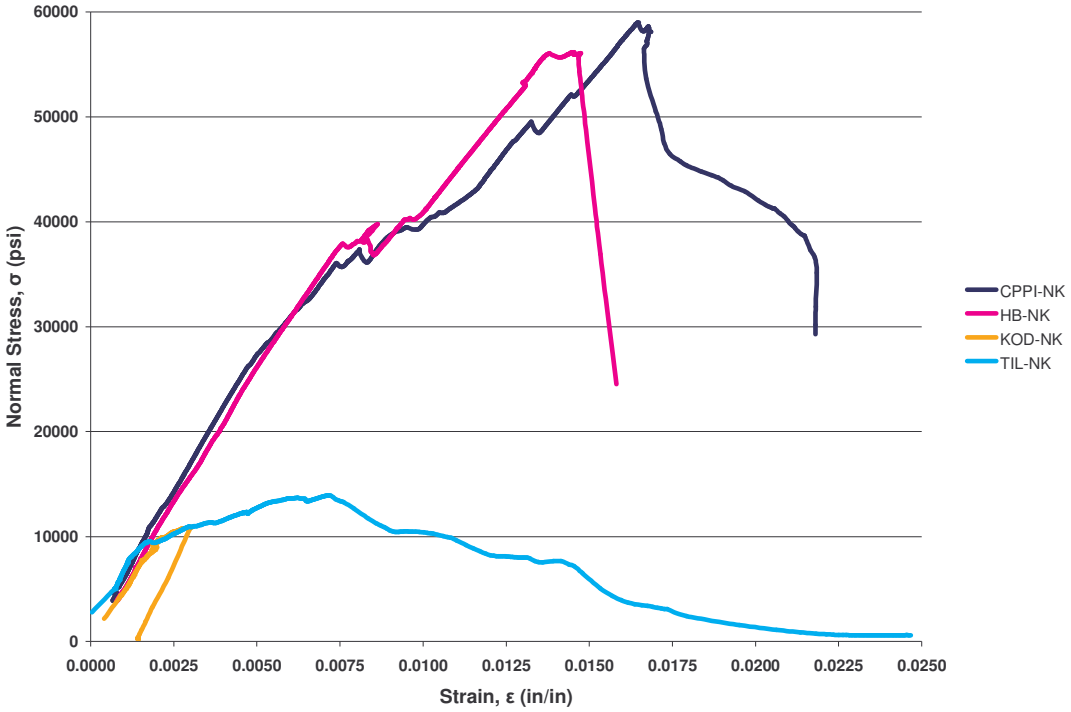

Figure H.23 Tensile Stress vs. Strain for Nicked at 100℉ for 18 Months

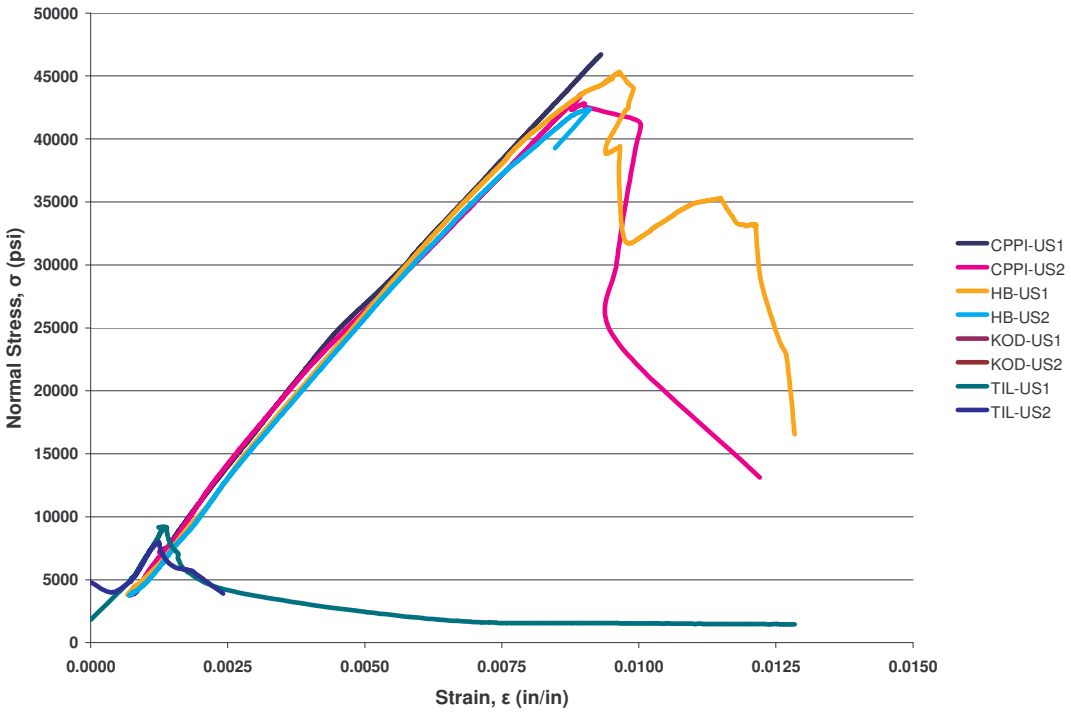

Figure H.24 Tensile Stress vs. Strain for Unscathed at 130℉ for 18 Months

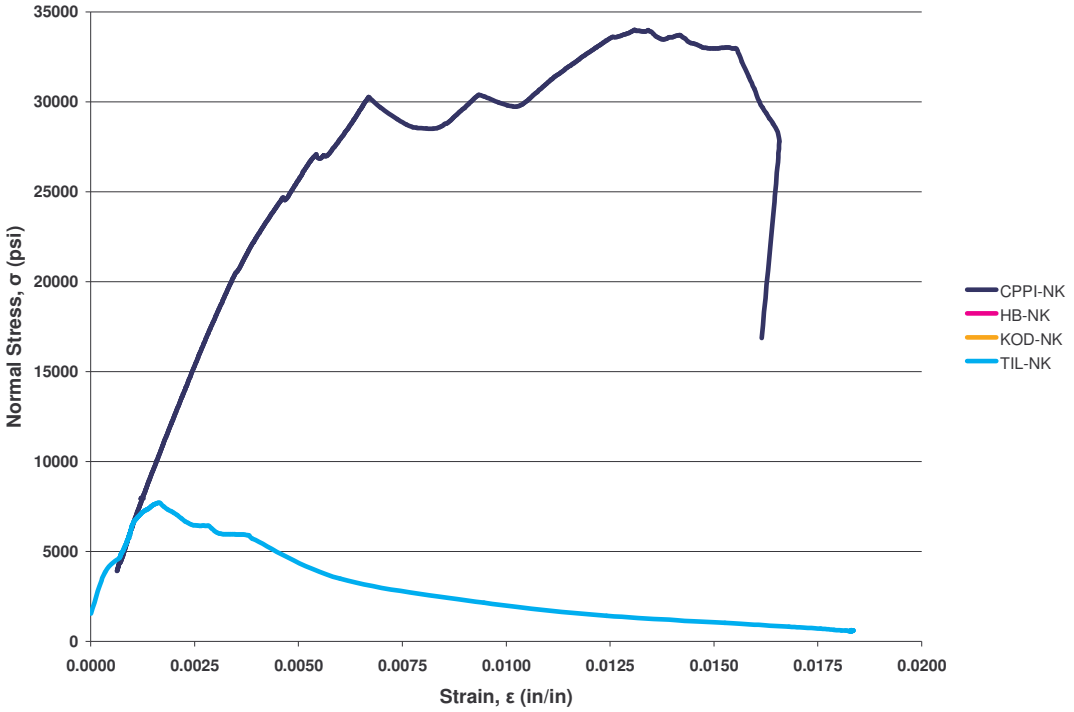

Figure H.25 Tensile Stress vs. Strain for Nicked at 130°F for 18 Months

Appendix I – Bond-Stress vs. Slippage Displacement Diagrams

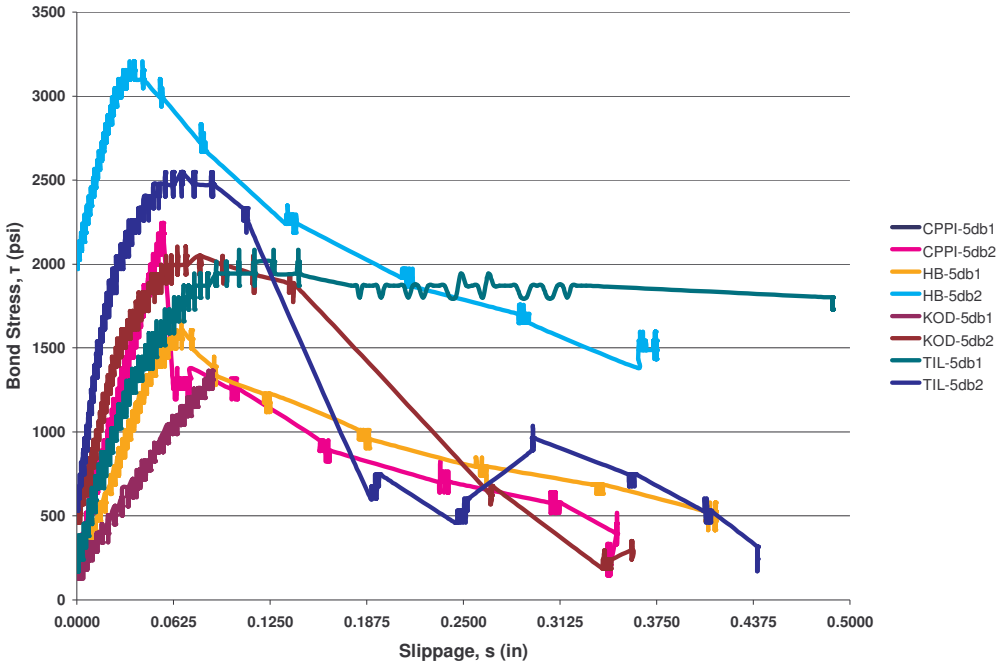

Figure I.1 Bond Stress vs. Slippage Displacement for $5Ø_b$ at Dry Conditions for 6 Months

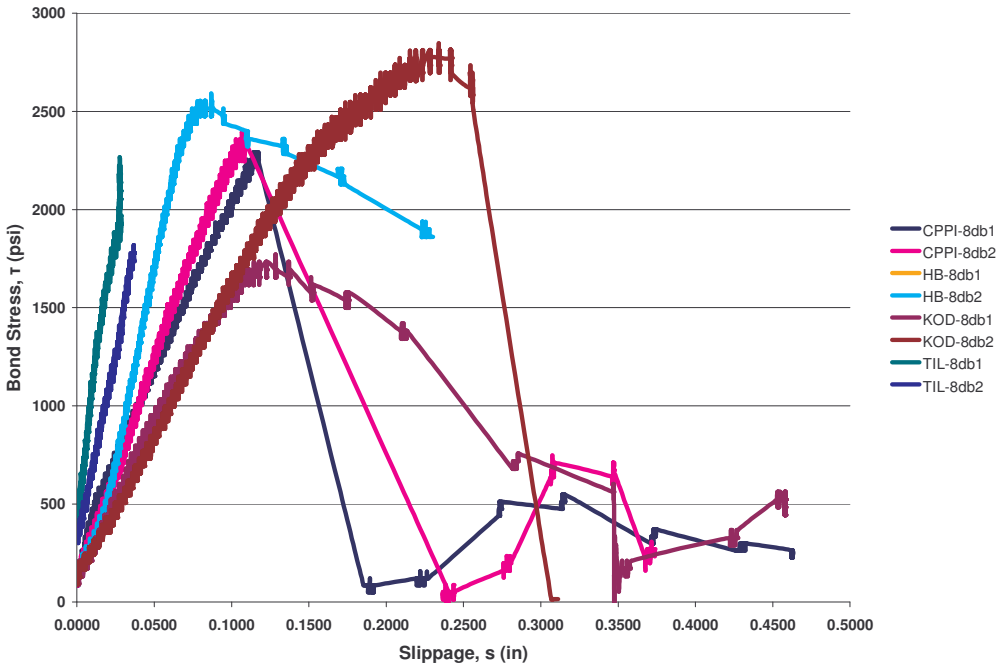

Figure I.2 Bond Stress vs. Slippage Displacement for $8Ø_b$ at Dry Conditions for 6 Months

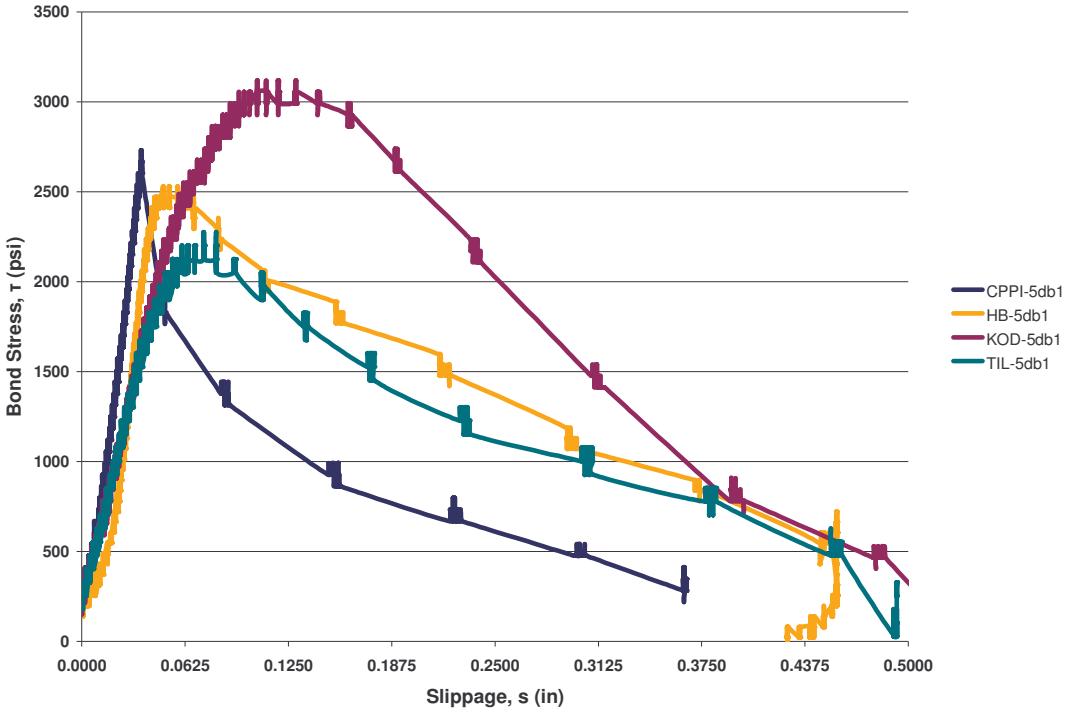

Figure I.3 Bond Stress vs. Slippage Displacement for $5Ø_b$ at Room Temperature for 6 Months

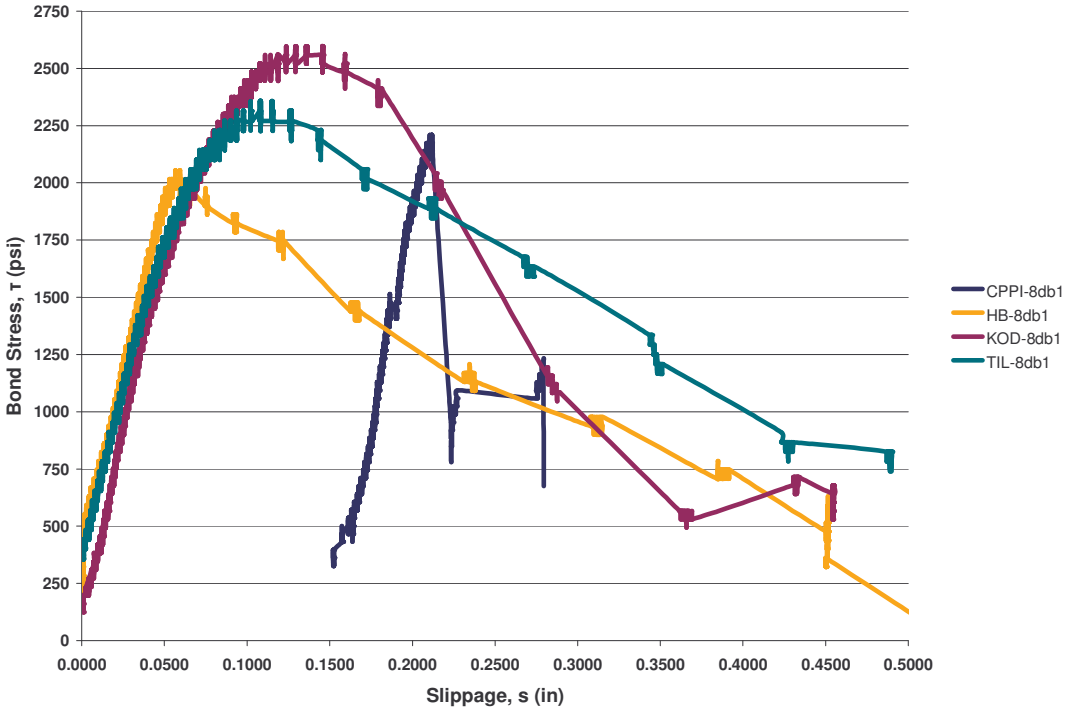

Figure I.4 Bond Stress vs. Slippage Displacement for $8Ø_b$ at Room Temperature for 6 Months

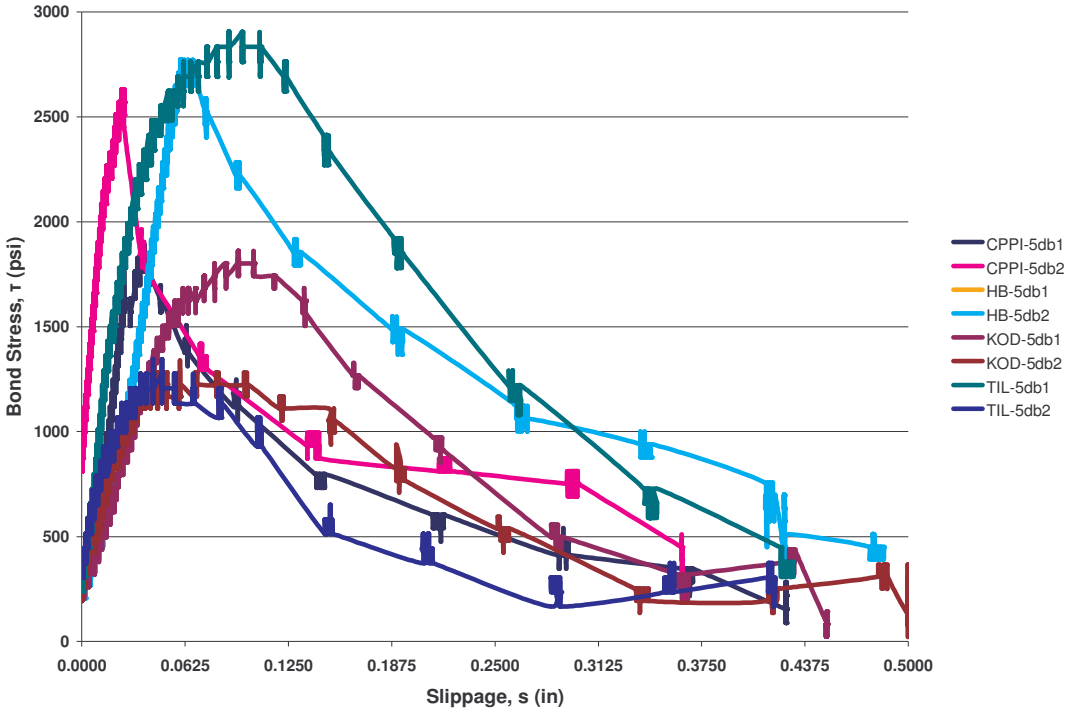

Figure I.5 Bond Stress vs. Slippage Displacement for 5$Ø_b$ at 100℉ at 6 Months

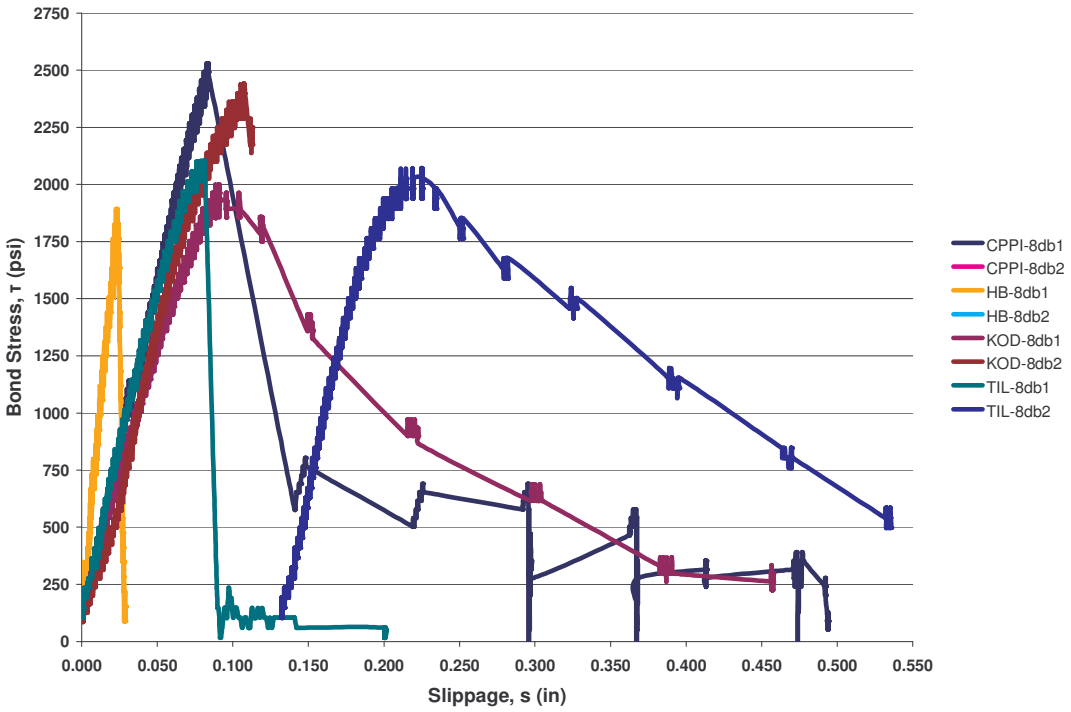

Figure I.6 Bond Stress vs. Slippage Displacement for 8$Ø_b$ at 100℉ for 6 Months

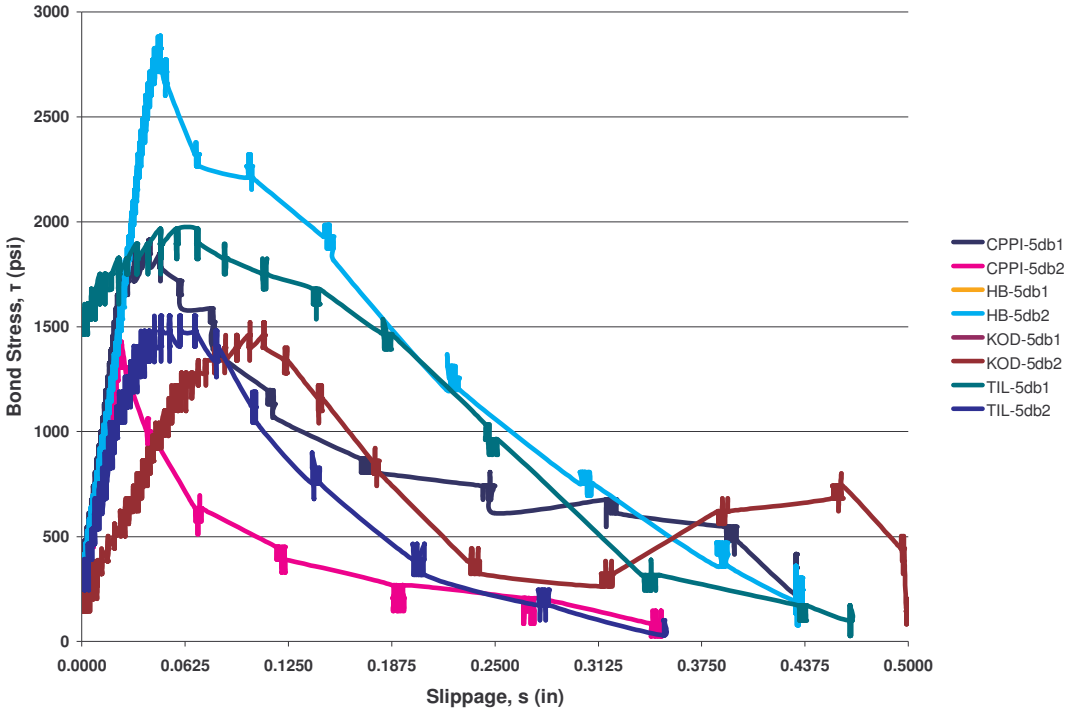

Figure I.7 Bond Stress vs. Slippage Displacement for 5$Ø_b$ at 130°F for 6 Months

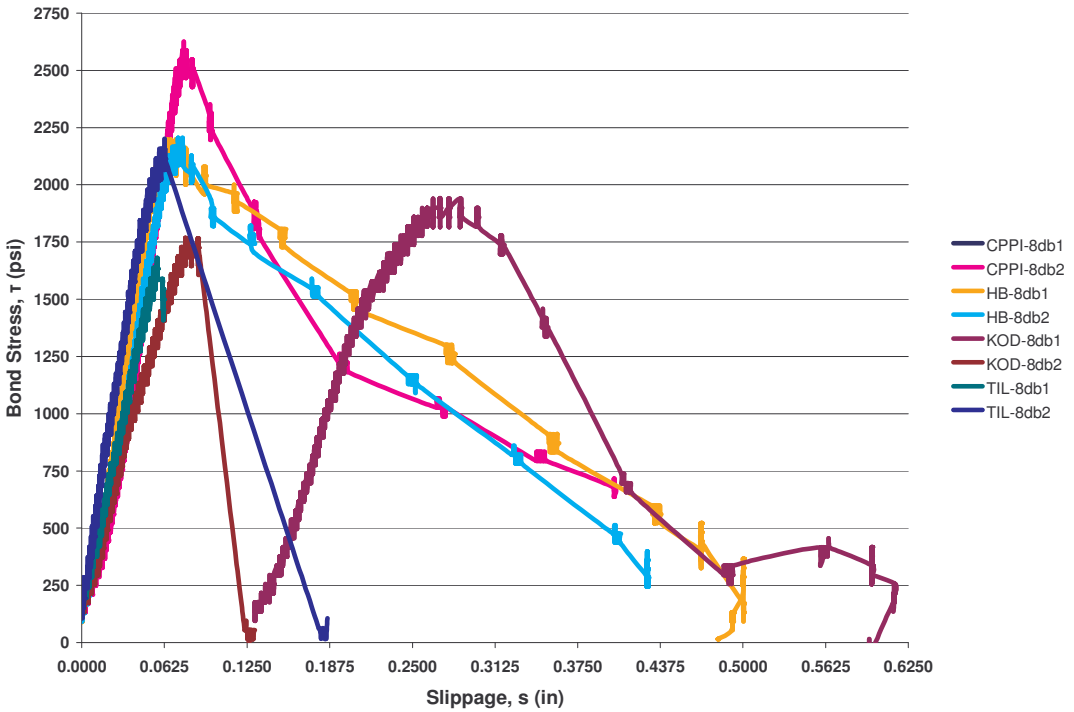

Figure I.8 Bond Stress vs. Slippage Displacement for 8$Ø_b$ at 130°F for 6 Months

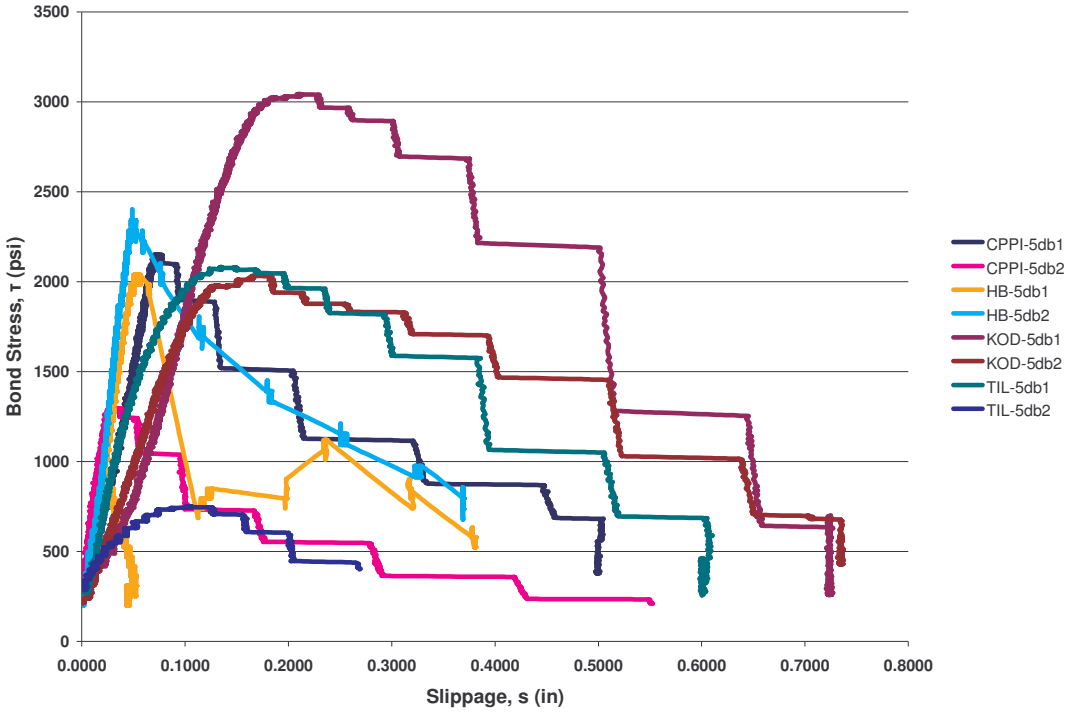

Figure I.9 Bond Stress vs. Slippage Displacement for $5Ø_b$ at Dry Conditions for 12 Months

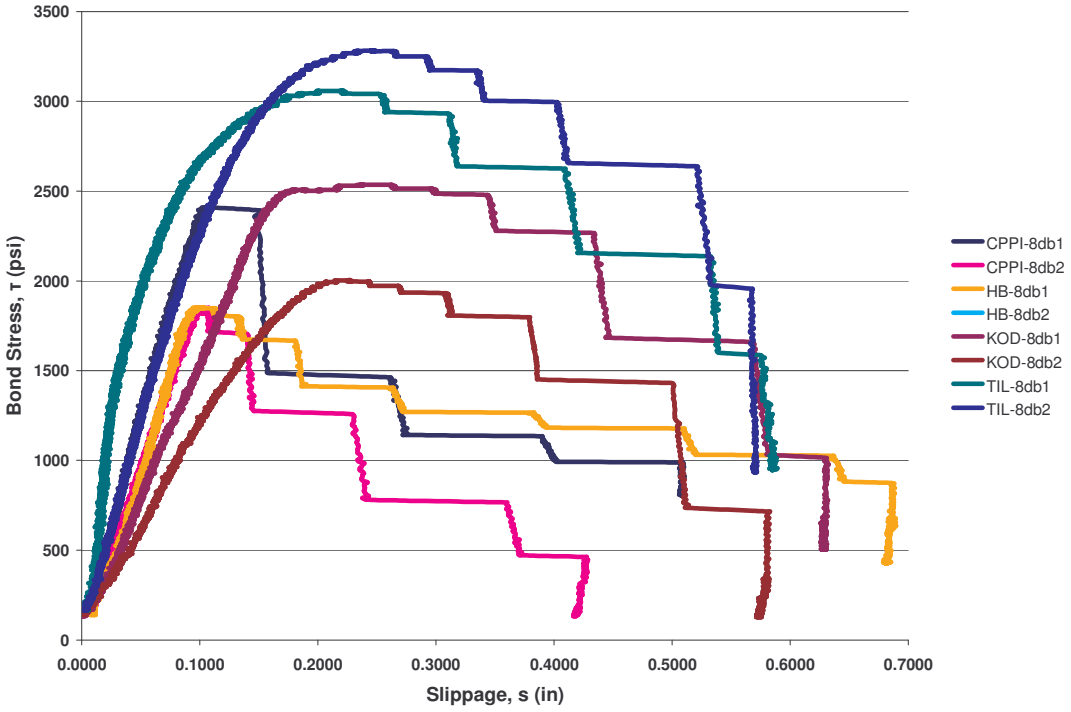

Figure I.10 Bond Stress vs. Slippage Displacement for $8Ø_b$ at Dry Conditions for 12 Months

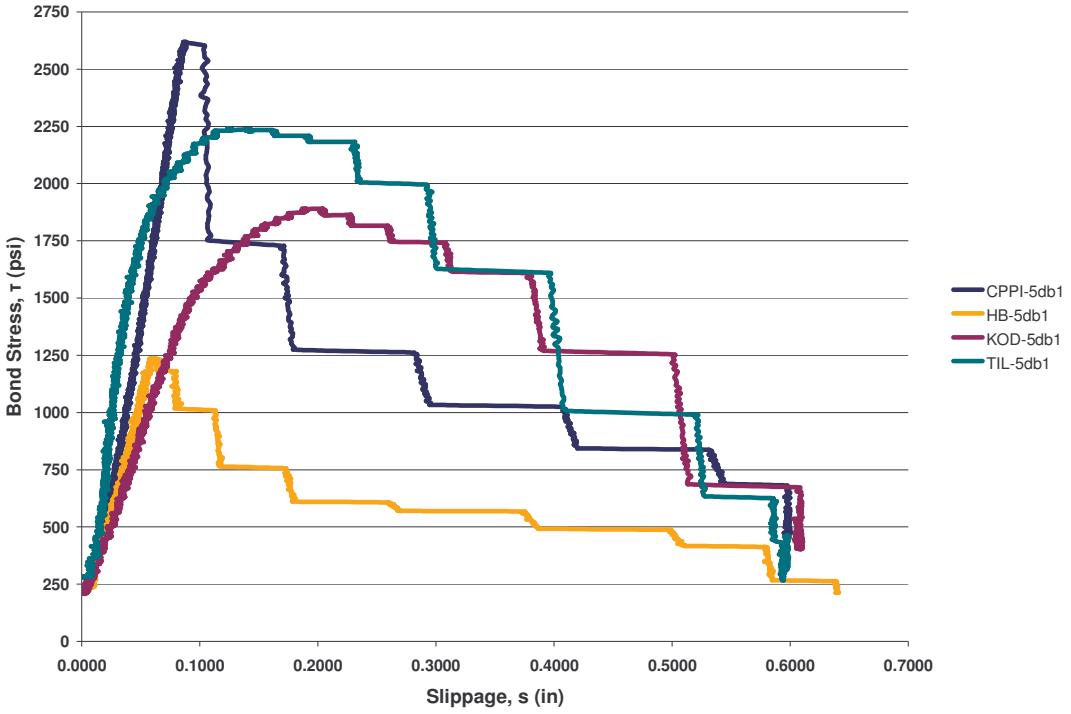

Figure I.11 Bond Stress vs. Slippage Displacement for $5Ø_b$ at Room Temperature for 12 Months

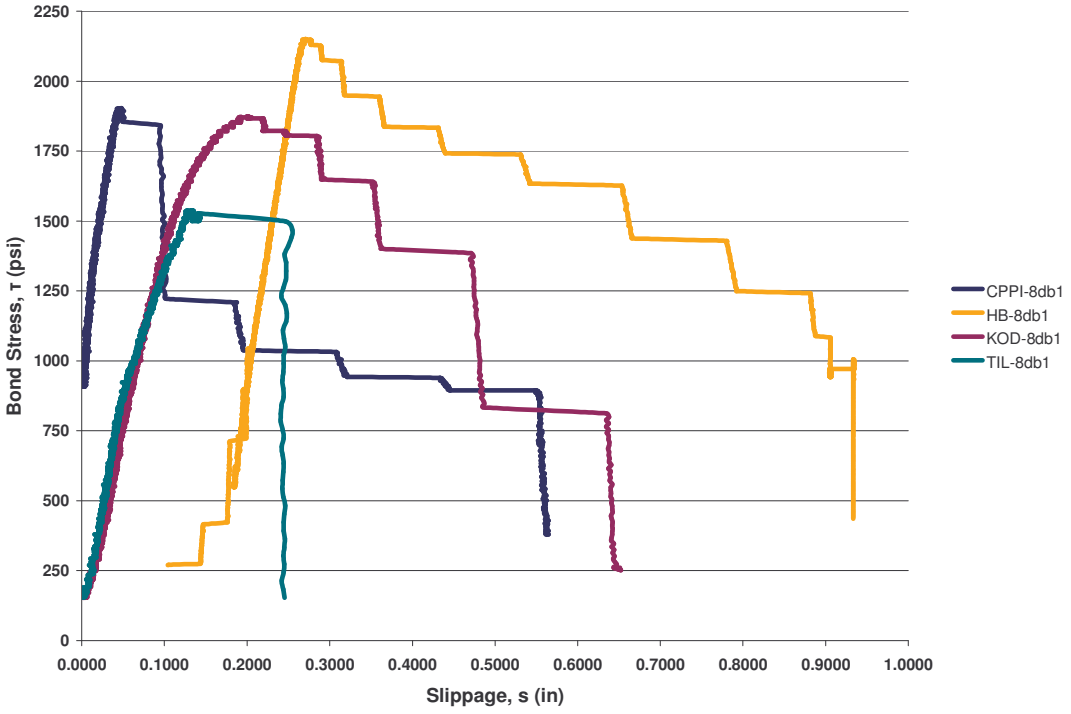

Figure I.12 Bond Stress vs. Slippage Displacement for $8Ø_b$ at Room Temperature for 12 Months

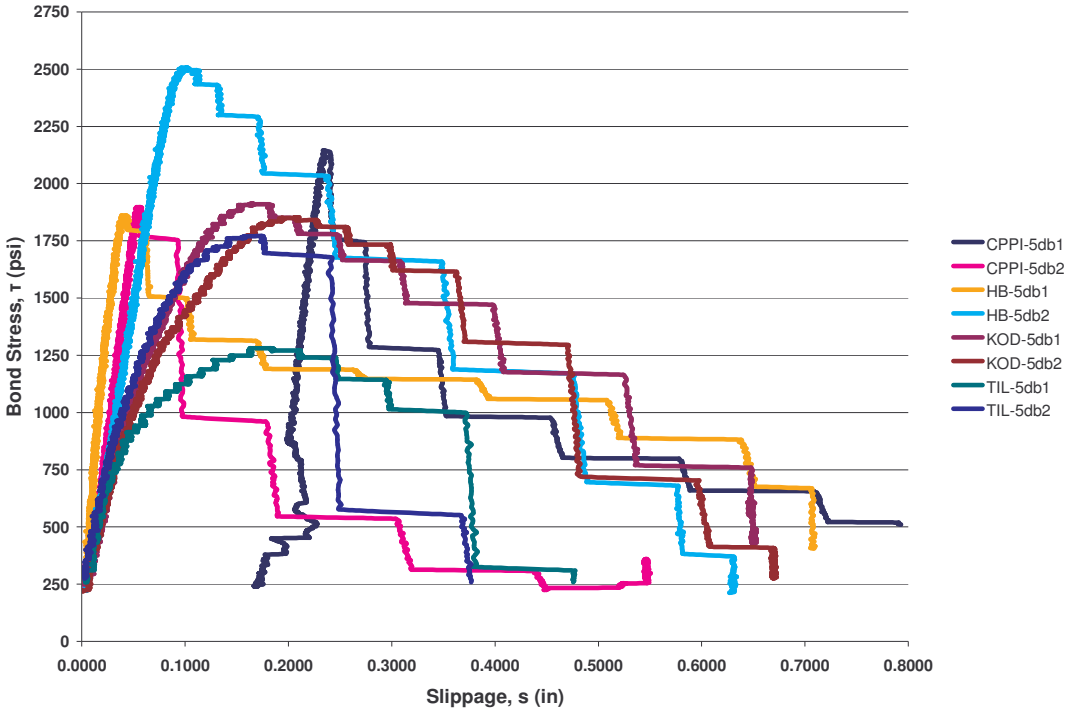

Figure I.13 Bond Stress vs. Slippage Displacement for $5Ø_b$ at 100°F for 12 Months

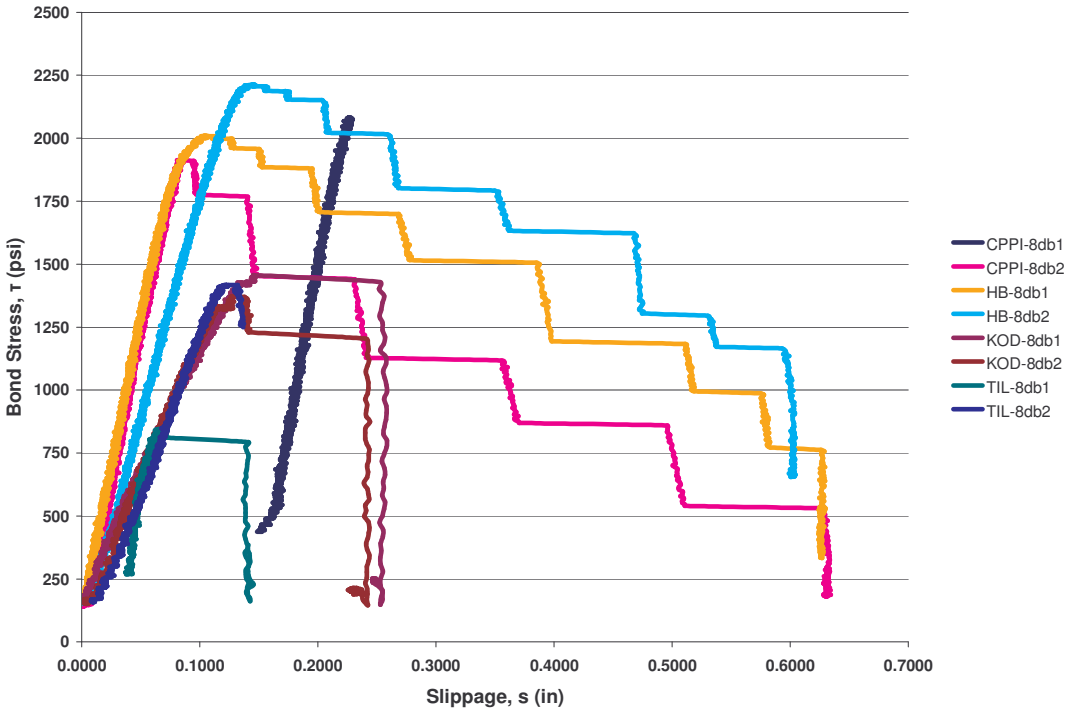

Figure I.14 Bond Stress vs. Slippage Displacement for $8Ø_b$ at 100°F for 12 Months

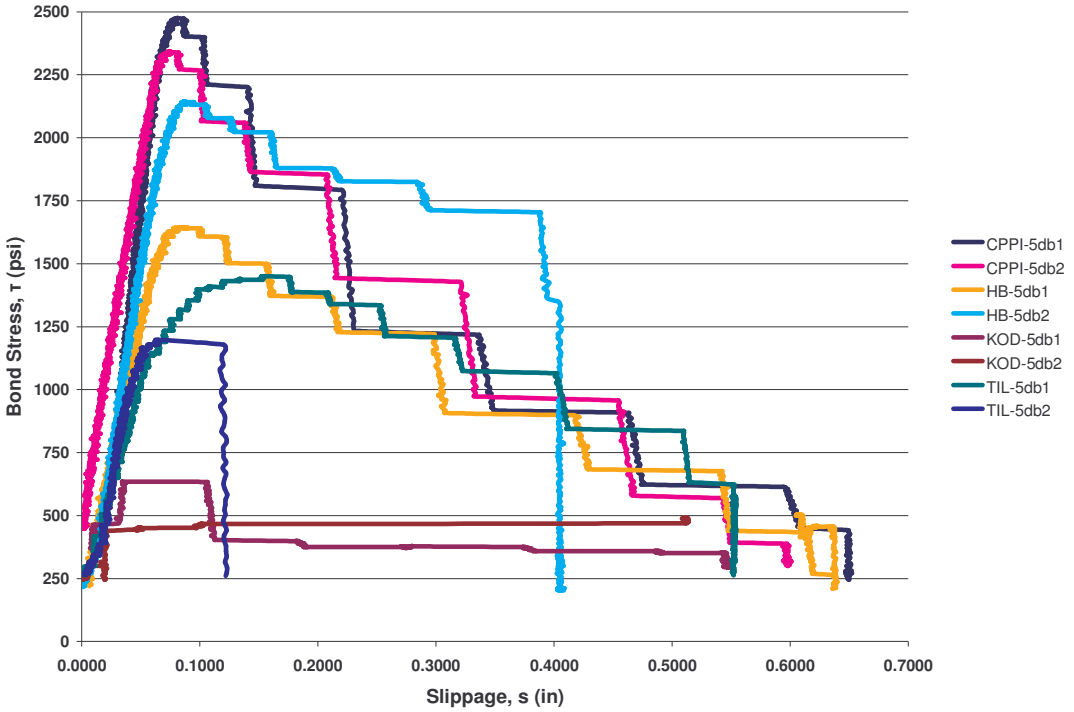

Figure I.15 Bond Stress vs. Slippage Displacement for 5$Ø_b$ at 130°F for 12 Months

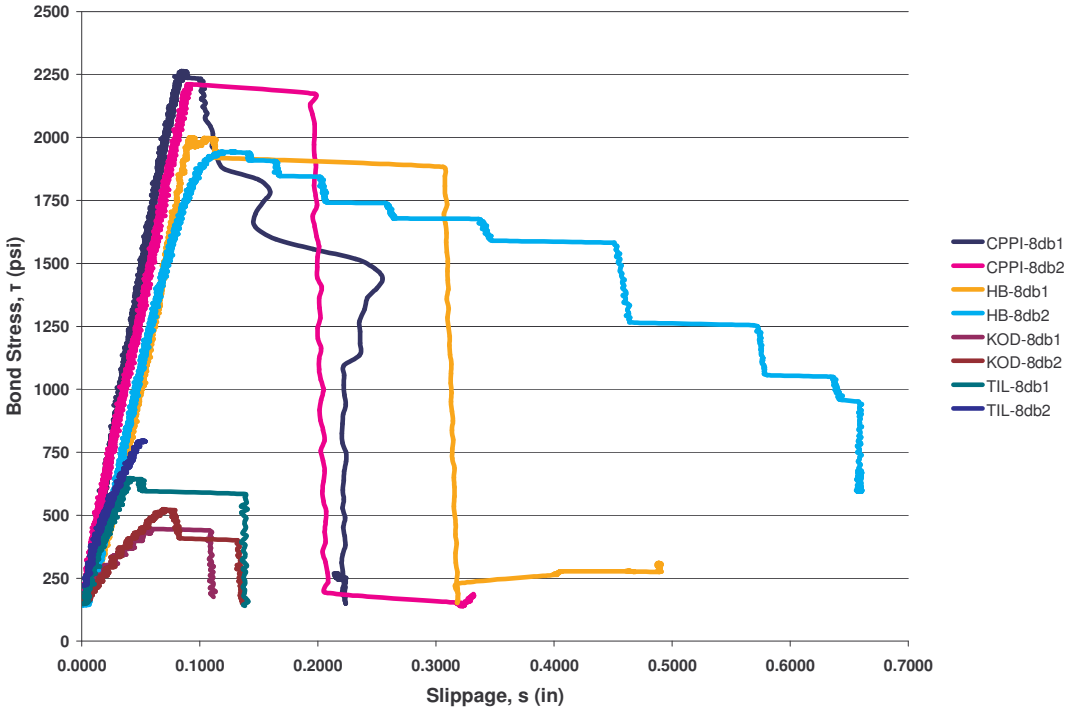

Figure I.16 Bond Stress vs. Slippage Displacement for 8$Ø_b$ at 130°F for 12 Months

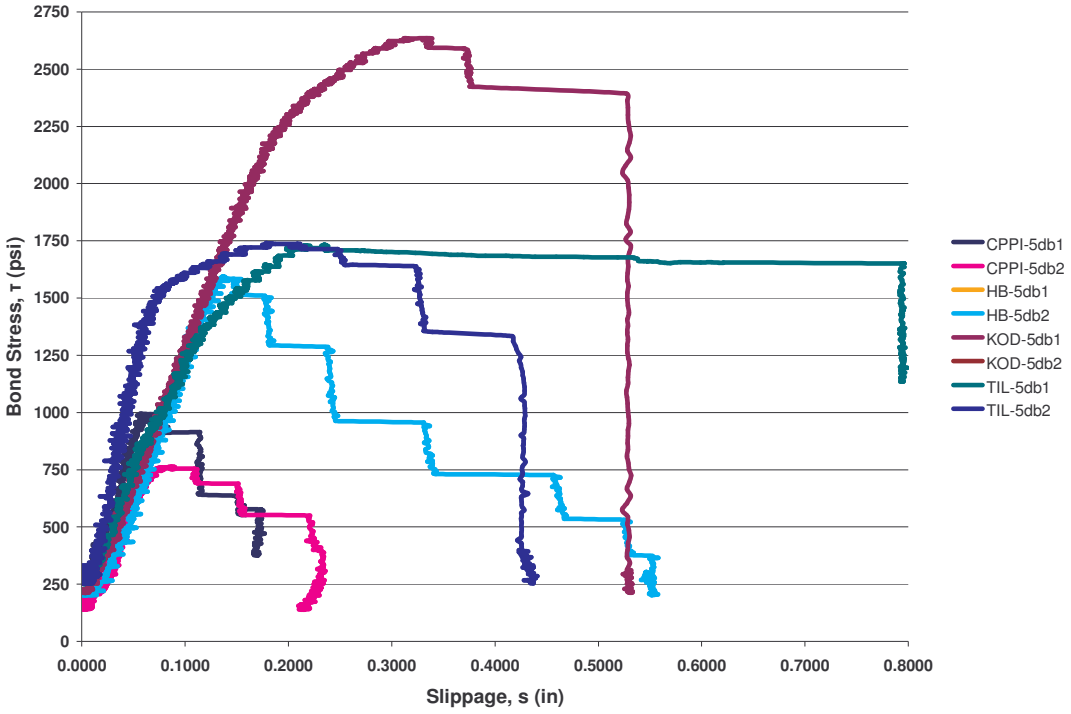

Figure I.17 Bond Stress vs. Slippage Displacement for 5$Ø_b$ at Dry Conditions for 18 Months

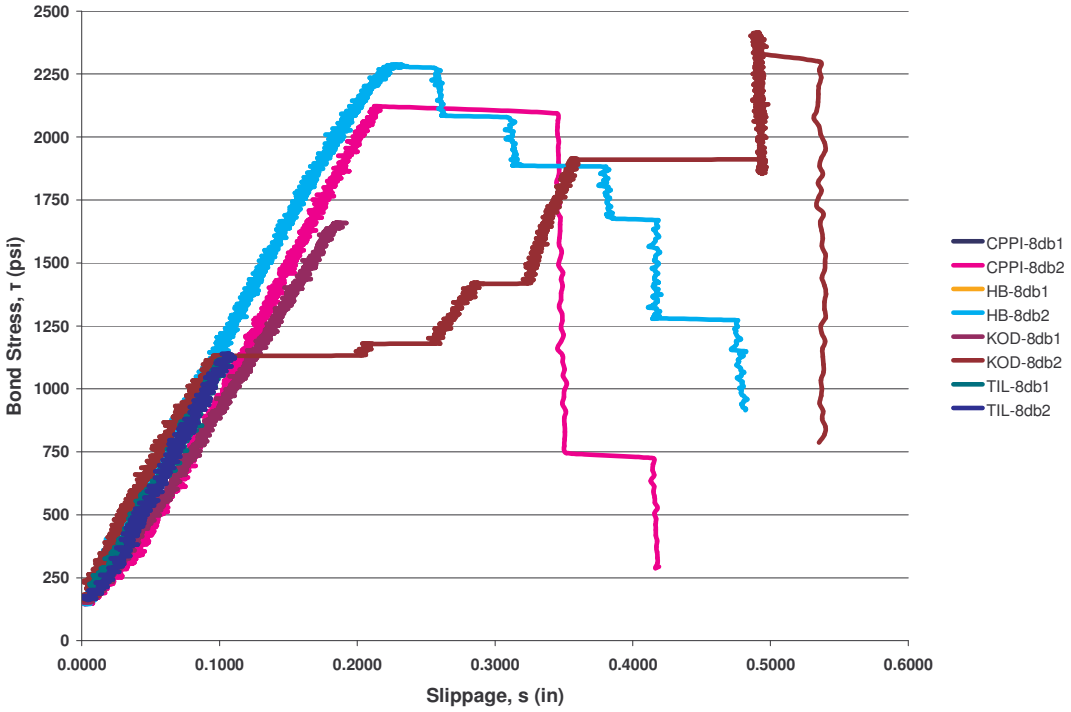

Figure I.18 Bond Stress vs. Slippage Displacement for 8$Ø_b$ at Dry Conditions for 18 Months

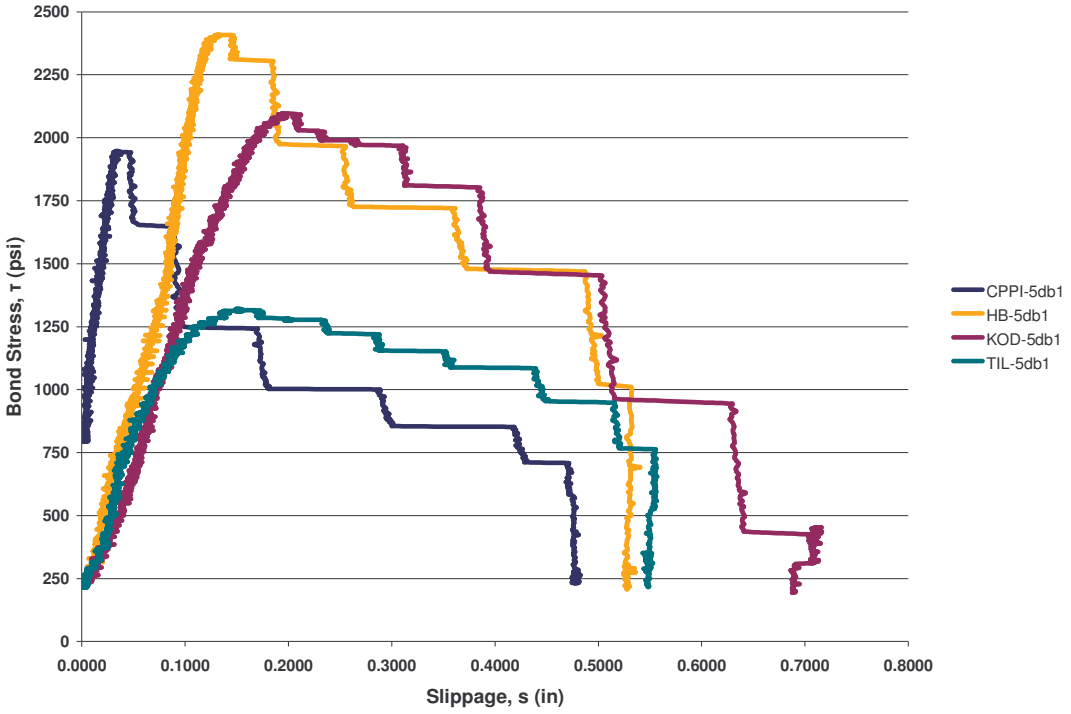

Figure I.19 Bond Stress vs. Slippage Displacement for $5Ø_b$ at Room Temperature for 18 Months

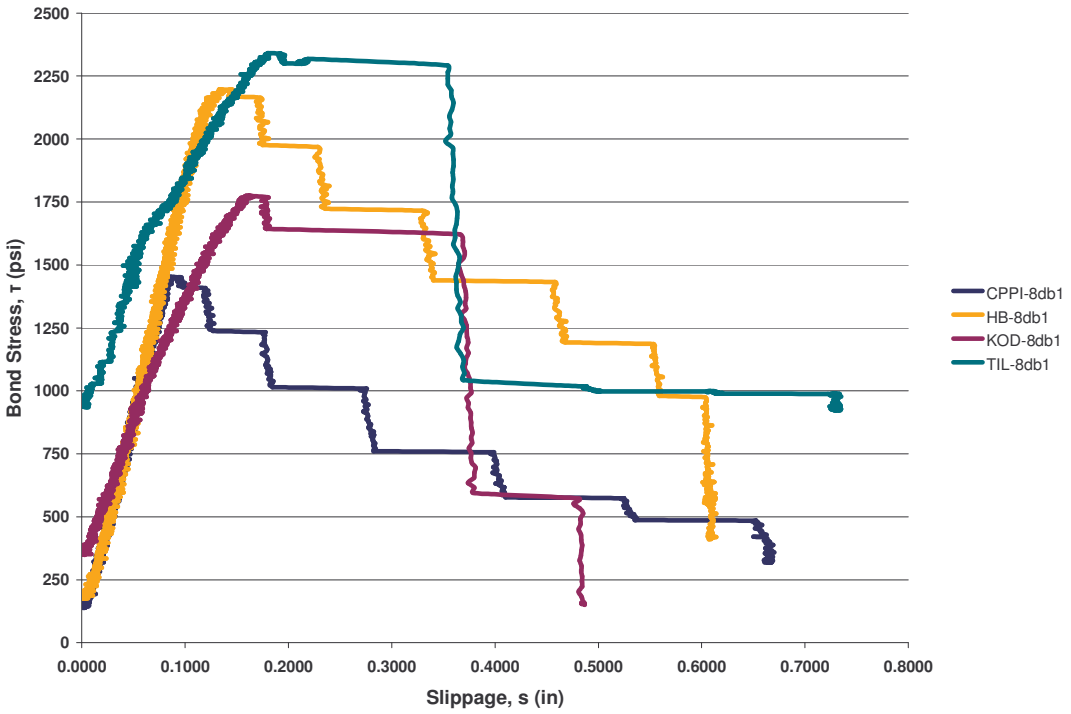

Figure I.20 Bond Stress vs. Slippage Displacement for $8Ø_b$ at Room Temperature for 18 Months

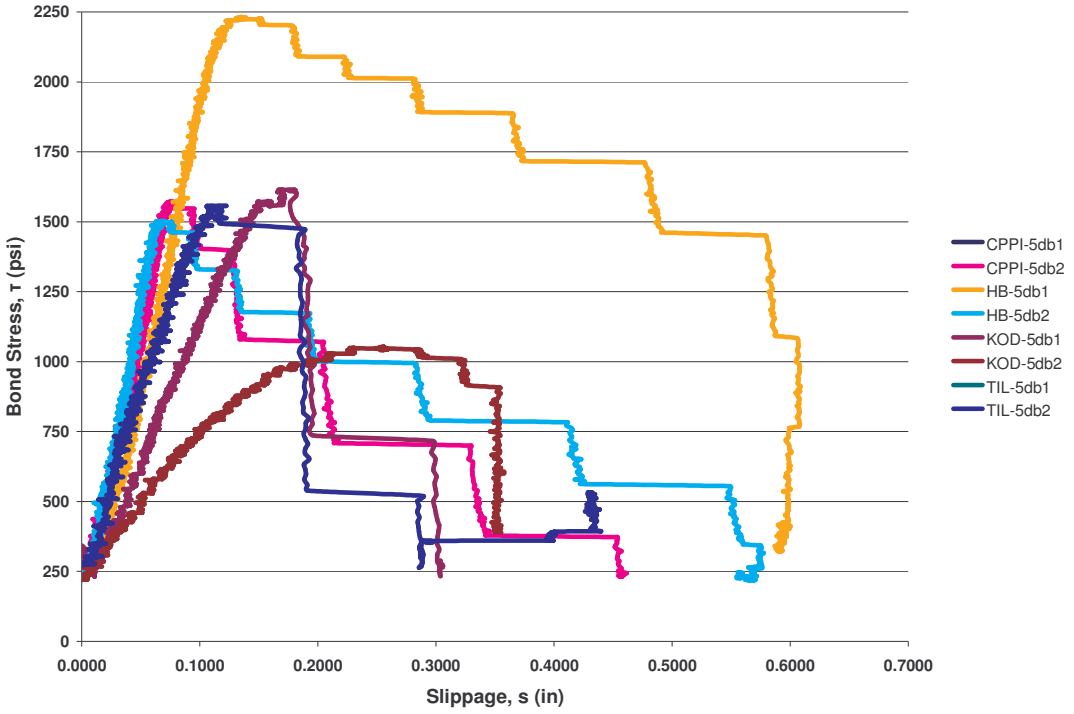

Figure I.21 Bond Stress vs. Slippage Displacement for 5$Ø_b$ at 100°F for 18 Months

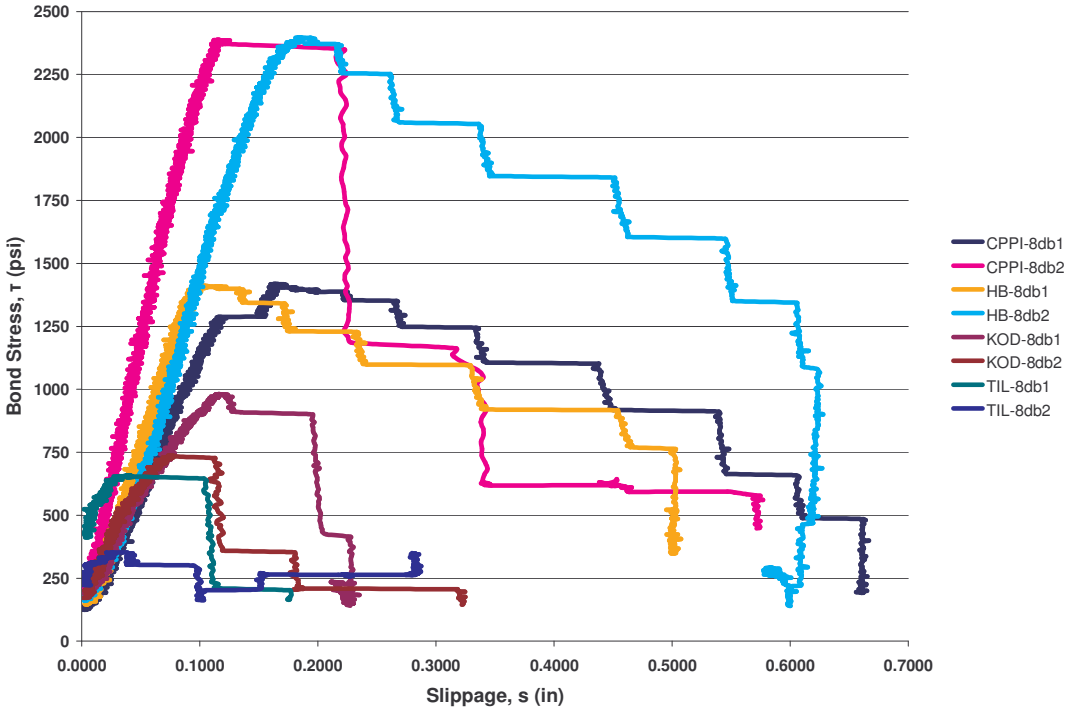

Figure I.22 Bond Stress vs. Slippage Displacement for 8$Ø_b$ at 100°F for 18 Months

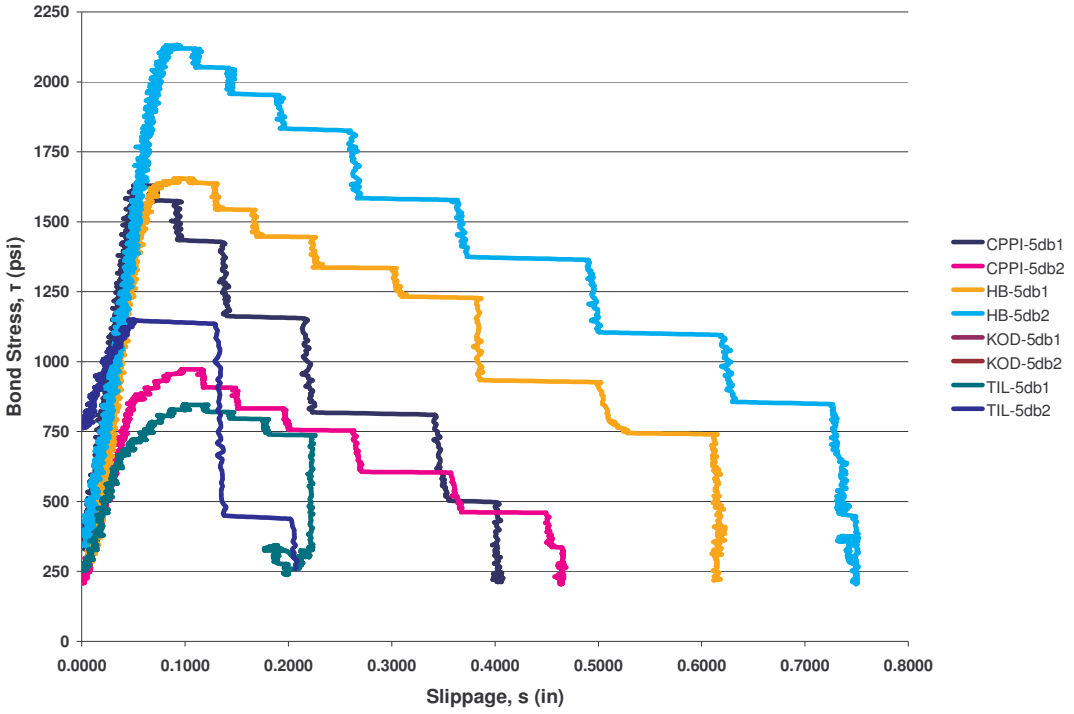

Figure I.23 Bond Stress vs. Slippage Displacement for 5$Ø_b$ at 130℉ at 18 Months

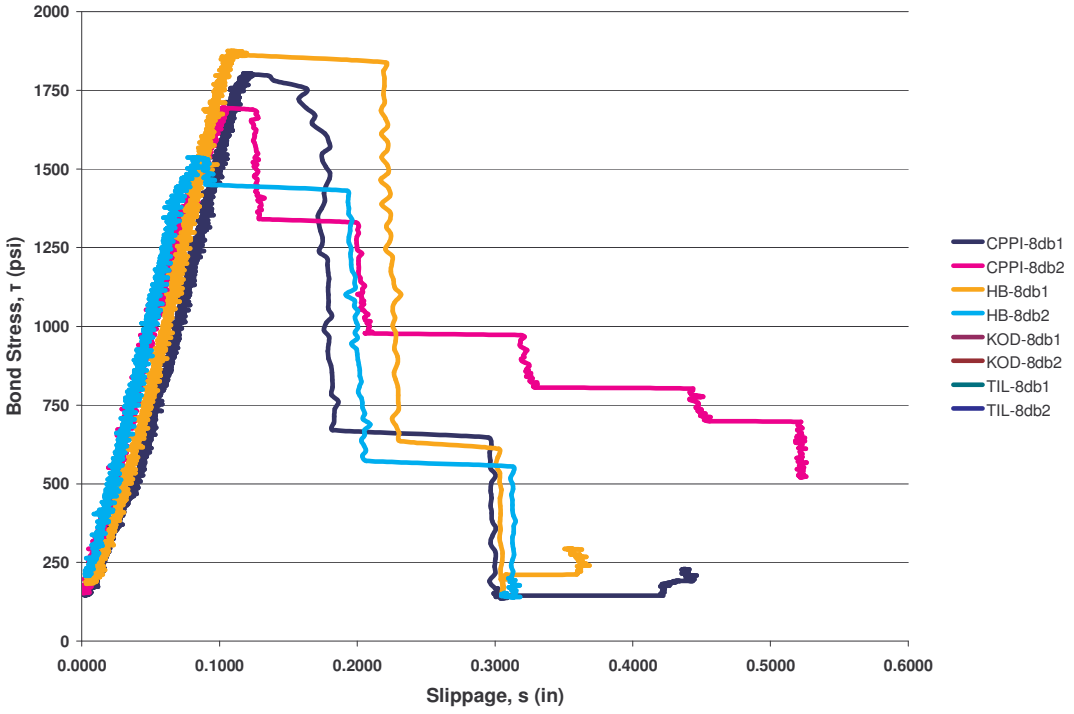

Figure I.24 Bond Stress vs. Slippage Displacement for 8$Ø_b$ at 130℉ for 18 Months